From Soil Legacy to Wheat Yield Decline: Studying the Plant-Soil Feedback Mechanisms in Wheat Rotations

Nikolaos Kaloterakis

Energie & Umwelt / Energy & Environment
Band / Volume 686
ISBN 978-3-95806-874-2

Mitglied der Helmholtz-Gemeinschaft

JÜLICH
Forschungszentrum

Schriften des Forschungszentrums Jülich
Reihe Energie & Umwelt / Energy & Environment Band / Volume 686

Forschungszentrum Jülich GmbH
Institut für Bio- und Geowissenschaften (IBG)
Agrosphäre (IBG-3)

From Soil Legacy to Wheat Yield Decline: Studying the Plant-Soil Feedback Mechanisms in Wheat Rotations

Nikolaos Kaloterakis

Schriften des Forschungszentrums Jülich
Reihe Energie & Umwelt / Energy & Environment Band / Volume 686

ISSN 1866-1793 ISBN 978-3-95806-874-2

Bibliografische Information der Deutschen Nationalbibliothek.
Die Deutsche Nationalbibliothek verzeichnet diese Publikation in der
Deutschen Nationalbibliografie; detaillierte Bibliografische Daten
sind im Internet über http://dnb.d-nb.de abrufbar.

Herausgeber und Vertrieb:	Forschungszentrum Jülich GmbH Zentralbibliothek, Verlag 52425 Jülich Tel.: +49 2461 61-5368 Fax: +49 2461 61-6103 zb-publikation@fz-juelich.de www.fz-juelich.de/zb
Umschlaggestaltung:	Grafische Medien, Forschungszentrum Jülich GmbH
Druck:	Grafische Medien, Forschungszentrum Jülich GmbH
Copyright:	Forschungszentrum Jülich 2025

Schriften des Forschungszentrums Jülich
Reihe Energie & Umwelt / Energy & Environment, Band / Volume 686

D 5 (Diss. Bonn, Univ., 2025)

ISSN 1866-1793
ISBN 978-3-95806-874-2

Vollständig frei verfügbar über das Publikationsportal des Forschungszentrums Jülich (JuSER)
unter www.fz-juelich.de/zb/openaccess.

Acknowledgements

"*The answer to the ultimate question of life, the universe, and everything is 42*"
The Hitchhiker's Guide to the Galaxy, Douglas Adams

Doing a PhD is no easy task. I spent countless hours designing my experiments and even more hours performing, analyzing and reporting them. The PhD journey is a unique experience that allowed me to grow, learn and most importantly, make a small contribution to the magical (and cryptic) world of plant-soil interactions. I am grateful for this valuable opportunity.

First, I would like to thank my supervisor, Nicolas Brüggemann, whose scientific support and guidance were crucial to the completion of my PhD project. His expertise in plant-soil interactions helped me greatly to gain a solid understanding of key concepts in this field and improve the quality of my work. It's through good supervision that a PhD student can effectively achieve critical and independent thinking.

I would like to thank my colleagues in the RhizoWheat project for the fruitful collaboration. Sharing their expertise has been a big advantage and I have learnt a lot from them. In particular, I want to thank Andrea Braun-Kiewnick and Adriana Giongo for their input in several chapters of this thesis and also for the nice times during their visit to Jülich and my visits to Braunschweig. Special thanks to Andrea for all the encouragement and the critical discussions on plant growth-promoting rhizobacteria. I appreciate the collaboration and discussions I had with Mehdi Rashtbari with whom I am glad to continue working in the second phase of the RhizoWheat project. Thanks also to Doreen Babin, Kornelia Smalla from Julius Kühn Institute, Bahar Razavi from the Christian Albrecht University of Kiel, Sibghat Ullah and Andrea Schnepf from Forschungszentrum Jülich for their insightful comments on several parts of this work.

Many thanks to the whole Plant-Soil-Atmosphere Exchange Processes group of Agrosphere (IBG-3) and especially Kerui, Matthias, Hella, Katharina, Daniel, Adrian and Moritz. Thank you for all the tea, lunch breaks and the fun we had. I also want to thank Rüdiger for introducing me to the well-designed rhizotrons back in 2020. Many thanks to Sirgit, Franz and Holger for all their help with the lab work. I also appreciate the support from Stephan Köppchen when working in the control area and the feedbacks from Harry Vereecken during my PhD report discussion. I also highly appreciate the support of Youri and Paulina with the automatic manifold system. I thank the technical assistant of Ayhan Egmen and his team in the construction department. Special thanks to Otávio for the collaboration and all the discussions on soil carbon and for bringing the Mediterranean (~ Brazilian) vibe to the group. Speaking of the Mediterranean, I would like to thank my French (subsp. Marseillaise) office mate. Samuel Le Gall, thank you for being the best office mate and, most importantly, a dear friend and fellow musician. I thoroughly enjoyed the times we spent hanging out, playing rebetiko, walking by the river, being nostalgic of the Mediterranean and experimenting (mostly with drought) on our office plants. Khadija Boughazi, I am grateful to have a friend and a great scientist from our neighboring institute and I

am especially thankful for the karaoke, basketball, cakes and the tasty tajines during these years; they kept me going. I could not be luckier to have you and Ousama as my family in Germany. Xinyue Cao, I am very glad that we met and I enjoyed our time together while you were working on your PhD in Jülich. I also appreciate that you introduced me to the amazing Chinese culture. See you soon in Crete or China. I met so many people in Jülich and I am sure I forgot to mention them all. I also want to thank several BSc and MSc students and especially Anne and Charlotte.

From my MSc in the Netherlands, I would like to thank Gerlinde De Deyn and Sander van Delden from Wageningen University and Research, for being true mentors and making me want to pursue a PhD. Also, many thanks to Wim van der Putten from the Netherlands Institute of Ecology (NIOO-KNAW) for introducing me to plant-soil feedbacks and their importance for plant succession. From my BSc in Greece, I would like to thank Konstantinos Loulakakis and Andriana Stavropoulou from the Hellenic Mediterranean University, for teaching me to appreciate science.

Many thanks to all my wonderful friends in Greece (Adam, Tzotzo, Nikonas, Nikitas, Fotini, Odisseas, Spiros, Titiki, Veronika, Giorgos, Eleni), Mexico (Francisco), Peru (Andrea), New Zealand (Michael) and the Netherlands (Sean and Juliana) for helping me reset each time we met and of course, many others scattered around the world that I hope to meet again soon. This has been a fundamental aspect of my PhD thesis. The same applies to my cats in Greece: Haroulis, Pipitsa and Chrisafis.

I want to thank Aliki and Liakos for their constant support and all the heartfelt experiences we have shared over the years. I am truly lucky to be surrounded by these loving and caring people who have taught me so much and supported me over the years. Aliki, you are full of imagination, and Liakos, you are a true “rebetis”.

I cannot express enough how grateful I am to my parents, Stelios Kaloterakis and Dimitra Kouveli. They have always been there for me since childhood, loving me unconditionally, motivating me and allowing me to grow, plan my future and achieve my dreams, even though they have been missing me all those years. Thank you for encouraging me to keep going in every challenge I have faced in life. Appreciating my parents who set the basis (or the roots as per this thesis is suggesting) of who I am today is the least I can do and I will always be grateful. And of course a big thank you to my sister Chrysoula and my little niece Artemis, to whom I plan to be the best uncle ever.

The acknowledgments section cannot end without thanking the most important person in my life: my colorful wife, Eleni Klainou. I am so fortunate that we are on this journey together and that you are teaching me how to be a better person and appreciate the things that really matter in life. You are always there to motivate me and I thank you for that. Living with you in Greece, the Netherlands and Germany has made this PhD possible, and I dedicate my thesis to you.

Abstract

Winter wheat is one of the most important crops cultivated globally. The yield of winter wheat is stagnating in several areas of the world since the 1990s. Continuous winter wheat cultivation is associated with a marked yield decline that is often attributed to the proliferation of the soil-borne pathogen *Gaeumannomyces tritici* (take-all). However, it is unlikely that this yield decline is solely due to take-all, but rather it is the outcome of more complex soil-microbe-plant interactions that drive plant-soil feedbacks in the rhizosphere of winter wheat. The soil legacy of the preceding crop is a major determinant of the growth and development of the succeeding plant, and it can be expected that the rotational position of winter wheat will influence the productivity of the following winter wheat. The aim of this thesis was to analyze plant-soil feedbacks in successive winter wheat rotations and better understand the observed yield decline. We specifically aimed at investigating how the rotational position of winter wheat affects the microbial communities and the associated nutrient cycling and enzymatic activity in the soil, and how the root system of winter wheat responds to these changes, thereby affecting plant growth and productivity. Finally, we looked into the potential of compost and plant growth-promoting rhizobacteria to compensate for the growth reduction in continuous winter wheat rotations and provide farmers with a sustainable toolbox to safeguard plant productivity and food production. We developed and used novel mesocosms for growing winter wheat and employing isotopic tracers to enable the quantification of important rhizosphere processes and assess above- and belowground carbon allocation, nitrogen uptake and water uptake from various soil layers. We found that there was much higher initial nitrate availability in the soil of winter wheat after oilseed rape at the germination and tillering growth stage compared to continuous winter wheat, especially in the subsoil. This was associated with nitrogen immobilization by the microbial community, which was associated with distinct root plastic responses and reduced winter wheat growth early in the growing season. Soil legacy of the preceding crop also had a strong influence on soil enzymatic activity and nitrogen cycling as indicated by changes in the activity of nitrogen-related enzymes and the abundance of microbial nitrogen-cycling genes. We also found a higher and sustained belowground allocation of freshly assimilated carbon at the flowering and grain ripening growth stages of winter wheat growing after oilseed rape that was available for microbial use, revealing a higher rhizodeposition in non-successive winter wheat rotations. Non-successive winter wheat converted more of the freshly assimilated carbon into biomass and achieved higher yields than continuous winter wheat. Winter wheat after oilseed rape exhibited distinct patterns in shaping its microbial community, with a higher abundance of taxa involved in important nutrient mineralization processes and capable of conferring plant protection against important soil pathogens. Application of both compost and plant growth-promoting rhizobacteria caused a positive plant-soil feedback in continuous winter wheat cultivation, compensating the growth reduction and yield decline. This work thus demonstrated that yield decline in successive winter wheat rotations is dependent on several key rhizosphere processes and that soil legacy of the preceding crop is an important driver of the

productivity of the succeeding plant. By understanding this phenomenon, we can design resilient, productive and multifunctional farming systems that can cope with the increasing adversities of climate change without compromising yield production and food security.

Zusammenfassung

Winterweizen ist eine der wichtigsten weltweit angebauten Nutzpflanzen. Seit den 1990er Jahren stagniert der Ertrag von Winterweizen in mehreren Regionen der Welt. Der kontinuierliche Anbau von Winterweizen ist mit einem deutlichen Ertragsrückgang verbunden, der häufig auf die Ausbreitung des bodenbürtigen Krankheitserregers *Gaeumannomyces tritici* (Schwarzbeinigkeit) zurückzuführen ist. Es ist jedoch unwahrscheinlich, dass dieser Ertragsrückgang ausschließlich auf die Schwarzbeinigkeit zurückzuführen ist. Vielmehr ist er das Ergebnis komplexerer Wechselwirkungen zwischen Boden, Mikroben und Pflanzen, die die Rückkopplungen zwischen Pflanzen und Boden in der Rhizosphäre von Winterweizen beeinflussen. Das Bodenvermächtnis der Vorfrucht ist ein entscheidender Faktor für das Wachstum und die Entwicklung der Nachfolgepflanze, und es ist zu erwarten, dass die Fruchtfolge von Winterweizen die Produktivität des nachfolgenden Winterweizens beeinflusst. Das Ziel dieser Arbeit war es, die Rückkopplungen zwischen Pflanzen und Boden in aufeinanderfolgenden Winterweizen-Fruchtfolgen zu analysieren und den Ertragsrückgang besser zu verstehen. Wir wollten insbesondere untersuchen, wie sich die Fruchtfolge von Winterweizen auf die mikrobiellen Gemeinschaften und die damit verbundenen Nährstoffkreisläufe und enzymatischen Aktivitäten im Boden auswirkt und wie das Wurzelsystem von Winterweizen auf diese Veränderungen reagiert und dadurch das Pflanzenwachstum und die Produktivität beeinflusst. Schließlich untersuchten wir das Potenzial von Kompost und pflanzenwachstumsfördernden Rhizobakterien, um die Wachstumsreduzierung in kontinuierlichen Winterweizenkulturen auszugleichen und den Landwirten ein nachhaltiges Instrumentarium zur Sicherung der Pflanzenproduktivität und Lebensmittelproduktion an die Hand zu geben. Wir entwickelten und verwendeten neuartige Mesokosmen für den Anbau von Winterweizen und setzten Isotopentracer ein, um die Quantifizierung wichtiger Rhizosphärenprozesse zu ermöglichen und die ober- und unterirdische Kohlenstoffverteilung, Stickstoffaufnahme und Wasseraufnahme aus verschiedenen Bodenschichten zu bewerten. Wir stellten fest, dass die anfängliche Nitratverfügbarkeit im Boden von Winterweizen nach Raps in der Keim- und Bestockungsphase viel höher war als bei kontinuierlichem Winterweizen, insbesondere im Unterboden. Dies führte zur Stickstoffimmobilisierung durch die Bodenmikroorganismen, was sich in deutlichen plastischen Reaktionen der Wurzeln und einem verringerten Wachstum des Winterweizens zu Beginn der Vegetationsperiode niederschlug. Die Beeinflussung des Bodens durch die Vorfrucht hatte einen starken Einfluss auf die enzymatische Aktivität des Bodens und den Stickstoffkreislauf, was sich in Veränderungen der Aktivität stickstoffassoziierter Enzyme und der Häufigkeit mikrobieller, mit dem Stickstoffkreislauf assoziierter Gene zeigte. Wir stellten auch eine erhöhte und anhaltende unterirdische Allokation von frisch assimiliertem Kohlenstoff in der Blüte- und Kornreifungsphase fest, der für die mikrobielle Nutzung zur Verfügung stand, was ein Indikator für eine höhere Rhizodeposition in nicht aufeinanderfolgenden Winterweizenfruchtfolgen war. Nicht aufeinanderfolgender Winterweizen wandelte mehr des frisch assimilierten Kohlenstoffs in Biomasse um und erzielte

höhere Erträge als kontinuierlicher Winterweizen. Die mikrobielle Gemeinschaft von Winterweizen nach Raps zeigte bei ihrer Bildung signifikante Muster, die sich durch eine höhere Präsenz von Taxa auszeichneten, die an essenziellen Prozessen der Nährstoffmineralisierung beteiligt sind und den Pflanzen Schutz vor bedeutenden Bodenpathogenen bieten. Sowohl die Anwendung von Kompost als auch von pflanzenwachstumsfördernden Rhizobakterien führte zu positiven Rückkopplungen zwischen Pflanze und Boden beim kontinuierlichen Winterweizenanbau und glich den Wachstums- und Ertragsrückgang aus. Diese Arbeit hat somit gezeigt, dass der Ertragsrückgang in aufeinanderfolgenden Winterweizen-Fruchtfolgen von mehreren wichtigen Rhizosphärenprozessen abhängt und dass das Bodenvermächtnis der Vorfrucht ein wichtiger Faktor für die Produktivität der Folgefrucht ist. Durch das Verständnis dieses Phänomens können wir resiliente, produktive und multifunktionale Anbausysteme entwickeln, die den zunehmenden Widrigkeiten des Klimawandels standhalten, ohne den Ertrag und die Ernährungssicherheit zu beeinträchtigen.

Contents

List of figures

List of tables

List of abbreviations

AOA	Ammonia-oxidizing archaea
AOB	Ammonia-oxidizing bacteria
AMO	Ammonia monooxygenase
BBCH	Biologische Bundesanstalt, Bundessortenamt und CHemical Industry decimal code system
BGU	*β*-glucosidase
BS	Bulk soil
C	Carbon
C_{mic}	Microbial biomass carbon
CO_2	Carbon dioxide
DAL	Days after labeling
DAS	Days after sowing
DOC	Dissolved organic carbon
DW	Dry weight
Fe	Iron
GLU	Glucose
Gt	*Gaeumannomyces tritici*
H	Hydrogen
K	Potassium

K_a	Catalytic efficiency
K_{CAL}	Plant-available potassium
K_m	Enzyme substrate affinity
LAP	Leucine aminopeptidase
N	Nitrogen
N_{mic}	Microbial biomass nitrogen
NH_4^+	Ammonium
N_2O	Nitrous oxide
NO_2^-	Nitrite
NO_3^-	Nitrate
O	Oxygen
OA	Organic amendments
P_{CAL}	Plant-available phosphorus
PGPR	Plant growth-promoting rhizobacteria
PSF	Plant-soil feedback
RA	Root-affected soil
R_{dia}	Average root diameter
RDW	Root dry weight
RH	Rhizosphere soil

RLD	Root length density
RMD	Root mass density
RP	Rhizoplane soil
RTD	Root tissue density
SO_4^{2-}	Sulfate
SOC	Soil organic carbon
SOM	Soil organic matter
SRL	Specific root length
TOC	Total organic carbon
Tt	Turnover time
TN	Total extractable nitrogen
V_{max}	Maximum enzymatic velocity
W1	First winter wheat after oilseed rape
W2	Second winter wheat after oilseed rape
W4	Fourth winter wheat after oilseed rape
WHC	Water holding capacity
WW	Winter wheat

1. Introduction

1.1 Rationale

Meeting the projected demand for increased agricultural production in the future will not be an easy feat. With significantly higher gross domestic product per capita by 2050, higher caloric and protein demand per capita will be needed for the different countries (Tilman et al., 2011). It is widely accepted that there is a need for enhancing crop yields while adopting new agricultural practices based on ecologically intensified and diversified (in time and space) agroecosystems (Bommarco et al., 2013). These practices will minimize the need for additional land clearing for food production, leading to sustainable farming and therefore food security (Tittonell, 2014). Uncertainties in the global winter wheat (WW, *Triticum aestivum* L.) supply chain are driving price surges and exacerbating food inequality (Zhang et al., 2022). This is particularly important given the importance of WW to global trade, as it is the most traded cereal in the world, with an estimated 25 % of the global production being exported (Erenstein et al., 2022).

WW is the most cultivated crop in the world and a staple food for billions of people worldwide, contributing significantly to many national economies (Enghiad et al., 2017; Shewry and Hey, 2015). Following a linear increase in several countries for many decades, annual WW yield growth has stagnated (Fig. 1.1), which is not due to achieving the maximum yield potential (Calderini and Slafer, 1998; Ray et al., 2013; Schauberger et al., 2018). To achieve food security by 2050, crop yields will need to increase by 2.4 % on an annual basis. For WW, the current yield growth of 0.9 % is far from what is needed to meet this demand (Ray et al., 2013). For most European countries, the year of stagnation was within the decade of 1989-1999 (Brisson et al., 2010).

There are several drivers behind these yield trends. Important agronomic drivers mainly include the increasing proportions of oilseed rape and decreasing proportions of legumes in the rotation, followed by an approximately 20 % reduction in the nitrogen (N) fertilization rate since the year 2000 (Brisson et al., 2010). The effects of climate change are also important drivers, accounting for approximately 10 % of WW yield decreases (Moore and Lobell, 2015). The higher frequency of heat stress during WW flowering is projected to be a major threat to WW yield in European farming (Semenov and Shewry, 2011). On an international level, climate change and especially hot, dry, and windy events as well as prolonged drought periods are expected to further increase the yield losses of WW (Zhao et al., 2022; Wang et al., 2024). With respect to soil organic carbon (SOC), it has been suggested that increasing SOC in agricultural soils can close nearly half of the yield gap for WW; however, the decrease in SOC due to climate change is forecasted to exacerbate WW yield losses (Reichstein et al., 2013; Crowther et al., 2016; Oldfield et al., 2019).

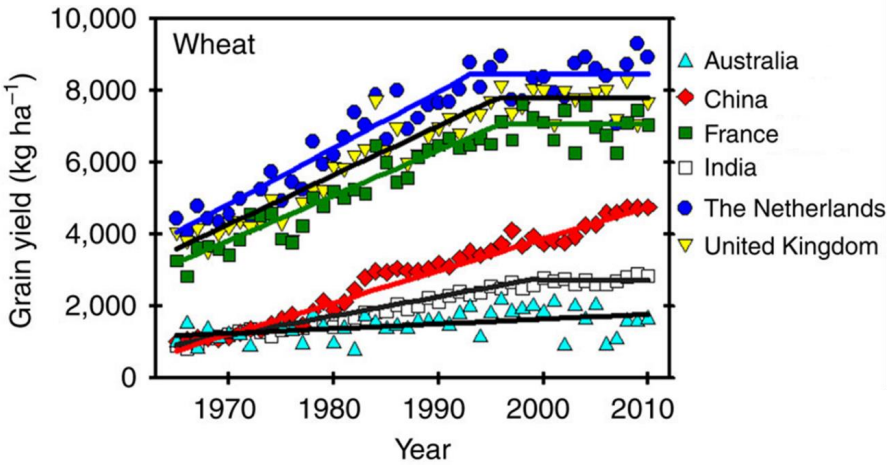

Figure 1.1 Historical grain yield trends for WW (Modified after Grassini et al., 2013).

Due to its high economic value, there is an increasing frequency of repeated WW cultivation in the same field during the rotation with only a late summer fallow as a break, ranging from 10 % at a Western European scale to 40 % at a global scale (Brisson et al., 2010; Angus et al., 2015; Yin et al., 2022). Higher proportions of WW are added in crop rotations, i.e., two or three WW crops grown before a break crop (Kwak and Weller, 2013). This, in turn, increases the risk for take-all disease (*Gaeumannomyces tritici*, Gt). Gt is the most important soil-borne fungus causing root rotting in WW plants and resulting in significant yield losses (Cook, 2003). Due to its ability to survive in a wide range of soil pH and soil moisture, it is a cosmopolitan WW pathogen (Kwak and Weller, 2013). WW self-succession has been shown to negatively affect the productivity of the subsequently grown WW (Sieling and Christen, 2015) by increasing the incidence of take-all (Smagacz et al., 2016). Exploiting the potential of rotations with increasing proportions of non-cereal crops such as oilseed rape has been shown to enhance the yield of the following WW (Angus et al., 2015; Weiser et al., 2017). When WW is grown after WW in a crop rotation, the residues of the previous crop infested with Gt are incorporated into the soil where the following WW is sown. The roots of new plants are in contact with those residues, increasing the risk of infection. For WW, more than half the root length is in contact with residues, depending on plowing depth and preceding crop (Watt et al., 2005). However, this yield decline has also been observed in years without an obvious Gt infestation (Arnhold et al., 2023a). In addition, it has been proposed that the preceding crop exerts a major influence on the rhizobiome of WW, further complicating the yield decline syndrome in successive WW rotations (Giongo et al., 2024). It is therefore imperative to research the most important drivers of the WW yield decline to improve our understanding of this complex phenomenon that is a global issue in WW cultivation and investigate potential measures to address it.

1.2 State of the art

1.2.1 The rhizosphere: a hotspot for interactions

The rhizosphere is the volume of soil that is directly affected by the roots and is estimated to range between 0.5-4 mm from the rhizoplane (RP, i.e., the root surface), which highly depends on the plant species (Kuzyakov and Razavi, 2019). It is a dynamic and heterogeneous microenvironment with intense interactions between roots, soil microbes, soil minerals, organic elements and gases (Fig. 1.2; Philippot et al., 2013; Pausch and Kuzyakov, 2018; Vetterlein et al., 2020). It is estimated that the active soil microbial biomass is 2-20 times higher in the rhizosphere than in the bulk soil (BS, Blagodatskaya et al., 2009). This high microbial biomass could contribute to the SOC pool due to rapid nutrient cycling and microbial life history strategies in the rhizosphere that promote the production of microbial necromass-related SOC (Ling et al., 2022; Wang et al., 2024). The microbial community composition in the rhizosphere is highly influenced by both abiotic and biotic factors. In addition, the plant species and genotype is a major determinant of the rhizosphere processes and soil microbial assembly in the rhizosphere (Philippot et al., 2013; Wang et al., 2018). The rhizosphere exhibits a dynamic spatial and temporal shape and the rhizosphere extent varies depending on the specific parameter, with a larger rhizosphere extent for carbon dioxide (CO_2) compared to pH (Kuzyakov and Razavi, 2019). Plants allocate freshly assimilated C belowground, which is used for root growth (biomass accumulation) and maintenance (as root respiration; Jones et al., 2009). Root exudates, sloughed root cells, mucilage and root-respired CO_2 are termed rhizodeposition and strongly modulate microbial growth and activity in the rhizosphere. The turnover time (Tt) for root exudates is very short. In contrast, mucilage, i.e., polysaccharides, turnover is much slower (Kuzyakov and Razavi, 2019). Important rhizosphere processes include water and nutrient acquisition by roots, active and passive rhizodeposition, microbial utilization of these rhizodeposits, O_2 and CO_2 consumption and release and physico-chemical processes that control the transformation of nutrients between different phases (Kuzyakov and Razavi, 2019).

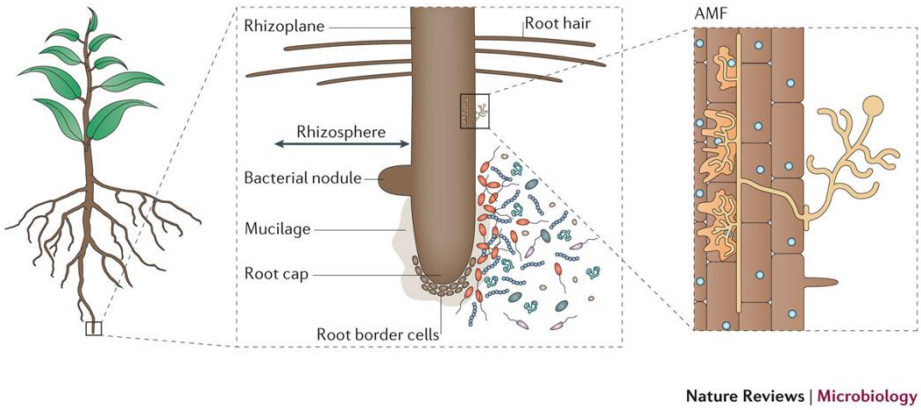

Figure 1.2 Magnified section of the root system showing the rhizosphere, soil saprophytic and symbiotic microbes, including arbuscular mycorrhizal fungi (reproduced with permission from Springer Nature; Philippot et al., 2013).

The secretion of low molecular weight organic compounds (sugars, amino acids, phenolic compounds and organic acids), stimulates the microbial activity or acts as signals for both mutualists and parasites (Hernández-Calderón et al., 2018; Mohan et al., 2020). Especially for soil pathogens, the rhizobiome is considered an important line of defense, with nutrient and microsite competition, parasitism and antibiosis being the most prominent mechanisms conferring this defense (Philippot et al., 2013). Organic acids, such as oxalic, lactic, acetic and citric acids, comprise up to 10% of the soil labile C and are known to stimulate mineral weathering and nutrient availability for plant uptake (Macias-Benitez et al., 2020). Root tips are the most important root part for exudation and the sensing module of the plant for a soil nutrient gradient thereby initiating changes in root system architecture for more effective foraging for available nutrients (Canarini et al., 2019). The release of primary metabolites (polysaccharides and proteins) to the soil due to root exudation creates hotspots for microbial growth, which stimulates soil enzymatic activity and nutrient mineralization. Soil microbes also affect root exudation and the chemical composition of root exudates through a process called “systemically induced root exudation of metabolites” (Korenblum et al., 2020). These interactions influence plant productivity by inducing changes in root system architecture and therefore nutrient and water uptake (Galloway et al., 2020).

1.2.2 Soil legacy: plant-soil feedbacks

Plants are constantly interacting with their environment and influence soil resource availability and thus, soil microbial community shape and activity. This so-called plant-soil feedback (PSF) determines plant succession, survival and growth (Bennett and Klironomos, 2019). PSFs can be positive, enhancing the growth and dominance of conspecific plants, or negative, favoring heterospecific plants and promoting coexistence in diverse plant communities. However, in monocultures, negative PSFs often result from soil pathogen accumulation, leading to yield decline

in successive WW rotations (van der Putten et al., 2013; Cortois et al., 2016). Several mechanisms have been proposed to drive PSF (Fig. 1.3). Plants affect the nutrient content of the soil through exudation, nutrient uptake, changes in the quality of their decaying litter and the recruitment of soil microbes in their rhizosphere and their associated enzymatic activity. Cellulose-degrading and protein-hydrolyzing enzymes, such as BGU and LAP, respectively, affect nutrient availability and preferentially enrich copiotrophic and deplete oligotrophic microbes in the rhizosphere, thus affecting PSFs (Razavi et al., 2016; S. Liu et al., 2022). The release of fragmented extracellular self-DNA (from decomposing plant residues, root exudates, or dead cells) originating from conspecifics makes the root system more susceptible to soil pathogens and results in negative PSF (Mazzoleni et al., 2015; Idbella et al., 2024). Nutrient depletion and production of low-quality residues (high C:N ratio) are usually associated with a negative PSF and suppress the performance of heterospecific plants. Negative PSF is mostly due to pathogen accumulation, while positive PSF are often linked to the presence of mutualistic symbionts (mainly mycorrhiza) and a favorable microbial community (de Vries et al., 2023). It has been suggested that the effects of soil biota-induced PSF can outweigh that of nutrient-induced PSF (Bennett and Klironomos, 2019). Finally, the release of phytotoxic compounds that cause either autotoxicity or allelopathy in conspecifics and heterospecifics, respectively, contributes to PSF. Plants also respond to the accumulation of soil pathogens by excreting secondary metabolites (e.g., flavonoids) into their rhizosphere, which induces systemic resistance and is often associated with a plant fitness cost (Heil, 2002; Vlot et al., 2020; Pang et al., 2021).

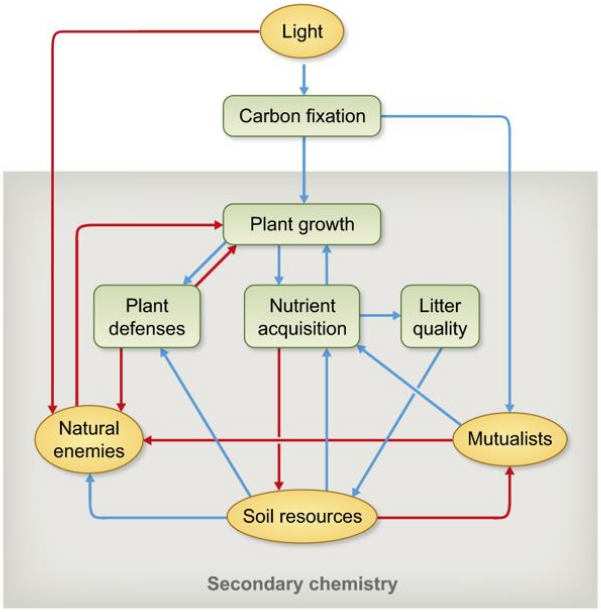

Figure 1.3 Mechanisms underlying plant-soil feedbacks. Blue arrows indicate positive relationships; red arrows indicate negative relationships (reproduced from Bennett and Klironomos, 2019).

Preceding crops influence the microbial communities in the rhizosphere of WW, possibly by controlling the quantity and quality of the secreted exudates, leading to changes in the relative abundance of certain taxa (Hilton et al., 2018; Babin et al., 2019; Jones et al., 2019; Wen et al., 2022). Oilseed rape is known to recruit microbial taxa that enhance the growth of the following WW (Vujanovic et al., 2012). This might be linked to the control that the preceding crops exert over root exudate profiles, soil nutrient dynamics and finally bacterial and fungal abundance (Town et al., 2023; Wang et al., 2023). Sun et al. (2024) showed that increasing crop diversity was associated with a higher microbial network complexity with a more diverse ecological functioning. This effect of the preceding crop can in turn influence root system architecture, including axial and lateral root length, width and convex hull area, holding important implications for root adaptations under biotic and abiotic stresses and root foraging for nutrients (Freschet et al., 2021; Cope et al., 2024). Rhizosphere N cycling is especially important for PSFs, since it controls N availability to roots and microbes and can be greatly affected by the preceding crop (Wang et al., 2023). N cycling in the rhizosphere, quantified as the abundance of N-fixing, nitrifying, and denitrifying genes, determines soil N mineralization, transformation and availability for plant and microbial uptake (Thion et al., 2016; Liao et al., 2024).

1.2.3 Employing isotopes to study plant-soil interactions

Isotopes have the same number of protons but a different number of neutrons and therefore different masses. This results in different physical properties such as reaction kinetics that cause fractionation events. The different isotopologues of carbon (C), N, hydrogen (H) and oxygen (O) are frequently used to assess C flow (^{13}C, ^{14}C), nutrient cycling (^{15}N, ^{33}P) as well as water flow and transport (^{18}O, ^{2}H; He et al., 2009; Brüggemann et al., 2011; Stumpp et al., 2018).

H and O isotopes are informative tracers and indicators of root water uptake dynamics. With the use of water isotopes, the contribution of different water sources to plant water uptake can be quantified (Penna et al., 2020). The soil legacy of the preceding crop exerts control over the root shape and growth and could therefore influence water uptake patterns for the following plant. Combining $^{2}H/^{18}O$ with ^{15}N labeling has been proven an insightful approach for studying water and N uptake from different soil layers (Chen et al., 2021). This makes them very promising for studying PSF in WW rotations.

The ^{13}C stable isotopic composition of CO_2 has been extensively used to study C cycling. Due to fractionation events associated with C fixation and turnover in the different plant parts and also in the soil (CO_2 diffusion, carboxylation, photorespiration and dark respiration), tracing the ratio of CO_2 isotopologues can provide useful information about the source (isotopic signature) and C allocation and therefore the atmosphere-plant-soil interactions (Brüggemann et al., 2011). ^{13}C pulse labeling allows assessing root exudation quantity and quality (compound-specific composition) and allows distinguishing the root-derived ^{13}C from native SOC. It is a useful approach to investigate C allocation across the soil profile and within the different plant organs (Bahn et al., 2013) and is greatly influenced by root system architectures and plant developmental stage (Sun et al., 2019). The fate of fresh assimilates and their incorporation into microbial biomass is an important feature of ^{13}C pulse labeling. Multiple pulses can be implemented across different plant growth stages to obtain root-derived C input to the soil in high temporal resolution.

1.2.4 Green waste compost amendment in the soil to improve wheat productivity

According to the Council Directive 1999/31/EC, the European Countries aim to decrease the percentage of organic waste going to landfills by 50% by 2050. At the same time, the Sustainable Development Goals set by the United Nations in 2015 aim to address 17 important challenges by 2030 (Hettiarachchi et al., 2020). These policies and the increase in green urban planning favor the recycling of green waste, which is a sustainable, abundant (150 kg of green waste per person per year in Europe) and renewable resource (Sæbø and Ferrini, 2006; Viretto et al., 2021). At the same time, 2.46 Mg of soil ha^{-1} $year^{-1}$ are eroded in the EU with increasing degradation in a global setting (Borrelli et al., 2017; Panagos and Borrelli, 2017). It is therefore necessary to explore the potential of compost as an agricultural input to improve plant growth, soil quality and farmer's income and promote the transition to a circular economy.

Green waste compost is the result of the aerobic digestion of plant residues and/or plant cuttings after pruning. The final product is nutrient-dense and can be applied as a soil amendment to support soil structure and/or supply nutrients for plant growth. The composition of green waste compost can vary and include the slow decomposing lignin and the moderately decomposing hemicellulose and cellulose. Its composition is highly dependent on the plant species used as a composting source and the plant developmental stage among others (Reyes-Torres et al., 2018). Usually compost has a high SOC content, plant-available N, phosphorus (P_{CAL}) and potassium (K_{CAL}, Nobile et al., 2022; Siedt et al., 2021). The organic C of the compost acts as a binding agent, increasing soil aggregation, and also provides easily degradable C for microbial uptake, preventing mining of native soil organic matter (SOM), which is termed negative priming (Dijkstra et al., 2013; Siedt et al., 2021; Wang et al., 2022). Compost application at deeper soil layers also improves water retention and uptake by the plants (Uhlig et al., 2023; Feifel et al., 2024).

Being a nutrient-rich organic amendment (OA), compost can be considered a suitable candidate to address the yield decline in successive WW rotations. Given that the WW residues are usually of lower quality (C:N of 50-100) than green waste compost, it can be expected that a transient N immobilization by soil microbes early in the season causes a growth delay of the succeeding WW (Reichel et al., 2018). The mineralization of oilseed rape residues with a lower C:N than WW will not create N immobilization conditions in the soil and promote a better early establishment for the succeeding WW. However, the plant demand during this early growth is relatively small (up to 30 kg ha^{-1}; Sieling et al., 1999), so it is not clear whether distinct soil legacies in terms of residual mineral N influence the growth of WW during early growth. In contrast, it could be expected that, by matching the microbial stoichiometric C:N:P demand, the compost enriches the rhizosphere with copiotrophic microorganisms that exhibit a high enzymatic activity and increase nutrient availability in the soil, which further restores plant productivity. For successive WW rotations, this could mean that compost application could compensate for growth reduction and yield decline. The supply of additional macro- and micronutrients by compost application can create a nutritional benefit and thereby a positive PSF for successively grown WW. In addition, Tilston et al. (2005) showed that application of green waste compost reduced the incidence of Gt severity and yield losses of WW, demonstrating the multiple benefits arising from application of OA in crop rotations.

1.2.5 Inoculation with plant growth-promoting rhizobacteria to improve wheat productivity

Plant-microbe interactions are important drivers of plant productivity, influencing key rhizosphere processes. This knowledge has stimulated a relatively new field of research, which assesses the potential of beneficial bacteria to promote plant growth under various biotic and abiotic stresses. This has led to an extremely high growth rate of the biostimulants market with an estimated market size of USD 5.6 billion by the end of 2025 and an annual compound annual growth rate of 13.58% (Landeta and Marchant, 2022).

Plant growth-promoting rhizobacteria (PGPR) employ several direct and indirect mechanisms to confer plant growth promotion. Some rhizobacteria can enhance nutrient availability and uptake by solubilizing potassium (K), phosphate and iron (Fe) from inorganic and organic sources. Siderophores, e.g., pyoverdine, pyochelin, azotobactin, salicylic acid, and pseudomonine, organic acids, H_2S and exopolysaccharides production drive inorganic P solubilization, while various enzymes facilitate organic nutrient solubilization (Verma et al., 2011; Scavino and Pedraza, 2013; Raymond et al., 2021). PGPR also interfere with plant hormonal homeostasis, for example, through the production of cytokinins, gibberellins and indolyl-3-acetic acid (Ma et al., 2009; Sokolova et al., 2011; Flores-Félix et al., 2015). These changes modulate changes in root system architecture, rhizosphere size, and therefore nutrient uptake by the plants (Nacry et al., 2005; Khoso et al., 2024). By increasing important root foraging traits like root surface area, primary root elongation, lateral root development, exudation and branching, they can improve the nutrient uptake capacity of the plant (Brazelton et al., 2008; Vacheron et al., 2013). They are directly involved in disease suppression through niche exclusion and competition against soil pathogens in the rhizosphere (Beneduzi et al., 2012; Mariutto and Ongena, 2015). Studies have also highlighted the importance of biofilm formation in the RP and the stimulation of induced systemic resistance with jasmonic acid or salicylic acid of plants, effectively decreasing the disease incidence in the aboveground part of the plant (Pieterse et al., 2003; Danhorn and Fuqua, 2007; Beneduzi et al., 2012; Khoso et al., 2024).

The effects of PGPR vary depending on the specific isolate that is applied, the experimental conditions, mode of application, inoculum concentration, compatibility with the plant host, and plant growth medium (De Zutter et al., 2022; Khoso et al., 2024). The outcome of the interaction between a particular strain and the soil microbial community in field experiments can be challenging to predict due to the presence of competitive, mutualistic, and neutral relationships among microbes, although a recent meta-analysis suggested that the effects of beneficial rhizobacteria are equally observed in field and greenhouse studies (De Zutter et al., 2022). The plethora of research on PGPR application renders it a promising practice for the mitigation of reduced productivity in successive WW rotations.

Root exudation (mainly glucose; GLU) provides labile C to the rhizosphere, which is used as an energy source by soil microbes and can stimulate the activity of PGPR, which could manifest as enhanced enzymatic production leading to nutrient availability and uptake by WW (Mäder et al., 2011). In addition, a soil microbial dysbiosis has been observed by Wu et al. (2018) in WW monocropping. Plants actively try to overcome this microbial dysbiosis over the years by altering their root exudation profile, which acts as a “cry-for-help” signal to recruit beneficial microbes and combat the pathogens or herbivores, and this effect is thought to persist in the soil (Rolfe et al., 2019). Whether the external application of beneficial microorganisms can increase the disease suppressiveness of successive WW soils remains to be studied.

1.3 Experimental approach

In order to observe the yield decline in successive WW rotations, field studies are the most reliable experimental approach. However, field studies are often associated with certain technical limitations, especially with respect to access to deeper soil layers. Due to its complex spatial distribution and the dynamic interactions between microbes, nutrients and roots, the rhizosphere is very difficult to study (Moran and McGrath, 2021). Therefore, mesocosms and rhizotrons are useful tools to study plant-soil interactions when the rhizosphere is at the core of the experiment.

This thesis capitalized on recent technical and scientific innovations to study the rhizosphere processes in successive WW rotations. The rhizotrons used in the experiments of this thesis have been developed at Forschungszentrum Jülich, IBG-3, and are described in detail in Reichel et al. (2022). They are suitable for root digital imaging, soil sampling from the bulk, root-affected (RA) and rhizosphere (RH) soil compartment, and facilitate online isotopic measurements. They are also non-restrictive for plant growth with dimensions of 2.5 cm × 35 cm × 100 cm (W × L × H), resulting in 8750 cm^3 volume. On the front and backside of the rhizotrons, several hundreds of holes (8 mm ⌀) have been made to allow for soil sampling. Self-adhesive transparent sheet is placed on the inside of the rhizotrons. Side holes enable the installation of gas-permeable tubing at different depths for online isotopic applications. The rhizotrons are also suitable for the application of novel in situ imaging of soil enzymes and GLU using optodes (Vandooren et al., 2013; Razavi et al., 2016; Hoang et al., 2022). The rhizotrons used in *Chapter* 6 were further optimized to control soil temperature and to achieve a relatively realistic soil temperature profile along the rhizotron by connecting it to an external cooling unit using insulated tubing. As an additional passive insulation step, the rhizotrons were fitted into a polystyrene case to minimize heat exchange with the environment. More information on the rhizotrons is shown in *Chapter* 2, *Chapter* 3, *Chapter* 4 and *Chapter* 6. Custom-made cylindrical polyvinyl chloride (PVC) sewage pipe mesocosms (135 cm height, 10.5 cm ⌀) with a perforated PVC sleeve at the bottom for drainage of seepage water, and perforated opposite sides for minimally destructive soil sampling were used in *Chapter* 5. The mesocosms were placed inside the empty space of a lysimeter pit and insulated against ambient weather conditions using polystyrene layers. A detailed description of this system is described in *Chapter* 5. In order to quantify the belowground C allocation in real time, we designed an automatic manifold system, based on Rothfuss et al. (2015), for sampling CO_2 and water vapor at different soil depths of the rhizotrons. Gas-permeable tubing was installed at six soil layers in the rhizotrons. Dry synthetic air was directed to the isotope-specific analyzers through the gas-permeable tubing after ^{13}C pulse labeling, and the $\delta^{13}C$ of the soil respired CO_2 was recorded, providing information on root derived C over a period of several weeks. A detailed overview of the manifold system is presented in *Chapter* 3.

1.4 Objectives, hypotheses and outline of this thesis

The yield decline in successive WW rotations has been extensively reported in the past and is most commonly attributed to the accumulation of certain soil pathogens, mostly Gt. However, the

mechanisms underlying this decline and the soil legacy of contrasting WW rotations have not been adequately described. The overall objective of this thesis was to understand how the soil legacy of different rotational positions of WW drives PSFs and the performance of the succeeding WW and how we can use this knowledge to adopt management practices that aim to mitigate this yield decline. The research questions and hypotheses of this thesis were as follows:

1. How does the rotational position of WW affect the early growth of WW and specifically the soil nutrient availability, root growth, bacterial and archaeal community composition, their associated enzymatic activity and GLU release in the bulk and RH? (*Chapter 2*)

We hypothesized that there would be reduced rhizodeposition in self-successional WW, resulting in distinct changes in the microbial community composition and reduced production of hydrolytic enzymes. The reduced rhizodeposition in self-successional WW would be followed by changes in the microbial community composition and a decreased microbial activity, influencing nutrient (especially mineral N) uptake by the plant and plant biomass.

2. i) How does the rotational position of WW affect the soil microbial activity and specifically the activity of C and N acquiring enzymes, and consequently WW growth and productivity; and ii) how does the rotational position of WW affect the abundance of the bacteria and archaea and N-related genes? (*Chapter 3*)

We hypothesized that the rotational position of WW would affect the bacterial and archaeal community, leading to distinct changes in the bacterial and archaeal community composition. Soil microbial activity would be affected by the WW rotational position, resulting in differences in N cycling and uptake by the following WW and ultimately influence crop growth and yield.

3. How do contrasting rotational positions of WW influence the allocation of freshly assimilated C in above- and belowground plant parts and its subsequent translocation to the rhizosphere of WW? (*Chapter 4*)

We hypothesized that the negative soil legacy of successive WW rotations with a lower residual mineral N will: i) reduce plant and root growth, which will lead to a limited assimilate supply to the root system and the associated microorganisms; and ii) the reduction in root growth will be coupled with a decrease in the storage of freshly assimilated C in aboveground plant parts and especially sink organs (grains).

4. i) Can the application of green-waste compost compensate for yield losses in successive WW rotations; and ii) how does the application of green-waste compost affect soil above- and belowground C allocation patterns, plant N and water uptake in contrasting WW rotations? (*Chapter 5*)

We hypothesized that the negative soil legacy of successive WW rotations with a lower residual mineral N will: i) reduce C allocation above- and belowground in the successive WW rotation

following a reduction in root growth; ii) compost application would increase C allocation above- and belowground, which would stimulate soil microbial activity by enhancing C and N cycling enzymes, and iii) this would promote root growth, followed by increased N uptake, enhanced subsoil water uptake and finally a higher yield.

5. How does the inoculation of WW with the plant growth promoting rhizobacterium *Bacillus pumilus* affect the productivity of successive and non-successive WW rotations? (*Chapter 6*)

We hypothesized that *Bacillus pumilus* inoculation would alleviate the negative PSF of successively grown WW.

Chapter 7 provides a synthesis of the conducted experiments, seeks to link their findings to an in-depth view of the yield decline syndrome in successive WW rotations, and suggests potential management practices to compensate for these yield losses.

This thesis has strived to acquire and link fundamental knowledge on PSFs in contrasting WW rotations and, based on this knowledge, to test mitigation practices that can be applied by farmers worldwide, who are facing increasingly higher yield variability, largely due to climatic conditions and global socio-economic uncertainties, as well as an increased need for a more efficient natural resource management in favor of crop yields, economic stability and environmental protection.

2. Preceding crop legacy modulates the early growth of winter wheat by influencing root growth dynamics, rhizosphere processes, and microbial interactions

---

Based on:
Kaloterakis, N., Rashtbari, M., Razavi, B.S., Braun-Kiewnick, A., Giongo, A., Smalla, K., Kummer, C., Kummer, S., Reichel, R., Brüggemann, N., 2024. Preceding crop legacy modulates the early growth of winter wheat by influencing root growth dynamics, rhizosphere processes, and microbial interactions. *Soil Biology and Biochemistry* 191, 109343. https://doi.org/10.1016/j.soilbio.2024.109343

2.1 Introduction

Due to its high economic importance, higher proportions of WW are added to crop rotations by growing two or more WW crops after a break crop (Kwak and Weller, 2013). The positive effects of adding non-cereal break crops to the rotation have been well established. On a global scale, up to 40 % of the cultivated wheat is grown successively, with only a late summer fallow as a break (Angus et al., 2015; Yin et al., 2022). However, growing WW successively in the same field increases the risk of soil-borne infections, such as the take-all dis- ease caused by Gt, which is the most important soil-borne fungal pathogen of WW, causing root rotting and significant yield losses (Cook, 2003; Kwak and Weller, 2013). Plant yield is negatively affected by the self-succession of wheat in the same field (Sieling and Christen, 2015) due to the increased incidence of (Smagacz et al., 2016). The take-all disease persists in wet and dry conditions and can cause a yield decline of up to 50 % (Palma-Guerrero et al., 2021). However, it has been recently demonstrated that the yield reduction is evident in a dry year with no obvious Gt infection (Arnhold et al., 2023a). Adding non-cereal break crops to the rotation, such as oilseed rape, has been shown to enhance the yield of the following WW (Angus et al., 2015; Weiser et al., 2017). Nevertheless, the complex interactions between pre-crop plants and microorganisms in the rhizosphere remain unclear.

WW allocates 20–30 % of the assimilated C belowground through the root (Kuzyakov and Domanski, 2000), known as rhizodeposition. Rhizodeposition shapes a dynamic and heterogeneous micro- environment in the rhizosphere, which is estimated to extend between 0.5 mm and 4 mm for different plant species (Kuzyakov and Razavi, 2019) and to be governed by mutualistic, parasitic, and neutral interactions between roots and soil microorganisms (Pausch and Kuzyakov, 2018). Root exudates are a highly influential pool of organic compounds with a low molecular weight, referred to as rhizodeposits, which are secreted into the rhizosphere. They provide a nutrient source for soil microbes, stimulating their activity, but also acting as signals for both mutualists and parasites, with consequences for plant health (Hernández-Calderón et al., 2018; Mohan et al., 2020). The efflux of primary metabolites to the soil due to root exudation creates a plant C source, which fuels microbial growth and nutrient mineralization, affecting plant performance and health. Soil microbes, in turn, influence root exudation by producing extracellular enzymes and polymeric sub- stances (Costa et al., 2018; Korenblum et al., 2020). Both processes require significant amounts of energy and are therefore an investment from both the plant and microbial sides to stimulate their nutrient acquisition as well as proliferation in the soil (Costa et al., 2018; Canarini et al., 2019). For plants, this can be exhibited as the stimulation of root growth. Plants also excrete secondary metabolites (e.g., flavonoids) into their rhizosphere in response to biotic stress and herbivores to induce systemic resistance (ISR; Pang et al., 2021; Vlot et al., 2020). Labile SOM and N mineralization following enhanced enzymatic activity (e.g., protein and cellulose-degrading enzymes) are thus mediated by root exudation and indirectly increase plant nutrient uptake (Meier et al., 2017). These interactions can induce changes in the root system architecture and, in turn, influence nutrient and water uptake (Galloway et al., 2020).

WW shapes its rhizosphere microbial community through rhizodeposition (Wen et al., 2022), enhancing nutrient uptake and plant performance. In particular, oilseed rape and legumes

as preceding crops have been associated with the selection of beneficial microbial taxa, and the suppression of pathogenic microbial taxa, in WW (Vujanovic et al., 2012). This is mainly due to differences in the residue quality that affect its decomposition process (Kerdraon et al., 2019). WW residues mainly contain cellulose and have a higher lignin content than oilseed rape, decelerating their decomposition rate (Pascault et al., 2010). In addition to the soil legacy effect of the residues of the preceding crop, GLU release in the rhizosphere of the growing WW, which is affected by root growth and functioning, can shape microbial communities and therefore affect the productivity of WW (Qi et al., 2022). GLU is the most abundant monosaccharide in the root exudates of WW (Yahya et al., 2021) and is a readily available C source for the soil microbiome. As such, it can fuel both mutualistic, competitive, and pathogenic interactions between soil microorganisms and plants that might affect plant productivity (Philippot et al., 2013). Besides root pathogens that can directly affect plant health, such as Gt, the prevalence of other detrimental microorganisms in the rhizosphere can compete with roots for available nutrients (Kuzyakov and Xu, 2013). This leads to reduced root growth and exudation, which further increases the C cost for the soil microbial community, creating negative plant–soil feedback (Cortois et al., 2016; Bennett and Klironomos, 2019). Diversified WW rotations with oilseed rape as a preceding crop are known to increase WW yield compared to successively grown WW (Kirkegaard et al., 2008; Ramanauskienė et al., 2018). Most studies show a positive effect on WW pathogen suppression, soil structure, and a high residual N content after oilseed rape harvest (Sieling and Christen, 2015; Weiser et al., 2017; Hilton et al., 2018), although these positive effects have not always been consistently observed (Arnhold et al., 2023b).

Our study aimed to investigate the underlying mechanisms that govern the productivity of WW grown in self-succession as opposed to WW grown after a break crop, such as oilseed rape. Specifically, we focused on the quantification of root growth parameters and the associated biochemical parameters (C and N translocation) as well as on the microbial (bacterial and archaeal) compositions in the rhizosphere (RH) and bulk (BS) soil of WW grown in different rotational positions. We hypothesized that there would be reduced rhizodeposition in self- successional WW, resulting in distinct changes in the microbial community composition and reduced production of hydrolytic enzymes. This would result in a decreased microbial activity, influencing nutrient (especially mineral N) uptake by the plant and biomass production.

To test these hypotheses, an outdoor rhizotron experiment was conducted, contrasting three rotational positions of WW. We combined zymography and GLU imaging on WW at the onset of stem elongation to observe changes in the activity of two important C- and N- acquiring enzymes, β-glucosidase (BGU), and leucine aminopeptidase (LAP) as well as GLU release in its rhizosphere. We also combined soil biochemical and microbiome analyses to assess nutrient and C availability as well as microbial community composition in the rhizosphere of WW and to understand the mechanisms underlying WW performance in those rotational positions.

2.2 Materials and Methods

2.2.1 Experimental design

The soil was collected in September 2021 from the experimental farm Hohenschulen, Faculty of Agricultural and Nutritional Sciences, Kiel University, 54°19′05″N, 9°58′38″E, Germany. The crop rotation trial was established in 1989. It included the following factors: a) rotational position (oilseed rape, first wheat after oilseed rape, third wheat grown continuously), b) WW varieties (4 levels), and c) N fertilization levels (4 levels). Composite soil samples for rhizobox experiments were taken from oilseed rape (WW grown in this soil is termed W1), first wheat plots (WW grown in this soil is termed W2), and third wheat plots (WW grown in this soil is termed W4) (n = 12 replications) containing the WW cultivar "Nordkap" (SAATEN-UNION GmbH, Isernhagen, Germany) and optimal N fertilization (240 kg N ha^{-1}). Soil was collected from the topsoil (0–30 cm) and subsoil (30–50 cm) and sieved to 2 mm. The residues of the preceding crop were not removed from the soil before sampling, and the field was ploughed after sampling. The crop rotations are referred to as rotational positions hereinafter. After the harvest of the different preceding crops, the plant residues remained on the field. The soil is a Cambic Luvisol of sandy loam texture (44 % sand, 35 % silt, and 21 % clay; (Sieling, 2005). The lack of effervescence in our soil samples after adding 10 % HCl indicated the absence of carbonates, which was confirmed by an average $\delta^{13}C$ value of -26.92 ‰ of soil samples analyzed before the start of the experiment. Table 2.1 shows some important initial soil biochemical parameters specific to the three rotational positions.

We conducted an outdoor rhizotron experiment (May 4, 2022 to June 30, 2022) using newly designed rhizotrons with a height of 100 cm, a width of 35 cm, and an inner thickness of 2.5 cm (Reichel et al., 2022). Each rhizotron was wrapped in a 50-mm-thick, aluminum-coated Rockwool foil to reduce soil temperature fluctuations inside the rhizotron. Bulk density was adjusted to 1.35 g cm^{-3} and deionized water was added to adjust soil moisture to 70 % water-holding capacity (215 g H_2O soil kg^{-1}) at $_{the}$ onset of the experiment. The plants were subsequently rain-fed throughout the experiment. The rhizotrons were placed on the campus of Forschungszentrum Jülich, Germany. All rhizotrons were consistently inclined at 45^{o} to facilitate root growth along the lower side of the rhizotrons. WW seeds (cultivar "Nordkap") were germinated on petri dishes with sterile filter paper for 24 h in the dark at 23 °C. One germinated seed was subsequently sown into each rhizotron. The plants were not fertilized for the duration of the experiment. The plants were harvested at the stem elongation stage Zadoks growth stages 30 (Zadoks et al. 1974); hereafter termed "BBCH" from the Biologische Bundesanstalt für Land- und Forstwirtschaft, Bundessortenamt und CHemische Industrie decimal code system).

Table 2.1 Initial rotational position (Rot_pos) specific soil NO_3^-, NH_4^+, plant-available P_{CAL}, K_{CAL}, sulfate (SO_4^{2-}), magnesium (Mg), C:N ratio, pH, dissolved organic C (DOC), microbial biomass carbon (C_{mic}), microbial biomass nitrogen (N_{mic}) and C_{mic}:N_{mic}. Data are mean ± S.E. (n = 9). Different lowercase letters in each column denote significant differences between the rotational positions at p value ≤ 0.05 using Bonferroni correction for multiple comparisons. ANOVA main effects of rotational position are indicated as follows: ns= not significant; * $p \leq 0.05$; ** $p \leq 0.01$; *** $p \leq 0.001$.

Rot_pos	NO_3^-	NH_4^+	P_{CAL}	K_{CAL}
	mg N kg^{-1}		mg kg^{-1}	
W1	3.89 ± 0.03a	0.11 ± 0.01	19.3 ± 0.1a	51.3 ± 0.8a
W2	3.38 ± 0.11b	0.14 ± 0.02	16.1 ± 0.2b	27.8 ± 0.7c
W4	3.09 ± 0.00b	0.18 ± 0.03	18.4 ± 1.0ab	35.4 ± 0.2b
ANOVA	***	ns	*	***
Rot_pos	SO_4^{2-}	Mg	soil C:N	pH
	mg kg^{-1}			
W1	5.3 ± 0.3a	75.2 ± 1.7	9.74 ± 0.02	6.73 ± 0.003
W2	3.5 ± 0.2b	76.8 ± 1.4	9.63 ± 0.03	6.76 ± 0.009
W4	2.9 ± 0.0b	84.6 ± 3.0	9.68 ± 0.08	6.75 ± 0.008
ANOVA	***	ns	ns	ns
Rot_pos	DOC	C_{mic}	N_{mic}	C_{mic}:N_{mic}
	mg kg^{-1}		mg kg^{-1}	
W1	29.5 ± 0.3a	57.0 ± 2.0b	8.2 ± 0.2a	7.0 ± 0.3b
W2	22.6 ± 0.7b	41.2 ± 3.4c	4.3 ± 0.5b	9.6 ± 0.3a
W4	29.0 ± 0.2a	75.3 ± 1.2a	9.3 ± 0.2a	8.1 ± 0.3b
ANOVA	***	***	***	**

2.2.2 Above and belowground plant growth analyses

The aerial plant parts were split at harvest into pseudostems (hereinafter referred to as stems) and leaves. The lower sides of the rhizotrons were then removed, and images of the root system along the soil profile were taken with a camera (DSLR Nikon D3500 Kit AF-P VR 18–55 mm, Nikon Corp., Tokyo, Japan). The soil profile was then divided into three layers (0–30 cm, 30–60 cm, and 60–100 cm), and soil samples were taken from two soil compartments, i.e. RH sampled with microspatulas from ≤5 mm away from the rhizosphere of primary roots and root-free BS. We pooled and mixed subsamples to form a composite sample, and then split it into several parts to ensure sufficient soil was collected for every planned analysis. For analysis of microbial biomass C and N (C_{mic} and N_{mic}), we sampled RA soil from a distance between 5 mm and 20 mm away from the RP of primary roots. This measure was taken to ensure that a sufficient amount of soil (20 g per sample) was sampled to be used for this specific analysis. The roots were then retrieved

after washing off the soil through a 1 mm sieve and stored in 30 % ethanol. They were scanned at 600 dpi (Epson Perfection V800 Photo, Epson, Japan) and analyzed with WinRhizo® software (Regent Instruments Inc., Quebec, Canada) for the following root growth traits: root length, average root diameter (R_{dia}), root surface area, and root volume. The roots were split into seven diameter classes: 0–0.05 mm, 0.05–0.1 mm, 0.1–0.5 mm, 0.5–1 mm, 1–1.5 mm, 1.5–2 mm, and ≥2 mm. Using these root growth traits, we computed the root length density (RLD), the specific root length (SRL), and the proportion of root length for the seven root diameter classes. Estimates of root tissue density (RTD) were made as described in Rose (2017). All plant materials were oven-dried at 60 °C to constant weight (maximum three days) to record their dry weight (DW). Ball-milled (MM 400, Retsch, Germany) above- and belowground plant samples, as well as soil samples, were weighed into tin capsules (HEKAtech, Wegberg, Germany) to determine the C and N content using an elemental analyzer coupled to an isotope-ratio mass spectrometer (EA-IRMS, Flash EA, 2000, coupled to Delta V Plus; Thermo Fisher Scientific Inc., Waltham, MA, USA).

2.2.2 Biochemical soil analyses

At harvest, soil samples were stored at -25 °C before analysis of mineral N, dissolved organic carbon (DOC), and total extractable nitrogen (TN). For the analysis, they were thawed and extracted using 0.01 M $CaCl_2$ (soil-to-solution ratio of 1:4 w/v), vortexed, shaken horizontally for 2 h at 200 rpm, centrifuged for 15 min at 690×g, and filtered through 0.45 µm PP-membrane filters (Ø 25 mm; DISSOLUTION ACCESSORIES, ProSense B.V., Munich, Germany). Soil solution was stored overnight at 4 ◦C before DOC and TN analysis. Ammonium (NH_4^+) was measured by continuous-flow analysis (Flowsys, Alliance Instruments GmbH, Freilassing, Germany). Nitrate (NO_3^-) and sulfate (SO_4^{2-}) were measured by ion chromatography (Metrohm 850 Professional IC Anion – MCS, Metrohm AG, Herisau, Switzerland). Mg was measured by inductively coupled plasma optical emission spectroscopy (iCAP 6500; Thermo Fisher Scientific Inc., Waltham, MA, USA). The pH was measured in the same solution using a glass pH electrode (SenTix® 940, WTW, Xylem Analytics, Weilheim, Germany). DOC and TN were quantified with a total organic C (TOC) analyzer (TOC-V + ASI-V + TNM, Shimadzu, Japan). Using 0.01 M calcium acetate lactate (CAL) instead of $CaCl_2$ and following the same extraction protocol, the P_{CAL} and K_{CAL} were measured with inductively coupled plasma optical emission spectroscopy (ICP- OES, iCAP 6500; Thermo Fisher Scientific Inc., Waltham, MA, USA).

The chloroform-fumigation extraction (CFE) method was used to estimate C_{mic} and N_{mic}. Ten grams of fresh soil stored at 4 °C were weighed in beakers and placed inside a desiccator. They were incubated with ethanol-free chloroform (80 mL) at room temperature for 24 h. Soil samples were then extracted with 0.01 M $CaCl_2$ and analyzed with a TOC analyzer, as described previously. Non-fumigated soil samples were extracted using the same protocol. The difference between extracted C and N from fumigated and non-fumigated soil samples was used to calculate C_{mic} and N_{mic}, using the correction factors 0.45 and 0.4 as the extractable parts of C_{mic} (kEC) and N_{mic} (kEN), respectively (Wu et al., 1990; Joergensen, 1996).

2.2.3 Glucose imaging

Soil GLU imaging was applied to all rhizoboxes according to Hoang et al. (2022). Accordingly, phosphate powder (Sigma P7994) was dissolved in distilled water to make a 100 mL buffer solution with a concentration of 0.05 M (pH 7.4). Added to the solution were 1.7 unit/ml GLU oxidase from *Aspergillus niger* (Sigma G7141), 1.5 unit/ml peroxidase from horseradish (Sigma P8125), and 200 µM Ampliflu red (Sigma 90,101, Sigma-Aldrich, Darmstadt, Germany) dissolved in 60 µL dimethylsulfoxide. Installed rhizotrons were gently removed to avoid cutting roots. Polyamide membrane filters (pore size 0.45 mm – Tao Yuan, China) were cut into 10 × 20 cm strips. These membranes were saturated with the prepared reaction mixture solution before being attached to the rooted area. After 20 min of incubation (an optimal incubation time was tested in advance; time may differ between plant species (Hoang et al., 2022), membranes were quickly removed, placed in a dark container, and immediately transferred to the dark room under UV light with a wavelength of 355 nm. The magenta-colored area on the membrane indicated GLU exudation as hydrogen peroxide generated from a reaction between GLU and GLU oxidase enzymes, which was catalyzed by horseradish peroxidase to convert colorless Ampliflu red into magenta-colored resorufin (Zhou et al., 1997).

2.2.4 Zymography

Zymography (BGU and LAP activity) was performed according to the protocol developed by Razavi et al. (2019). A 4-methylumbellifer- yl-β-glucoside (MUF-β) and L-leucine-7-amino-4-methylcoumarin hydrochloride (AMC-L) (Sigma Aldrich, Germany) solutions were prepared in MES buffer ($C_6H_{13}NO_4SNa_{0.5}$, Sigma-Aldrich, Darmstadt, Germany) and TRIZMA ($C_4H_{11}NO_3 \cdot HCl$, $C_4H_{11}NO_3$, Sigma-Aldrich, Darmstadt, Germany), respectively, to make a fluorescent solution of 12 mM. The same polyamide membrane filters (Tao Yuan, China) with a pore size of 0.45 mm were selected to reduce enzyme diffusion through the pores (Razavi et al., 2016). The membranes were soaked in the fluorescent solution and then directly applied to the root-exposed side of the rhizoboxes before being subsequently covered with aluminum foil to avoid exposure to light and drying out. After 1 h of incubation, the membranes were quickly removed, cleaned with a soft brush, and exposed to UV light with an excitation wavelength of 355 nm in a dark room.

All images were taken with a digital camera (Canon EOS 6D, Canon Inc.) and a Canon lens EF 24–105 mm 1: 4 L IS II USM with the setting of aperture and shutter speed at f/5.6 and 1/10 s (for GLU imaging) and 1/8 s (for zymography), respectively. The calibration lines for GLU imaging were prepared by soaking a 4 cm^2 membrane in a GLU solution at respective concentrations of 0 mM, 2 mM, 4 mM, 6 mM, 8 mM, and 10 mM. The membranes were soaked in the respective reaction mixture solution in the same way as mentioned above. Fluorescent signals of GLU release on an area basis were calculated based on the volume of substrate solution taken up by a fixed membrane size.

Zymography processing was calibrated by soaking individual 4 cm^2 membranes in MUF solution at respective concentrations of 0 mM, 0.2 mM, 0.5 mM, 1 mM, 2 mM, 4 mM, 6 mM, 8 mM, and 10 mM. These membranes were exposed to UV light in the same way as the samples.

Calibrated values were used to quantify the color intensity and to link BGU activity to the grey value. Fluorescent signals of MUF on an area basis were calculated based on the volume of substrate solution taken up by a fixed membrane size.

The image processing and analysis were conducted using the software package ImageJ. The hotspot percentage was calculated based on the pixel size proportion of the hot area to the entire image. In other words, hotspot areas were determined to have the 25 % higher pixel- wise enzyme activities after subtracting background values at zero concentration of the calibration line from all zymograms and GLU release images (Ma et al., 2018). Meanwhile, the rhizosphere extent of each root was calculated from the root surface. The rhizosphere extent was determined for root segments for the following parameters: 1) GLU release and 2) BGU and LAP (soil zymograms). To measure the rhizosphere extent, five horizontal transects (angle to the root ~90°) were randomly drawn across five randomly selected roots for the GLU release image and BGU zymogram using ImageJ. In total, this yielded 25 lines per image as pseudo-replicates, and their mean was used for each rhizobox (as a true replicate) (Bilyera et al., 2021).

2.2.5 Enzyme kinetics and turnover time

The kinetics of hydrolytic enzymes involved in C and N cycles were measured by fluorimetric microplate assays of 4-methylumbelliferone (MUF) and 7-amino-4-methyl coumarin (AMC) (Dorodnikov et al., 2009). A fluorogenic substrate based on MUF and one type based on AMC were used to assess enzymatic activities: 4-methylumbelliferyl-β-D-glucoside to detect BGU activity; L-Leucine-7-amino-4-me- thylcoumarin to detect LAP activity. All substrates and chemicals were purchased from Sigma-Aldrich (Darmstadt, Germany).

According to German et al. (2011), 1.0 g of soil was suspended in 50 mL of distilled water, of which 50 µL aliquots were pipetted into labeled wells of a 96-well microplate (Thermo Fisher, Denmark). A 50 µL buffer (MES/Trizma) and 100 µL respective substrate solution were then added to each well. The activity of enzymes was measured at three time points: 30 min, 60 min, and 120 min using CLARIOstar Plus (BMG LABTECH, Germany) at an excitation wavelength of 355 nm and an emission wavelength of 460 nm. We determined enzyme activities over a range of substrate concentrations from low to high (0 µmol g^{-1} soil, 20 µmol g^{-1} soil, 40 µmol g^{-1} soil, 60 µmol g^{-1} soil, 80 µmol g^{-1} soil, 100 µmol g^{-1} soil, 200 µmol g^{-1} soil, and 400 µmol g^{-1} soil) to ensure the appropriate saturating concentration.

Enzyme activities were denoted as released MUF/AMC in nmol per g dry soil per hour (nmol MUF/AMC g^{-1} soil h^{-1}) (Awad et al., 2012), and the affinity constant for each enzyme (K_m) was expressed in µmol substrate per g dry soil (µmol g^{-1} soil). Simultaneously, MUF/AMC concentrations of 0 nM, 10 nM, 20 nM, 30 nM, 40 nM, 50 nM, 100 nM, and 200 nM were prepared to calibrate the measurement. The Michaelis-Menten equation was used to determine the parameters of the activity of the enzyme (V):

$$V = \frac{Vmax[S]}{Km[S]} \quad (1)$$

where V_{max} is the maximum enzyme velocity (a function of enzyme concentration), S is the substrate concentration, and K_m is the substrate concentration at half-maximal enzyme activity. Both V_{max} and K_m parameters were approximated by the Michaelis–Menten equation (1) with the non-linear regression routine of SigmaPlot (v. 12.3). Catalytic efficiency (K_a) was calculated as the V_{max}-to-K_m ratio (Panikov et al., 1992). The substrate turnover rate was calculated by equation (2), where Tt is the turnover time (hours) (Zhang et al., 2020).

$$Tt = \frac{Km \times [S]}{Vmax + [S]} \quad (2)$$

2.2.6 Soil DNA extraction and 16S rRNA gene amplicon sequencing

The distinct microbial communities (bacteria and archaea) were accessed using a metabarcoding approach (16 S rRNA amplicon sequencing). Total DNA was extracted from 0.5 g of BS and RH soil samples using the FastDNA SpinKit for Soil (MP Biomedicals Fast Prep- 24 5G) according to the manufacturer's instructions. This included weighing the soil into the 2 mL bead-beating tubes containing the lysis matrix. After adding 978 µL sodium phosphate buffer and 122 µL of the MT buffer provided by the kit, samples were vortexed and adjusted for bead beating using the FastPrep-24 (2 × 30 s with a 5-min rest, speed 4). Samples were kept on ice until 250 µL of PPS (protein precipitation solution) were added. Extraction was performed according to the manufacturer's protocol, and DNA was eluted in 100 µL of DES water.

The quantity and integrity of the DNA were checked by Nanodrop and on 0.8 % agarose gels, respectively. The libraries from the 16 S rRNA gene amplicon using Uni341 F and Uni806 R primers and Illumina adaptors (Illumina, San Diego, USA) were performed at Novogene (UK) using Illumina MiSeq v2 (2 × 250 bp) chemistry according to the manufacturer's instructions (Illumina, San Diego, USA). Unassembled raw amplicon data were deposited in the National Center for Biotechnology Information (NCBI) Sequence Read Archive (SRA) under Bio-Project PRJNA942109.

2.2.7 Amplicon sequence analyses

The soil sample sequences were analyzed and categorized using the Divisive Amplicon Denoising Algorithm (DADA2 v.1.12.1 pipeline; Callahan et al. (2016) in R (v4.2.1; R Core Team, 2022). The "FilterAndTrimmed" function was utilized for the quality trimming and filtering processes. Reads of less than 100 bp were discarded, and two expected errors were permitted for each read. The subsequent steps involved error inference, denoising, and chimera removal. Following quality filtering, denoising, and chimera removal, the 16 S rRNA gene amplicon depths of 48 samples produced 1,558,139 high-quality 16 S rRNA gene reads, or 32,461 per sample. The amplicon sequencing variations (ASVs) were assigned taxonomically using the SILVA database version 138 (Quast et al., 2013) and then imported into the phyloseq tool in R (McMurdie and Holmes, 2013). Unassigned ASVs at the phylum level and any remaining ASVs identified as chloroplasts,

mitochondria, or eukaryotes were omitted from the studies. Amplicon sequencing yielded 46,725 unique ASVs.

2.2.8 Data analysis

General linear models (GLMs) were used to test the difference be- tween the means of the response variables at a significance threshold of $\alpha = 0.05$. The factors in the GLM were rotational position (W1, W2 and W4), soil compartment (BS, RH), and soil depth (0–30 cm, 30–60 cm, and 60–100 cm). The Shapiro–Wilk and Levene tests as well as a visual inspection of QQ plots were used to test for normality of the residual distribution and homogeneity of variance, respectively. Pairwise comparisons were made for soil chemical and enzymatic data using Bonferroni correction to identify differences between the response variables. Data transformation was performed when the assumptions of GLM failed. Yeo–Johnson (Yeo and Johnson, 2000), Box–Cox (Box and Cox, 1964), and log transformations were used. The transformation used for a certain variable is mentioned in the respective table. Correlation analysis was performed using Pearson's correlation for the response variable and for every level of the rotational position of WW (W1, W2, and W4). Since the soil sampling for microbiome data was performed only for soil depths of 0–30 cm and 30–60 cm, we calculated correlation coefficients for these two depths only, excluding the 60–100 cm layer from our analysis. Where applicable, we also show the variables related to BS and RH. The abovementioned statistical analyses were performed with IBM SPSS Statistics for Windows, version 23 (IBM Corp., Armonk, N.Y., USA). Graphs were generated with the *ggplot2* package in R (v4.2.1; R Core Team, 2022).

Relative abundances, alpha and beta diversities, and statistical tests were determined in R using specialized R package functions. Rarefaction analysis within the *vegan* R package examined the sequencing depth (Oksanen et al., 2022). The rarefaction curves tended to reach a plateau, indicating that the sequencing method supplied sufficient sequences to cover most of the sample diversity. Microbial sequences were rarefied for the lowest number of sequences identified among all samples, generating a dataset with 22,158 sequences per sample. The alpha diversity indices were computed for each rarefied sample using the *phyloseq* (McMurdie and Holmes, 2013) and *microbiome* (Lahti and Shetty, 2017) R packages. Using 10,000 permutations, Kruskal–Wallis tests were employed to evaluate for statistically significant changes in alpha diversity. The microbial composition of samples was assessed after transformation to relative abundance. The differences in phyla and taxa across samples were visualized using the *phyloseq* package (McMurdie and Holmes, 2013). Permutational multivariate analysis of variance (PERMANOVA) was performed to identify significant differences in the WW microbial community composition. The beta diversity of the microbial communities was visualized by a principal coordinate analysis (PCoA) using the Bray–Curtis distance.

2.3 Results

2.3.1 Effects of rotational position, soil compartment and soil depth on winter wheat growth

The preceding crop history had a pronounced effect on the biomass of the following WW. W2 and W4 plants had 43 % and 45 % reduced DW, respectively, compared to W1 (Table A.1; Fig. 2.1a). The decline in wheat DW was attributed to a reduction in root and stem biomass for W2, and root, stem, and leaf biomass for W4 when compared to W1 (Fig. 2.1a). Higher shoot N concentration resulted in a lower C:N ratio for W1 compared to W2 and W4 (Table A.1; Fig. 2.1b). In all rotational positions, there was a similar C:N ratio increase within roots, stems, and leaves (Table A.1).

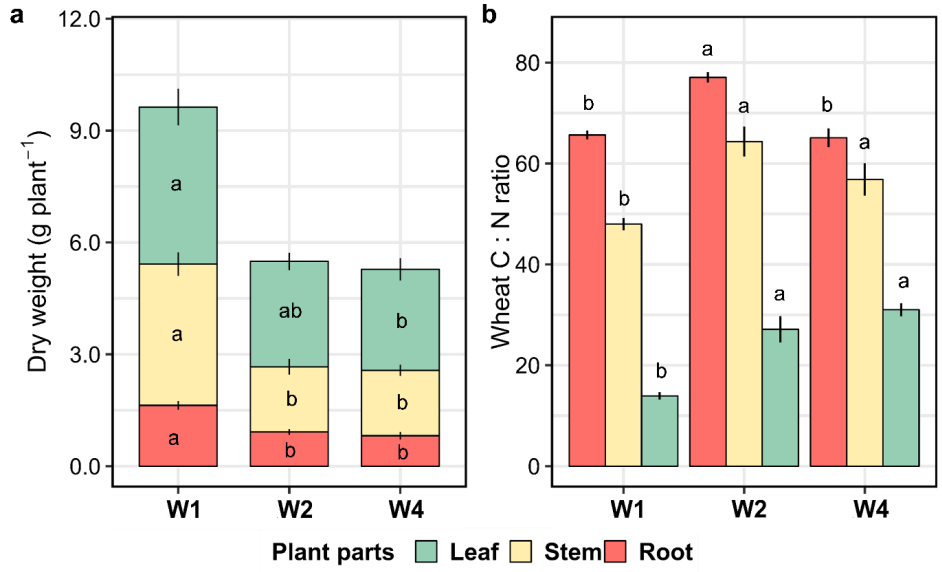

Figure 2.1 Effect of the rotational positions on root, stem, leaf dry weight (a) and C:N ratio (b) of the following winter wheat at onset of stem elongation (BBCH 30). W1 = first wheat, W2 = second wheat, and W4 = fourth wheat after oilseed rape in soil from the experimental farm Hohenschulen in Kiel, Germany. Within each plant part, different lowercase letters denote significant differences between rotational positions at $p \leq 0.05$ according to ANOVA with Bonferroni correction for multiple comparisons.

There was a strong response of root growth traits to WW rotational position with an overall reduction in RLD of 29 % and 31 % for W2 and W4, respectively, mainly in the upper 30 cm of the soil (Table A.2; Fig. 2.2a). However, even at a greater depth (60–100 cm), W1 had the highest

difference in RLD compared with W4. At this depth, W2 increased its RLD greater than W4, which had the lowest values of all three rotational positions.

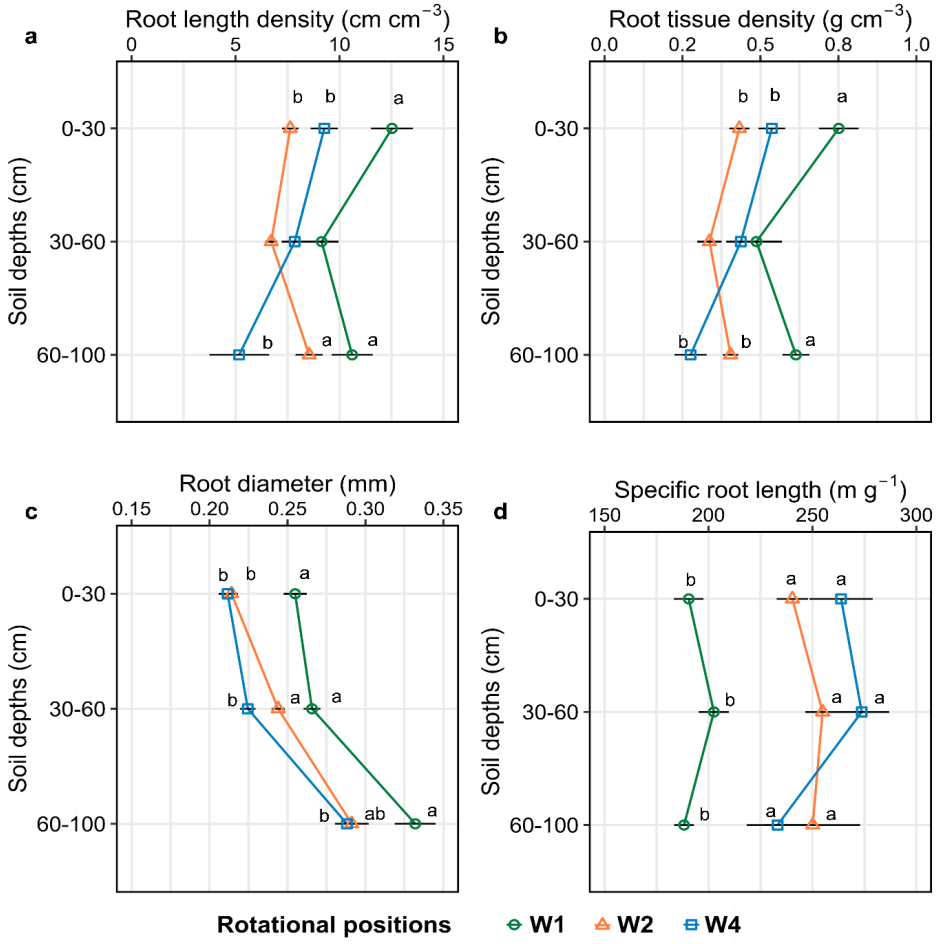

Figure 2.2 Effect of the rotational positions on root length density (a), root tissue density (b), average root diameter (c) and specific root length (d) of the following winter wheat at the onset of stem elongation (BBCH 30) at soil depths 0-30 cm, 30-60 cm and 60-100 cm). W1 = first wheat, W2 = second wheat, and W4 = fourth wheat after oilseed rape in soil from the experimental farm Hohenschulen in Kiel, Germany. Within each soil depth, different lowercase letters denote significant differences between rotational positions at $p \leq 0.05$ according to ANOVA with Bonferroni correction for multiple comparisons. No letters indicate non-significant differences.

Similarly, W1 had the highest RTD of all rotational positions, with 58 % and 48 % higher RTD values than W2 and W4, respectively (Table A.2; Fig. 2.2b). These differences were apparent in both the topsoil and the subsoil. Overall, W1 had thicker roots with an Rdia of 0.28 mm compared to 0.25 mm and 0.24 mm for W2 and W4, respectively, a trend that was observed throughout the soil profile (Table A.2, Fig. 2.2c). The Rdia of all three rotational positions increased at greater soil depth (Table A.2). Finally, W2 and W4 increased their SRL by 28 % and 33 % compared to W1, with significant differences along the complete soil profile (Table A.2, Fig. 2.2d).

2.3.2 Effects of rotational position, soil compartment, and soil depth on biochemical soil properties

More NH_4^+ and NO_3^- were found in the RH compared to BS and in the 0-30 cm soil layer compared to subsoil layers (Table A.3). The rotational position of WW strongly affected mineral N, with a 42 % and 48 % lower NH_4^+ concentration in W1 overall compared to W2 and W4, respectively (Fig. 2.3a). In particular, in the uppermost soil depth of W1, there was much less NH_4^+ than in the same depth of W2 (-54 %) and W4 (-58 %).

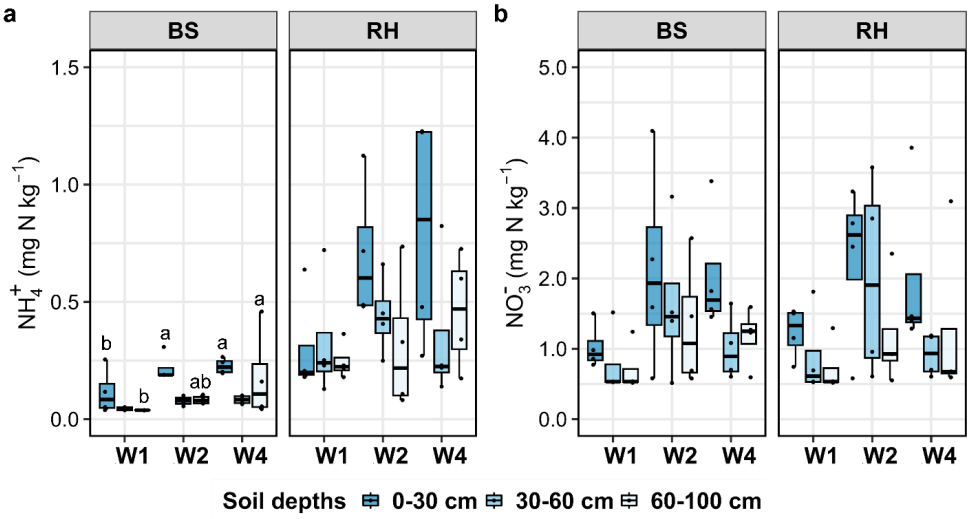

Figure 2.3 Effect of the rotational positions on soil NH_4^+-N (a) and NO_3^--N (b) of the following winter wheat at onset of stem elongation (BBCH 30) at soil depths 0-30 cm, 30-60 cm and 60-100 cm and two soil compartments bulk soil (BS) and rhizosphere soil (RH). W1 = first wheat, W2 = second wheat, and W4 = fourth wheat after oilseed rape in soil from the experimental farm Hohenschulen in Kiel, Germany. Within each soil depth and soil compartment, different lowercase letters denote significant differences between rotational positions at $p \leq 0.05$ according to ANOVA with Bonferroni correction for multiple comparisons. No letters indicate non-significant differences.

In addition, a similarly lower NO3- content was found in W1 (-49 % and -36 % compared to W2 and W4, Fig. 2.3b). Cmic and Nmic were also highly impacted by the rotational position, as shown in Fig. 2.4. Cmic was lower by 37 % and 43 % in W1 compared to W2 and W4, respectively (Fig. 2.4a). Nmic values of W1 were 50 % and 57 % lower than those of W2 and W4 (Fig. 2.4b). Most Cmic and Nmic were found in the topsoil (Table A.2).

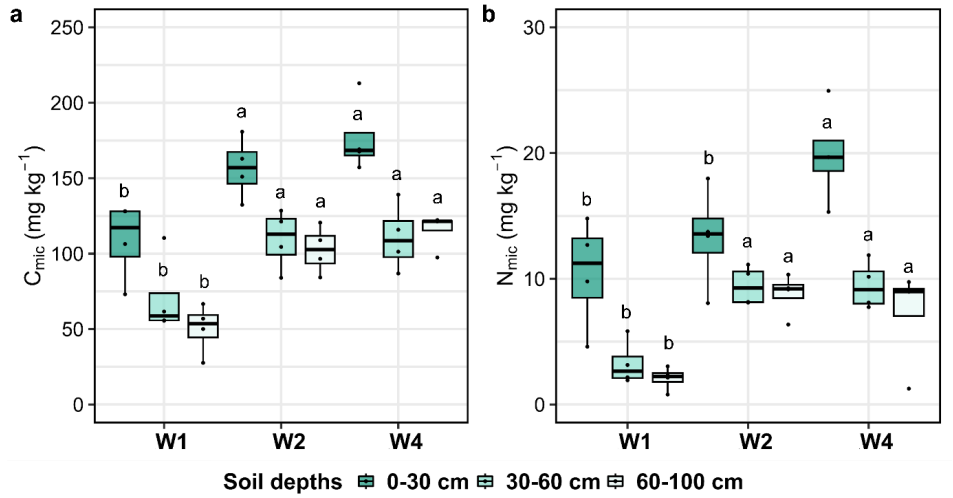

Figure 2.4 Effect of the rotational positions on microbial biomass carbon (C_{mic}, a) and microbial biomass nitrogen (N_{mic}, b) of the following winter wheat at onset of stem elongation (BBCH 30) at soil depths 0-30 cm, 30-60 cm and 60-100 cm. W1 = first wheat, W2 = second wheat, and W4= fourth wheat after oilseed rape in soil from the experimental farm Hohenschulen in Kiel, Germany. Within each soil depth, different lowercase letters denote significant differences between rotational positions at $p \leq 0.05$ according to ANOVA with Bonferroni correction for multiple comparisons. No letters indicate non-significant differences.

The rotational position also had a major influence on DOC levels (Table A.3). W1 soil had 68 % and 150 % higher DOC concentrations than W2 and W4, respectively (Fig. A.2). A significant main effect of soil compartment was shown, with a 74 % higher DOC content in the RH compared to BS. Interestingly, the DOC level in the RH of W1 at both subsoil depths (30-60 and 60-100 cm) was 1.7 and 4.1 times higher than W2 and W4, respectively (Fig. A.2). Similar DOC concentrations were observed in the BS in the rotational position and at all three soil depths.

2.3.3 Effects of rotational position, soil compartment, and soil depth on extracellular enzymes activities

The V_{max} of BGU was higher in W2 compared to W4 (by 27 %). No differences were observed between BS and RH, while higher values were observed in the first 30 cm of the soil profile (Table A.4). The interaction between rotational position, soil compartment, and soil depth revealed a 91 % and 169 % higher BGU V_{max} in the RH of W1 at 30-60 cm and 60-100 cm of the subsoil, respectively, compared to W4. In contrast, W2 and W4 had a higher BGU V_{max} in the topsoil compared to W1 (by 83 % and 89 %, respectively; Fig. A.5a). The response of the BGU K_m to the rotational position revealed a 64 % and 68 % reduction in affinity for W2 and W4 compared to W1, which was evident in all soil layers (Fig. A.5b). A higher K_a was observed in W1 compared to W2 and W4, while a lower substrate Tt was seen in W1 and W2 compared to W4 (Table A.4). The V_{max} of the LAP of W1 equaled that of W2 and was 32 % higher than that of W4 (Fig. A.5c). It was also increased in BS compared to RH, with no obvious differences in its response between soil depths. Higher values of V_{max} were observed in the BS of W1 in the subsoil layers compared to W2 and W4. Soil compartment had a significant effect, with LAP affinity increasing in the RH compared to BS (Table A.4). LAP K_m was also affected by the rotational position, as shown in Fig. A.5d. W2 had a much higher LAP affinity in the RH than BS, while it did not fluctuate significantly between the two soil compartments for W1 and W4. LAP K_m was higher in W1 compared to W4 in the BS (58 %) and RH (76 %) (Fig. A.5d). Finally, both K_a and Tt were increased in W4 compared to W1 and W2 (Table A.4).

Zymography revealed significant differences between WW rotations (Table A.5), with the BGU rhizosphere extent of W1 averaging 5.3 mm compared with 2.5 mm for W2 and W4. This response was mainly driven by major differences in the lowest soil depth, where the rhizosphere extent for BGU was 9 mm compared to 4 mm for W2 and 3 mm for W4 (Fig. 2.5a). In a similar manner, the rhizosphere extent for LAP was, on average, 0.36 mm for W1, which was significantly higher than for W4 (0.16 mm, Fig. 2.5b). We found a similar, though insignificant, trend of a reduced LAP rhizosphere extent for W2 (0.19 mm). In terms of BGU and LAP activity, there were no pronounced differences among the fixed factors of the experiment (Fig. 2.5c, d). The same was true for the BGU hotspot area, with a decreasing hotspot area percentage at greater soil depths that was nonetheless insignificant (Fig. 2.5e). Lastly, the LAP hotspot area for W1 was 96 % higher than W2 in the deep subsoil of 60-100 cm (Fig. 2.5f).

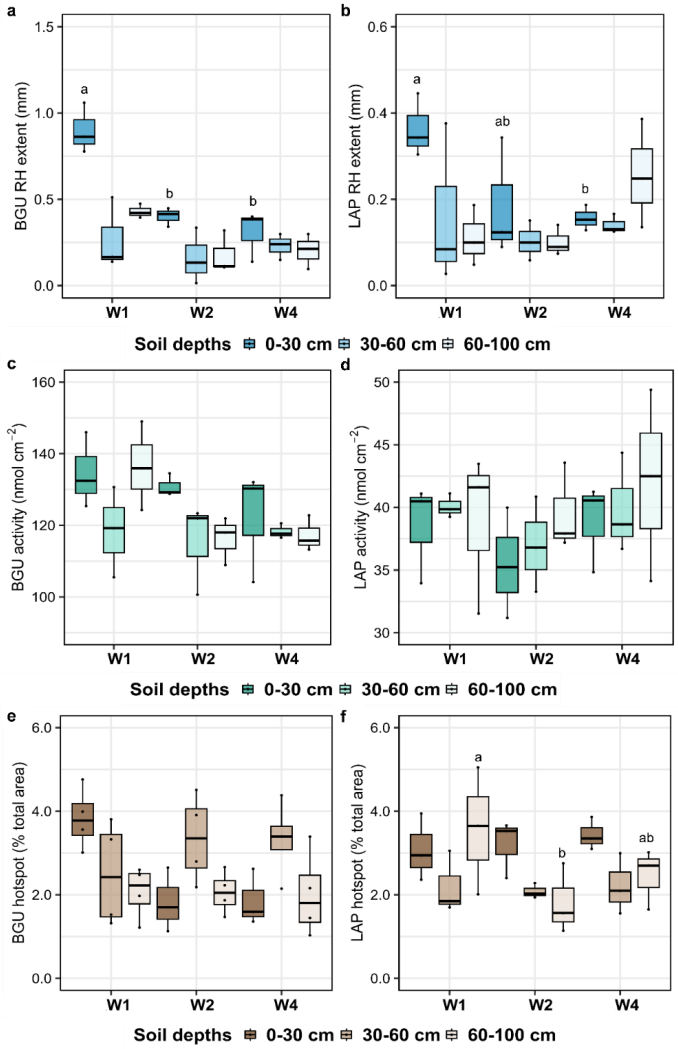

Figure 2.5 Effect of the rotational positions on rhizosphere extent (RH), activity and hotspot percentage of *β*-glucosidase (BGU) (a, c, e) and leucine aminopeptidase (LAP) (b, d, f) of the following winter wheat at onset of stem elongation (BBCH 30) at soil depths 0-30 cm, 30-60 cm and 60-100 cm. W1 = first wheat, W2 = second wheat, and W4 = fourth wheat after oilseed rape in soil from the experimental farm Hohenschulen in Kiel, Germany. Within each soil depth and soil compartment, different lowercase letters denote significant differences between rotational positions at $p \leq 0.05$ according to ANOVA with Bonferroni correction for multiple comparisons. No letters indicate non-significant differences.

GLU imaging revealed significant differences between the GLU rhizosphere extent and hotspot area between the three soil layers (Table A.5). This trend followed that of the root growth data. We also observed a decreasing rhizosphere extent for GLU in successively grown WW that was, however, insignificant (Fig. 2.6a). The same was found for GLU release per surface area (Fig. 2.6b), with a lower relative amount of GLU release in W2 and W4, although there was no significant main effect of the rotational position. However, a significant decline was recorded in the GLU hotspot area in the 60-100 cm layer of the soil profile in W2 (-53 %) compared to W1 (Fig. 2.6c).

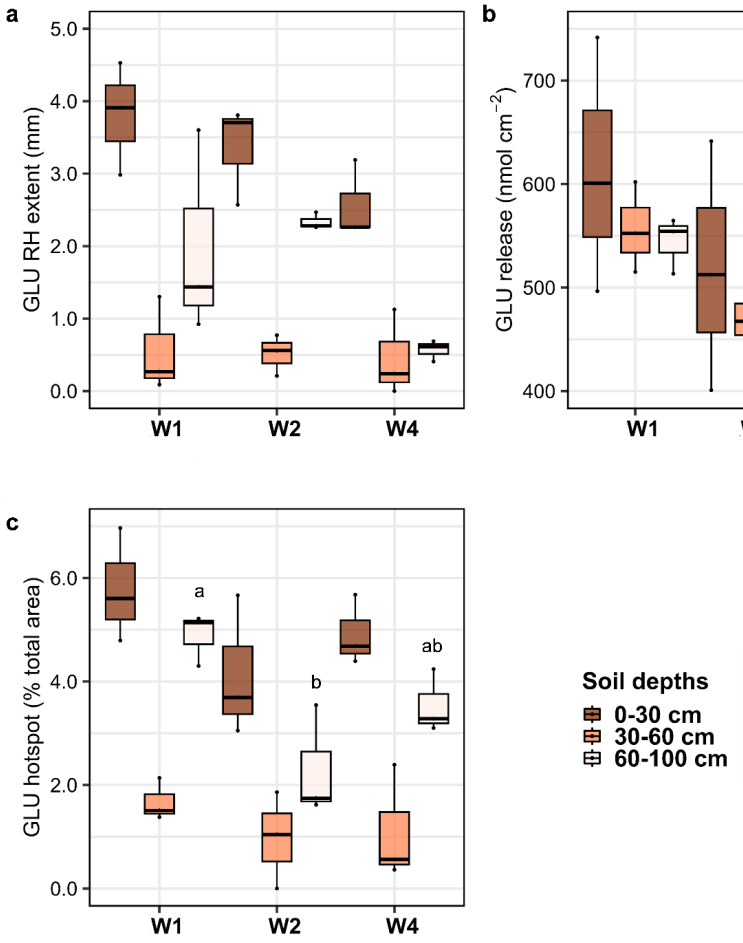

Figure 2.6 Effect of the rotational positions on glucose rhizosphere extent (RH, a), release (b) and hotspot percentage (c) of the following winter wheat at onset of stem elongation (BBCH 30) at soil depths 0-30 cm, 30-60 cm and 60-100 cm. W1 = first wheat, W2 = second wheat, and W4 =

fourth wheat after oilseed rape in soil from the experimental farm Hohenschulen in Kiel, Germany. Within each soil depth and soil compartment, different lowercase letters denote significant differences between rotational positions at $p \leq 0.05$ according to ANOVA with Bonferroni correction for multiple comparisons. No letters indicate non-significant differences.

2.3.4 Effects of rotational position, soil compartment, and soil depth on microbial community structure and composition

A significant difference in species richness between W1 and W4 was observed in the BS compartment and in the uppermost 30 cm of soil, where W4 presented a higher number of species than W1 (Fig. A.6a). Interestingly, there was no influence on the microbial community diversity and species evenness distribution expressed as the Pielou index and Shannon index, respectively (Fig. A.7a, b). The soil depth had a main effect on the beta diversity parameters (Fig. A.6b). According to the PERMANOVA results, the rotational position explained 10.5 % of the variation ($F = 3.51$; $p < 0.001$) in the microbial community, while soil depth explained 12.3 % of the variation observed ($F = 5.97$; $p < 0.001$).

The main components of the microbial community composition at the phylum level were *Actinobacteriota*, *Proteobacteria*, *Chloroflexi*, *Gemmatimonadota*, and *Crenarchaeota*. The relative abundance of several taxa from *Acidobacteriota*, *Gemmatimonadota*, *Nitrospirota*, and *Chloroflexi* was significantly affected by the rotational position in the BS and RH soils and at different soil depths. While in the BS of the plants, the relative abundance of *Acidobacteriota* was not significantly different, we recorded a significantly higher relative abundance of *Acidobacteriota* in the RH of the topsoil and subsoil of W1 compared to both W2 and W4 (Fig. 2.7a). A decreasing relative abundance of *Gemmatimonadota* in W4 compared to W1 was found in both soil compartments, while the difference between W1 and W2 remained insignificant (Fig. 2.7b). With regard to *Nitrospirota*, W1 and W2 had similar relative abundances in both BS and the RH (Fig. 2.7c). In the RH, the relative abundance of *Nitrospirota* was significantly higher in both the topsoil and subsoil of W2 compared to W4. Finally, in W1 and W2, there was a much lower relative abundance of *Chloroflexi* compared to W4, and this difference was consistently found in BS and RH soil (Fig. 2.7d).

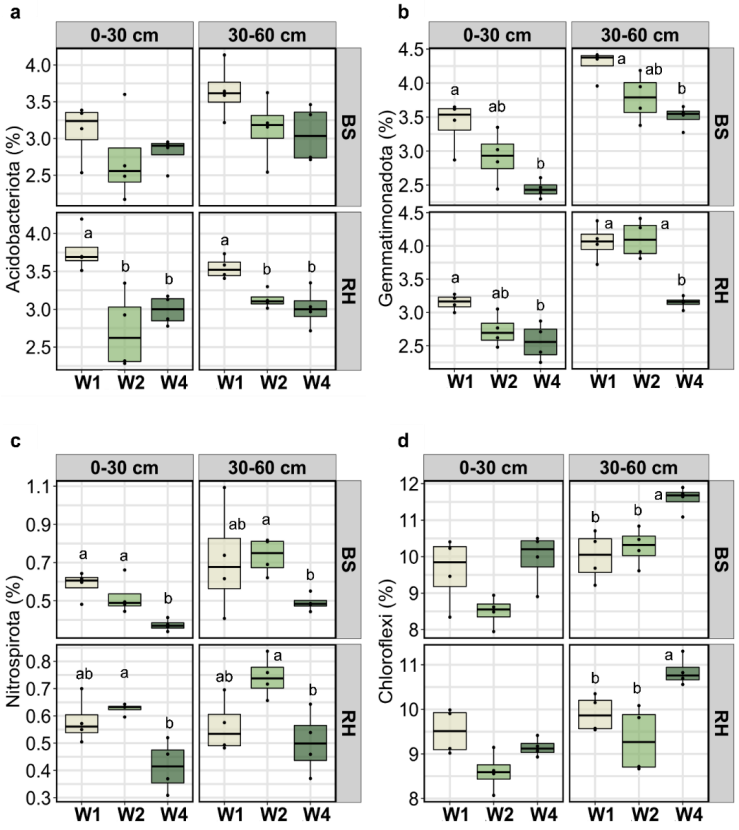

Figure 2.7 Effect of the rotational positions on the relative abundance of (a) *Acidobacteriota*, (b) *Gemmatimonadota*, (c) *Nitrospirota* and (d) *Chloroflexi* at soil depths 0-30 cm and 30-60 cm, in the two soil compartments bulk soil (BS) and rhizosphere (RH). W1 = first wheat, W2 = second wheat, and W4 = fourth wheat after oilseed rape in field soil from the experimental farm Hohenschulen in Kiel, Germany. Within each soil depth and soil compartment, different lowercase letters denote significant differences between rotational positions at $p \leq 0.05$ according to ANOVA with Bonferroni correction for multiple comparisons. No letters indicate non-significant differences. Effect of the rotational positions on the relative abundance of (a) *Acidobacteriota*, (b) *Gemmatimonadota*, (c) *Nitrospirota* and (d) *Chloroflexi* at soil depths 0-30 cm and 30-60 cm, in the two soil compartments bulk soil (BS) and rhizosphere (RH). W1 = first wheat, W2 = second wheat, and W4 = fourth wheat after oilseed rape in field soil from the experimental farm Hohenschulen in Kiel, Germany. Within each soil depth and soil compartment, different lowercase letters denote significant differences between rotational positions at $p \leq 0.05$ according to ANOVA with Bonferroni correction for multiple comparisons. No letters indicate non-significant differences.

In order to examine the relationship between the measured parameters in each rotational position and their influence on the different bacterial phyla, we conducted correlation analyses (Tables A9-A11). At 0-30 cm, the root dry weight (RDW) of W1 was negatively correlated with the relative abundance of *Gemmatimonadota* in the rhizosphere compartment. At 30-60 cm, it was positively correlated with the soil NO_3^- content in the BS, K_{CAL} in the RH, and the relative abundance of *Nitrospirota* in the RH, but negatively correlated with *Chloroflexi* in the RH and *Acidobacteriota* in the BS (Table A.9). For W4, the RDW was negatively correlated with the relative abundance of *Chloroflexi* in the RH and *Nitrospirota* in the RH (Table A.11). For W1 and at 30-60 cm, DOC was positively correlated with P_{CAL} in the RH. DOC was also positively correlated with both the BGU and LAP reaction rates in the BS. Finally, DOC positively correlated with the relative abundance of *Nitrospirota* in the RH (Table A.9). For W2 and at 0-30 cm, DOC was negatively correlated with K_{CAL} in the BS. In the RH, there was a negative correlation between DOC and C_{mic} and a positive correlation between DOC and the relative abundance of *Acidobacteriota*. As for W4, there was a negative correlation between DOC in the RH and BGU rhizosphere extent (Table A.11). C_{mic} exhibited a positive correlation with the LAP hotspot at 0-30 cm of W1, while it was negatively correlated with *Gemmatimonadota* in the BS. At 30-60 cm, it was positively correlated with both NO_3^- of the RH and N_{mic} (Table A.9). C_{mic} of W2 was negatively correlated with both *Chloroflexi* and *Acidobacteriota* in the RH at 0-30 cm. In the subsoil, it was negatively correlated with DOC in the RH (Table A.10). Finally, in the topsoil of W4, C_{mic} was positively correlated with both NH_4^+ and NO_3^- in the RH and BS, respectively (Table A.11).

2.4 Discussion

2.4.1 Root plastic responses drive nutrient supply and plant biomass accumulation in winter wheat rotations

Successively grown WW appeared to prioritize soil exploration, shaping a thinner and less dense root system, as indicated by its higher SRL, lower R_{dia}, and RTD. It should be noted that the overall RLD and SRL followed a similar trend for each measured diameter class in the rotational positions. In a field trial with silty loam soil, (Arnhold et al., 2023b) found no differences in RLD between the first WW after oilseed rape, the second WW after oilseed rape, and WW monoculture at the end of tillering. However, when they measured RLD during late flowering in a year with high summer precipitation, the wheat after oilseed rape had a significantly higher RLD than the successively grown WW in the topsoil. In the sandy loam soil of our study, we documented an early reduction in RLD in successive WW rotations during the relatively dry period of the trial (Fig. A.1). Therefore, the soil type and environmental conditions are strong determinants of the effect of the WW rotational position on its plant biomass accumulation.

Differences in root growth patterns might explain the more efficient N, P, and K uptake in W1, leading to lower mineral N, P, and K concentrations in the soil of W1 at BBCH 30 and, therefore, an increased N, P, and K supply to the plants, which is reflected in the lower C:N ratios

of W1 compared to W2 and W4 (Fig. 2.1a and b; Table A.6). A higher N uptake by maize plants was previously found in diversified crop rotations (maize, soybean, three-year wheat rotation with red clover and rye cover crops) and was associated with a higher C and N enzymatic activity of soil microbes (Bowles et al., 2022). In our study, there was a positive correlation between the RDW and the K_{CAL} in the topsoil of W1, but this was not the case for W2 and W4. In the topsoil, the SRL of W1 was negatively correlated with NH_4^+ in the RH and K_{CAL} (Table A.9). The SRL of plants tends to increase under biotic and abiotic stresses (Kramer-Walter et al., 2016; Kaloterakis et al., 2021; Lopez et al., 2023), while RLD and R_{dia} are reduced (Kramer-Walter et al., 2016; Lopez et al., 2023). Accordingly, the SRL of W2 was negatively correlated with RLD and the RDW (Table A.10). Kelly et al. (2022) found a higher SRL in WW landraces grown under conditions of low nutrient availability, while landraces with a higher proportion of coarse roots were associated with higher extractable C pools in the RH. The higher NH_4^+ was positively correlated with the R_{dia} of W1, especially in the subsoil (Table A.9). W1 is also associated with high residual mineral N in the soil after harvest (10–20 kg N ha^{-1}) that is readily available for uptake by W1 (Weiser et al., 2017). Our data suggest that this available N stimulated the early growth of W1, enabling the vigorous establishment and exploitation of the rhizobox soil volume. Due to their initial root growth reduction, W2 and W4 did not fully utilize the N reservoir of the soil, resulting in higher mineral N in the soil at the end of the experiment.

2.4.2 High microbial biomass and low labile C in the soil of successive winter wheat rotations induce N immobilization

In a recent field experiment, Yang et al. (2022) found that C_{mic} and N_{mic} increased in parallel with WW dry matter accumulation throughout the growth period. In our experiment, the highest plant biomass-yielding rotational position, W1, had much lower C_{mic} and N_{mic} values at all three soil depths, confirming the results of the afore- mentioned study. Typically, higher root biomass is associated with increased C_{mic} (Lange et al., 2015). However, changes in root biomass may be more accurately linked to changes in microbial diversity, thus explaining the trends observed (Fig. A.6) in this experiment (Ren et al., 2017). Hansen et al. (2019) reported a similar decline in C_{mic} when oilseed rape was introduced into successive wheat mono- cultures and attributed this effect to the biocidal properties of its secondary metabolite, isothiocyanate. The initial soil biochemical properties of the three rotational positions (Table 2.1) showed a higher C_{mic} in the soil of W4 and a higher C_{mic}:N_{mic} ratio for W2 compared to W1. The higher C_{mic}, C_{mic}:N_{mic} ratio, and lower soil mineral N indicate a significant initial N limitation of the soil microbial community of successively grown WW. The high initial DOC content of the soil (Table 2.1) induced rapid microbial regrowth after the initial adjustment of the water-holding capacity (WHC), resulting in N immobilization that may have affected plant growth. The higher C_{mic} measured at the end of the experiment was not utilized as an N source (i.e. mineralization of microbial biomass and N release) by W2 and W4, leading to lower plant biomass and a higher plant C:N ratio.

2.4.3 Microbial activity in the rhizosphere of winter wheat is highly dependent on its rotational position

The combination of zymography with the quantification of enzyme kinetic parameters complemented each other and improved our understanding of the microbial activity and the nutrient transformations in the rhizosphere of WW. Zymography is an invaluable technique to demonstrate the dynamics of enzymatic activity at very small spatial scales (Razavi et al., 2019; Guber et al., 2021). Soil microbes in successive WW rotations invested less in BGU and LAP secretion compared to those in the RH of W1, especially in the subsoil. The absence of the main effect of soil depth on soil enzymatic activity, together with the high root growth and DOC content in the subsoil, imply that the soil microbes sustained their metabolic function at greater depth. This was evident for all three rotational positions.

The zymograms of BGU and LAP showed a narrower rhizosphere extent in the topsoil of W2 and W4 compared to W1 (Fig. 2.5). This suggests that the root system of W1 stimulated microbial activity, increasing GLU and leucine release, which can be directly utilized by microbes. As a result, the microbes in the RH of W1 (and partially of W2) (such as taxa belonging to the *Gemmatimonadota*, *Acidobacteriota*, and *Nitrospirota*) were able to utilize the DOC and N in the RH more effectively than the microbes in the RH of W4 (Fig. 2.3, Fig. A.2). Plants as well as bacteria and archaea (Singh et al., 2016; Bilyera et al., 2021) produce BGU, an enzyme important in the first step of cellulose degradation, which is the major component of plant cell walls. Microbes have a weaker ability to utilize low molecular weight C when competing with plants for available nutrients, with DOC content being a strong determinant of the outcome of this interaction (Kuzyakov and Jones, 2006; Song et al., 2020). Complementing our findings on the DOC of the RH, we found a larger GLU hotspot area in W1 compared to W2 and W4. Labile C is considered critical for maintaining the pathogen-suppressive qualities of agricultural soils, irrespective of the total SOM content (Bongiorno et al., 2019), which could have confounded the biocidal soil legacy of oilseed rape.

Depth-specific comparisons revealed differences in the activity of the previous C- and N-cycling soil enzymes between all three rotational positions. Interestingly, BGU activity was significantly higher in the RH and in the topsoil of W2 and W4 than in W1. This pattern could be explained by the accumulation of less labile organic matter from the wheat residues in the uppermost soil layers in successively grown WW (Cenini et al., 2016; Ni et al., 2020; Luan et al., 2022), which may have stimulated the growth of cellulose-degrading microbes. This, in turn, led to higher BGU activity in the topsoil and C_{mic} throughout the soil profile (Zhao and Zhang, 2018; Reichel et al., 2022). Soil microorganisms thus synthesize BGU in response to the presence of a decomposable substrate that must be degraded (Turner et al., 2002; Veres et al., 2015).

The larger LAP hotspot area in W1 compared to successively grown WW indicates a larger overall rhizosphere size, which affects a larger soil volume and thus induces positive soil feedback for W1. This may have contributed to the observed N limitation of successively grown WW. Protein-derived N accounts for 40 % of total soil N and is a crucial N source for microbes and plants, but it is also a precursor for mineral N production that is available for plant uptake (Rillig

et al., 2007; Paungfoo-Lonhienne et al., 2008; Näsholm et al., 2009). It is likely that these differences in the form of organic N in the soil of the rotational position stimulated LAP activity in W1 and repressed it in successively grown WW, with an increasing size of effect from W2 to W4. Emmett et al. (2020) showed that plant N uptake and LAP activity are coupled in sunflower (*Helianthus annuus* L.), buckwheat (*Fagopyrum esculentum* Moench), Sudan grass (*Sorghum* x *drummondii* (Nees ex Steud.) Millsp. & Chase), Japanese millet (*Echinochloa esculenta* (A. Braun) H. Scholz), and maize (*Zea mays* subsp. *mays* L.) during flowering, and attributed this to the priming of soil organic N that is available for plant uptake. We observed that higher concentrations of DOC and NH_4^+ were accompanied by higher LAP activity and substrate affinity in the RH (Fig. A.5, Fig. 2.5). However, the literature is inconclusive regarding the impact of inorganic N on LAP activity (Cenini et al., 2016; Shi et al., 2016).

2.4.4 The rotational position of WW shapes the soil microbial community composition

The higher richness of bacterial taxa in the BS of W4 compared to W1 and W2 suggests that successive wheat cultivation selects a broader spectrum of bacteria that are better adapted to the specific soil conditions (Mayer et al., 2019). Previous research has shown that pre- ceding crops affect the microbial communities in the wheat rhizosphere (Hilton et al., 2018; Babin et al., 2019). Oilseed rape is known to recruit microbial taxa that enhance the growth of the following WW (Vujanovic et al., 2012). This might be linked to the control that the preceding crops exert over the quantity and quality of the secreted exudates, leading to changes in the relative abundance of certain taxa (Jones et al., 2019; Wen et al., 2022). In addition, we observed only minor differences between BS and RH compartments, which is in contrast to other studies reporting pronounced differences between soil- and root-associated communities (Schreiter et al., 2014; Bziuk et al., 2021). These findings suggest that our non-destructive sampling technique using micro- spatulas may have been constrained by the distance at which we were able to collect soil samples from the vicinity of the plant roots (≤ 5 mm). Although more precise techniques, such as the wet needle technique (Tian et al., 2020) or Stomacher blending to wash off tightly adhering soil particles directly from the roots, could provide a better distinction between BS and RH microbial communities, they are mainly suitable for only very small sample sizes in terms of soil weight, or they require more root material. Nevertheless, we aimed for a compromise in sampling RH and BS to be able to link all gathered data, i.e. soil biochemical, enzymatic, and microbial community data.

We observed shifts in the bacterial composition at the phylum level between different WW rotational positions (Fig. 2.7) that might explain a potential imbalance or dysbiosis effect in successively grown WW, leading to less efficient nutrient uptake and lower plant biomass yields. In general, the microbial community structures of W1 and W2 were more similar compared to W4 (Fig. A.6b). It appears that the higher rate of WW residue return in the soil of WW monocropping may have favored a higher species richness, resulting in microbial taxa competing for slowly

degradable C sources (straw) but causing less efficient plant nutrient supply and thus an early reduction of plant growth.

In more detail, we observed a higher relative abundance of *Acidobacteriota* in the RH of W1 throughout the soil profile compared to W2 and W4. *Acidobacteriota* is considered a keystone phylum in the rhizosphere of wheat (Kavamura et al., 2020). Bacteria belonging to this phylum have been found to induce auxin (IAA) production in *Arabidopsis*, increase Fe uptake following siderophore synthesis, and secrete exopolysaccharides, forming biofilms (Kielak et al., 2016; Kaloterakis et al., 2021). In the subsoil of W2, the high C_{mic} was negatively associated with the relative abundance of *Acidobacteriota* (Tables A9–A10), which was not the case for W1, thus highlighting the rotational position-specific effect on supporting the proliferation of certain bacterial phyla. *Chloroflexi* and *Nitrospirota* are considered to be NO_2^- oxidizers, contributing to nitrification and, therefore, soil NO_3^- production (Pivato et al., 2021; Yuan et al., 2023). *Nitrospirota* was more prevalent in W1 and W2 compared to W4 in the RH. In the topsoil of W1, we found that *Nitrospirota* was negatively associated with *Chloroflexi* in the RH (Table A.9), indicating a competition for the same resources. In a rape–rice rotation, (Yuan et al., 2023) correlated the relative abundance of *Nitrospirota* to urease activity, which generates NH_4^+ and, therefore, allows N turnover due to nitrification. We found that W1 formed a more extensive root system and accumulated more N in its biomass. It could thus exploit the newly produced NH_4^+ and NO_3^- more effectively than W2 and W4, leading to an increase in biomass in W1. These findings suggest functional differences in the bacterial communities of the rotational positions, underscoring the dynamic biochemical soil processes that lowered the performance of successively grown wheat.

Understanding the shape of the fungal communities of the rotational positions would help us to better comprehend the complex plant–microbe interactions. (Woo et al., 2022) found a strong effect of the rotational position of wheat grown after pea on shaping bacterial and fungal diversity. In another study, fungal community composition responded more than bacterial composition to crop rotation, with a higher relative abundance of beneficial microbes in rotation canola compared to oilseed rape monocropping (Town et al., 2023). Finally, differences in the stability of bacterial and fungal necromass (reflected in the stability be- tween peptides and chitin/chitosan) could determine the mineralization rate of immobilized N by microorganisms and, therefore, the subsequent mineral N release (Camenzind et al., 2023) that is available for uptake by WW.

2.5 Conclusions

In this study, three rotational positions of WW were contrasted to assess their impact on soil microbial dynamics, extracellular enzymatic activity, and the performance of WW. We linked the activities of C-acquiring (BGU) and N-acquiring (LAP) enzymes to changes in biochemical soil processes and microbiome community in the rhizosphere of successive WW rotations. The reduced root growth and labile C in the rhizosphere of successive WW rotations led to decreased microbial and enzymatic activity and, finally, plant nutrient uptake and biomass accumulation. Our results

greatly increase our understanding of the preceding crop's soil legacy, which drives the reduction in biomass growth during the early growth of WW.

3. Rotational diversity shapes the bacterial and archaeal communities and confers positive plant-soil feedback in winter wheat rotations

---

Based on:
Kaloterakis, N., Giongo, A., Braun-Kiewnick, A., Rashtbari, M., Priscilla, Z., Razavi, B.S., Smalla, K., Reichel, R., Brüggemann, N., 2025. Rotational diversity shapes the bacterial and archaeal communities and confers positive plant-soil feedback in winter wheat rotations. *Soil Biology and Biochemistry* 203, 109729. https://doi.org/10.1016/j.soilbio.2025.109729

3.1 Introduction

WW is the second most cultivated cereal in the world, grown on approximately 217 million hectares in 2018 and providing one-fifth of the world's caloric and protein demand (Shewry and Hey, 2015; Erenstein et al., 2022). Following a linear increase of 35 % since 1994, the yield growth of WW is currently stagnating, not meeting the forecasted global demand (Moore and Lobell, 2015; Schauberger et al., 2018; Erenstein et al., 2022).

It is estimated that up to 40 % of the global WW is cultivated in monocropping systems (Angus et al., 2015; Yin et al., 2022). This self-succession of WW is associated with yield reduction, mainly attributed to the fungal root pathogen Gt (Palma-Guerrero et al., 2021). However, yield decline has also been observed in years lacking evident Gt infestation (Arnhold et al., 2023b, 2023a). This suggests that the yield decline in successive WW rotations is more complex, not limited to a single factor.

Temporal crop diversification by implementing suitable crop rotations holds great potential for addressing part of the WW yield decline problem. This can occur by either mitigating the negative PSF caused by the suppression of soil pathogens, or by conferring positive PSF, such as selecting beneficial microbes in the rhizosphere or increasing the enzymatic activity and nutrient availability. Increasing crop rotation diversity has also been associated with higher microbial activity and/or a higher incidence of plant-beneficial taxa (D'Acunto et al., 2018; Sun et al., 2023; Giongo et al., 2024). The addition of oilseed rape in the rotation as a preceding crop of WW is considered beneficial for attaining higher yields compared to less diverse crop rotations (Groeneveld et al., 2024). The positive soil legacy of oilseed rape includes suppression of pathogens through the production of secondary metabolites with biocidal properties or by simply breaking the pathogen life cycle in the soil (survival on host plant/straw residues), improving aggregate formation and soil structure, and increasing post-harvest residual N (N; Sieling et al., 2005; Weiser et al., 2017; Hegewald et al., 2018; Hansen et al., 2019; Kerdraon et al., 2019).

The positive legacy of oilseed rape can be expected to strongly affect the growth of the plants that, in turn, become more efficient in exploring the soil volume and utilizing the available nutrients in the top and subsoil. Root adaptations are strong indicators of soil resource acquisition and are controlled by both the genotype and the growing conditions of plants (H. Liu et al., 2022). Previous research on WW rotations has shown that factors affecting soil mineral N availability strongly affect root plasticity, at least during the early growth stages of WW (Kaloterakis et al., 2024b), which could potentially enhance nutrient and water uptake in more diverse WW rotations (Giongo et al., 2024).

Changes in the soil, and especially in the plant's rhizobiome, might reveal important information and enhance our understanding of PSFs in plant successions. The rhizosphere (RH), the interface between plants and soil microbiota, is characterized by intense microbial activity due to plant secretion of large amounts of photosynthesized C, either by exudation of low-molecular-weight compounds or of mucilage (Sasse et al., 2018). Together with the decomposing senesced roots, the rhizodeposited C stimulates microbial growth and activity in the rhizosphere, promotes nutrient cycling, and acts as a signal to recruit the rhizospheric microbial community (Benizri et

al., 2007; Yuan et al., 2018; Koprivova and Kopriva, 2022; George et al., 2024). The RH is governed mainly by copiotrophic r-strategists that provide different soil functions (such as C and N cycling; Ling et al., 2022). The secretion of secondary metabolites, such as benzoxazinoids, in the RH of WW following oilseed rape is known to induce microbial community composition changes to recruit beneficial microbes to cope with pathogens, which could potentially lead to a growth tradeoff of the following WW (Hu et al., 2018; Mwendwa et al., 2021). A potential dysbiosis in the rhizosphere of monocultures, involving the depletion of keystone species that protect plants from root pathogens, reduces the disease suppressiveness of the soil compared to crop rotations (Zhou et al., 2023). In addition, plants respond by fine-tuning their rhizospheric microbial communities under N-limiting conditions (Alegria Terrazas et al., 2022). Crop rotation is an important driver of N-related gene expression (R. Liu et al., 2023). Despite its importance, a deeper look into the effect of WW rotational position on the diversity, composition, and activity or function of the soil bacterial and archaeal community is currently lacking, especially with respect to N cycling.

To investigate the complex processes and plant-soil interactions, we conducted a greenhouse rhizotron experiment contrasting two WW rotational positions, i.e., W1 and W2. Our research questions were: i) how does the rotational position of WW affect the soil microbial activity and specifically the activity of C and N acquiring enzymes, and consequently WW growth and productivity; and ii) how does the rotational position of WW affect the abundance of the bacteria and archaea and N-related genes. We hypothesized that the rotational position of WW would affect the bacterial and archaeal community, leading to distinct changes in the bacterial and archaeal community composition. Soil microbial activity would be affected by the WW rotational position, resulting in differences in N cycling and uptake by the following WW, and ultimately influence crop growth and yield.

3.2 Materials and Methods

3.2.1 Experimental design

The soil was collected in September 2020 from the topsoil (0-30 cm) and subsoil (30-50 cm) of field plots immediately after oilseed rape cultivation and after one year of WW cultivation following oilseed rape at the Experimental Farm Hohenschulen, Faculty of Agricultural and Nutritional Sciences, Christian-Albrechts University of Kiel (54°19′05″N, 9°58′38″E), Germany. Hereafter, they are referred to as WW rotational positions. The plots from which the soil was collected were optimally fertilized with N (240 kg N ha^{-1}) and sown with the WW cultivar "Nordkap" (SAATEN-UNION GmbH, Isernhagen, Germany). The residues of the preceding crop, i.e., oilseed rape and WW for W1 and W2, respectively, were not removed from the soil, and the field was not ploughed before soil collection. The soil is classified as a carbonate-free Cambic Luvisol of a sandy loam texture (44 % sand, 35 % silt, and 21 % clay; Sieling et al., 2005). A detailed description of the soil properties and a comparison of the initial soil biochemical properties of this experiment is reported in Kaloterakis et al. (2024a). The residual soil NO_3^-, P_{CAL},

K_{CAL}, DOC and C_{mic} and N_{mic} following oilseed rape cultivation were significantly higher than following WW (Kaloterakis et al., 2024a).

Eight rhizotrons were placed in the greenhouse (Forschungszentrum Jülich, Germany). One plant was grown in each rhizotron filled with soil that had been cultivated either with oilseed rape or WW for one year before the start of the experiment (W1 and W2, respectively). Each rotational position was replicated four times (n = 8). All rhizotrons were kept inclined at 45° to facilitate root growth along the lower side of the rhizotrons. The soil was sieved to 2 mm and, subsequently, packed into the rhizotrons to reach a bulk density of 1.45 g cm^{-3}. Deionized water was added to adjust soil moisture to 70 % WHC (215 g H_2O soil kg^{-1}) at the onset of the experiment. After that, soil moisture was monitored gravimetrically and kept at 70 % WHC with deionized water to ensure well-watered conditions. WW seeds from the cv. "Nordkap" were germinated in Petri dishes on sterile filter paper for 24 h in the dark at 20 °C. After germination, one seedling was planted in each rhizotron. Each plant was fertilized with 0.78 g of calcium ammonium nitrate fertilizer (13.5 % NO_3^--N, 13.5 NH_4^+-N, 4 % CaO, 1 % Mn, YaraBela® CAN™, YARA GmbH & Co. KG, Dülmen, Germany) corresponding to an application rate of 240 kg N ha^{-1}. It was applied in three doses of 80 kg N ha^{-1} N ha each at the plant developmental stage BBCH 25, 30-/31 and 50, corresponding to 38, 62 and 96 days after sowing (DAS) in our experiment.

3.2.2 Soil sampling at tillering

The non-destructive soil sampling was performed at BBCH 29 (28 DAS; tillering, hereafter called T1). The sampling was performed as described in Reichel et al. (2022) with minor modifications. We sampled soil from two soil compartments i.e., RH and RA soil. For mineral N determination, we sampled soil from three soil layers i.e., 0-30 cm, 30-60 cm and 60-100 cm of four plant replicates (n = 48). Due to limitations in the maximum number of samples that could be quantified for microbiome and enzymatic analyses, we sampled soil from two soil layers i.e., 0-30 cm and 30-60 cm of three plant replicates (n = 24). Briefly, we sampled the RH soil near well-developed first-order lateral roots using a custom-made punching tool with which a hole was punched into the self-adhesive foil of the rhizotrons. Next, a soil core was extracted (2.5 cm length × Ø 0.8 cm) by inserting an Ø 0.8 cm metal cylinder through the perforated holes of the rhizotron's plates. For the RH soil samples, the first cm of the soil core was kept for the analysis, corresponding to a volume of 0.5 cm^3. We also sampled RA from holes with no apparent root growth, but which was likely affected by the dense root system that was only partly visible on the transparent plate of the rhizotron. After soil sampling, a polyamide screw (length of 6.5 cm × Ø 0.8 cm) resealed the hole created by the metal cylinder. To reduce soil heterogeneity in our samples, we pooled five soil sub-samples to form a composite sample at each soil compartment and soil depth. Soil samples for enzymatic analyses were stored at 4 °C and all other samples were stored at -20 °C until further processing. A preliminary analysis revealed no significant differences in the response variables (mentioned in the following subparagraphs) between RH and RA. Therefore, we combined the two soil compartments in specific analyses, which are detailed below, to increase the statistical power of our planned analyses.

3.2.3 Soil sampling at grain ripening and plant harvest

At the grain ripening stage (180 DAS; BBCH 90; hereafter called T2), the plants were harvested by splitting the aerial plant parts into tillers, leaves, husks, and grains. By removing the lower plate of the rhizotrons, the roots growing along the surface of the soil were exposed, and the soil profile was divided into the same soil layers described before. Since roots occupied the entire soil volume at this growth stage, we considered all the soil RH and did not distinguish between RA and RH. For mineral N determination, we sampled soil from three soil layers i.e., 0-10 cm, 10-20 cm, 20-40 cm, 40-70 cm and 70-100 cm of four plant replicates (n = 40). For microbiome and enzymatic analyses, we sampled soil from two soil layers i.e., 0-30 cm and 30-60 cm of three plant replicates (n = 12). Following soil sampling, the roots were carefully extracted and washed over a 1-mm sieve to retrieve most of the root system. They were stored in 30 % (v/v) ethanol before analysis. They were then scanned at 600 dpi (Epson Perfection V800 Photo, Epson, Japan) and analyzed with the WinRhizo® software (Regent Instruments Inc., Quebec, Canada).

All plant biomass was oven-dried at 60 °C to constant weight for three days before determining the DW. The plant material was then ball-milled (MM 400, Retsch, Germany) and weighed into tin capsules (HEKAtech, Wegberg, Germany) for C and ^{15}N content determination using an elemental analyzer coupled to an isotope-ratio mass spectrometer (EA-IRMS, Flash EA 2000, coupled to Delta V Plus; Thermo Fisher Scientific, Waltham, MA, USA).

3.2.4 Processing of soil samples

Soil samples were extracted with 0.01 M $CaCl_2$ (soil-to-solution ratio of 1:4 w/v), vortexed, shaken horizontally for 2 h at 200 rpm, centrifuged for 15 min at 690 × *g*, and filtered through 0.45 µm PP-membrane filters (Ø 25 mm; DISSOLUTION ACCESSORIES, ProSense B.V., München, Germany). Soil solution was analyzed for DOC with a TOC analyzer (TOC-V + ASI-V + TNM, Shimadzu, Japan). NH_4^+ was measured by continuous-flow analysis (Flowsys, Alliance Instruments GmbH, Freilassing, Germany). NO_3^- was measured by ion chromatography (Metrohm 850 Professional IC Anion – MCS, Metrohm AG, Herisau, Switzerland). Enzymatic activity of BGU and LAP, two hydrolytic enzymes involved in soil C and N cycling, was measured as reported by Kaloterakis et al. (2024a), following German et al. (2011). The kinetics of BGU and LAP were measured by fluorimetric microplate assays of 4-methylumbelliferone (MUF) and 7-amino-4-methyl coumarin (AMC; Razavi et al., 2017).

3.2.5 Soil DNA extraction and 16S rRNA gene amplicon sequencing

Total genomic DNA from bacteria and archaea was extracted from 0.5 g of RA and RH soil samples using a bead-beating method according to the manufacturer's description (FastDNA SpinKit for Soil, MP Biomedicals, Eschwege, Germany) and established protocols (Braun-Kiewnick et al., 2024). DNA quantity and quality were checked by Nanodrop and on 0.8 % agarose gels, and amplification efficiency of appropriate DNA dilutions (10-20 ng μL^{-1}) was tested by a pre-Illumina PCR using a fragment of the V3-V4 region of the 16S rRNA gene with the same

primers as for amplicon sequencing, except for the adaptors (Uni341F (5′ CCTAYGGGRBGCASCAG 3′) and Uni806R (5′ GGACTACHVGGGTWTCTAAT 3′)) (Yu et al., 2005; Caporaso et al., 2011; Sundberg et al., 2013). PCR products were checked on 1 % agarose gels before sending genomic DNA to amplicon sequencing (Novogene, Cambridge, UK). Amplicon libraries with the primers Uni341F-Uni806R and Illumina adaptors (Illumina, San Diego, USA) were then generated and sequenced at Novogene using Illumina MiSeq v2 (2 x 250 bp) chemistry according to the manufacturer's instructions (Illumina, San Diego, USA). Unassembled raw amplicon data were deposited at the National Center for Biotechnology Information (NCBI) Sequence Read Archive (SRA) under PRJNA1146588.

3.2.6 Amplicon sequence analyses

The downstream analysis was conducted in R (v4.2.1; R Core Team, 2022). The amplicon sequencing analysis was performed in the Divisive Amplicon Denoising Algorithm (DADA2 v.1.12.1 pipeline; Callahan et al., 2016). A total of 1,668,656 high-quality reads with a maximum of two expected errors were retained from 32 samples corresponding to eight plants, two soil layers 0-30 cm and 30-60 cm and two soil compartments i.e., RH and RA. The taxonomic classification of amplicon sequence variants (ASVs) was conducted using the SILVA database v.138 (Quast et al., 2013) and the 'phyloseq' package (McMurdie and Holmes, 2013). Unassigned ASVs at the phylum level and any remaining ASVs identified as chloroplasts, mitochondria, or eukaryotes were omitted from the studies. A taxonomic level called "Annotation" was manually included in the taxonomic table, which included the latest taxonomic information for each ASV. The dataset was subjected to rarefaction analysis to ensure an equal level of sequencing depth (Schloss, 2024), with the minimum number of sequences (34,391) observed in all samples. The rarefaction curves tended to reach a plateau, indicating that the sequencing method supplied sufficient sequences to cover most of the sample diversity.

Alpha diversity indices were calculated using the 'phyloseq' and 'microbiome' packages (Lahti and Shetty, 2017). Significant changes were determined using Kruskal-Wallis tests and post-hoc Wilcoxon-Mann-Whitney tests. The analysis of beta diversity employed square root transformed ASV count data using the 'vegan' package (Oksanen et al., 2022) and was visualized through multidimensional scaling (MDS) plots. The study evaluated variations in beta diversity centroids by applying permutational multivariate analysis of variance ('adonis'), PERMANOVA tests, and ANOSIM. Differential abundance (DA) analysis was performed using DESEeq2 negative-binomial Wald test (Love et al., 2014). Taxa were considered significant if their adjusted *p*-value was less than 0.05 after the Benjamini-Hochberg correction. Additionally, the putative prediction of the functions of the bacterial and archaeal communities from 16S rRNA gene sequencing data was performed using the software Tax4Fun2 v1.1.5 (Wemheuer et al., 2020). Log-transformed data from the differentially abundant taxa in each group of samples were used to obtain predicted relative values for different KEGG orthologues. KEGG functional pathways and N metabolism genes were selected based on five keywords, "nitrogen", "ammonium", "ammonia", "nitrate", and "nitrite".

3.2.7 Quantification of total bacteria (16S rRNA), bacterial 16S rRNA *amoA* (AOB) *nirS*, *nosZ*, and *nifH* genes and archaeal 16S rRNA and *amoA* genes (AOA) by qPCR

Quantitative PCR (qPCR) was used to measure the absolute abundance of bacterial 16S rRNA gene copies and N cycle-related genes, including the ammonia monooxygenase (AMO) alpha subunit (*amoA*), NO_2^- reductase (*nirS*), nitrous oxide reductase (*nosZ*), and N_2-fixing nitrogenase (*nifH*) genes in both RA and RH samples. To quantify absolute bacterial abundance, the BACT1369F, PROK1492R, and TM1389F primers, labeled with 5'-FAM and 3'-TAMRA, were used in a specific TaqMan assay, following the protocol described by (Suzuki et al., 2000). To determine the absolute abundance of the bacterial *amoA* gene (ammonia-oxidizing bacteria, AOB) the primers *amoA*-1F and *amoA*-2R developed by (Rotthauwe et al., 1997) were employed as described in Meyer et al. (2013). For quantifying the *nirS* gene the primers cd3aF and R3cd (Throbäck et al., 2004), and for the *nifH* gene, the forward primer FPGH19 (Simonet et al., 1991) was used along with the reverse primer PolR (Poly et al., 2001). Finally, for the *nosZ* gene quantification, the *nosZ*-2F and *nosZ*-2R primers were used (Henry et al., 2006). All reactions were conducted in a total volume of 20 µL containing 10 µ: of 2 x Luna Universal qPCR Master Mix (New England Biolabs, Ipswich, USA), 0.1 mg mL^{-1} BSA, 200 nM (*amoA*) or 400 nM (*nirS*, *nifH*, *nosZ*) of each primer and 5 µL of template DNA (1:5 diluted) per reaction. PCR cycling conditions were 1 min at 95 °C, followed by 40 cycles of 15 sec at 95 °C and 30 sec at 60 °C. The specificity of the amplification products employing SYBR green chemistry (New England Biolabs, Ipswich, USA) was confirmed through melting curve analyses after completion of amplification cycles (60 °C-95 °C, Δ 0.5 °C every 5 sec).

The quantification of all target gene copies in the samples was determined by comparing them to adequate standard curves of cloned and purified target gene copies, and all measurements were based on 1 g of soil (gene copies per g of soil). Standard curves were generated by serial dilutions of target genes (ranging from 10^{-2} to 10^{-7}). Reference DNAs for bacterial *nirS*, *nifH*, *nosZ*, and *amoA* genes were used based on purified gene fragments inserted into either the pEASY-T1 (*nirS*, *nifH*, *nosZ*) or pCR2.1 (*amoA*) cloning vectors and transformed into *Escherichia coli*. All measurements were run in duplicates (= technical replications) on a CFX96 Real-Time System (Bio-Rad, Laboratories GmbH, München, Germany). Precautions were taken to ensure that the data from each duplicate fell within 0.5 threshold cycle (Ct), and clear outliers (>2 standard deviations) were removed before calculating the average Ct of each treatment, with each treatment having three biological replications, resulting in six data points per measurement. Melting curves and non-template controls were used to assess run reliability. There was no detectable amplification arising from non-template controls in any of the assays. The amplification efficiencies of all qPCR assays ranged from 91 % to 98 %, calculated from the equation:

$$Eff = 10 \times \left(\frac{-1}{slope}\right) - 1$$

Archaea-specific qPCRs were conducted to quantify total archaea and *amo*A (AOA) gene copies of archaea, archaea-specific qPCRs were conducted. To quantify the absolute abundance of archaea, the ARC787F_YU, ARC1059R_YU, and ARC915F_YU probe (with 5'-FAM and 3'-TAMRA labels) were used in a TaqMan assay, following the protocol described by (Yu et al., 2005). For quantification of the archaeal AMO alpha subunit (*amoA*) the forward primer amo19F (Leininger et al., 2006) and reverse primer CrenamoA616r48x (Schauss et al., 2009) were used according to the protocol described by Meyer et al. (2013). PCR reactions were conducted in a total volume of 20 µL, containing 10 µL of 2 x Luna Universal qPCR Master Mix (New England Biolabs, Ipswich, USA), 0.1 mg mL^{-1} BSA, 600 nM of each primer and 5 µl of template DNA (1:5 diluted, ca. 10-20 ng μL^{-1}) per reaction. PCR cycling conditions were 10 min at 94 °C, followed by 40 cycles of 45 sec at 94 °C, 45 sec at 60 °C, and 45 sec at 72 °C. The specificity of amplification products employing SYBR green chemistry was confirmed through melting curve analyses after completion of amplification cycles (72-95 °C, Δ 0.5 °C every 5 sec). The quantification of target gene copies was conducted as described above, and reference DNA for total archaea was based on 10-fold serial dilutions of purified PCR product 16S rRNA gene from *Methanobacterium oryzae* (ca 1300 bp, cloned into pGEM-T transformed in *E. coli*). Reference DNA for the archaeal *amoA* gene was based on 10-fold serial dilutions of purified archaeal *amoA* gene fosmid clone 54d9 (656 bp) from *Crenarchaeota* cloned into pCR2.1 and transformed into *E. coli*. Calculations of total archaea and AOA gene copy numbers were performed as described above.

3.2.8 Data analysis

After assessing normality and homogeneity of variances using the Shapiro-Wilkinson and Levene test, respectively, we conducted ANOVA with the Bonferroni correction at $p \leq 0.05$, using the rotational position of WW (two levels) and soil depth (three levels) as fixed factors. When the assumptions of normality were not met, we transformed the data using the Yeo-Johnson transformation (Yeo and Johnson, 2000). The transformation used for a certain variable is mentioned in the respective table. Data analysis was performed with IBM SPSS Statistics for Windows, version 23 (IBM Corp., Armonk, NY, USA). The packages 'ggplot2' (Wickham, 2016) and 'ggstatsplot (Patil, 2021) in R were used to create the graphs and correlograms of Spearman rank correlation matrices.

3.3 Results

3.3.1 Soil mineral N and enzymatic activity at tillering and grain ripening growth stage

At T1, the rotational position of WW strongly influenced soil NO_3^- ($p = 0.002$), soil NH_4^+ ($p = 0.001$), BGU ($p < 0.001$) and LAP activity ($p = 0.007$), while soil depth affected only soil NO_3^- ($p < 0.001$; Table B.1). More specifically, we measured 55.9 % higher NH_4^+ in the soil of W2 compared to W1, which was mainly evident in the 0-30 cm and 30-60 cm layers of the soil (Fig. 3.1a). In the soil of W1, NO_3^- was on average 87.5 % higher than in W2, mainly due to large

differences in the deep subsoil of 60-100 cm (Fig. 3.1b). With respect to enzymatic activity, BGU V_{max} of W2 was 351.4 % higher than in W1, with significant differences in both 0-30 cm and 30-60 cm layers (Fig. 3.1c). The opposite trend was recorded for LAP V_{max} with an 18.3 % reduction in W2 compared to W1 (Fig. 3.1d). At T2, the rotational position of WW significantly influenced soil NO_3^- ($p < 0.001$) and soil NH_4^+ ($p = 0.001$), while BGU and LAP activity remained unaffected (Table B.1). Soil depth had the same main effect on soil NO_3^- ($p = 0.015$) and soil NH_4^+ ($p < 0.001$), with no effect on BGU and LAP activity. We recorded a 24.0 % higher NH_4^+ content in the soil of W1 compared to W2 (Fig. 3.1e) while the opposite was detected for NO_3^-, with a 51.2 % reduction in W1 compared to W2 that was evident throughout the soil profile (Fig. 3.1f). No differences were observed for the enzymatic activity of BGU and LAP between the rotational positions (Fig. 3.1g, h).

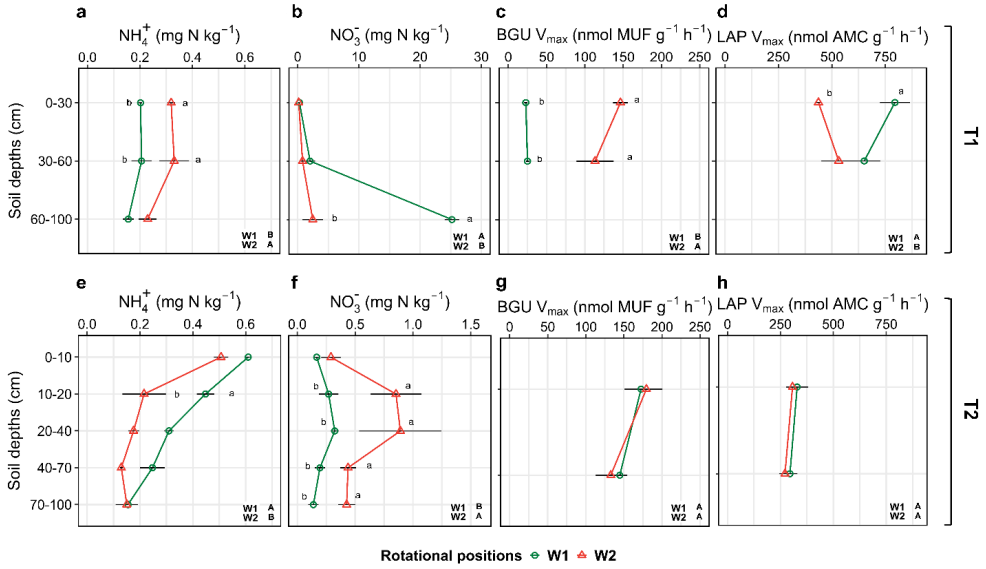

Figure 3.1 Effect of the rotational positions on soil NH_4^+-N (a, e), soil NO_3^--N (b, f), maximum velocity (V_{max}) of β-glucosidase (BGU; c, g) and leucine aminopeptidase (LAP; d, h) of the following winter wheat at tillering (BBCH 29, 28 DAS) and grain ripening (BBCH 90, 180 DAS). W1 = first wheat, W2 = second wheat after oilseed rape. Different uppercase letters in each subplot indicate significant differences between the rotational positions. Within each soil depth, different lowercase letters denote significant differences between rotational positions at $p \leq 0.05$. Four plant replicates were analyzed for mineral N (n = 48 for T1 and n = 40 for T2) and three plant replicates were analyzed for BGU and LAP (n = 24 for T1 and n = 12 for T2).

3.3.2 N-related genes at the tillering and grain ripening growth stage

At T1, there was no significant influence of the rotational position of WW on the absolute abundance of 16S gene copy numbers for both bacteria (Fig. 3.2a, e; Table B.2) and archaea (Fig. B.4a, d; Table B.3) at both WW developmental stages. In contrast, the rotational position of WW ($p = 0.017$) and soil depth ($p < 0.001$) had a significant main effect on the *amoA* gene copy number of AOB (Table B.2), with a much higher *amoA* abundance in the topsoil of W2 compared to W1 (Fig. 3.2b). We also noted a significant increase of bacterial *nifH* gene copy numbers only in the topsoil of W2 compared to W1 (Fig. 3.2c). In addition, both the rotational position of WW ($p < 0.001$) and soil depth ($p < 0.001$) significantly influenced bacterial *nirS* gene copy numbers, with higher bacterial *nirS* abundance in both the top and subsoil of W2 compared to W1 (Fig. 3.2d). At T2, the main effects of rotational position of WW and soil depth were insignificant (Table B.2). However, we did find higher *amoA* copy numbers of AOB and a higher bacterial *nirS* gene abundance in the topsoil of W2 compared to W1 (Fig. 3.2f, h).

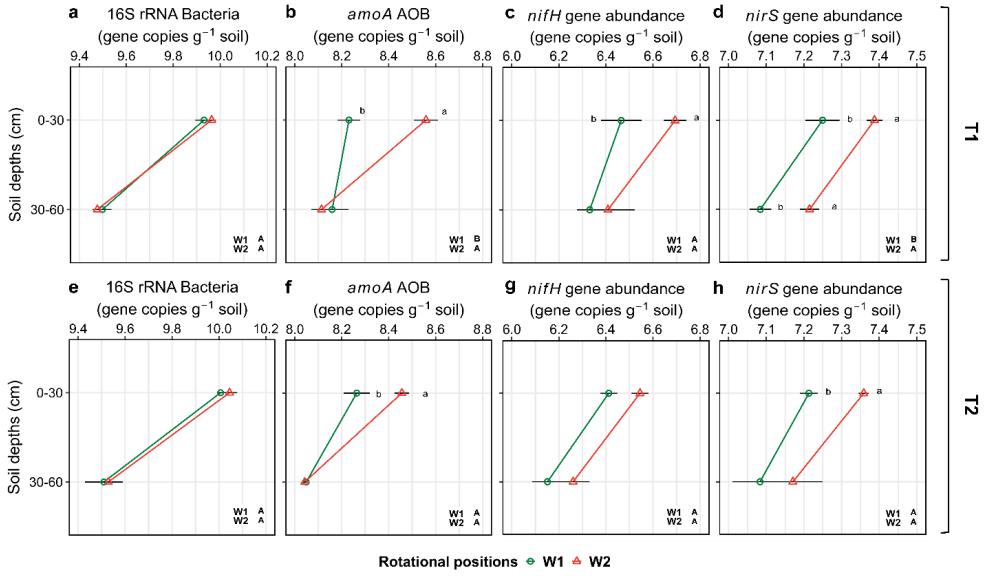

Figure 3.2 Effect of the rotational positions on the 16S rRNA gene copy number of Bacteria (a, e), ammonia-oxidizing bacteria *amoA* gene abundance (AOB; b, f), bacterial *nifH* gene abundance (c, g) and bacterial *nirS* gene abundance (d, h) of the following winter wheat at tillering (BBCH 29, 28 DAS) and grain ripening (BBCH 90, 180 DAS). W1 = first wheat and W2 = second wheat after oilseed rape. Different uppercase letters in each subplot indicate significant differences between the rotational positions. Within each soil depth, different lowercase letters denote significant differences between rotational positions at $p \leq 0.05$. Three plant replicates were analyzed for the response variables (n = 24 for T1 and n = 12 for T2).

At the same time, no differences were evident for bacterial *nifH* gene abundance at this late growth stage (Fig. 3.2g). Finally, no differences were found in *amoA* gene copy number of AOA (Fig. B.4b, e) and bacterial *nosZ* gene abundance (Fig. B.4c, f) between the rotational positions and the sampling time points (Table B.3).

3.3.3 Characterization of the bacterial and archaeal communities

We used 16S rRNA gene amplicon sequencing to characterize the bacterial and archaeal communities obtained from different samples. No significant differences in alpha diversity (microbial diversity within samples) were observed between the specific bacterial and archaeal communities of W1 and W2 at T1 or T2 across all microhabitats (Fig. 3.3a). Regarding beta diversity (comparison among communities), depth and rotation were the primary factors influencing the soil bacterial and archaeal diversity and composition at T1 (Bray-Curtis distances, Depth, $R^2 = 0.10$; Rotation, $R^2 = 0.07$; $p < 0.001$) (Fig. 3.3b). Since the microhabitat (RH and RA) was the variable that affected the bacterial and archaeal communities the least (contributing to 5.2 % of the variation; $p < 0.040$), samples were combined. At T2, without sampling across different microhabitats, rotation and depth continued to shape the soil microbial diversity and composition across different rotational positions (Fig. 3.3c, Depth, $R^2 = 0.16$; Rotation, $R^2 = 0.15$; $p < 0.001$). The ten most abundant taxa, including *Bacillus*, *Gaiella*, and *Sphingomonas*, were the same at T1 and T2, except for a taxon belonging to the family Methyloligellaceae (among the top 10 in T1) and a taxon from the Subgroup 7 (Acidobacteriota; Holophagae; among the top ten at T2). A taxon belonging to the archaeal family Nitrososphaeraceae presented an overall relative abundance of 1.1 % of the total sequences.

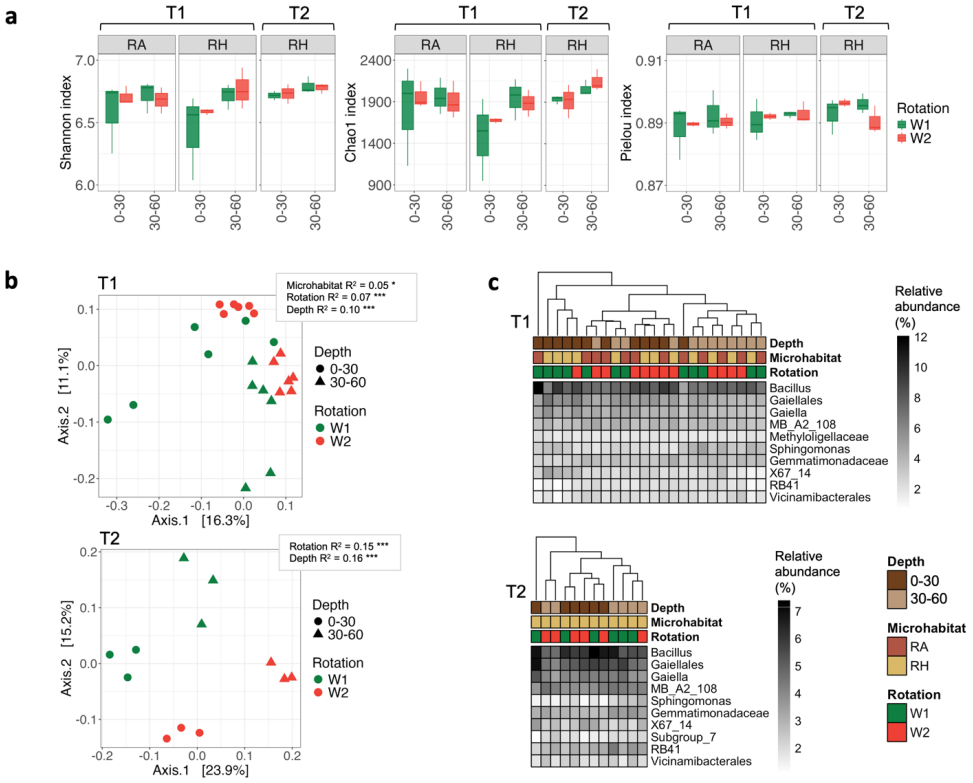

Figure 3.3 Bacterial and archaeal diversity at two plant developmental stages (T1 = BBCH 29, 28 DAS, tillering; T2 = BBCH 90, 180 DAS, grain ripening), separated by soil depth (0-30 cm; 30-60 cm), microhabitat (RA = root-affected soil; RH = rhizosphere), and rotational position (W1 = first wheat after oilseed rape; W2 = second wheat after oilseed rape), based on 16S rRNA gene amplicon sequencing data. (a) Alpha diversity metrics, including Shannon's diversity, Chao1's richness, and Pielou's evenness (analyzed using the Mann–Whitney U test with p-values adjusted by the Bonferroni method). Vertical bars represent standard errors. (b) Beta diversity was measured using Bray-Curtis dissimilarity and visualized through multidimensional scaling (MDS), with statistical analysis performed using PERMANOVA. (c) Relative abundance of the ten most prevalent taxa in T1 and T2. Significance levels: * $p < 0.05$; *** $p < 0.001$. Three plant replicates were analyzed for the response variables (n = 24 for T1 and n = 12 for T2).

When comparing the effect of WW rotational positions on the bacterial and archaeal communities at different plant developmental stages and depths, we observed that significantly more taxa were differentially abundant at T1 than at T2 (Fig. 3.4). At T1 and in the 0-30 cm soil layer, eleven out of twelve differentially abundant taxa were more prevalent in W1, including

Corynebacterium, *Moraxella*, *Neisseria*, *Noviherbaspirillum*, and a taxon belonging to the family Xanthobacteraceae. *Tumebacillus* was the only taxon significantly more abundant in W2 (Figure 4a). At T1 and in the 30-60 cm soil layer, twelve taxa were significantly more abundant in W1 than W2, including *Phenylobacterium* and a taxon belonging to the family Xanthobacteraceae. Conversely, four taxa, including *Dyella* and *Rhodobium*, were more abundant in W2. Notably, *Phenylobacterium* and a taxon from the family Xanthobacteraceae were consistently more abundant in W1 at both depths. At T2, *Shinella* was significantly more abundant in W1 than in W2 in the 0-30 cm soil layer, while the cluster ANPR, *Acinetobacter*, and a taxon from the family Devosiaceae were more abundant in W2 than W1 (Figure 4b). Interestingly, *Caulobacter*, *Gemmatimonas, Streptomyces*, and *Verrucosispora* were more prevalent in W1 compared to W2. In contrast, *Devosia* and a taxon from the same family, Devosiaceae, were among the taxa significantly more abundant in W2 than W1.

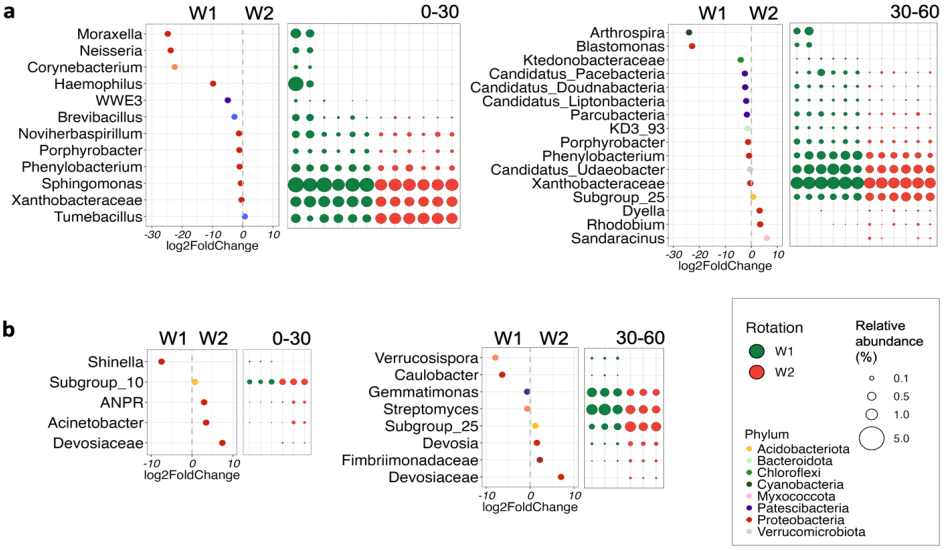

Figure 3.4 Differentially abundant (DA) taxa between crop rotational positions (W1 = first wheat after oilseed rape as a pre-crop; W2 = second wheat after oilseed rape) at two plant developmental stages: (a) T1 (BBCH 29, 28 DAS, tillering) and (b) T2 (BBCH 90, 180 DAS, grain ripening), separated by soil depth (0-30 cm; 30-60 cm). The lowest confident taxonomic classifications are shown, with each corresponding phylum represented by a unique color. Negative log2FoldChange values indicate a significantly higher abundance in W1, while positive log2FoldChange values indicate a higher abundance in W2. The relative abundance of each significantly different taxon is depicted by round shapes, varying in size from 0.1 % to 3 % of the total sequences. *p* values < 0.05 were adjusted using the Benjamini-Hochberg correction. Three plant replicates were analyzed for the response variables (n = 24 for T1 and n = 12 for T2).

Using Tax4Fun2, we searched for the relative abundance of N-related genes that matched genes related to NO_3^-, nitrite (NO_2^-) or ammonia/ NH_4^+ metabolism in the differentially abundant taxa in each group of samples. No statistical significance was found between depths or rotations ($p > 0.05$), except for the decrease in N-related genes in 30-60 cm compared with 0-30 cm in W2 at T1 ($p = 0.002$) (Fig. B.1a). N metabolism regulators, regulatory proteins and components of the NtrC gene family were found in higher abundance at T1, either W1 or W2 samples ($p < 0.01$) (Fig. B.1b). NO_3^-/ NO_2^- response regulators belonging to NarL are significantly higher in T2, 30-60 cm ($p = 0.004$), so as the assimilatory NO_3^- reductase.

Correlation analyses at T1 and in the 0-30 cm soil layer revealed a significant positive correlation between NO_3^- and *Moraxella*, *Neisseria*, *Corynebacterium* and *Haemophilus* in W1, but not in W2 (Fig. B.2). In this soil layer, BGU V_{max} was also positively correlated with LAP V_{max} in W1, but not in W2. Gene abundance of bacterial *nifH* and *nirS* in the topsoil of W2 was positively correlated with *Porphyrobacter* and *Noviherbaspirillum*, respectively, while this was not the case for W1. In the 30-60 cm soil layer, we found a positive correlation between NO_3^- and *Rhodobium* in W1, while in W2 they were negatively correlated (Fig. B.3). Bacterial *nifH* gene abundance positively correlated with *Arthrospira* and *Blastomonas* in W1 and with *Candidatus* Doudnabacteria in W2.

3.3.4 Effect of rotational position on WW biomass accumulation and root growth

The rotational position of WW had a strong effect on plant biomass accumulation. W1 produced 51.5 % more biomass than W2 ($p < 0.001$; Table B.4), mainly due to differences in grain, husk and RDW (Fig. 3.5a). Overall, C:N ratio remained unaffected by the rotational position of WW, but W2 had a higher stem C:N ratio compared to W1 (Fig. 3.5b). Regarding root growth traits we noted a significantly higher RDW ($p < 0.001$; Table B.5; Fig. 3.5c) and root mass density (RMD, $p < 0.001$; Fig. 3.5d) in W1 compared to W2, which was evident throughout the soil profile. Fig. 3.5c and Fig. 3.5d have been adapted from Kaloterakis et al. (2024a).

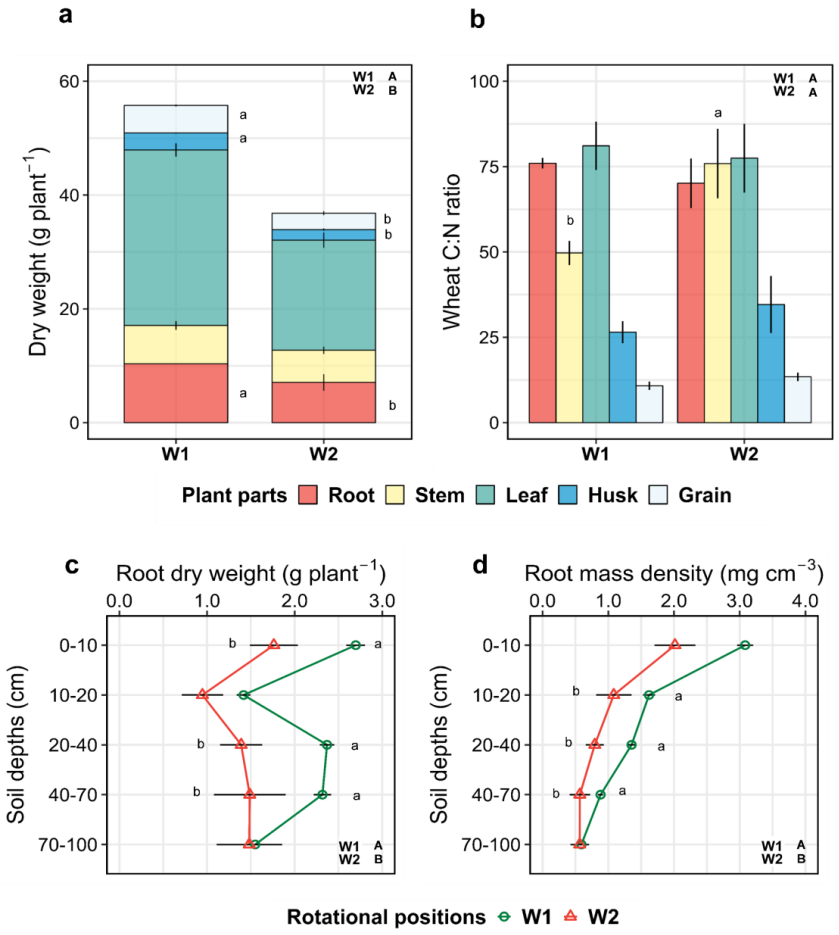

Figure 3.5 Effect of the rotational positions on root, stem, leaf, husk and grain dry weight (a), C:N ratio (b), root dry weight (c), and root mass density (d) of the following winter wheat at grain ripening (BBCH 90, 180 DAS). W1 = first wheat, W2 = second wheat after oilseed rape. Different uppercase letters in each subplot indicate significant differences between the rotational positions. Within each plant part (panels a, b) and soil depth (panels c, d) different lowercase letters denote significant differences between rotational positions at $p \leq 0.05$ level according to ANOVA with Bonferroni correction for multiple comparisons. Fig. 3.5c and Fig. 5d adapted from Kaloterakis et al. (2024b). Four plant replicates were analyzed for the response variables (n = 40 for the response variables).

3.4 Discussion

3.4.1 Distinct soil legacies of the preceding crops on WW growth

The rotational position of WW modulated changes in soil nutrient content, microbial community structure and enzymatic activity, which ultimately translated into yield discrepancies. Given that at the early growth stage of T1 the root system was mainly located in the upper 50 cm of the rhizotrons, the higher NO_3^- content in the 60-100 cm of W1 can be directly linked to the initial soil NO_3^- content at the start of the experiment and the microbial activity (Kaloterakis et al., 2024a). The N-rich residues of oilseed rape (with a lower C:N compared to WW) were mineralized faster, creating an N-rich environment for the following WW. This is also supported by the enhanced LAP activity in W1 compared to W2. LAP activity degrades proteins into amino acids that can be further degraded into ammonia. This higher activity in W1 is likely due to the protein-rich organic material of oilseed rape residues that were decomposing in the soil during WW growth, thus contributing to the higher NO_3^- levels in the soil of W1. On the contrary, the increased BGU activity in W2 compared to W1 can be expected due to the higher C:N ratio of WW residue with a higher cellulose content than that of oilseed rape. At T1, BGU K_m was significantly affected by WW's rotational position and it was significantly higher in W2 compared to W1 meaning that the soil microbes in W2 had a much lower enzymatic affinity for BGU than those in W1 (Table B.6). This means that BGU was released by different microbial groups despite the lack of a significant shift in the bacterial and archaeal community composition. The absence of significant differences for LAP K_m indicates that the bacterial and archaeal communities of W1 and W2 produced more enzymes to degrade the protein-rich organic material in the soil. At T2, both BGU and LAP were released by different microbial groups in W1 and W2, as shown by the significant effect of the WW's rotational position of BGU and LAP K_m (Table B.6).

The soil microbes in the soil of W2 are faced with an early N immobilization in its rhizosphere, which has been previously observed during the early growth of successively grown WW (Kaloterakis et al., 2024b). In the same study, the authors also recorded a much lower root growth in the successive WW rotation, which negatively correlated with soil NH_4^+ as opposed to WW after oilseed rape. Although we did not measure root growth at T1, we nevertheless detected less NH_4^+ in the 0-30 cm and 30-60 cm layers of the soil profile in W1 compared to W2, which might reveal the same mechanism given that we used the same soil from the same experimental plots as Kaloterakis et al. (2024a). This points towards the early disadvantage of the successive WW rotation in accessing available mineral N, and conversely the advantage of W1 with much higher NO_3^- in the deep subsoil of 60-100 cm that is available for plant uptake at later growth stages when the root system is more advanced and the subsoil nutrient and water reserves become increasingly important. Under these temporary N-limiting conditions of W2 soil, increasing BGU activity could be a way for the soil microbes to accelerate the breakdown of the cellulose-rich WW residues.

Regarding the soil legacy of the preceding crop on the bacterial and archaeal alpha diversity, we expected that the rotational position of WW would exert control over the shape of

the bacterial and archaeal community structure. We did not find differences in the diversity and richness metrics of the microbial community between the rotational positions of WW, which is consistent with other studies assessing the effect of the rotational position of WW on bacterial and archaeal diversity (Braun-Kiewnick et al., 2024; Giongo et al., 2024; Kaloterakis et al., 2024b). In contrast, both the rotational position of WW and soil depth had a strong influence on beta diversity in accordance with previous studies (Town et al., 2023; Giongo et al., 2024; Kaloterakis et al., 2024b). The effects on alpha and beta diversity were similar throughout the growth cycle of WW, measured at the tillering and grain ripening stages. It should be noted that we did not measure the fungal diversity and composition, which is considered an additional or complementary driver of the observed yield reduction in the successive crop rotations (Gao et al., 2019; Wang et al., 2019; Sun et al., 2023; Town et al., 2023; Yu et al., 2024).

The differential abundance analysis revealed important shifts in the microbial taxonomic composition, which influenced soil enzymatic activity, N cycling processes and root growth of the following WW. Although our methodology did not allow us to attribute functions to specific microbial groups, we were able to discuss potential functions of previous studies in relation to our study. Town et al. (2023) found a consistent bacterial community composition between monocropped WW and WW after oilseed rape or pea, which contrasts with our findings, possibly due to differences in soil type, which strongly affects microbial assemblages. In our experiment, *Moraxella* was significantly more abundant in the 0-30 cm soil layer in W1 than in W2, at tillering. This is consistent with its role in denitrification (Zheng et al., 2023), which is in line with the higher soil NO_3^- content in W1 at this growth stage. *Neisseria* abundance has been shown to increase in a WW-maize rotation compared to monocropped WW (Navarro-Noya et al., 2013). *Neisseria* is known to enhance cellulose hydrolysis (Sakai et al., 1996), which could have contributed to the higher LAP activity in W1 at T1. The same is true for *Noviherbaspirillum* which includes bacterial species that are involved in cellulose degradation (Maheshwari et al., 2023). Bacilio-Jiménez et al. (2001) linked a *Corynebacterium* species with endophytic growth and growth enhancement in rice, which we found to be significantly more abundant in the topsoil of W1 than W2 at T1 and could have stimulated plant growth at this stage. Certain *Brevibacillus* species have been found to promote organic sulfur and N mineralization, increasing soil NH_4^+ content, which boosts plant growth (Santana et al., 2013, 2021). This is consistent with the higher soil NH_4^+ content in W1 at T2, suggesting that the *Brevibacillus* may be an important genus in the degradation of the protein-rich residues of oilseed rape, thereby increasing mineral N availability for W1 uptake. Adesina et al. (2007) highlighted the antagonistic effect of *Brevibacillus* against *Rhizoctonia solani* and *Fusarium oxysporum*, which are important WW pathogens. Kaloterakis et al. (2024b) suggested that a more beneficial microbial community in W1 might be due to the selection of antagonists that confer protection against soil pathogens. Members of the Xanthobacteraceae family are known to be positively correlated with protease activity and soil DOC (Imparato et al., 2016), thus affecting N cycling and mineral N availability, which was evident in our study by the higher LAP activity at T1 and the higher soil NH_4^+ at T2 in W1.

At the grain ripening stage, we observed a much lower number of differentially abundant taxa at both soil depths compared to the tillering stage, with limited information in the literature

about the potential functions of the different taxa. *Devosia* species are plant-beneficial bacteria (Jeewani et al., 2021; Cerecetto et al., 2024) with antifungal properties (Chen et al., 2022), capable of N fixation (Wolińska et al., 2017), which is in line with the higher *nifH* gene abundance in W2 at T1. Their higher abundance in the subsoil of W2 compared to W1 could be the reaction of W2 plants to enrich their rhizobiome with beneficial microbes due to the potential microbial dysbiosis in the soil that is frequently reported for monocropping systems (Zhou et al., 2023; Giongo et al., 2024). *Gemmatimonas,* a genus associated with organic matter decomposition and high gene copy numbers found in nutrient-rich soils (Banerjee et al., 2016), was more abundant in the subsoil of W1 compared to W2.

3.4.2 The effect of the rotational position of WW on N cycling

We hypothesized that due to changes in soil microbial community structure between the two rotational positions of WW would be accompanied by varying N-related gene abundances. Therefore, we investigated specific functional genes involved in soil N cycling as indicators of ecosystem functionality, involved in key N cycling processes in agricultural soils exposed to single or successional WW cropping. Ammonia-oxidation is the rate-limiting step of nitrification, converting ammonia to NO_2^-, and is catalyzed by AMO, which is encoded by the *amoA* gene (Alves et al., 2018). Elevated *amoA* gene copy numbers have been shown to be positively correlated with the relative abundance of NO_2^- oxidizers from the phylum Nitrospirota (Daims et al., 2015). No differences were observed between W1 and W2 for *amoA* of AOA, which suggests that AOB were the main ammonia-oxidizers in both soils (Sterngren et al., 2015). This is in accordance with previous studies reporting a less important role of AOA in soils with high mineral fertilization (Levičnik-Höfferle et al., 2012; Chen et al., 2023). The higher initial NH_4^+ in W2 at T1 could have stimulated the *amoA* of AOB, due to the increase in available substrate for oxidation. This stimulated nitrification in response to the increased NH_4^+ availability from the decomposing residues of the preceding WW. Over time, this trend weakened, as shown by the insignificant overall main effect of the rotational position on *amoA* of AOB at T2 and the higher NH_4^+ in W1 than W2.

Bacterial *nirK* and *nirS* genes encode NO-producing NO_2^- reductase. NO is then reduced to nitrous oxide (N_2O) during denitrification, further reduced to N_2 by nitrous oxide reductase encoded by *nosZ* (Zumft, 1997). Liu et al. (2023) described crop rotation as an important moderator of N-related genes. Both *nirK* and *nirS* are considered important predictors of N losses via N_2O emissions (Yajun Yang et al., 2022). (Giongo et al., 2024) assessed the relative abundance of bacterial N-cycling genes in the RA, RH and RP soil of two rotational positions of WW, i.e., first WW after oilseed rape and a 15-year WW monocropping in silty loam Luvisol. Although soil depth was an important driver of microbial community composition, they did not find differences between the rotational positions of WW. In our study, although there was no effect of the rotational position of WW on bacterial *nosZ* gene copy numbers, we found a significant increase in *nirS* gene copy numbers in W2 in both topsoil and subsoil at tillering. *nirS* genes are linked to denitrification, the major N loss pathway that reduces NO_3^- to N_2 or N_2O (Wei et al., 2015). The higher bacterial *nirS* gene abundance indicates a higher conversion of NO_2^- to NO in the second step of

denitrification (Wei et al., 2015) and therefore a more active denitrification in W2 compared to W1. Even though we found more NO_3^- in the soil of W1 at T1, the increase of bacterial *nirS* gene copy numbers in W2 suggests that NO_3^- is rapidly used and transformed by denitrifiers and thus lost for uptake by the WW roots. Perhaps, the secretion of certain compounds derived from oilseed rape residues suppresses the denitrifiers, which in turn leads to a higher NO_3^- content in the soil of W1 than W2.

A higher rate of N-fixing bacteria (increase of bacterial *nifH* gene copy numbers that encode for the nitrogenase enzyme) was noticed only at tillering and in the topsoil of W2 compared to W1, possibly hinting at a higher conversion of N_2 to NH_4^+ in the rhizosphere of continuous WW. These N-fixing bacteria seemed to be relatively more abundant under the N-limiting conditions of W2 (Chen et al., 2024), possibly contributing to the increase of soil NH_4^+ from T1 to T2, while the respective increase in soil NH_4^+ from T1 to T2 in W1 was mainly due to enhanced root exudation, growth and turnover (Kaloterakis et al., 2024a). The microbial community is obviously adapting to the initial nutrient limitation (at least during the early growth) by shifting to more N-fixing bacteria. Plants actively participate in this interaction through root exudation to recruit N-fixing microbes under N-deficient conditions (Wassermann et al., 2023), as reflected in the exudation of flavonoids by maize under N-limiting conditions (Yu et al., 2021). The lower and higher activity of LAP and BGU, respectively, in W2, might be indicative of the response of the bacterial community to increasing soil N content by stimulating the breakdown of cellulose-rich residues of the preceding WW and increasing the abundance of *nifH* genes. Under increased soil mineral N content, the relative abundance of *nifH* genes is known to decrease (Hao et al., 2022), similar to what we observed in the soil of W1 at T1. According to the ecological theory, at relatively higher mineral N conditions, diazotrophs will preferentially use mineral N, since it is a more energetically efficient strategy than fixing atmospheric N_2 (Contosta et al., 2011).

3.4.3 Contrasting drivers of soil N cycling among the rotational positions of WW contribute to yield discrepancies

In a $^{13}CO_2$ pulse labeling experiment, (Kaloterakis et al., 2024a) showed that successive WW rotations invest a lower amount of photosynthates above- and belowground compared to WW after oilseed rape, which contributes to reduced plant growth. They also reported a long-lasting effect of increased belowground $^{13}CO_2$ fluxes from flowering until grain ripening for WW grown following oilseed rape. Extending the outcome of this study, we show here that the positive PSF of WW grown after oilseed rape is also strongly related to its ability to utilize the residual soil mineral N pool. We argue that this is mainly due to distinct changes in the N cycling in the soil of W1 compared to W2.

At the grain ripening stage, the higher soil NH_4^+ content in W1 and the lower *amoA* abundance from AOB indicate that, relative to NH_4^+, more soil NO_3^- was taken up by W1 plants compared to W2 and thus significantly less soil NO_3^- was found in W1 soil. The higher nitrification activity in W2 converted more of the available NH_4^+ to NO_3^-, which was not utilized by the plants due to the reduced root growth throughout the soil profile. The higher LAP activity of W1 at

tillering could have stimulated organic N mineralization, resulting in higher NH_4^+ content at the end of the experiment, which was complemented by its larger root system, with a higher amount of root debris and rhizodeposition fueling the turnover of organic matter (Yang et al., 2023).

3.5 Conclusions

We assessed the effect of two rotational positions of WW on soil bacterial and archaeal abundance and their dynamics by measuring extracellular enzymatic activity, N cycling and yield of WW. Our results highlight the vulnerability of successive WW rotations and the benefit of introducing the N-rich oilseed rape in the rotation. The soil legacy of the preceding crops caused distinct PSFs by shaping the microbial communities and enzymatic activities, which affected N availability for the subsequent growth and yield of WW. The higher grain yield in W1 was due to increased root growth and soil mineral N during its early growth phase. Conversely, W2 exhibited distinct responses to the lower initial soil N as observed by the higher abundances of N-fixing genes, nitrification and denitrification-related genes, which were unable to compensate for this early N limitation, resulting in substantial yield losses. This study improves our mechanistic understanding of how the preceding crops influence key rhizosphere processes that create unique soil legacies for the following WW.

4. Reduced belowground allocation of freshly assimilated C contributes to negative plant-soil feedback in successive winter wheat rotations

---

Based on:
Kaloterakis, N., Kummer, S., Le Gall, S., Rothfuss, Y., Reichel, R., Brüggemann, N., 2024. Reduced belowground allocation of freshly assimilated C contributes to negative plant-soil feedback in successive winter wheat rotations. *Plant and Soil*. https://doi.org/10.1007/s11104-024-06696-6

4.1 Introduction

WW is the most cultivated staple crop in the world and a staple food for billions of people worldwide, contributing significantly to many national economies (Shewry and Hey, 2015; Enghiad et al., 2017). Following a linear increase for many decades, annual WW yield growth is currently stagnating, not meeting the forecasted global demand (Calderini and Slafer, 1998; Ray et al., 2013; Moore and Lobell, 2015; Schauberger et al., 2018). A 2.4 % increase in crop yields is required annually to achieve food security by 2050. For WW, the current 0.9 % annual yield growth is markedly lagging behind this target (Ray et al., 2013; Crespo-Herrera et al., 2018). Brisson et al. (2010) attributed this observation to agronomic (cereal rotations with more oilseed rape and fewer legumes, lower N fertilization), climatic (drought stress), and political causes (agricultural policies), while genetic progress did not appear to be an underlying cause.

Plant community diversity and succession has been associated with distinct changes in the abiotic and biotic parameters of the soil exerting positive or negative PSF, de Vries et al., 2023; van der Putten et al., 2013). Among those, changes in nutrient input as well as contrasting quantity and quality (C:N ratio) of plant litter induce significant changes in the microbial community diversity and composition (Bennett and Klironomos, 2019; Thakur et al., 2021; De Long et al., 2023). Linking the PSF theory to arable farming, the beneficial effect of a non-cereal pre-crop on WW productivity has been well established and yet it is estimated that up to 40 % of the global WW cultivation is grown successively (Angus et al., 2015; Yin et al., 2022). This trend is expected to continue in the future due to the focus of agrochemical and breeding companies on the staple crops such as WW (Hegewald et al., 2018). This practice is associated with a high risk of soil-borne pathogens and specifically the necrotrophic fungus Gt, which causes early root senescence, rotting, and yield decline (Cook, 2003; Kwak and Weller, 2013). Gt can persist in the soil as a saprotroph after WW, has been harvested and its severity increases with increasing frequency of WW self-succession (Palma-Guerrero et al., 2021). However, the soil legacy of wheat monocropping is not limited to Gt as this has been observed in years without obvious Gt symptoms, suggesting that other soil microbes might contribute to the observed effect (Arnhold et al., 2023a; Donn et al., 2015). The inclusion of oilseed rape in crop rotations has been widely appreciated for its importance to soil structure, suppression of WW pathogens, high post-harvest residual N and the production of secondary metabolites i.e., isothiocyanate (Sieling et al., 2005; Weiser et al., 2017; Hegewald et al., 2018; Hansen et al., 2019). Therefore, the soil legacy of the WW preceding crop to the following WW can be expected to exert major control over the productivity of WW.

Plants allocate photosynthetic C belowground for root growth and maintenance, as indicated by biomass buildup and root respiration (Jones et al., 2009). A part of that C is exuded from the roots into the rhizosphere, which is a hotspot for microbe-root interactions. This process is termed rhizodeposition and, in combination with root litter and DOC, it constitutes a readily available energy source for soil microorganisms (Kuzyakov and Domanski, 2000; Loeppmann et al., 2019). Rhizodeposition may provide positive or negative feedback for plant nutrient acquisition as indicated by accelerated or decelerated nutrient mineralization by rhizosphere microorganisms (Tian et al., 2013; Cheng and Kuzyakov, 2015; Meier et al., 2017). It has been

established that the rhizodeposition-to-root biomass ratio shows very small variation, meaning that factors affecting root growth are also expected to affect C allocation belowground (Pausch et al., 2013; Heinemann et al., 2023). The combination of heterotrophic microbial respiration of rhizodeposits with autotrophic root respiration constitutes the root-derived CO_2 and can be used to estimate the fate of freshly assimilated C in plants (Loeppmann et al., 2019; Henneron et al., 2022). Whether successively grown WW invests more C belowground to stimulate root growth, root biomass and/or microbial activity, or whether it invests less C belowground due to negative soil legacy of the preceding crop, remains unknown.

^{13}C labeling of plants is a common and valuable approach to distinguish and quantify the rhizodeposited C from native soil organic C (SOC). It allows for the investigation of C allocation patterns throughout the soil and within the different plant parts (Bahn et al., 2013). In addition, recording the time lag between ^{13}C fixation and rhizodeposition belowground provides important information regarding the C use within plants as well as the availability of photosynthates to soil microorganisms (Brüggemann et al., 2011). Studying C partitioning to the different plant parts and to rhizodeposition has great potential to improve our understanding of C allocation patterns in high-input agricultural systems that are governed by intense microbial interactions and often abiotic stress factors. C allocation dynamics vary depending on plant species, plant genotype, plant developmental stage (higher exudation during earlier growth stages), biotic and abiotic factors (Pausch and Kuzyakov, 2018; Williams and de Vries, 2020; Chai and Schachtman, 2022). In WW, higher exudation for increased nutrient uptake is observed from early growth until flowering with a decreasing trend thereafter until full maturity (Sun et al., 2018). At this late developmental stage, C is transported to the head during starch synthesis of the grains (Sun et al., 2019). Rhizodeposition moderates microbial-plant competition by the provision of labile C and the resulting enhanced nutrient cycling when the nutritional demands of the plants are maximal (Hernández-Calderón et al., 2018; Mohan et al., 2020).

In light of no Gt-resistant WW cultivars (Palma-Guerrero et al., 2021), the projected unfavorable climatic conditions for WW cultivation both at European and global scale (Senapati et al., 2021; Zhu et al., 2022) and the premature status of the Gt-specific biocontrol research (Osborne et al., 2018; G. Zhao et al., 2023), there is an urgent need to decipher the mechanisms by which the rotational positions of WW influences its productivity. Here, we investigated how different rotational positions of WW influence the allocation of freshly assimilated C in above- and belowground plant parts and its subsequent translocation to the rhizosphere of WW. We hypothesized that WW self-succession would result in:

I. a limited assimilate supply to the root system and the associated soil microorganisms in successively grown WW due to negative soil legacy feedback and its associated decreased plant and root growth.
II. reduced storage of freshly assimilated C in aboveground plant parts and especially sink organs (grains) due to reduced root performance.

To test these hypotheses, a greenhouse rhizotron experiment was set up with three contrasting rotational positions of WW. The plants were pulse-labeled with enriched $^{13}CO_2$, and the allocation

of freshly assimilated C was traced in the top- and subsoil over a 25-day period, spanning from flowering until grain filling stage.

4.2 Materials and Methods

4.2.1 Experimental design

Soil was collected in September 2020 from the experimental farm Hohenschulen (54°19′05″N, 9°58′38″E), Faculty of Agricultural and Nutritional Sciences, Christian-Albrechts-University of Kiel, Germany. The crop rotation that is implemented in the experimental farm is: faba beans - oats - oil seed rape - WW -WW -WW. The soil is a Cambic Luvisol of sandy loam texture (44 % sand, 35 % silt and 21 % clay; Sieling, 2005) with no carbonates. Soil was collected from the topsoil (0-30 cm) and subsoil (30-50 cm), from W1, first W2 and W4, and sieved to 2 mm. Hereafter, they are referred to as rotational positions. The initial soil properties are summarized in Table 4.1. The WW cultivar "Nordkap" was sown on the plots where the soil was collected. They were fertilized with N (240 kg N ha^{-1} split into three doses of 80 kg N ha^{-1} and applied at BBCH 25, 30/31 and 50/51. The residues of the preceding crop were not removed from the soil, and the field was not plowed before sampling. Note that the presence of Gt experimental plots is well documented (Sieling et al., 2005).

We conducted a greenhouse rhizotron experiment (May 10, 2021 to November 12, 2021), using newly designed rhizotrons with a height of 100 cm, width of 35 cm and inner thickness of 2.5 cm (Reichel et al., 2022). The greenhouse was located on the campus of Forschungszentrum Jülich, Germany. The experiment was organized in a full factorial and completely randomized design, consisting of the three rotational positions W1, W2 and W4 with four replicates each, resulting in 12 experimental units (rhizotrons). The rhizotrons were rotated randomly on a weekly basis. For the online isotopic measurements that are described below, we took measurements of W1 and W4 but not W2, as W1 and W4 comprised the most extreme rotational positions and showed the most pronounced differences in their root growth. Three replicates from W1 and W4 were used for the isotopic measurements. Those rhizotrons were equipped with gas-permeable tubing (KM-PPMF_O-2020-KF-0201, Katmaj Filtration, Poland; 35 cm length, 0.155 cm wall thickness, 0.55 cm i.d., 0.86 cm o.d., 0.2 µm pore size) and polyethylene/aluminum tubing (Synflex® 1300, ¼" o.d., Eaton, Bonn, Germany). The gas-permeable tubing was positioned horizontally in the soil at six depths (5, 15, 25, 35, 65 and 85 cm) and connected to the sampling system with the Synflex® tubing. The tubing was sealed until it was used for the isotopic measurements. In this way, air exchange between the inner volume of the gas-permeable tubing and the ambient air in the greenhouse could be avoided and water vapor loss minimized.

Table 4.1 Initial soil NO_3^-, NH_4^+, plant-available P_{CAL}, K_{CAL}, sulfate (SO_4^{2-}), magnesium (Mg), C:N ratio, pH, DOC, microbial biomass carbon (C_{mic}), microbial biomass nitrogen (N_{mic}) and C_{mic}:N_{mic} for the soil from the different rotational positions. The soil for these analyses was collected from the 0-30 cm soil depth. Data are mean ± S.E. (n = 3 for rotational position). Different lowercase letters in each column denote significant differences between the rotational positions at $p \leq 0.05$ using Bonferroni correction for multiple comparisons. ANOVA main effects of rotational position are indicated as follows: ns = not significant; * $p \leq 0.05$; ** $p \leq 0.01$; *** $p \leq 0.001$.

Soil parameter	Unit	Rotational position			ANOVA
		W1	W2	W4	
NO_3^-	mg N kg^{-1}	3.89 ± 0.03a	3.38 ± 0.11b	3.09 ± 0.00b	***
NH_4^+	mg N kg^{-1}	0.11 ± 0.01	0.14 ± 0.02	0.18 ± 0.03	**ns**
P_{CAL}	mg kg^{-1}	19.3 ± 0.1a	16.1 ± 0.2b	18.4 ± 1.0ab	*
K_{CAL}	mg kg^{-1}	51.3 ± 0.8a	27.8 ± 0.7c	35.4 ± 0.2b	***
SO_4^{2-}	mg kg^{-1}	5.3 ± 0.3a	3.5 ± 0.2b	2.9 ± 0.0b	***
Mg	mg kg^{-1}	75.2 ± 1.7	76.8 ± 1.4	84.6 ± 3.0	**ns**
soil C:N		9.74 ± 0.02	9.63 ± 0.03	9.68 ± 0.08	**ns**
pH		6.73 ± 0.00	6.76 ± 0.01	6.75 ± 0.01	**ns**
DOC	mg kg^{-1}	29.5 ± 0.3a	22.6 ± 0.7b	29.0 ± 0.2a	***
C_{mic}	mg kg^{-1}	57.0 ± 2.0b	41.2 ± 3.4c	75.3 ± 1.2a	***
N_{mic}	mg kg^{-1}	8.2 ± 0.2a	4.3 ± 0.5b	9.3 ± 0.2a	***
C_{mic}:N_{mic}		7.0 ± 0.3b	9.6 ± 0.3a	8.1 ± 0.3b	**

All rhizotrons were kept inclined at 45° to facilitate root growth along the lower side of the rhizotrons. Bulk density was adjusted to 1.45 g cm^{-3} using topsoil (collected from 0-30 cm) for the first 30 cm and subsoil (collected from 30-50 cm) for the following 70 cm. Deionized water was added to reach 70 % WHC (215 g H_2O soil kg^{-1}) at the onset of the experiment. Thereafter, soil moisture was readjusted gravimetrically every 2-3 days to 70 % WHC to ensure well-watered conditions. WW seeds (cultivar "Nordkap") were germinated on petri dishes with sterile filter paper for 24 h in the dark at 20 °C. Subsequently, one germinated seed was sown into each rhizotron. Each plant was fertilized with 0.78 g of calcium ammonium nitrate fertilizer (13.5 % NO_3^-N, 13.5 NH_4^+-N, 4 % CaO, 1 % Mn, YaraBela® CAN™, YARA GmbHand Co. KG, Dülmen, Germany) applied at a rate of 240 kg N ha^{-1}, split to three doses of 80 kg N ha^{-1} each at BBCH 25, BBCH 30/31 and BBCH 50. The plants were harvested at the grain ripening stage (BBCH 92). The environmental conditions during the experiments are shown in Fig. C.4.

4.2.2 $^{13}CO_2$ labeling during flowering

In order to quantify the C allocation pattern above- and belowground, we conducted $^{13}CO_2$ pulse labeling during late flowering (BBCH 69). Technical challenges associated with the automatic manifold system that was used to measure the ^{13}C-CO_2, did not allow for earlier labelling during early flowering. The plants were labeled with highly enriched 99 atom-% ^{13}C-CO_2 (Campro Scientific GmbH, Berlin, Germany). Custom-made polymethyl methacrylate plant chambers (Fig. C.1), constructed by the workshop of Forschungszentrum Jülich were fitted onto the rhizotrons shortly before the labeling. The chamber comprised a 55° triangle-shaped base (opposite of 5 cm × hypotenuse of 6 cm × adjacent 5 cm, wall thickness of 1 cm) with a rubber seal and the plant compartment (height of 60.7 cm, length of 40.7 cm and width of 8.7 cm, wall thickness of 0.35 cm; total volume of 19 240 cm^3). Two fans (252 N. DC axial fan, 12 V, 25 × 25 × 8 mm, EBM-Papst Mulfingen GmbH and Co. KG, Mulfingen, Germany) were fixed at the top corners of the chamber to ensure thorough air mixing. A rubber seal port at the uppermost side of the chamber was used to inject the $^{13}CO_2$.

Prior to $^{13}CO_2$ pulse labeling, we monitored the assimilation rate of unlabeled CO_2 inside the chamber by applying four injections of 20 ml pure unlabeled CO_2 to reach a mixing ratio of 1400 ppm CO_2 in the chamber. This was done to adjust the timing of the $^{13}CO_2$ injections as well as to accurately estimate the $^{13}CO_2$ assimilation time by the plants without the need to keep the gas exchange analyzer connected to the plant chamber during the labeling. Prior to the pulse labeling, the soil surface was covered with thick gas-impermeable foil to minimize diffusion of $^{13}CO_2$ into the soil. Air temperature, relative humidity, and mixing ratio of unlabeled CO_2 was monitored with an infrared gas exchange analyzer (Li-8100, Li-COR, Lincoln, NE, USA). When the plants had assimilated most of the CO_2 and its concentration had dropped to sub-ambient levels, another injection was made to reach a CO_2 mixing ratio of 1500 ppm inside the chamber. We repeated this procedure for a different set of environmental factors (temperature range: 25.5-29.5 °C, relative humidity range: 34-50 %, light intensity range: 243-618 µmol m^{-2} s^{-1}) to obtain accurate information on how the assimilation rate of the unlabeled CO_2 would change with changes in abiotic conditions. For $^{13}CO_2$ labeling, we made four injections of 20 ml of $^{13}CO_2$ (99 atom % ^{13}C) each in 20-min intervals to ensure that adequate amounts of ^{13}C were fixed by the plants.

In order to facilitate the online isotopic measurements, an automatic valve-switching unit was constructed (Fig. C.2) following the setup of Rothfuss et al. (2013, 2015). The time course of soil $\delta^{13}C$ CO_2 at the six abovementioned depths was monitored with an isotope ratio infrared spectrometer (IRIS, Delta Ray™, Thermo Fisher Scientific, Inc., Waltham, MA, USA) after the $^{13}CO_2$ pulse labeling. Data was recorded 2 hours after labeling (0 days after labeling, DAL), for two consecutive DAL and on the tenth and twenty-fifth DAL. Every time we fitted the chamber onto the rhizotron, the soil surface was covered with gas-impermeable foil to prevent gas exchange between the soil and the chamber interior. For the online time-series measurement, we contrasted W1 and W4. W2 plants were also labelled on the same day as W1 and W4 but were not used for these online measurements. The $\delta^{13}C$ was measured at harvest in the plant biomass and in various soil pools in all three rotational positions. The excess ^{13}C CO_2 was calculated based on the atom%

^{13}C excess of every sample, its biomass and C content. All calculations were corrected for the background unlabeled ^{13}C, assuming a $\delta^{13}C$ CO_2 of -27 ‰ of our cereal-dominated soil at the beginning of the experiment. We expressed the excess ^{13}C CO_2 as a flux of $mg^{13}C$ CO_2 min^{-1} by using the flow rate of 100 mL min^{-1} of CO_2-free air that was used in the automatic manifold system and the CO_2 measurements at each soil depth.

4.2.3 Plant harvest and analyses

At harvest (BBCH 92) the aerial plant parts were split into pseudo-stems (hereafter called stems), leaves, husks and grains. The rhizotron plates were removed, and the soil profile was then divided into seven layers (0-10, 10- 20, 20-40, 40-50, 50-70, 70-80 and 80-100 cm) and samples from all soil depths were taken. Due to the extensive root growth throughout the rhizotron, there was no root-free BS. Therefore, we considered the soil to be RA. Within every soil depth, several soil aliquots were pooled to form a composite sample and then split into several samples before the analysis. The roots were retrieved after washing off the soil through a 1-mm sieve and stored in 30 % ethanol. They were scanned on a flatbed scanner (Epson Perfection V800 Photo, Epson, Japan) at 600 dpi to retrieve root growth parameters using the WinRhizo® software (Regent Instruments Inc., Quebec, Canada). All plant material was ball-milled (MM 400, Retsch, Germany) and weighed into tin capsules (HEKAtech, Wegberg, Germany) for determination of ^{13}C content of the various plant parts (roots, stems, leaves, husks and grains) using an elemental analyzer coupled to an isotope-ratio mass spectrometer (EA-IRMS, Flash EA 2000, coupled to Delta V Plus; Thermo Fisher Scientific Inc., Waltham, MA, USA).

$$\delta^{13}C = \frac{R_{sample}}{R_{VPDB}} - 1 \quad (1)$$

Where R is the isotope ratio ($^{13}C/^{12}C$) of the sample (R_{sample}) and of VPDB (Vienna Peedee Belemnite, R_{VPDB} = 0.0111802; Werner and Brand, 2001) respectively. The excess ^{13}C of the total plant biomass was calculated based on the atom% ^{13}C excess of every sample, its biomass and C content. All calculations were corrected for the background unlabeled ^{13}C, using the fourth unlabeled replicate of each rotational position.

The chloroform-fumigation extraction (CFE) method (Wu et al., 1990; Joergensen, 1996) was used to estimate C_{mic} and N_{mic}. Ten grams of fresh soil stored at 4 °C were weighed in beakers and placed inside a desiccator. They were incubated with ethanol-free chloroform (80 ml) at room temperature for 24 h. Soil samples were then extracted with 0.01 M $CaCl_2$ and analyzed with a TOC analyzer (TOC-V + ASI-V + TNM, Shimadzu, Japan). Non-fumigated soil samples were extracted with the same protocol. C_{mic} and N_{mic} were estimated as the difference between the extracted C and N from fumigated and non-fumigated soil samples. The correction factors, kEC = 0.45 and kEN = 0.4, were used for the calculation of the extractable part of C_{mic} and N_{mic}. Ten milliliters of extracted fumigated and non-fumigated soil solution were freeze-dried in polypropylene vials and stored in a desiccator until further processing. Then, 120 µl of deionized H_2O were added into every PP vial to solubilize the precipitate. The solution was then pipetted

into 5 mm × 9 mm silver capsules and air-dried for 2 days. The capsules were placed into a desiccator connected to a vacuum pump and incubated with 200 ml HCl for 1 day. After that, they were placed onto a heating plate at 40 °C for 3 hours and stored in the freezer at -20 °C overnight. They were then freeze-dried again and fitted into 10 mm × 10 mm silver capsules before ^{13}C analysis with the elemental analyzer as described before. These steps were done to measure the $\delta^{13}C$ of DOC and C_{mic}. The C_{mic} $\delta^{13}C$ was calculated according to Werth and Kuzyakov (2008). The excess ^{13}C of DOC and C_{mic} was calculated based on the atom% ^{13}C excess of every sample and its DOC and C_{mic}, respectively. All calculations were corrected for the background (initial) unlabeled ^{13}C DOC and C_{mic} values measured at the start of the experiment.

Regarding the initial soil properties, soil samples were analyzed for mineral N, DOC, and TN. They were extracted using 0.01 M $CaCl_2$ (soil-to-solution ratio of 1:4 w/v), vortexed, shaken horizontally for 2 h at 200 rpm, centrifuged for 15 min at 690 × g, filtered through 0.45 µm PP-membrane filters (Ø 25 mm; DISSOLUTION ACCESSORIES, ProSense B.V., Munich, Germany) stored 4 °C and measured on the following day. The pH was measured in the same solution using a glass pH electrode (SenTix® 940, WTW, Xylem Analytics, Weilheim, Germany). NH_4^+ was measured by continuous-flow analysis (Flowsys, Alliance Instruments GmbH, Freilassing, Germany). NO_3^- and SO_4^{2-} were measured by ion chromatography (Metrohm 850 Professional IC Anion – MCS, Metrohm AG, Herisau, Switzerland). DOC and TN were quantified with a TOC analyzer (TOC-V + ASI-V + TNM, Shimadzu, Japan). Magnesium was with inductively coupled plasma optical emission spectroscopy (ICP-OES, iCAP 7600; Thermo Fisher Scientific Inc., Waltham, MA, USA). The P_{CAL} and K_{CAL} were measured with ICP-OES (iCAP 6500; Thermo Fisher Scientific Inc., Waltham, MA, USA) after soil extraction with 0.01 M CAL instead of $CaCl_2$ and following the same extraction protocol as mentioned before.

4.2.4 Data analysis

Data were checked for normality using the Shapiro-Wilkinson test and for homogeneity of variances using the Levene test. For data not meeting the assumptions of normality the Yeo-Johnson (Yeo and Johnson, 2000) and log transformation were applied. The transformation used for a certain variable is mentioned in the respective table that reports the statistical outcome. The factors in the general linear models (GLM) were rotational position (three levels) and soil depth (seven levels). The data on $\delta^{13}C$ of soil respiration measured on five dates was analysed with repeated measures ANOVA. Date (five levels), rotational position (two levels) and soil depth (three levels) were defined as fixed factors. Bonferroni correction was used for multiple comparisons to identify differences between the contrasted factors at $p \leq 0.05$. Data analysis was performed using R and IBM SPSS Statistics for Windows, version 23 (IBM Corp., Armonk, N.Y., USA). Graphs were made with 'ggplot2' (Wickham, 2016) and visualizations of Spearman rank correlation matrices were made with 'ggstatsplot' (Patil, 2021), using R Statistical Software (v4.2.1; R Core Team, 2022).

4.3 Results

4.3.1 Excess ^{13}C fluxes of soil respiration

Online measurement of the pulse-labeled excess 13C of soil respiration at six soil depths revealed different allocation patterns of the freshly assimilated C during flowering of WW (Fig. 4.1). Translocation of photosynthates to greater soil depths (> 30 cm) peaked at two DAL, with a total of 0.006 mg 13C excess min-1 and decreased gradually thereafter until 25 DAL. Rotational position had a strong effect (Table C.1) on root-derived 13C fluxes during the measurement period of 25 DAL. During the first three measurement time points, there were no significant differences between the rotational positions (Fig. 4.1a,b,c). The observations during the last two measurement of 10 DAL and 25 DAL, revealed a strong influence of the rotational position on soil respiration of freshly assimilated C. More specifically, there was 87.2 % higher 13C excess of the soil respired CO2 in W1 compared to W4, with the greater differences been measured in the topsoil layers of 25 cm and 35 cm. Interestingly, the fluxes of 13C-CO2 were 125 % higher in W1 compared to W4 25 DAL. This was evident in both the topsoil (151.7 % increase at 25 cm and 160.9 % increase at 35 cm) and the subsoil (80.1 % increase at 65 cm and 61.9 % increase at 85 cm; Fig. 4.1d,e).

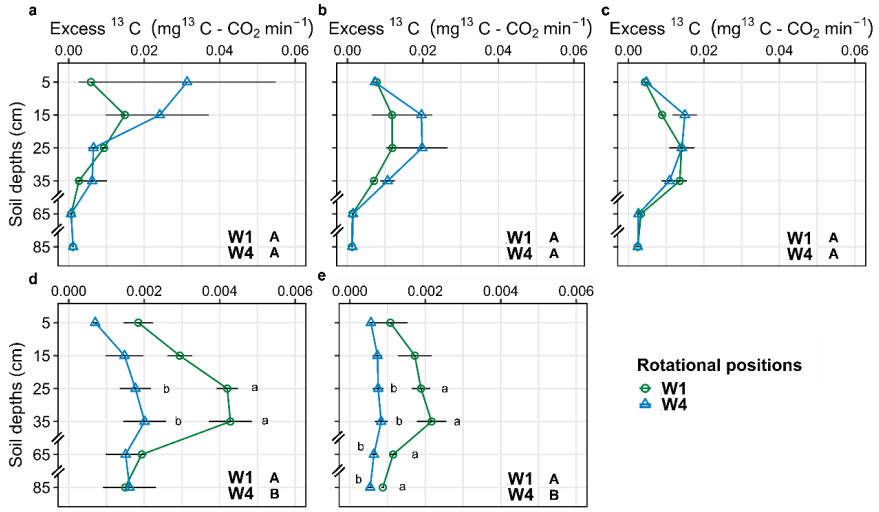

Figure 4.1 Excess ^{13}C of soil respiration in two contrasting winter wheat rotational positions 0 (a), 1 (b), 2 (c), 10 (d) and 25 (e) days after labeling (DAL). Plants were labeled during late flowering (BBCH 69). W1 = first wheat and W4 = fourth wheat after oilseed rape. Different uppercase letters in each subplot indicate significant differences between the rotational positions. Different lowercase letters indicate significant differences between rotational positions at each soil depth at $p \leq 0.05$ level according to repeated measured ANOVA with Bonferroni correction for multiple comparisons.

4.3.2 Plant excess ^{13}C and yield

Rotational position strongly affected (Table C.2) the allocation of freshly fixed C in WW biomass with a significant increase in absolute excess ^{13}C in W1 compared to W2 and W4 (Fig. 4.2). C allocation also strongly varied between plant parts, with 11.1 mg excess ^{13}C measured in leaves, followed by grains (5.7 mg), stems (5.5 mg), husks (3.3 mg) and roots (0.3 mg). Pairwise comparisons between the rotational positions for every plant part followed the overall trend of decreased excess ^{13}C in W2 and W4 compared to W1. More specifically, there was a significant reduction in absolute and normalized excess ^{13}C of W1 compared to W2 and W4 in grain (12.0 mg vs 2.5 mg and 2.7 mg), husk (7.9 mg vs 1.4 mg and 0.5 mg) stem (11.4 mg vs 3.6 mg and 1.7 mg, insignificant for W2) and leaf (23.1 mg vs 2.4 mg and 7.9 mg) ^{13}C in W1 but not in root ^{13}C (0.4 mg vs 0.2 mg and 0.3 mg, Fig. 4,2a,b). W2 plants exhibited a clear shift in their relative allocation of ^{13}C compared to W1 and W4 with lower leaf excess ^{13}C to higher stem excess ^{13}C (Fig. 4.2c). Finally, the biomass data revealed a similar trend, with 51.5 % and 45.0 % higher total plant DW in W1 compared to W2 and W4, which was mainly due to differences in leaf and root biomass (Fig. 4.2d).

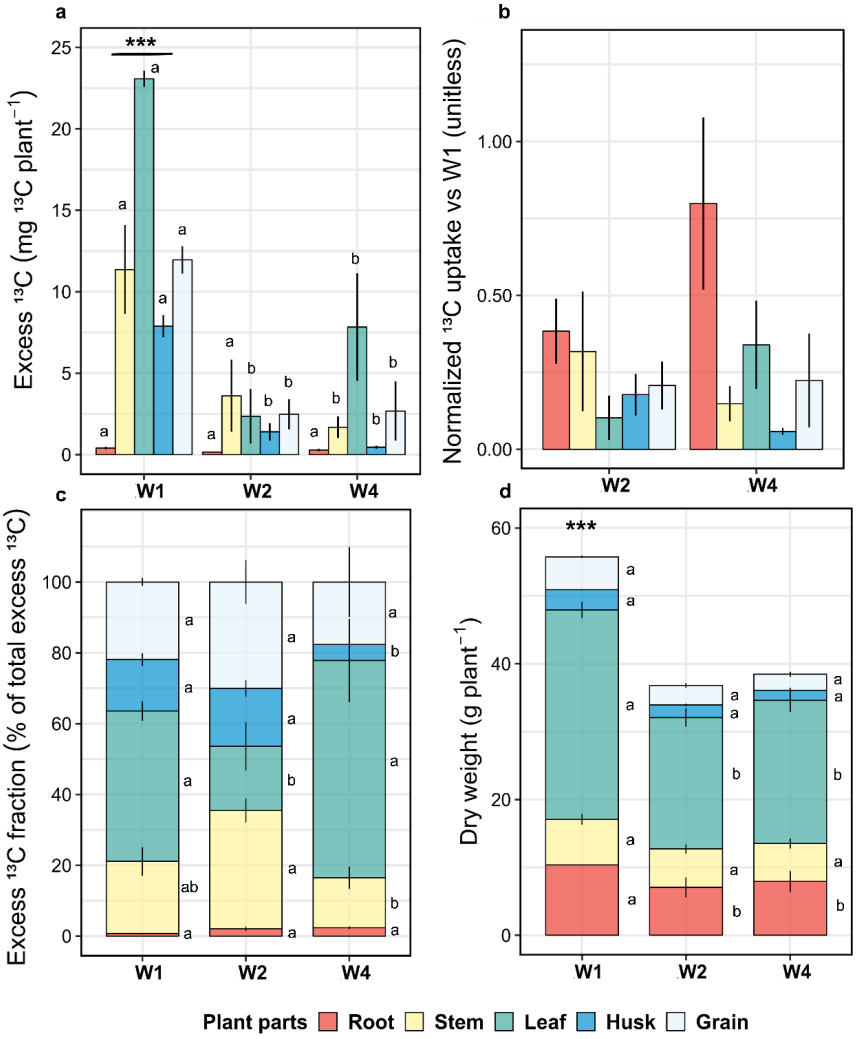

Figure 4.2 (a) Absolute excess ^{13}C, (b) normalized ^{13}C uptake of W2 and W4 compared to W1, (c) relative excess ^{13}C fraction and (d) dry weight of roots, stems, leaves, husks and grains of three rotational positions of winter wheat at grain ripening stage (BBCH 92). W1 = first wheat, W2 = second wheat, and W4 = fourth wheat after oilseed rape. Asterisks indicate significant differences between the rotational positions over all plant parts with $*p \leq 0.05$; $**p \leq 0.01$; $***p \leq 0.001$. Within each plant part, different lowercase letters indicate significant differences between the rotational positions at $p \leq 0.05$ level according to ANOVA with Bonferroni correction for multiple comparisons.

4.3.3 Excess ^{13}C of belowground pools

Freshly assimilated C was also traced in the microbial biomass (excess ^{13}C C_{mic}), DOC (excess ^{13}C DOC) and root (excess ^{13}C root) pool with decreasing amounts at greater depths (Fig. 4.3a,b,c; Table C.3). Rotational positon had a significant impact on the excess ^{13}C of those three pools (Table C.3) with W2 having lower values compared to W1 and W4 overall (Fig. 4.3 a,b,c). Pairwise comparisons revealed a 41.1 % reduction in the DOC excess ^{13}C measured in the 10-20 cm of W2 compared to W1 (Fig. 4.3b). At the same time, there was a 77.1 % decrease in the root excess ^{13}C of W2 compared to W1 in the 0-10 cm soil layer (Fig. 4.3c).

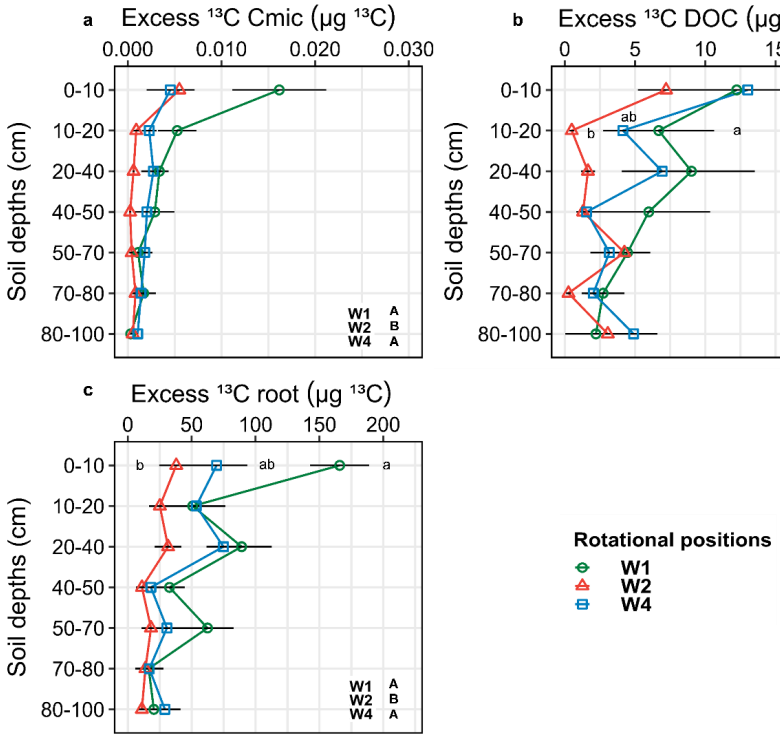

Figure 4.3 Absolute excess ^{13}C of the (a) microbial biomass C (C_{mic}), (b) dissolved organic carbon (DOC) and (c) root biomass in three rotational positions of winter wheat at grain ripening stage (BBCH 92). W1 = first wheat, W2 = second wheat, and W4 = fourth wheat after oilseed rape. Different uppercase letters in each subplot indicate significant differences between the rotational positions. Different lowercase letters indicate differences between rotational positions at each soil depth at $p \leq 0.05$ level according to ANOVA with Bonferroni correction for multiple comparisons.

4.3.4 The effect of rotational position on root growth

There was a significant main effect of the rotational position on RDW, RMD and RLD (Table C.4; Fig. 4.4). W1 had a 46.4 % and 44.2 % higher RDW as well as a 49.9 % and 51.1 % higher RMD compared to W2 and W4. For RDW, the difference was evident in the 0-10 cm and 20-40 cm (Fig. 4.4a) while for RMD, it was evident only in the 20-40 cm (Fig. 4.4b). W1 showed an 36.8 % increase in RLD compared to W2 which was mainly due to differences in both top soil (0-10 cm) and subsoil (40-70 cm and 70-100 cm; Fig. 4.4c). The RLD of W4 did not differ significantly from W1 and was overall 16.1 % lower than W1. There was an indication of lower RLD in the 40-70 cm and 70-100 cm of W4; however, this trend was also insignificant.

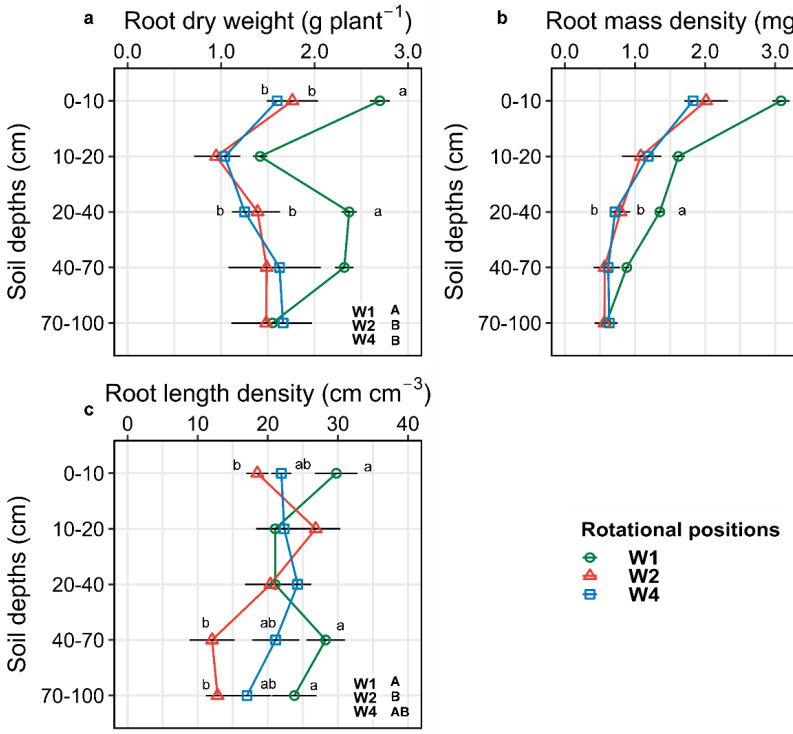

Figure 4.4 Root dry weight (a), root mass density (b) and root length density (c) of three rotational positions of winter wheat at grain ripening stage (BBCH 92). W1 = first wheat, W2 = second wheat, and W4 = fourth wheat after oilseed rape. Different uppercase letters in each subplot indicate significant differences between the rotational positions. Different lowercase letters indicate differences between rotational positions at each soil depth at $p \leq 0.05$ level according to ANOVA with Bonferroni correction for multiple comparisons.

4.3.5 Rotational position-specific correlation analysis

Correlation analysis (Fig. C.5) of the response variables, for each rotational positon, revealed a significant positive correlation between the absolute excess ^{13}C of the root, DOC and C_{mic} in W1.The absolute excess ^{13}C of plant biomass was negatively correlated with RDW and RMD in W1, but positively correlated in W2 and W4. The RLD was positively correlated with plant biomass in W1, but not in W2 and W4. Finally, the RLD of W2 and W4 was negatively correlated with the absolute excess ^{13}C of plant biomass while there was no significant correlation in W1.

4.4 Discussion

Using a novel experimental approach, employing real-time quantification of root-derived ^{13}C from $^{13}CO_2$ pulse labeling, we showed that preceding crop legacy is a strong determinant of the above- and belowground C allocation in WW. To our knowledge, this is the first time that such non-destructive and real-time method is used to track the fate of photosynthesized C and understand the soil legacy effect of preceding crops to WW.

4.4.1 Winter wheat rotational position strongly influences the translocation of freshly assimilated C belowground

Belowground C allocation is a determinant of several processes, including C and N mineralization rates, residue turnover and microbial community composition (Brüggemann et al., 2011; Pausch and Kuzyakov, 2018). Freshly assimilated C has a strong stimulatory effect on rhizosphere processes, including rhizosphere priming and nutrient cycling that are governed by microbial activity (Frey, 2019; Wang et al., 2021). C translocation from WW biomass into soil was already evident two hours post $^{13}CO_2$ labeling with high detectable excess ^{13}C fluxes of the soil respiration (Fig. 4.1). This rapid C translocation to soil has been previously observed in a mountain grassland labeling study assessing diurnal variations in photoassimilate supply to the roots (Bahn et al., 2009). We hypothesized that the soil legacy of successively grown WW will lead to reduced allocation of freshly fixed C due to a negative soil legacy feedback. Initially there was similar excess ^{13}C of the soil respiration in the rhizosphere of W1 and W4. Considering the difference in the C_{mic} of W4 and W1 (Table 4.1), this finding suggests that the microbial community of W1 consumed the rhizodeposits faster than that of W4. The much higher excess ^{13}C of the soil respiration of W1 compared to W4 at 10 and 25 DAL (Fig. 4.1), provides evidence for accelerated senescence of the root system of W4. Increased belowground C allocation can help plants cope with biotic and abiotic stresses by increasing rhizodeposition and investing more in extensive root systems (Sanders and Arndt, 2012; Chandregowda et al., 2023).

In the soil of successive WW cultivation, the lower excess ^{13}C CO_2 of the soil respiration could be a potential strategy to invest more energy into the production of plant defensive secondary metabolites i.e., benzoxazinones to cope with a less favorable microbial community which can come at the expense of biomass accumulation (Bass, 2024; Gfeller et al., 2024). In our experiment, there was no difference in the relative allocation of freshly assimilated C to the root in W2 and W4

compared to W1 suggesting that successive WW (Fig. 4.2) rotations can not overcome the negative PSF by increasing the translocation of freshly assimilated C to the roots. Reduced rhizodeposition could be also complemented by reduced root growth as both can happen simultaneously (Pausch and Kuzyakov, 2018; Heinemann et al., 2023). This was evident in our study, as shown by the marked decline in RDW, RMD and RLD in successive WW rotation and especially in W2 as well as by the negative correlation between biomass and RLD in the successive WW rotations (Fig. C.5). It should be noted that separating autotrophic to heterotrophic respiration is experimentally challenging (Kuzyakov and Larionova, 2005).

4.4.2 Uptake of ^{13}C by the rotational position of winter wheat

The excess ^{13}C of the plant biomass of successively grown WW was much lower than that of WW grown after oilseed rape (Fig. 4.2), which was partially reflected in the lower C translocation belowground (Fig. 4.1). W1 benefited from the preceding oilseed rape with a higher uptake of ^{13}C compared to self-successional wheat, which was accompanied by a much higher biomass, especially leaf biomass. The aboveground allocation of freshly assimilated C therefore contributed to the negative PSF in successive WW rotations. The highest amount of excess ^{13}C was measured in the aboveground plant biomass, followed by soil respiration, extractable DOC, and C_{mic}. This is consistent with a $^{14}CO_2$ pulse labeling experiment with WW, in which most of the recovered ^{14}C was found in plant biomass and soil respiration, whereas root ^{14}C constituted the smallest pool of the total traced C (Sun et al., 2018). Although we observed relatively low ^{13}C enrichment in the root biomass C pool, we found a higher ^{13}C enrichment of the C_{mic} (Fig. 4.3), which is opposite to what has been described previously for wheat (Van de Broek et al., 2020) but also other plant species, such as chicory and alfalfa (Hafner and Kuzyakov, 2016). For the experiment of Van De Broek et al. (2020), this could relate to the much higher amount of ^{13}C label that entered the system with weekly ^{13}C-pulses as opposed to our single ^{13}C-pulse. However, in another ^{13}C-pulse labeling experiment on maize (Meng et al., 2013), the authors found very low recovery rates for root ^{13}C at grain filling stage compared to elongation phase, while they observed the opposite trend for shoot biomass. This can be attributed to the dynamic C investment strategy of plants that prioritize root elongation during tillering for acquiring nutrients and water over root maintenance, while C translocation to the grain is dominant following anthesis (Sun et al., 2018). Indeed, plants allocated a big portion of the labeled C on aboveground plant parts and especially in the leaves and heads, with lower amounts allocated in the stems and roots. This clearly shows a remobilization and increased translocation of the assimilated ^{13}C towards the reproductive plant organ and thus, the grains of the plants. Thus, the differences in the amount and pattern of ^{13}C allocation between W1 on the one hand, and W2 and W4 on the other hand, suggest a change in the plants' growth strategies depending on the rotational position of WW.

4.4.3 The fate of freshly assimilated C belowground

The amount of ^{13}C traced in the microbial biomass can vary greatly depending on the plant species and variety (Elias et al., 2017; Van de Broek et al., 2020). In addition to autotrophic respiration by

the roots, heterotrophic (microbial) respiration substantially contributes to total soil respiration (Brüggemann et al., 2011). In the rhizosphere, heterotrophic respiration is a very important sink of fresh photoassimilates. Similar to other isotopic tracer experiments, we found a strong link between belowground allocation of freshly fixed C and soil respiration, DOC and soil microbial biomass (Bahn et al., 2013; Tavi et al., 2013; Sommer et al., 2016; Weng et al., 2017; Van de Broek et al., 2020). It has been proposed that under conditions of reduced assimilate supply, the lack of carbohydrate reserves in microbes contributes to a faster decline in their respiration rate (Brüggemann et al., 2011). This was not evident in our experiment, as the excess ^{13}C of the soil respiration of W4 was significantly lower compared to W1 during the later growth stage of the plants, while the two rotational positions did not differ in the ^{13}C content of their C_{mic} in the grain ripening stage (Fig. C.3). More importantly, we found a higher excess ^{13}C C_{mic} of W1 and W4 compared to W2 (Fig. 4.3). Both W1 and W4 had higher initial C_{mic} values than W2 at the start of the experiment (Table 4.1), while there was no significant difference among the rotational positions at the end of the experiment (Fig. C.3). This means that the microbial community of W1 and W4 used more freshly assimilated C for growth compared to W2. Previous research has shown the modulating role of the rotational position on microbiome community structure with distinct changes in the relative abundance of various bacteria and archaeal phyla in successive WW rotations (Giongo et al., 2024; Kaloterakis et al., 2024b).

Soil respiration of root-derived ^{13}C in the subsoil was much lower than the topsoil, especially during the first two DAL, while this effect was only partly evident 25 DAL (Fig. 4.1). This means that the soil microorganisms were not severely C-limited in the subsoil even if there were lower ^{13}C amounts of the excess ^{13}C C_{mic}. Therefore, they must have utilized similar amounts of rhizodeposited C under these non C-limiting conditions. This is similar to what Van De Broek et al. (2020) reported, with the topsoil layers being more enriched in $\delta^{13}C_{Cmic}$ compared to the subsoil, but this trend was not significant. Alternatively, it has been proposed that differences in the C use efficiency of the microbes at the different soil depths could explain the insignificant effect of soil depth on $\delta^{13}C_{mic}$ (Li et al., 2021). We also observed a significant main effect of soil depth on the distribution of the excess ^{13}C DOC (Table C.3). This suggests that the ^{13}C pool of DOC was largely influenced by the distribution of root biomass and/or rhizodeposits along the soil profile. In addition, we observed a strong effect of rotational position in the excess ^{13}C DOC. There was more ^{13}C traced in the DOC of W1 compared to W2 in both the top- and subsoil as hypothesized. DOC sources include decomposing C compounds from plant residues and litter as well as root exudates, such as organic acids, amino acids and sugars (Kindler et al., 2011; Panchal et al., 2022). Due to its fast turnover time, DOC is an important pool that encompasses changes in old and new C cycling in the soil, and as such is a major determinant of soil respiration (Brüggemann et al., 2011). Here, we found a strong negative correlation between RLD, excess ^{13}C of the overall plant biomass and specifically of the root biomass (Fig. C.5). Increasing RLD to compensate for the negative soil legacy of self-succession comes at the expense of incorporating less freshly assimilated C into biomass, contributing to the negative PSF in W2 and W4.

4.5 Conclusions

Overall, our results on the ^{13}C traced in soil respiration, plant biomass, labile C and C_{mic} after ^{13}C pulse labeling suggest increased incorporation of recently assimilated C into biomass, followed by increased C translocation to the rhizosphere of WW after oilseed rape compared to successively grown WW. More of this translocated C was incorporated into microbial biomass directly through root exudation or indirectly through the heterotrophic utilization of root litter. The findings of our experiment enhance our understanding on the PSF of contrasting WW rotational positions with respect to above- and belowground allocation of freshly assimilated C. The indirect effect of reduced C allocation in successively grown WW likely caused by a negative soil legacy effect, results in reduced root performance and thus potentially lower yield compared to more complex crop rotations with higher C allocation below ground. The increased and sustained C investment in the root system of W1 is overcompensated by higher and longer overall plant vigor, ultimately leading to higher yield.

5. Compost application compensates yield loss in a successive winter wheat rotation: evidence from a multiple isotope labeling study

---

Based on:

Kaloterakis, N., Rashtbari, M., Reichel, R., Razavi, B.S. and Brüggemann, N. 2025. Compost Application Compensates Yield Loss in a Successive Winter Wheat Rotation: Evidence From a Multiple Isotope Labelling Study. *Journal of Sustainable Agriculture and Environment*. https://doi.org/10.1002/sae2.70079

5.1 Introduction

Due to its high economic importance, higher proportions of WW are added to crop rotations by growing two or more WW crops after a break crop (Kwak and Weller, 2013). On a global scale, up to 40 % of the cultivated WW is grown successively, with only a late summer fallow as a break (Angus et al., 2015; Yin et al., 2022). Growing WW successively in the same field increases the risk of soil-borne infections, such as the take-all disease caused by Gt, which is the most important soil-borne fungal pathogen of WW, causing root rotting and significant yield losses (Cook, 2003; Kwak and Weller, 2013). However, this yield decline has also been observed in years lacking evident Gt infestation (Arnhold et al., 2023a). Recent studies have shown that the soil microbial community structure is affected by the rotational position of WW, suggesting that yield decline in successive WW rotations is a complex phenomenon, not limited to Gt (Giongo et al., 2024; Kaloterakis et al., 2024b).

Adding non-cereal break crops to the rotation, such as oilseed rape, has been shown to enhance the yield of the following WW (Angus et al., 2015; Weiser et al., 2017). The improvement of pathogen suppression, soil aggregation, soil structure and high post-harvest residual N (N; approximately 70 kg N ha^{-1}) are among the most frequently reported benefits of oilseed rape addition to the rotation, although it might come at the expense of increased environmental N losses (Sieling et al., 2005; Sieling and Kage, 2006; Weiser et al., 2017; Hegewald et al., 2018; Hansen et al., 2019; Kerdraon et al., 2019). In successive WW rotation, this beneficial effect is missing, and the following WW experiences a long-lasting growth reduction that is exacerbated by reduced plant and soil C allocation and plant nutrient uptake. Previously, successive WW rotations have been associated with divergent bacterial and archaeal communities (Giongo et al., 2024; Kaloterakis et al., 2024b) and C allocation patterns (Kaloterakis et al., 2024a). Whether the beneficial effect of oilseed rape can be achieved in successive WW rotation by adopting certain management practices, such as incorporating organic fertilizers, remains unknown.

The use of OA, such as compost, could increase the productivity of conventional farming systems in a sustainable manner (Keeling et al., 2003; Lee et al., 2021) by promoting the build-up of SOM and nutrient supply to plants, while avoiding nutrient losses, mainly through leaching (Agegnehu et al., 2017; Heisey et al., 2022; Duan et al., 2023). OA have been recognized for their multifunctionality in agricultural production mainly due to their high SOM content and, in the case of compost, plant-available N, P_{CAL} and K_{CAL} (Siedt et al., 2021; Nobile et al., 2022). OA positively influence soil structure and C storage, with organic C acting as a soil-binding agent, which improves soil aggregation (Siedt et al., 2021). Compost effectively prevents C mining and loss of stabilized native SOM by providing labile C for microbial uptake, thus contributing to C stabilization in the soil (Wang et al., 2022). Soil microbes preferentially use the labile C substrate from the compost and reduce decomposition of the relatively stable SOM, causing a negative priming effect (Dijkstra et al., 2013). Depending on the soil depth at which the compost is applied, the associated increase in SOM is expected to have a positive effect on water retention and potentially on water uptake by plants, especially in deeper soil layers (Uhlig et al., 2023; Feifel et al., 2024). OA have also been found to increase plant water uptake and help plants recover quickly

from drought, although this effect is likely to be dependent on the components of the compost (Nguyen et al., 2012; Kowaljow et al., 2017; Soudek et al., 2024).

The ability of compost to influence the C transfer between plants and microbes may be an appropriate strategy to mitigate yield losses in successive WW rotations. By increasing the substrate availability for microbes, compost can stimulate enzymatic activities and promote plant nutrient availability and uptake, especially under the limited N supply conditions of successive WW rotations. Tilston et al. (2005) reported a benefit of the application of green-waste compost in reducing take-all severity and yield losses in WW, showing that compost application not only provides plant-available nutrients, but also supports microbial activity and enhances plant health. Thus, the multifunctionality of compost offers an effective soil management practice to address the yield decline in successively grown WW by addressing multiple soil health aspects.

However, the key question remains open whether the benefits of compost application influence the processes that are already occurring in the rhizosphere of WW, which in turn are influenced by the soil legacy of the preceding crop, such as rhizodeposition. Plants allocate a significant fraction of the assimilated C below ground through active and passive processes such as root respiration, root exudation, emission of volatile organic compounds, mucilage production and root wilting (Brüggemann et al., 2011; Kuzyakov and Xu, 2013). For WW, an estimated 20-30 % of this assimilated C is deposited in the soil via the roots (Kuzyakov and Domanski, 2000; Loeppmann et al., 2019). This labile C is fueling microbial activity and its associated nutrient cycling in the soil, and this process is particularly intense in the rhizosphere (Jones et al., 2009). In fact, plants actively recruit microbial taxa that compete with pathogens for the available resources in the rhizosphere, produce inhibitory metabolites that prevent pathogen growth, mobilize nutrients or influence plant hormonal expression (Philippot et al., 2013).

Recent studies have explored the mechanisms underlying yield decline in successive WW rotations (Kaloterakis et al., 2024a, 2024b), but the influence of compost on the rhizosphere processes of successive WW rotations and potential mitigating mechanisms for the associated yield decline remain unknown. Therefore, our objectives were to: 1) assess the potential of green-waste compost (referred to as compost hereafter) application to compensate for yield losses in successive WW rotations, and 2) assess the effect of compost application on plant and soil C allocation patterns, plant N uptake and water uptake in contrasting WW rotations. We hypothesized that (i) there would be reduced C allocation above- and below ground in the successive WW rotation, while compost application would increase C allocation above- and below ground and stimulate microbial activity by enhancing C and N cycling enzymatic activity, and (ii) this would result in enhanced root growth, followed by increased N uptake, enhanced subsoil water uptake and finally increased yield. To test these hypotheses, an outdoor mesocosm experiment was conducted, contrasting two rotational positions of WW, i.e., WW grown after oilseed rape compared with WW grown in self-succession. We combined biochemical, enzymatic and isotopic analyses to assess nutrient and C availability in the soil of the different rotational positions and to understand the potential mechanisms of underlying compost effects on the successive WW rotation.

5.2 Materials and Methods

5.2.1 Experimental design

The soil used in the experiment was collected from an experimental farm located near Harste in Germany (51°36′23.5″N, 9°51′55.8″E) and was classified as a silty loam Luvisol. A detailed overview of the agricultural management and the crop rotations that were implemented on the farm, has been provided by Arnhold et al. (2023b). The soil was collected from 0-30 cm and 30-50 cm soil depth after one season of oilseed rape cultivation and after one year of WW after oilseed rape cultivation. After the harvest of the preceding crops, the plant residues were not removed from the field and the soil was not ploughed before the soil was collected for the experiment. The following rotational positions of WW were simulated in this study, after sowing WW on the collected soil: 1) W1, and 2) W2, each treatment replicated six times.

Table 5.1 Initial soil NO_3^-, NH_4^+, plant-available phosphorus (P_{CAL}), plant-available potassium (K_{CAL}), sulfate (SO_4^{2-}), magnesium (Mg), C:N ratio, pH, DOC, microbial biomass carbon (C_{mic}), microbial biomass nitrogen (N_{mic}) and C_{mic}:N_{mic} for the soil from the different rotational positions. The soil for these analyses was collected from the 0-30 cm soil depth. Data are mean ± S.E. (n = 3 for rotational position). Different lowercase letters in each column denote significant differences between the rotational positions at $p \leq 0.05$ using Bonferroni correction for multiple comparisons. Main effects identified by ANOVA of rotational position are indicated as follows: ns = not significant; * $p \leq 0.05$; ** $p \leq 0.01$; *** $p \leq 0.001$.

Soil parameter	Unit	Rotational position		ANOVA
		W1	W2	
NO_3^-	mg N kg^{-1}	18.0 ± 0.06a	12.5 ± 0.73b	**
NH_4^+	mg N kg^{-1}	0.14 ± 0.02	0.12 ± 0.01	**ns**
P_{CAL}	mg kg^{-1}	40.4 ± 0.2	35.5 ± 1.9	**ns**
K_{CAL}	mg kg^{-1}	58.8 ± 0.4a	27.3 ± 5.0b	**
SO_4^{2-}	mg kg^{-1}	7.0 ± 0.2ba	1.8 ± 0.1b	***
Mg	mg kg^{-1}	72.5 ± 0.8a	47.0 ± 1.2b	***
soil C:N		8.75 ± 0.12	8.93 ± 0.12	**ns**
pH		6.81 ± 0.003	6.79 ± 0.004	**ns**
DOC	mg kg^{-1}	38.9 ± 0.3a	30.9 ± 0.6b	***
C_{mic}	mg kg^{-1}	70.4 ± 2.4a	52.3 ± 4.2b	*
N_{mic}	mg kg^{-1}	10.2 ± 0.3a	5.6 ± 0.4b	***
C_{mic}:N_{mic}		6.9 ± 0.04b	9.3 ± 0.06a	***

We conducted an outdoor experiment (November 8, 2022 to July 18, 2023) using custom-made cylindrical polyvinyl chloride (PVC) sewage pipes (135 cm height, 10.5 cm inner diameter,

Fig. D.1b) with a perforated PVC sleeve at the bottom for drainage. Two opposite sides of the pipes were perforated vertically with resealable 20-mm holes to enable soil sampling during plant growth. The distance between the holes was 5 cm for the first 30 cm of the pipe, followed by 10 cm distance between the holes for the remaining depth of the pipe. Custom-made PVC screws were inserted in every hole and sealed with O-rings. The pipes were placed inside the empty space of a lysimeter pit (120 cm depth × 105 cm width × 105 cm length) in an outdoor lysimeter area of Forschungzentrum Jülich, Germany (50°54′31.9″N 6°24′11.0″E). To expose the plants to realistic field conditions, we placed two layers of Styrofoam™ in the first 42 cm of the pit. Six 10.5-cm holes were created in the Styrofoam™ to insert the pipes and minimize air exchange between the pit and the environment (Fig. D.1a). The treatments included the W1 and W2 rotational position without and with compost (W1C and W2C) with 6 replicates each. We used a total of 4 pits and 24 pipes. The experimental unit was the pipe, in which a single plant was growing. A temperature sensor was placed in two of the four pits at a depth of 70 cm to record temperature fluctuations throughout the experiment.

Green-waste compost (GABCO Kompostierung GmbH, Würselen, Germany) was applied at a rate of 40 t fresh mass ha^{-1} once and thoroughly mixed with the top soil (0-30 cm) of each pipe before sowing. The compost consisted of kitchen and green waste (gardening and landscaping waste, including tree and hedge cuttings, plant leaves and grass clippings). The compost contained (on a fresh mass basis): 30.7% water, 21.6% C, 1.29% total N (C:N ratio of 13), 1.19 % organic N, 0.97 % mineral N (95 % NH_4^+-N and 5 % NO_3^--N), 0.3% total P 1 % total K, 0.31 % total Mg and had a pH (1:5 w/v H_2O) of 9.1. The composition of the compost was certified by the German Institute for Quality Assurance (RAL Deutsches Institut für Gütesicherung und Kennzeichnung e.V., Bonn, Germany).

Soil bulk density was adjusted to 1.35 g cm^{-3} in the topsoil and to 1.45 g cm^{-3} in the subsoil (30-100 cm). The bottom 30 cm of the pipes was filled with 1.80 g cm^{-3} quartz sand for drainage. Deionized water was added to adjust soil moisture to 70 % water-holding capacity (corresponding to 227 g H_2O soil kg^{-1}) at the onset of the experiment. Thereafter, the plants were kept rain-fed throughout the experiment (Fig. D.2). WW seeds (cultivar "Nordkap") were germinated on a Petri dish with sterile filter paper for 24 h in the dark at 23 °C. Subsequently, one germinated seed was planted into each pipe. The plants were fertilized with 80 kg N ha^{-1} of calcium ammonium nitrate (CAN, 13.5 % NO_3^--N, 13.5 % NH_4^+-N; Raiffeisen Waren-Zentrale Rhein-Main eG, Cologne, Germany) at BBCH 25, 30/31 and 50/51, resulting in a total of 240 kg N ha^{-1} applied throughout the experiment. The fertilizer was mixed with 10 atom% $(^{15}NH_4)_2SO_4$ (Merck KGaA, Darmstadt, Germany) to reach a target $\delta^{15}N$ of 5000 ‰.

5.2.2 $^{13}CO_2$ pulse labeling at early flowering

When the plants reached early flowering (BBCH 60/61 at 205 DAS, hereafter called T1), we conducted $^{13}CO_2$ pulse-labeling. First, the soil surface was covered with a thick gas-impermeable PVC membrane to minimize diffusion of $^{13}CO_2$ into the soil. Thereafter, custom-made polymethyl methacrylate plant chambers, constructed by the workshop of Forschungszentrum Jülich, were fitted onto the pipes shortly before the labeling. The chamber consisted of a base (3 cm height ×

10.5 cm diameter; 0.35 cm wall thickness) and the plant compartment (60 cm height × 20 cm diameter; 0.35 cm wall thickness). Two fans (252 N. DC axial fan, 12 V, 25 × 25 × 8 mm, EBM-Papst Mulfingen GmbH and Co. KG, Mulfingen, Germany) were fixed at opposite sides of the upper part of the chamber for air mixing. A rubber seal port on the top plate of the chamber was used to inject the $^{13}CO_2$, while another port was used to measure the temperature inside the chamber. $^{13}CO_2$ pulse labeling was done by injecting 20 mL of 99 atom-% ^{13}C-CO_2 (Campro Scientific GmbH, Berlin, Germany) inside the chambers. Prior to $^{13}CO_2$ pulse labeling, we monitored the decay rate of unlabeled CO_2 inside the chamber by injecting 20 mL of pure unlabeled CO_2 to reach a mixing ratio of 1500 ppm CO_2 inside the chamber. This allowed us to adjust the timing of the CO_2 injections and to record the CO_2 assimilation time of the plants. Air temperature, relative humidity, and mixing ratio of unlabeled CO_2 was monitored with an infrared gas exchange analyzer (Li-8100, Li-COR, Lincoln, NE, USA). When the concentration dropped to sub-ambient CO_2 levels, another injection of 20 mL was made to reach a CO_2 mixing ratio of 1500 ppm inside the chamber. For $^{13}CO_2$ labeling, a total of three injections of 20 mL of $^{13}CO_2$ each were made in 20-min intervals to ensure that a sufficient amount of ^{13}C was fixed by the plants.

5.2.3 $^{1}H^{2}HO$ and $H_2{}^{18}O$ labeling and soil sampling at flowering and grain ripening

Three days after the $^{13}CO_2$ labeling, the first soil sampling was conducted by temporarily lifting the pipes out of the pits to gain access to the holes on the side of the pipes and to collect soil. From each of three soil depths (0-30 cm, 30-60 cm and 60-100 cm), we sampled 60 g of soil with 20 g sampled from each of the three holes per depth using metal spatulas. The collected soil was then thoroughly mixed and divided into several subsamples for the various laboratory analyses. Subsequently, 90 ml of $^{1}H^{2}HO$ (enriched at $\delta^{2}H$ = 43000 ‰) and $H_2{}^{18}O$ (enriched at $\delta^{18}O$ = 5000 ‰; Cortecnet Europe, Les Ulis, France) were injected into the soil at a depth of 25 cm and 50 cm, respectively. The amount of water injected corresponded to the amount needed to increase the water-holding capacity from 60 to 100% in a 5 cm layer of soil.

The plants were harvested when they had reached the grain ripening stage (BBCH 90 at 252 DAS, hereafter called T2). The aboveground plant parts were divided into pseudostems (hereafter called stems), leaves, husks and grains. The pipes were then cut into three parts, i.e., 0-30 cm, 30-60 cm and 60-100 cm, and soil was sampled for the different analyses. For both soil sampling time points (T1 and T2), subsamples from all the side holes of each soil depth were pooled and mixed to form a composite and representative sample for each soil depth. They were stored in the freezer at -25 °C before processing. For the analysis of soil enzymatic activity, the samples were stored in the fridge at 4 °C and analyzed within one week. The roots were also retrieved after washing off the soil through a 1-mm sieve and stored in 30% ethanol. They were scanned at 600 dpi (Epson Perfection V800 Photo, Epson, Japan) and analyzed with the software WinRhizo® (Regent Instruments Inc., Quebec, Canada). The following root growth traits were measured: root length, R_{dia}, root surface area and root volume. Seven root diameter classes were selected: 0-0.05 mm, 0.05-0.1 mm, 0.1-0.5 mm, 0.5-1 mm, 1-1.5 mm, 1.5-2 mm, ≥ 2 mm. Using

these root growth traits, the RLD, the SRL and the proportion of root length were computed for the seven root diameter classes. Estimates of RTD were made as described in Rose (2017). Plant DW was determined after oven-drying at 60 °C to constant weight (for a maximum of three days). Ball-milled (MM 400, Retsch, Germany) plant and soil samples were weighed into tin or silver capsules (HEKAtech, Wegberg, Germany) for determination of $\delta^{13}C$, $\delta^{15}N$, $\delta^{2}H$ and $\delta^{18}O$ using an elemental analyzer coupled to an isotope-ratio mass spectrometer (EA-IRMS, Flash EA 2000, coupled to a Delta V Plus; Thermo Fisher Scientific Inc., Waltham, MA, USA). All biochemical analyses were performed as described in detail in Kaloterakis et al. (2024b). The quantification of isotopes and isotopic calculation were done as described in Kaloterakis et al. (2024a). Calculations for the atom% ^{2}H and ^{18}O of the biomass were corrected for the background (initial) unlabeled ^{2}H and ^{18}O content of the different plant parts using the following values for ^{2}H and ^{18}O, respectively: 39.3 ‰ and -32.9 ‰ for the grains, 33.3 ‰ and -88.7 ‰ for the husks, 20.5 ‰ and -128.6 ‰ for the leaves, 27.2 ‰ and -99.1 ‰ for the stems, and 25.1 ‰ and -88.1 ‰ for the roots. These values were obtained from earlier experiments, and since the ^{2}H and ^{18}O enrichment levels were very high and the labeling uniform throughout the plants, the comparisons between the treatments are sufficiently precise.

5.2.4 Statistical analysis

The following fixed factors were included in the analysis: rotational position (W1 and W2), OA (with and without compost application) and, whenever applicable, soil depth (0-30 cm, 30-60 cm and 60-100 cm) and plant part (grain, husk, leaf, stem and root). The following statistical analysis was performed in R (v4.2.1. (R Core Team, 2022). We conducted PERMANOVA with 10,000 permutations using the 'vegan' package (Oksanen et al., 2022) to account for deviations from normality and homoscedasticity of the data, using the Benjamini-Hochberg *p* adjustment procedure to control the false discovery rate. We conducted follow-up between-subjects t-tests with the 'RVAideMemoire' package in R (Hervé, 2023). The significance threshold was set to $\alpha = 0.05$. Visualizations of Spearman rank correlation matrices were made with 'ggstatsplot (Patil, 2021) for the response variables and for each rotational position of WW with and without OA application. Graphs were generated with the 'ggplot2' package (Wickham, 2016).

5.3 Results

5.3.1 Soil biochemical properties at T1 and T2

At T1, we found a significant effect of the rotational position, compost application and soil depth on soil NO_3^- and NH_4^+ (Table D.1). More specifically, the topsoil of W1 had the lowest concentration of NO_3^-, followed by W1C and W2C. W2 had 164.9% and 250.0% higher NO_3^- content compared to W1C and W1, respectively, with no significant difference between W2 and W2C (Fig. 5.1a). In the 60-100 cm layer, W2 had 150.2% higher NO_3^- content compared to W2C.

Compost addition increased the soil NH_4^+ content of both rotational positions, with 235.9% higher soil NH_4^+ in W1C compared to W1, and 180.3% higher soil NH_4^+ in W2C compared to W2

(Fig. 5.1b). Compost amendment also increased the overall DOC content of W2C by 45.7% compared to W2, with no obvious differences between W1, W1C and W2. (Fig. 5.1c). C_{mic} was also significantly elevated by 22.5% in the 60-100 cm layers of W2C compared to W1, W1C and W2 (Fig. 5.1d). The V_{max} of BGU was significantly increased in the compost-amended W1C (Fig. D.3a), while the highest V_{max} of LAP was found in W1 compared to W1C, W2 and W2C (Fig. D.3b). At T2, there were no differences in NO_3^-, NH_4^+ and DOC between the rotational positions with and without compost addition (Table D.2; Fig. 5.1e, f, g). However, there was a 41.8% and 25.4% higher C_{mic} in W2C compared to W1 and W2, respectively, in the topsoil (Fig. 5.1h).

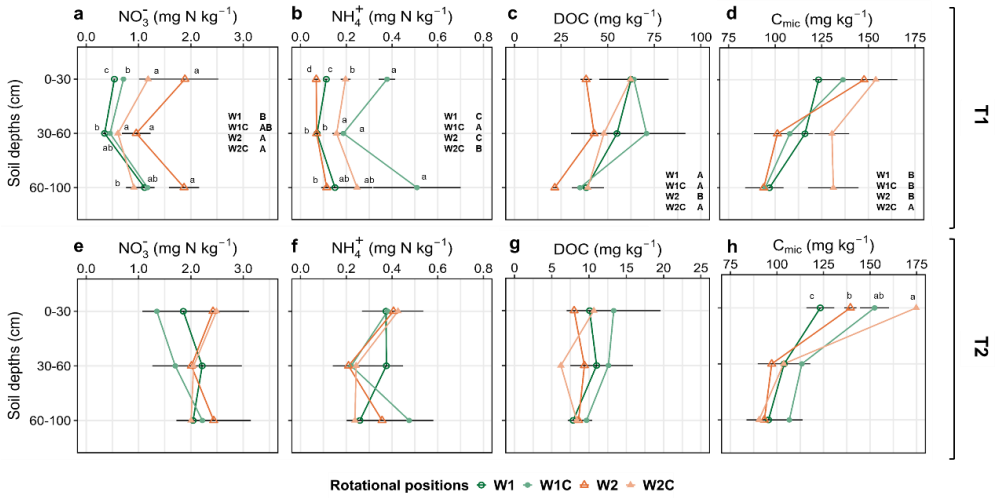

Figure 5.1 Effect of the rotational positions on soil NO_3^--N (a, e), soil NH_4^+-N (b, f), dissolved organic C (DOC; c, g) and microbial biomass C (C_{mic}; d, h) of the following winter wheat at flowering (BBCH 61, T1) and grain ripening (BBCH 90, T2), for the first wheat after oilseed rape without (W1) and with (W1C) compost addition, and the second wheat after oilseed rape without (W2) and with (W2C) compost addition. Different uppercase letters in each subplot indicate significant differences between the rotational positions. Within each soil depth, different lowercase letters denote significant differences between rotational positions at $p \leq 0.05$ level according to PERMANOVA with Benjamini-Hochberg *p* adjustment. Absence of letters indicates non-significant differences.

5.3.2 Belowground allocation of ^{13}C and ^{15}N at T1 and T2

An 18.1% higher absolute excess of ^{13}C (hereafter called ^{13}C excess) of the soil in W2C compared to W1 was found in W2C at T1 across all depths (Fig. 5.2a). Soil was significantly enriched in ^{13}C in the compost amended rotational positions, which was not the case for the ^{13}C excess of DOC and C_{mic} (Table D.1). However, we found higher ^{13}C excess of DOC in W2C and W2 compared to W1 (Fig. 5.2b), with no differences in ^{13}C excess of C_{mic} and ^{15}N excess of the soil between the

rotational positions (Fig. 5.2c, 2d). At T2, soil depth and not rotational position or compost application had a significant main effect on the abovementioned response variables (Table D.2; Fig. 5.2e, f, g), except the ^{15}N excess of the soil, where a higher ^{15}N excess in W1 and W1C was observed compared to W2C (Fig. 5.2h).

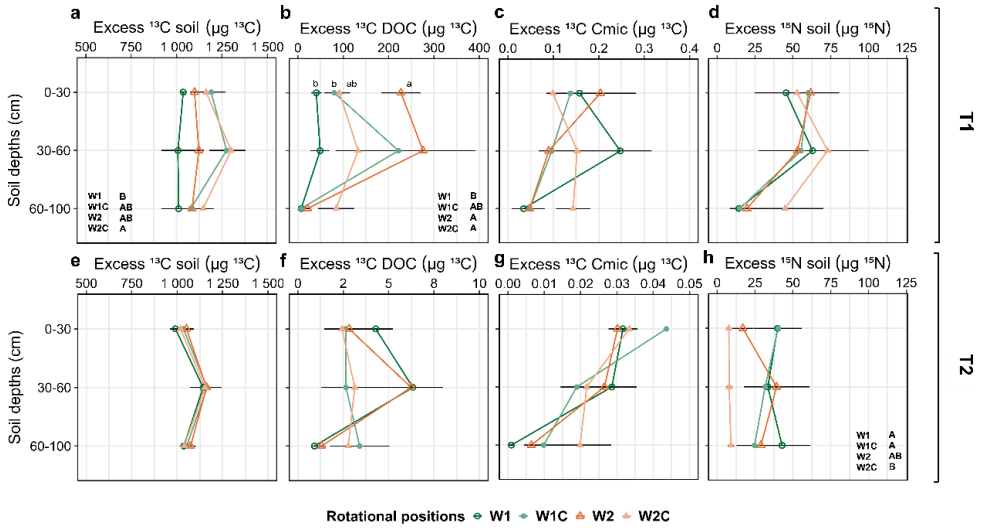

Figure 5.2 Effect of the rotational positions on the absolute ^{13}C excess of the soil (a, e), dissolved organic carbon (DOC; b, c) and microbial biomass C (C_{mic}; c, g) and on the absolute ^{15}N excess of the soil (d, h) of the following winter wheat at flowering (BBCH 61, T1) and grain ripening (BBCH 90, T2), for the first wheat after oilseed rape without (W1) and with (W1C) compost addition, and the second wheat after oilseed rape without (W2) and with (W2C) compost addition. Different uppercase letters in each subplot indicate significant differences between the rotational positions. Within each soil depth, different lowercase letters denote significant differences between rotational positions at $p \leq 0.05$ level according to PERMANOVA with Benjamini-Hochberg *p* adjustment. Absence of letters indicate non-significant differences.

5.3.3 Allocation of ^{13}C, ^{15}N, ^{2}H and ^{18}O within the plant and biomass accumulation

Compost addition to W1C increased root biomass and reduced leaf biomass compared to W1 (Table D.3; Fig. 5.3a). W2 exhibited a 23.2% reduction in biomass compared to W1, which was evident for all plant parts except the leaves and the husks (Fig. 5.3a). The addition of compost significantly compensated for the reduction in biomass of W2 in all plant parts (Fig. 5.3a). Plant C:N ratio was also strongly affected by rotational position and compost addition (Table D.3). We observed a 19.2% and 22.3% reduction in the C:N ratio of W1 and W2C compared to W2 (Fig. 5.3b). Compost addition did not change the overall plant C:N ratio of W1C plants compared to

W1, but increased the C:N ratio of their roots. Compost addition resulted in 46.2% higher ^{13}C excess in the biomass of W2C compared to W2 (Table D.4; Fig. 5.3c). Notably, the ^{13}C excess of W2 grains was significantly lower than that of W1, W1C and W2C. This was also the case for all plant parts except the leaves and husks.

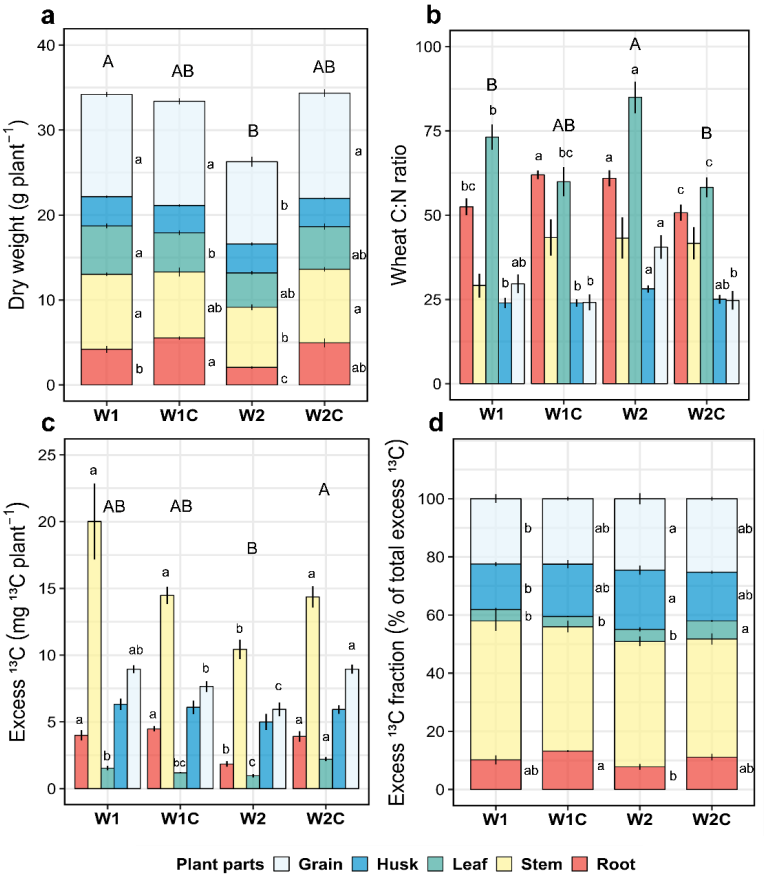

Figure 5.3 Dry weight (a) and C:N ratio (b), absolute ^{13}C excess (c) and relative ^{13}C excess fraction of roots, stems, leaves, husks and grains (d) of two rotational positions of winter wheat at grain ripening stage (BBCH 90, T2), for the first wheat after oilseed rape without (W1) and with (W1C) compost addition, and the second wheat after oilseed rape without (W2) and with (W2C) compost addition. Different uppercase letters indicate significant differences between the rotational positions over all plant parts with *$p \leq 0.05$; **$p \leq 0.01$; ***$p \leq 0.001$. Within each plant part, different lowercase letters indicate significant differences between the rotational positions at $p \leq 0.05$ level according to PERMANOVA with Benjamini-Hochberg p adjustment. Absence of letters indicate non-significant differences.

We also found an increase in the relative allocation of ^{13}C to grains and husks in W2 compared to W1 (Fig. 5.3d). Compost addition also increased the relative allocation of ^{13}C to roots in both W1C and W2C compared to their unamended counterparts W1 and W2.

W2 showed a decreased ^{15}N excess in all plant parts, except for the husks, compared to W1 and W1C (Fig. 5.4a). Compost addition increased the ^{15}N excess in all plant parts in W2C, except for stems and husks, compared to W2. A similar trend was observed when measuring the ^{2}H excess of the different plant parts of the rotational positions. The grains of W1, W1C and W2C had a 26.4%, 41.8% and 46.2% higher ^{2}H excess compared to W2, respectively (Fig. 5.4b). Compost addition increased the ^{2}H of the stems in both W1C and W2C compared to their unamended couterparts. We also obeserved a signficant decrease in the overall ^{18}O excess of W2C compared to W1 (Fig. 5.4b). Compost addition reduced the amount of ^{18}O incorporated into the grains of W1C and W2C compared to W1 and W2, repectively. Plant biomass was positively correlated with the ^{13}C, ^{15}N, ^{2}H and ^{18}O excess in W1 and W2, with and without compost addition (Fig. D.4).

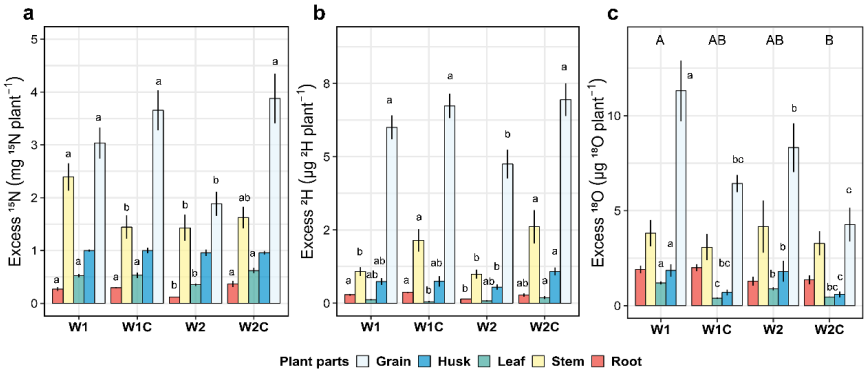

Figure 5.4 Absolute ^{15}N (a), ^{2}H (b) and ^{18}O (c) excess of roots, stems, leaves, husks and grains of two rotational positions of winter wheat at grain ripening stage (BBCH 90, T2), for the first wheat after oilseed rape without (W1) and with (W1C) compost addition, and the second wheat after oilseed rape without (W2) and with (W2C) compost addition. Different uppercase letters indicate significant differences between the rotational positions over all plant parts with *p ≤ 0.05; **p ≤ 0.01; ***p ≤ 0.001. Within each plant part, different lowercase letters indicate significant differences between the rotational positions at p ≤ 0.05 level according to PERMANOVA with Benjamini-Hochberg p adjustment. Absence of letters indicate non-significant differences.

The ^{13}C excess of the W2 roots in the topsoil was on average 64.4%, 71.7% and 44.3% lower compared to W1, W1C and W2C, respectively (Table D.5; Fig. 5.5a). In the 60-100 cm soil layer, compost addition increased the ^{13}C excess of the roots of W2C compared to W2. A similar trend was observed with respect to the ^{15}N excess with W2C, with increased values compared to W2 throughout the soil profile (Fig. 5b). RDW was significantly reduced in the topsoil of W2 compared to W1, W1C and W2C (Fig. 5.5c). In the 60-100 cm soil layer, compost addition

increased RDW in W2C compared to W2. Finally, RLD was similar across all rotational positions (Fig. 5.5d).

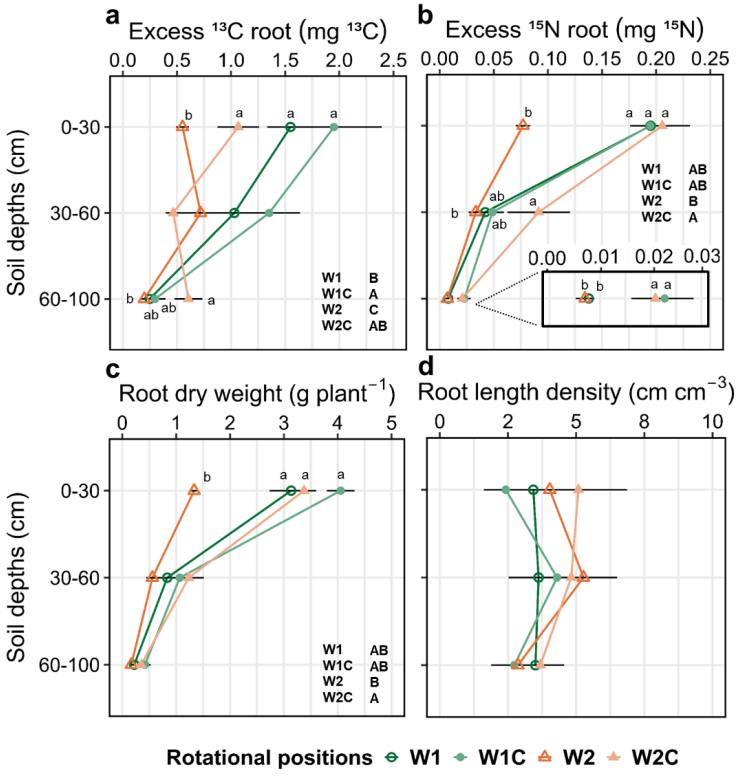

Figure 5.5 Absolute ^{13}C (a) and ^{15}N (b) excess of roots, root dry weight (c) and root length density (d) of two rotational positions of winter wheat at grain ripening stage (BBCH 90, T2), for the first wheat after oilseed rape without (W1) and with (W1C) compost addition, and the second wheat after oilseed rape without (W2) and with (W2C) compost addition. Different uppercase letters indicate significant differences between the rotational positions over all plant parts with *$p \leq 0.05$; **$p \leq 0.01$; ***$p \leq 0.001$. Within each plant part, different lowercase letters indicate significant differences between the rotational positions at $p \leq 0.05$ level according to PERMANOVA with Benjamini-Hochberg p adjustment. Absence of letters indicate non-significant differences.

5.4 Discussion

5.4.1 Initial soil characteristics as the basis for legacy effects on plant performance

The soil legacy of the preceding crop of WW had a significant impact on the soil nutrient status and thus, on nutrient availability and uptake of the following WW. Previous studies have shown that the soil after oilseed rape contains high levels of mineral N that is directly available for plant uptake (Groeneveld et al., 2024; Kaloterakis et al., 2024b). In these studies, the higher C_{mic} buildup at the tillering stage in W2 compared to W1 was suggested to induce N immobilization and, as a result, reduced N availability for WW. A potential dysbiosis in the soil of W2 was also discussed as a confounding factor for this early growth reduction in successively grown WW. In our experiment, a higher mineral N content (both NO_3^- and NH_4^+) and a generally higher nutrient content were measured in the soil of W1 compared to W2, together with a higher C_{mic} (Table D.1). This confirmed the beneficial management practice of cultivating oilseed rape before WW.

Although the residues of oilseed rape are rich in N, the higher content of other nutrients, such as SO_4^{2-}, Mg, P_{CAL} and K_{CAL}, provided the basis for a better early establishment of W1 in the field compared to W2. The initial C_{mic} of W1 was significantly higher than W2, which was associated with a higher DOC content. These two variables respond similarly in cases where accelerated decomposition produces more GLU in the soil that can be directly used by the microbes and be incorporated into C_{mic}. Together with the higher mineral N content in W1, this suggests that microbes are neither C- nor N-limited and do not immobilize N early in the growing season.

5.4.2 Evidence of soil legacy at later growth stages and compensation of initial disadvantages of W2 by addition of compost

Flowering is a very important stage that determines the grain yield of WW and, as such, it was important to assess the soil biochemical conditions and the potential growth-promoting role of the compost addition. At T1, the soil NO_3^- content was already very low, indicating high N uptake rates by WW and/or high N losses due to denitrification, which was not the focus in our study. The higher NH_4^+ content at T1 for the compost-amended W1C and W2C showed that compost stimulated N mineralization and provided a slow and steady supply of nutrients that could be utilized by plants and microbes. In fact, it is estimated that only a small portion of OA is mineralized within the first year after its application, depending on its composition (Agegnehu et al., 2017). The low C:N ratio of 13 of the green-waste compost applied in this study should make the compost more readily available for microbial (especially bacterial) use, which was probably the reason why higher N mineralization occurred in compost-amended soils, a possible cause of the significant compensation of yield losses in the self-successive WW rotation. The higher NH_4^+ availability in W2C compared to W2 is linked to its higher C_{mic}, which was also the highest among all rotational positions. This means that even though W2 started with a lower C_{mic} and DOC compared to W1, compost amendment compensated for this initial difference, which potentially

led to a higher NH_4^+ in W2C. This is further supported by the higher DOC in W2C compared to W2.

According to our first hypothesis, compost application stimulated GLU release, as shown by the high BGU activity, but only in W1C and not in W2C. LAP activity was the highest in W1, suggesting that LAP stimulated organic N mineralization and the production of NH_4^+ (Yang et al., 2023). Kaloterakis et al. (2024b) found a higher BGU activity in W2 compared to W1 at tillering and attributed this to the quality of the preceding crop residues (higher N content of the residues of oilseed rape compared to WW). In our study, the BGU activity was more linked to compost mineralization at T1 than decomposition of the preceding crop residues. In contrast to mineral fertilizers, compost provides nutrients in organic forms that need to be mineralized first before they become available for plant uptake, acting as a slow-release fertilizer (Amlinger et al., 2003; Al-Bataina et al., 2016). Furthermore, compost addition to soil is known to induce higher exudation rates that in turn stimulate nutrient solubilization and uptake by plants (Rosa et al., 2021; Kumar et al., 2024). Another potential explanation for the increased NH_4^+ in the compost-amended treatments may be that compost application boosted root growth. The larger root system of W2C may have increased the C input either through increased rhizodeposition or increased root litter decomposition (Remus et al., 2022), which fueled microbial activity, N mineralization and thus, NH_4^+ production.

5.4.3 Belowground allocation of ^{13}C and ^{15}N at the flowering and grain ripening growth stages

At T1, we traced ^{13}C in different belowground pools and found that soil depth had a strong influence on the transfer of the ^{13}C label in the C_{mic} pool, with lower values in the 60-100 cm soil layer, which is in contrast to previous studies (Van de Broek et al., 2020; Kaloterakis et al., 2024a). The amount of ^{13}C label that ends up in the C_{mic} pool is dependent on the C use efficiency of the microbes, which changes at different depths (Li et al., 2021). Soil depth strongly affected the ^{13}C excess in the DOC pool, which is linked to the root distribution across the soil profile but also exudation intensity and root litter turnover (Kaloterakis et al., 2024a).

According to our first hypothesis, we found that a significantly higher amount of the ^{13}C label ended up in the soil of compost-amended WW, especially W2C. This shows that WW benefited from the compost by stimulating root growth and, as a result, increased ^{13}C translocation below ground. This higher ^{13}C in the soil of W2C compared to W2 was utilized by the larger microbial pool of W2C, indicated by higher C_{mic} values. At T2, the ^{13}C label had already been consumed by the soil microbes, resulting in no differences in the ^{13}C excess of the soil. The increased ^{13}C of the DOC in W2 compared to W1 at T1 contradicts the findings of (Kaloterakis et al., 2024a), who observed higher ^{13}C of the DOC in the sandy loam of W1 compared to W2 at late flowering and linked this to the increased and sustained belowground allocation of photosynthates. Here, the higher ^{13}C of the DOC in W2 might be the result of accelerated C turnover as a response to short-term nutrient availability. Increased root decay in W2 due to accumulation of soil pathogens, a common observation in monocropping systems, could be an alternative explanation

(Peralta et al., 2018). Over time, the ^{13}C in the soil pool was utilized by soil microbes (used for growth and maintenance), resulting in no differences at T2. The significantly lower ^{15}N excess of the soil in W2C compared to W1, W1C and W2 suggests that W2C plants took up the labelled N earlier in the season, or that N losses were higher in W2C compared to the other rotational positions. W1 and W1C had a higher soil ^{15}N excess and had incorporated similar amounts of ^{15}N into their biomass as W2C, favoring the possibility of earlier ^{15}N uptake or increased N losses. WW is known to utilize the available N more efficiently when compost is applied (Keeling et al., 2003), most likely due to the supply of other important plant-available nutrients.

5.4.4 Compost addition mitigated yield decline of W2 by improving plant growth, nutrient and water uptake from the subsoil

The initial soil legacy of W2 persisted through the late growth stages of WW and resulted in a large yield decline compared to W1. This is consistent with previous studies that reported a reduction in growth of successively grown WW (Arnhold et al., 2023b; Kaloterakis et al., 2024a). W2 exhibited reduced root growth as indicated by the reduction in RDW. This was not associated with distinct changes in RLD between W1 and W2. Arnhold et al. (2023a) did not observe differences in the RLD between W1 and W2 at tillering in a field experiment, but found higher RLD in W1 at late flowering in a year with high summer precipitation. In the current experiment, W1 allocated more freshly assimilated C to the roots than W2, which was followed by a more efficient utilization of the ^{15}N-labeled fertilizer. Compost addition strongly affected the ^{13}C content of the root in both the topsoil and subsoil of W1C and W2C. The enhanced root growth in W2C improved the N uptake, indicated by the significantly higher ^{15}N excess of the roots at all three measured soil depths.

The plant biomass was closely related to the excess of all four isotopes applied and measured in the plant biomass, as indicated by the correlation analyses. The positive PSF in WW after oilseed rape was associated with a significantly higher ^{13}C excess in W1 compared to W2. Even though compost addition increased the root biomass of W1C, it was not associated with any yield gain compared to W1. The addition of compost to W2C proved to be a very beneficial management practice that significantly mitigated the yield decline of W2. Compost is known to promote WW yield and reduce take-all severity at both lower and higher application rates than the 40 t ha^{-1} used in this study (Tilston et al., 2005; Demelash et al., 2014). Compost addition boosted soil nutrients and promoted N mineralization and thus supply of fresh NH_4^+ available for plant and microbial uptake. As hypothesized, this promoted root growth, nutrient uptake and plant performance, increasing the amount of ^{13}C and ^{15}N measured in plant biomass and especially in the grains. The increased N uptake in W2C compared to W2 was also reflected in the significant decrease in the plant C:N ratio for all plant parts except the husks, which is similar to the reported increased N uptake at tillering by W1 by Kaloterakis et al. (2024b). Thus, compost application increased the N use efficiency of the successively grown WW that could not use the large amount of mineral N from the fertilization.

Compared to W2, W1 increased the relative amount of water uptake from the topsoil and subsoil, as indicated by the higher ^{2}H and ^{18}O excess, respectively. This is most likely related to the larger and better functioning root system of W1, resulting from the soil legacy of oilseed rape. Compost addition did not affect the relative contribution of the tospoil to plant water uptake but resulted in a significant increase of ^{2}H excess in W2C. This observation is linked to the enhanced root growth and nutrient uptake by W2C, highlighting the multi-faceted beneficial properties of compost amendment which was hypothesized to compensate the growth reduction in the successive WW rotation. W2 had a relatively lower water uptake from the ^{18}O-enriched depth compared to W1. Compost addition reduced the contribution of the subsoil to total plant water uptake, possibly by increasing the root growth and the WHC of the topsoil compared to the unamended soils, which was the case at least for W2C.

5.5 Conclusions

In this study, we compared two different compost-amended and unamended rotational positions of WW to assess the potential of compost to mitigate yield losses in successive WW rotations. The beneficial soil legacy of oilseed rape led to enhanced performance of the following WW compared to the soil legacy of WW. This effect was substantial and evident at the flowering and grain-ripening stages. According to our hypotheses, compost application notably mitigated the initial disadvantage of W2 by promoting belowground allocation of freshly assimilated C, enzymatic activity, nutrient mineralization, root growth, N and water uptake by WW, thereby effectively compensating for the substantial yield loss of the successively grown WW. Our results provide empirical evidence and a mechanistic understanding on the beneficial role of compost amendment in mitigating yield decline in successively grown WW. We showed that green-waste compost is a promising management practice to increase yield in successive WW rotations. However, further experiments on the long-term effect of compost application on successive WW rotations are needed to assess the duration of the yield loss compensation.

6. *Bacillus* seed coating mitigates early growth reduction in successive winter wheat without altering rhizosphere bacterial and archaeal communities.

Based on:
Kaloterakis, N., Braun-Kiewnick, A., Rashtbari, M., Giongo, A., Doreen, B., Priscilla, Z., Razavi, B.S., Smalla, Reichel, R., Brüggemann, N. *Bacillus* seed coating mitigates early growth reduction in successive winter wheat without altering rhizosphere bacterial and archaeal communities. Manuscript under review in *BMC Biology*.

6.1 Introduction

The potential of PGPR in enhancing plant growth is receiving a lot of attention, mainly due to their multifunctionality under different biotic and abiotic conditions (Nkebiwe et al., 2024). This is depicted by the very high annual growth rates of the biostimulants market, which was estimated to be 13.58% in 2022 and worth approximately USD 5.6 billion by the end of 2025 (Landeta and Marchant, 2022). The projected adverse climatic conditions in the coming decades, coupled with environmental concerns about the overuse of mineral fertilizers, present a unique opportunity to address decreasing yields by harnessing the potential of soil life for plant growth.

Whether dealing with salinity and water stress, nutrient deficiency, heavy metal contamination or biotic stress, several experiments have highlighted the positive effect of PGPR in alleviating plant stress (Groppa et al., 2012; Köberl et al., 2013; Vacheron et al., 2013; Goswami et al., 2016; Rosier et al., 2018; Kaloterakis et al., 2021). PGPR affect plant growth by modulating phytohormonal homeostasis and stress markers, thereby inducing systemic resistance responses or affecting the shape and size of the root system. Other important mechanisms include biological N fixation, phosphate, K and micronutrient solubilization following the release of organic acids by bacterial cells, as well as Fe chelation following siderophore production and phenol accumulation, mainly found in the genus *Pseudomonas*, and antibiotic production, mainly found in the genera *Bacillus* and *Pseudomonas* (Goswami et al., 2016; Rosier et al., 2018; Sharma et al., 2024). There is also evidence that certain PGPR, such as *Bacillus* spp. and *Trichoderma* spp., can alter the soil microbial community composition by increasing the relative abundance of microbes with antifungal properties (Xiong et al., 2017).

In the context of arable farming, the soil legacy following the growth of a certain plant species can affect the microbial community composition and the growth of the succeeding plant, which can result in a negative, neutral or positive PSF (van der Putten et al., 2013; de Vries et al., 2023). Rhizodeposition is one of the most important factors shaping the rhizobiome, in addition to abiotic soil properties (Paterson et al., 2007; Nannipieri et al., 2023). The released carbohydrates from root exudates and plant litter can be expected to stimulate the activity of PGPR in the rhizosphere and, therefore, improve some of the aforementioned functions, enhancing plant health and performance (Ling et al., 2022). PGPR can improve soil quality through enhancing soil enzymatic activity, nutrient availability and the yield of WW (Mäder et al., 2011). However, it is crucial to assess the root microhabitat, i.e., BS, RA, RH and RP, as well as the associated soil depth, since both factors strongly influence the microbial community assemblage strategies and rhizosphere functions (Jones et al., 2019; S. Liu et al., 2022; Giongo et al., 2024).

Applying the PSF theory to crop rotations, the beneficial effect of oilseed rape as a preceding crop to WW has been previously established (Weiser et al., 2017; Hegewald et al., 2018; Hansen et al., 2019; Arnhold et al., 2023a; Kaloterakis et al., 2024b). Up to 40% of the global WW cultivation is grown successively, and this succession affects the rhizobiome and leads to a significant yield decline due to the high occurrence of soil-borne fungal pathogens (Kwak and Weller, 2013; Angus et al., 2015; Palma-Guerrero et al., 2021; Yin et al., 2022; Giongo et al., 2024). It is, therefore, important to explore beneficial preceding crops to WW while evaluating the

potential of bio-effectors, such as PGPR, to restore the productivity of successively grown WW. Capitalizing on this knowledge, we can assume that the addition of a PGPR will act as a bio-effector and promote plant health and productivity in conditions of microbial dysbiosis in the rhizosphere of successive WW rotations (Nkebiwe et al., 2024). Recently, successive wheat rotations have been found to enrich the rhizosphere with plant-beneficial bacteria with fungal antagonistic activity, while early application of PGPR is a promising strategy to control the soil-borne pathogen Gt (Braun-Kiewnick et al., 2024).

One of the most common drawbacks of using single-strain PGPR is the weak extrapolation of the beneficial trends observed in lab or pot experiments to trends that persist under field conditions (Pineda et al., 2020). Therefore, it is crucial for the experimental conditions of pot experiments, which are the intermediate step between *in vitro* and field experiments, to resemble field climatic conditions. The objective of our study was to assess the effect of *Bacillus pumilus* on the productivity of successive and non-successive WW rotations. We hypothesized that *B. pumilus* inoculation would alleviate the negative PSF of successively grown WW.

6.2 Materials and Methods

6.2.1 Experimental design

An outdoor rhizotron experiment was set up from June 6 to July 31, 2023 on the campus of Forschungszentrum Jülich, Germany, using newly designed rhizotrons with a height of 100 cm, a width of 35 cm and an inner thickness of 2.5 cm (Reichel et al., 2022). The rhizotrons were optimized for active soil temperature regulation, by circulating cool water through the upper polyvinyl chloride plates of the rhizotrons. The water temperature was set to 5 $^{\circ}$C and controlled with a cooling unit. The rhizotrons were connected to the cooling unit with polyurethane tubing coated with a rubber insulating hose. In order to create a realistic soil temperature gradient along the rhizotron, the water was first directed into the bottom part of the rhizobox, then flowing upwards to the rhizotron/soil surface. Preliminary trials showed that the temperature changes, during the upward movement of the cooling water through the rhizobox material created a realistic temperature gradient in the soil profile. Passive insulation was provided by fixing a 4 cm insulation, consisting of a 1 cm thick rubber and a 3 cm thick styrofoam™ layer, on both plates of the rhizotrons (Fig. E.1). One rhizotron was dedicated to measuring soil temperature at three soil depths i.e., 10 cm, 40 cm and 80 cm throughout the experiment. Ambient weather conditions and the soil temperature gradient along the soil profile of the rhizotron are shown in Fig. E.2.

We contrasted W1 and W2 and soil was collected from the experimental farm Hohenschulen, Faculty of Agricultural and Nutritional Sciences, Christian-Albrechts-University of Kiel, 54°19′05″N, 9°58′38″E, Germany. The crop rotation trial was established in 1989. It included the following factors: a) rotational position (oilseed rape, first wheat after oilseed rape, third wheat grown continuously), b) WW varieties (4 levels), and c) N fertilization levels (4 levels). Composite soil samples for rhizobox experiments were taken from the topsoil (0-30 cm) and subsoil (30-50 cm) of field plots after oilseed rape and after one season of WW cultivation (n = 4 replications) with the WW cultivar “Nordkap” (SAATEN-UNION GmbH, Isernhagen, Germany)

and optimal N-fertilization (240 kg N ha^{-1}). After the harvest of the different preceding crops, the plant residues remained on the field. The residues of the preceding crops were not removed from the soil before sampling, and the field was ploughed after the sampling. The soil was a carbonate-free Cambic Luvisol of sandy loam texture (44 % sand, 35 % silt, and 21 % clay; Sieling et al., 2005). The soil properties of the specific plots where the soil was sampled were previously described in Kaloterakis et al. (2024).

Soil was sieved to 2 mm and repacked in the rhizotrons to reach a bulk density of 1.33 g cm^{-3} and 1.45 g cm^{-3} for 0-30 cm and 30-100 cm, respectively. Deionized water was added to adjust the soil moisture to 70 % water-holding capacity (215 g H_2O soil kg^{-1}) at the onset of the experiment. Thereafter, the plants were kept rain-fed throughout the experiment. All rhizotrons were kept inclined at 45° to facilitate root growth along the lower side of the rhizotrons. WW seeds (cultivar "Nordkap") were inoculated with either *B. pumilus* 45_39 (DSM117807, DSMZ, Braunschweig, Germany) or buffer solution (control) as described in (Braun-Kiewnick et al., 2024). Briefly, seeds were pre-germinated at room temperature for two days in the dark and then immersed in cell suspensions of *B. pumilus* vegetative cells from fresh overnight cultures. Bacterial cultures were grown in 50 mL R2A broth containing 100 µg mL^{-1} rifampicin in 300 mL Erlenmeyer flasks at 150 rpm and harvested by centrifugation (5000 g, 15 min at room temperature) using 50 mL conical tubes and washing three times in 10 mM $MgCl_2$ buffer. The cell pellet was resuspended in 5 mL 10 mM $MgCl_2$, and 5 mL of 2 % (v/v) sterile methyl cellulose was added as a coating agent. Approximately 25 pre-germinated seeds were submerged and soaked in the 10 mL cell suspension for one hour. The tubes were gently shaken throughout soaking to ensure even contact between each seed and the cell suspension. CFU counts conducted directly after seed treatment resulted in approximately *log* 9 CFU mL^{-1} per seed. Three WW seeds were sown in each rhizotron and thinned to one seedling per rhizotron three DAS. The plants were not fertilized for the duration of the experiment. The plants were harvested at the end of tillering stage BBCH 29.

6.2.2 Above and belowground plant growth analyses

The aerial plant parts were split at harvest into pseudostems (hereafter called stems) and leaves. The lower sides of the rhizotrons were then removed and the soil profile was divided into three layers (0-30 cm, 30-60 cm and 60-100 cm). Soil samples for biochemical analyses were taken from the RA and RH soil compartment, while soil samples for DNA extraction were taken additionally from the RP soil compartment. First, we sampled RA soil from ≥ 15 mm away from the root surface, using microspatulas. The visible roots were removed from the soil and gently shaken to retrieve the RH soil. We pooled and mixed subsamples to form a composite sample and then split it into several parts to ensure that enough soil was collected for every planned analysis. These roots together with the RH soil for the microbiome analysis were subsequently stored at 4 °C overnight until DNA extraction. The remaining roots were washed and stored in 30 % ethanol. They were scanned at 600 dpi (Epson Perfection V800 Photo, Epson, Japan) and analyzed with WinRhizo® software (Regent Instruments Inc., Quebec, Canada). The roots were split into six diameter classes, i.e., ≤ 0.1 mm, 0.1-0.2 mm, 0.2-0.3 mm, 0.3-0.4 mm, 0.4-0.5 mm, ≥ 0.5 mm. All plant materials

were oven-dried at 60 °C to constant weight (maximum three days) to record their DW. Ball-milled (MM 400, Retsch, Germany) above- and belowground plant samples, as well as soil samples, were weighed into tin capsules (HEKAtech, Wegberg, Germany) for determination of C and N content using an elemental analyzer coupled to an isotope-ratio mass spectrometer (EA-IRMS, Flash EA 2000, coupled to Delta V Plus; Thermo Fisher Scientific Inc., Waltham, MA, USA). Microwave digestions of ball-milled plant material in closed vessels were performed and measured for P, K and Fe content by inductively coupled plasma optical emission spectroscopy (ICP-OES; iCAP 7600; Thermo Fisher Scientific Inc., Waltham, MA, USA (adjusted from Hansen et al. (2019).

6.2.3 Soil samples processing

At harvest, soil samples were stored at -25 °C before analysis of mineral N, DOC, and TN. For the analysis, they were thawed and extracted using 0.01 M $CaCl_2$ (soil-to-solution ratio of 1:4 w/v), vortexed, shaken horizontally for 2 h at 200 rpm, centrifuged for 15 min at 690 × g, and filtered through 0.45 µm PP-membrane filters (Ø 25 mm; DISSOLUTION ACCESSORIES, ProSense B.V., Munich, Germany). Soil solution was stored overnight at 4 °C before DOC and TN analysis. NH_4^+ was measured by continuous-flow analysis (Flowsys, Alliance Instruments GmbH, Freilassing, Germany). NO_3^- and SO_4^{2-} were measured by ion chromatography (Metrohm 850 Professional IC Anion – MCS, Metrohm AG, Herisau, Switzerland). Mg was measured by ICP-OES (iCAP 6500; Thermo Fisher Scientific Inc., Waltham, MA, USA). The pH was measured in the same solution using a glass pH electrode (SenTix® 940, WTW, Xylem Analytics, Weilheim, Germany). DOC and TN were quantified with a TOC analyzer (TOC-V + ASI-V + TNM, Shimadzu, Japan). Soil enzymatic analysis as well as zymography were performed as in Kaloterakis et al. (2024).

6.2.4 Statistical analysis

The rotational position of WW (W1 and W2), PGPR inoculation status (‘+’ and ‘-‘), soil compartment (RA and RH), soil depth (0-30 cm, 30-60 cm and 60-100 cm) and plant part (root, stem, leaf) were considered fixed factors in the statistical analysis. We conducted PERMANOVA with 10000 permutations using the ‘vegan’ package (Oksanen et al., 2022) in R (v4.2.1. R Core Team, 2022) to account for normality violations and unequal variances of the data. Follow-up t-tests were made using the ‘RVAideMemoire’ package in R (Hervé, 2023) using the significant threshold $\alpha = 0.05$. We conducted a principal component analysis (PCA), using the prcomp() function in R, on standardized variables related to plant biomass, root growth, soil nutrients and soil enzymatic activity for the rotational position with and without *B. pumilus* inoculation. All figures were created using the ‘ggplot2’ package (Wickham, 2016).

6.3 Results

6.3.1 The effect of *Bacillus pumilus* inoculation on WW shoot and root growth

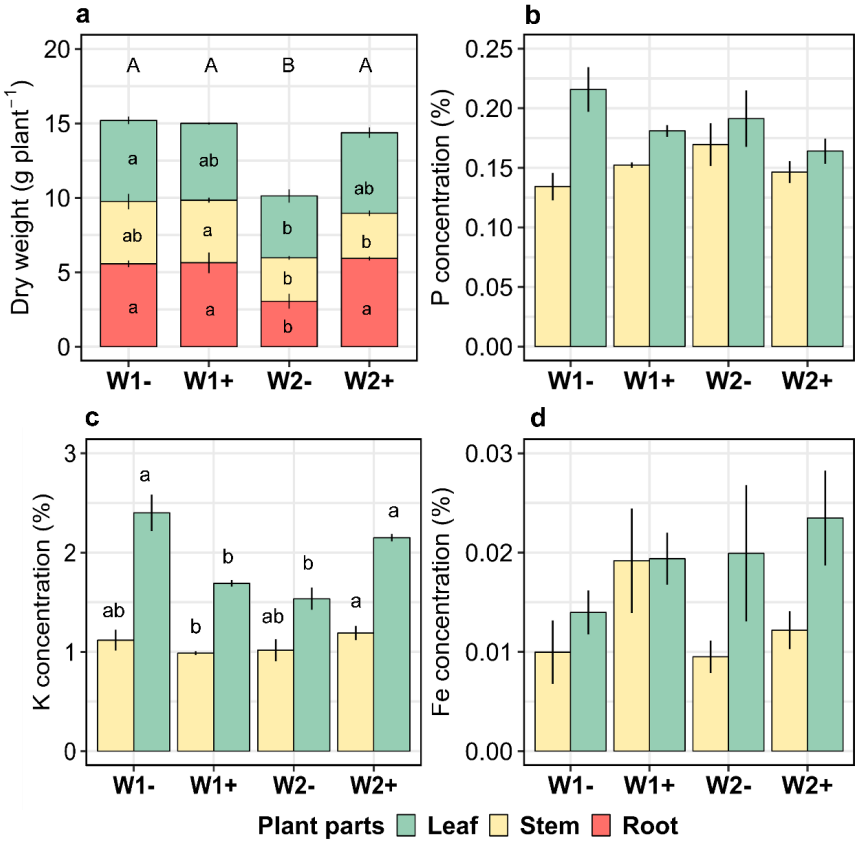

Figure 6.1 Dry weight (a), P content (b), K content (c) and Fe content (d) of roots, stems, leaves, husks and grains of winter wheat at the end of tillering (BBCH 29). First wheat after oilseed rape without (W1-) and with (W1+) *Bacillus pumilus*, and second wheat after oilseed rape without (W2-) and with (W2+) *Bacillus pumilus*. Different uppercase letters indicate significant differences between the rotational positions over all plant parts. Within each plant part, different lowercase letters indicate significant differences between the rotational positions at $p \leq 0.05$ level according to PERMANOVA. Absence of letters indicate non-significant differences.

Rotational position had a strong influence in biomass accumulation at the end of tillering (BBCH 29; Table E.1). There was a 50.1% plant biomass growth increase in W1- compared to W2- for leaf and RDW (Fig. 6.1a). *B. pumilus* inoculation in W1+ did not further increase plant biomass compared to W1-, but W2+ had a 41.0% increase in dry weight compared to W2-. Plant tissue analysis showed that the leaves had a significantly higher P, K and Fe content (Table E.1). There were no differences in P and Fe content between the rotational positions (Fig. 6.1b, d) while the leaves of W2+ had a 40.1% higher K% (Fig. 6.1c).

Root growth followed a similar pattern as plant DW, with W2- having significantly less root biomass compared to W1-, while *B. pumilus* inoculation compensated for this effect (Table E.2, Fig. 6.2a). W2- plants had on average 48.7%, 49.4% and 43.9% lower RLD compared to W1-, W1+ and W2+, respectively, which was evident across all three soil depths (Fig. 6.2b). SRL was also significantly affected by the rotational position of WW (Table E.2), with successively grown W2- having higher SRL than W1-, W1+ and W2+ in the 30-60 cm and 60-100 cm (Fig. 6.2c). Across all depths, W2- plants produced the thinnest roots with an average diameter of 0.259 mm, compared to 0.297 mm, 0.304 mm and 0.290 mm for W1-, W1+ and W2+, respectively (Fig. 6.2d). Successive WW inoculated with *B. pumilus* had thinner roots in the topsoil and thicker roots at both subsoil depths compared to non-inoculated successive WW. This was also evident from the higher proportion of thicker roots of W2+ compared to W2- belonging to the larger root diameter classes (Table E.3, Fig. E.3).

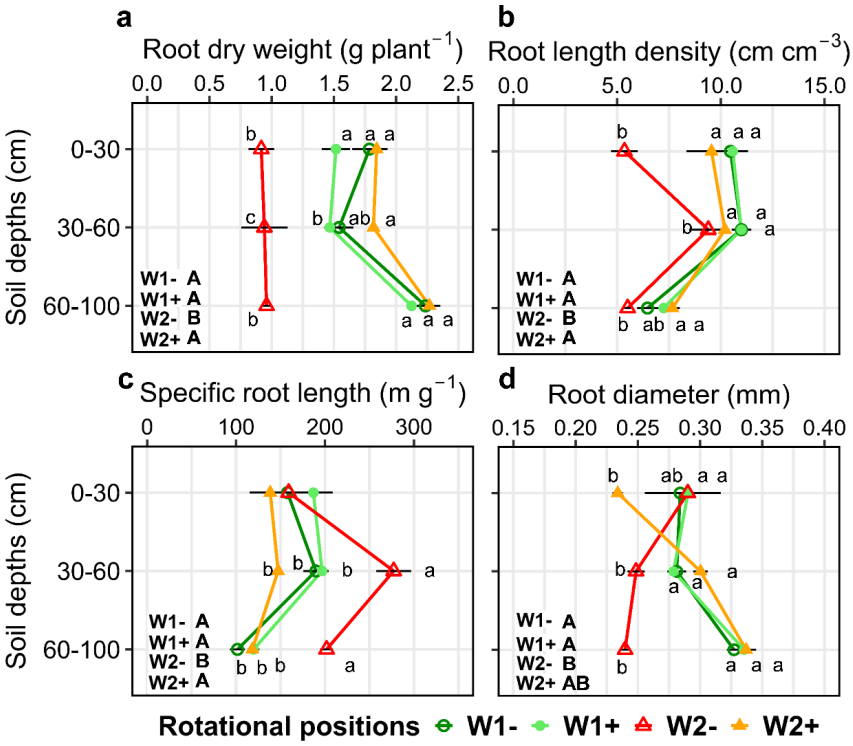

Figure 6.2 Root dry weight (a), root length density (b), specific root length (c) and average root diameter (d) of roots, root dry weight (c) and root length density (d) of two rotational positions of winter wheat at the end of tillering (BBCH 29) at soil depths 0-30 cm, 30-60 cm and 60-100 cm. First wheat after oilseed rape without (W1-) and with (W1+) *Bacillus pumilus*, and second wheat after oilseed rape without (W2-) and with (W2+) *Bacillus pumilus*. Different uppercase letters indicate significant differences between the rotational positions over all soil depths. Within each soil depth, different lowercase letters indicate significant differences between the rotational positions at $p \leq 0.05$ level according to PERMANOVA. Absence of letters indicate non-significant differences.

6.3.2 The effect of *Bacillus pumilus* inoculation on soil nutrient dynamics

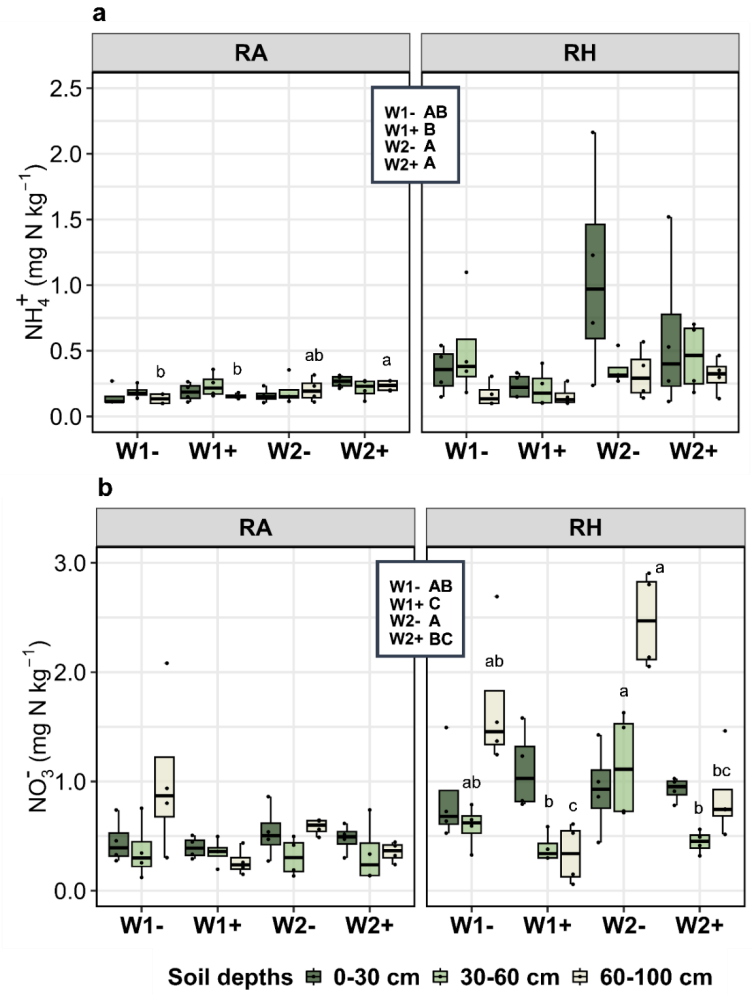

Figure 6.3 Effect of the rotational positions on soil NH_4^+-N (a) and soil NO_3^--N (b) of the following winter wheat at the end of tillering (BBCH 29) at soil depths 0-30 cm, 30-60 cm and 60-100 cm and in two soil compartments: root-affected soil (RA) and rhizosphere soil (RH). First wheat after oilseed rape without (W1-) and with (W1+) *Bacillus pumilus*, and second wheat after oilseed rape without (W2-) and with (W2+) *Bacillus pumilus*. Different uppercase letters indicate significant differences between the rotational positions over all soil depths. Within each soil depth, different lowercase letters indicate significant differences between the rotational positions at $p \leq 0.05$ level according to PERMANOVA. Absence of letters indicate non-significant differences.

Rotational position and *B. pumilus* inoculation had a marked impact on soil mineral N and DOC content (Table E.4). We measured higher soil NH_4^+-N in inoculated and non-inoculated W2 plants compared to W1 (Fig. 6.3a). There was significantly less soil NO_3^--N in the inoculated W1+ and W2+ than in their non-inoculated counterparts, which was especially evident for subsoil NO_3^--N. A higher soil content of NH_4^+-N was measured in the topsoil of W1- and W2- compared to NO_3^--N that was higher in the 60-100 cm soil layer in the same two treatments (Table E.4; Fig. 6.3). The soil compartment was a strong determinant of soil mineral N content, with a higher NO_3^--N and NH_4^+-N content measured in the RH than in the RA soil (Table E.4; Fig. 6.3). The same was the case for DOC (Table E.4; Fig. E.4). In addition, DOC was higher in the soil of W2 compared to W1, which was irrespective of the inoculation status (Table E.4). There was also an insignificant trend of higher DOC in the RH of W2+ compared to W2- especially in the 30-60 cm and 60-100 cm subsoil layers (Fig. E.4).

6.3.3 The effect of *Bacillus pumilus* inoculation on soil enzymatic activity

With respect to soil enzymatic activity, both rotational position and *B. pumilus* inoculation affected the kinetic parameters of BGU and LAP (Table E.5). Most of the differences in the BGU activity in the RA soil were found between W2- and W2+, with the latter having a lower BGU V_{max} in the 60-100 cm soil layer (Fig. 6.4a). In the more active soil compartment of the RH, there was also a lower BGU V_{max} in W2+ compared to W2-. The opposite was obvious for LAP V_{max} in both RA and RH soil (Fig. 6.4b). We observed a 71.8% and 31.5% increase in LAP V_{max} in the RA and RH soil, respectively, of W2+ compared to W2-. The RH soil had a higher enzymatic activity than RA soil, with higher BGU and LAP reaction rates (Table E.5). The RH extent for BGU was significantly higher across the soil profile in W1- than in W1+, W2- and W2+, while no significant trend was obvious for LAP (Fig. E.5). BGU K_m values were significantly affected by the rotational position and inoculation with *B. pumilus*, which was not the case for LAP K_m (Table E.5). In the RA soil, the substrate affinity for BGU was significantly increased following *B. pumilus* inoculation, with higher values for both W1+ and W2+ compared to their non-inoculated counterparts, while this was not the case for the RH soil (Table E.5).

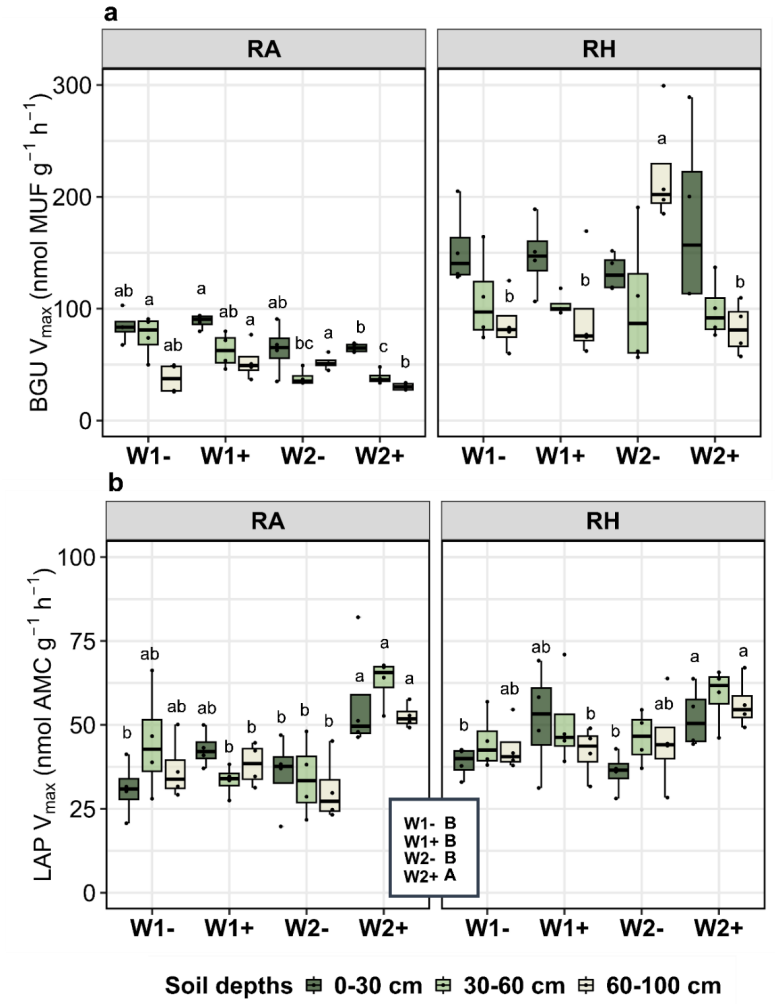

Figure 6.4 Effect of the rotational positions on maximum reaction rate of *β*-glucosidase (BGU; a) and leucine aminopeptidase (LAP; b) of the following winter wheat at the end of tillering (BBCH 29) at soil depths 0-30 cm, 30-60 cm and 60-100 cm and in two soil compartments: root-affected soil (RA) and rhizosphere soil (RH). First wheat after oilseed rape without (W1-) and with (W1+) *Bacillus pumilus*, and second wheat after oilseed rape without (W2-) and with (W2+) *Bacillus pumilus*. Different uppercase letters indicate significant differences between the rotational positions over all soil depths. Within each soil depth, different lowercase letters indicate significant differences between the rotational positions at $p \leq 0.05$ level according to PERMANOVA. Absence of letters indicate non-significant differences.

The two principal components explained 54.52 % of the total data set variance. PC3 and PC4 explained 11.68% and 10.35% of the variance, respectively. Plant biomass was positively associated with RLD (r = 0.75, p = 0.0008) and R_{dia} (r = 0.77, p = 0.0005), while it was negatively associated with soil NH_4^+-N (r = -0.56, p = 0.0234) and NO_3^--N (r = -0.56, p = 0.0242) and SRL (r = -0.74, p = 0.0009). There were significant differences in the variables associated with PC1 and PC2 between the rotational positions W1 and W2, while *B. pumilus* inoculation in W2+ resulted in distinct group clustering (Fig. 6.5). Plant biomass, RLD, and plant K content were strongly associated with W1- and W1+, while SRL, soil BGU V_{max}, NH_4^+-N and NO_3^--N were closely linked to the response of W2-. W2+ was more strongly aligned with LAP V_{max} and LAP RH extent (Fig. 6.5).

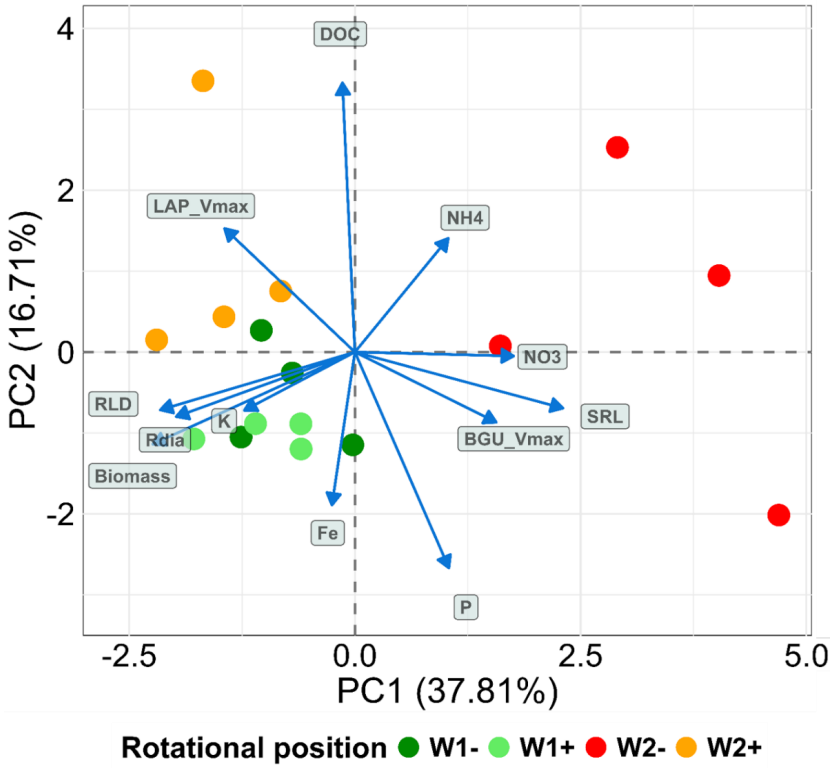

Figure 6.5 Redundancy analysis of the relationship between winter wheat biomass, nutrient uptake, root growth, soil chemical and enzymatic factors in two rotational positions of winter wheat at end of tillering (BBCH 29). First wheat after oilseed rape without (W1-) and with (W1+) *Bacillus pumilus* and second wheat after oilseed rape without (W2-) and with (W2+) *Bacillus pumilus*. BGU: *β*-glucosidase, LAP: leucine aminopeptidase, V_{max}: maximum enzymatic velocity, P: plant phosphorus, K: plant potassium, Fe: plant iron, RLD: root length density, SRL: specific root length, DOC: dissolved organic carbon.

6.4 Discussion

The addition of beneficial microbial inoculants is a sustainable agricultural practice due to their multiple functionalities that can address the major challenges of modern and future agriculture (Lugtenberg and Kamilova, 2009; Backer et al., 2018; Chieb and Gachomo, 2023). However, the research on PGPR and plant growth promotion is still in its primacy given the plethora of potential microbial candidates capable of plant growth promotion that have not been explored. Our study allowed the assessment of the complex interactions between the rotational position of WW, *B. pumilus* inoculation and their interaction in driving soil mineral N, release of labile C, root adaptations and their implications for plant performance and biomass accumulation.

6.4.1 *Bacillus pumilus* inoculation stimulates root growth and biomass accumulation in successive WW rotations

Successively grown WW benefited from PGPR inoculation and outgrew its non-inoculated counterpart. Changes in root morphology are crucial in understanding the biomass differences of the rotational positions. Root plasticity is a major response determining the overall fitness and productivity of plants (Schneider and Lynch, 2020). The observed 50.1% increase in biomass in W1- compared to W2- was largely driven by root plastic responses and soil nutrient uptake. In a recent meta-analysis, it was shown that R_{dia} is negatively correlated with SRL and positively associated with median root lifespan, which indicates that roots with a higher R_{dia} invest heavily in belowground C allocation per unit root length to achieve sufficient nutrient and water uptake (Hou et al., 2024). It has been shown that when WW is grown after oilseed rape, there is a higher and sustained belowground allocation of freshly assimilated C that is closely matched by root adaptations (Kaloterakis et al., 2024a). This sustained higher C allocation in non-successive WW rotations could be either a direct result of increased root biomass, but it could also be partly due to enhanced root exudation and root lifespan (Hou et al., 2024; Kaloterakis et al., 2024b). Even though we did not quantify the abundance of the soil-borne fungus Gt, enhanced root senescence due to root rot caused by Gt could be a prominent mechanism leading to yield decline in successive WW rotations (Arnhold et al., 2023a).

In our study, there was clear link between root growth traits and biomass accumulation, with RLD and plant biomass being negatively associated with SRL and NO_3^--N. Plants tend to increase their SRL in response to abiotic stresses and N limitation (Kaloterakis et al., 2021; Scheifes et al., 2024). In our experiment, SRL was negatively correlated with RLD, R_{dia} and plant biomass, revealing that root adaptations play a pivotal role in enhancing plant growth in plant successions. During the early growth stages of WW, Kaloterakis et al., (2024b) have shown that microbial immobilization of available mineral N is an important mechanism that causes lower N uptake by successively grown WW which is translated into a reduced biomass. It is this transient N limitation that the plants try to overcome by increasing their root absorptive surface and therefore soil exploration (Lynch, 2013). However, in the case of successive WW rotations, these root adaptations came with a significant C cost that did not compensate the biomass reduction.

Perhaps, it is more than merely the C cost that caused the observed effects: differences in the microbial community have been shown to strongly modulate the outcome of WW self-succession, with a potential microbial dysbiosis in the RH of the successive WW rotations (Kaloterakis et al., 2024b).

Earlier work on characterizing the *B. pumilus* strain used in this study showed the positive effect of *B. pumilus* inoculation on the shoot and especially root biomass of WW, which was independent of the presence of Gt in the soil (Braun-Kiewnick et al., 2024). This means that *B. pumilus* directly promoted plant growth, in addition to indirect ways, i.e., its effect on the microbial community composition and soil pathogen antagonism. The addition of *B. pumilus* to W2+ improved the root growth of successively grown WW, increased the proportion of larger root diameter classes and reduced the SRL. W1+ plants responded similarly to W1- and W2+ plants, with no further improvement of plant performance in the non-successive WW rotation. There is a plethora of studies reporting a beneficial effect of *B. pumilus* on root growth promotion of several crops (Win et al., 2018; Ngo et al., 2019; Liu et al., 2020; Braun-Kiewnick et al., 2024). Previous studies have also reported an upregulation of phytohormones by *B. pumilus* and especially gibberellins and auxins, which can directly promote root growth and, as a result, plant biomass accumulation (Gutiérrez-Mañero et al., 2001; Dobrzyński et al., 2022). That could be a possible link to the enhanced root growth of W2+ compared to W2-.

6.4.2 *Bacillus pumilus* inoculation stimulates soil enzymatic activity and nutrient uptake in successive WW rotations

Braun-Kiewnick et al. (2024) also showed that *B. pumilus* possesses a high production capacity of extracellular hydrolytic enzymes and siderophores and is capable of increasing the production of proteases, glucanases and cellulases in the soil. There are also reports of enhanced phosphatase and urease activity following *B. pumilus* in salt-tolerant rice (Kumar et al., 2021). In our study, we measured the activity and other kinetic parameters of the two very important enzymes BGU (C-cycling) and LAP (N-cycling). Using the novel technique of zymography for quantification and visualization of enzyme activity, we were also able to localize enzymatic hotspots and rhizosphere extent for both BGU and LAP in the RH of the WW plants (Razavi et al., 2019). Kaloterakis et al., (2024b) found an increased BGU and LAP activity in WW grown after oilseed rape compared to successive WW rotations, which was not the case in this experiment, where there were no significant differences between W1- and W2-. Nevertheless, we did measure a higher RH extent for BGU in W1- than W2- using zymography, but addition of *B. pumilus* in W2+ did not reverse this trend in the successive W2- rotation. However, *B. pumilus* inoculation significantly increased LAP activity in W2+ across all soil depths and soil compartments, and this was also reflected in the closer association of the W2+ plants with LAP activity in the PCA.

In addition to the overall effect on plant biomass, *B. pumilus* also improved plant K content in the successive wheat rotation. Increased plant Fe content was also observed, although not significant, while the plant P content was similar in W2+ and W2- plants. The PCA also revealed that *B. pumilus* inoculation improved plant K uptake, which was associated with higher above-

and belowground biomass. In our study, the addition of *B. pumilus* to both WW after oilseed rape and successively grown WW led to a significant decrease in soil NO_3^- compared to their non-inoculated counterparts. This observation suggests three potential mechanisms. *B. pumilus* could have induced important changes in the microbial community composition of the two rotational positions of WW (such as reduced abundance of ammonia-oxidizing bacteria), leading to inhibition of nitrification (Bozal-Leorri et al., 2022). In addition, it has been suggested that the exudation of certain compounds into the rhizosphere of cereals, termed biological nitrification inhibitors, can suppress the activity of nitrifiers, increasing soil NH_4^+-N and potentially plant N uptake (Subbarao et al., 2021; Bozal-Leorri et al., 2022; Kuppe and Postma, 2024). However, we did not observe an increase in soil NH_4^+ in the inoculated plants of both rotational positions. We measured an increase in soil NH_4^+ in the successive WW irrespective of inoculation status, which could be related to the quality and composition of the residues of the preceding crops. It has been shown that the residues of oilseed rape are quickly mineralized in the soil due to its high litter quality, which is evident in our experiment from the larger RH extent of BGU release (Trinsoutrot et al., 2000). Another and potentially most realistic mechanism may be that the soil NO_3^- was quickly depleted due to root growth promotion by *B. pumilus* that resulted in enhanced mineral N uptake by the plants, which is important for N uptake in both the top and subsoil (Thorup-Kristensen, 2001). All three mechanisms may co-exist and exert some influence on the performance of WW. From an environmental perspective, the significant reduction in soil NO_3^- after inoculation with *B. pumilus* could limit NO_3^- leaching and pollution of groundwater, giving additional value to the application of *B. pumilus* in WW rotations. Further analyses on the potential of *B. pumilus* to shape the microbial community will shed light on the complex interactions between PGPR and WW.

6.5 Conclusions

In this study, we tested the hypothesis of whether the inoculation of WW with *B. pumilus* can compensate for the reduced performance of successively grown WW. Our hypothesis was confirmed and the biomass growth reduction in the successive WW rotation was significantly alleviated by *B. pumilus*. The PGPR-inoculated successive WW showed a high LAP activity, root growth and K uptake that was translated into higher biomass. We demonstrated that PGPR application is a sustainable practice that can improve WW productivity during early growth. Our results advance our understanding of the potential of PGPR to modulate the plant-soil interactions in successive WW rotations and compensate for the negative PSF that is prevalent in such rotations.

7. Synopsis

7.1 Summary

Continuous cultivation of WW is associated with significant yield losses, a phenomenon widely observed but not yet fully understood. The lower yield is usually attributed to the high soil pathogen load in the soil of successive WW rotations and especially to the soil fungus Gt. However, this observation can also be made in years without obvious Gt symptoms, suggesting an important role for the soil microbiome and other soil factors in driving plant-soil interactions leading to this yield decline. Understanding the mechanisms that underlie this phenomenon is therefore crucial if we want to address the yield stagnation of WW.

The first approach (*Chapter* 2) was to investigate how contrasting rotational positions of WW affect soil nutrient dynamics, microbial assemblages, soil enzymatic activity and finally WW growth. An outdoor experiment was set up using sandy loam arable soil. W1, W2 and W4 were grown in rhizotrons. We applied zymography and harvested the plants at the onset of the stem elongation growth stage to observe changes in the activity of BGU and LAP as well as GLU imaging to observe GLU release patterns in the rhizosphere of WW. Several biochemical and microbial properties of the BS and the rhizosphere of the rotational positions were measured. W2 and W4 exhibited reduced growth compared to W1. Root growth traits exhibited a strong plastic response, with higher RLD, root mean diameter and lower SRL for W1 compared to W2 and W4. W1 soil had lower mineral N concentration and C_{mic} than W2 and W4, which translated to higher C:N ratio. Greater rhizosphere extent of BGU and LAP across the soil profile of W1 than W2 and W4 was evident from the zymography. Lower DOC and hotspot areas of GLU in the rhizosphere of successive WW possibly led to dysbiosis between plants and soil microbes. W4 had higher microbial species richness than W1, while soil depth and rotational position explained most of the variance in the soil microbial communities. *Actinobacteriota*, *Proteobacteria*, *Chloroflexi*, *Gemmatimonadota* and *Crenarchaeota* were the most abundant phyla with marked differences between the rotational positions at different soil depths. This study highlighted the effect of WW rotational positions on soil and plant properties as well as microbial community dynamics, and provided evidence for the pathways driving biomass decline in successively grown WW.

In *Chapter* 3, we aimed to assess the effect of the rotational positions on soil bacterial and archaeal communities, as well as N cycling, as potential drivers of WW yield decline in successively grown WW. W1 was compared with W2 in a rhizotron study using agricultural soil with a sandy loam texture. Samples were collected at tillering and grain ripening. At tillering, we found a higher NO_3^- content in W1 soil, especially in the 60-100 cm subsoil layer, associated with the N-rich residues of the preceding oilseed rape crop, while this trend was reversed at grain ripening. Analysis of enzyme kinetics revealed an increase in LAP activity in W1 and an increase in BGU activity in W2 at tillering, possibly related to the residue quality of the preceding crop. No differences in bacterial and archaeal alpha diversity were observed at both sampling times, but beta diversity showed a significant role of both rotational position and soil depth in shaping the microbial community. The gene copy numbers of *amoA* genes of AOB, *nifH* and *nirS* were significantly higher in W2 compared to W1 at tillering, suggesting a strong effect of rotational position on N cycling of the following WW. The abundances of *amoA* of AOB and *nirS* were also

higher in W2 at grain ripening. In this experiment, we showed that there is a persistent soil legacy effect of the preceding crop on both nutrient cycling and bacterial and archaeal community composition, contributing to yield reduction in successively grown WW.

In *Chapter* 4, we aimed to investigate how the rotational positions of WW affect the allocation of freshly assimilated C, an energy source for soil microbes, above- and belowground. A $^{13}CO_2$ pulse labeling rhizotron experiment was conducted in the greenhouse to study freshly fixed C allocation patterns in W1, W2 and W4. We used an automatic manifold system to measure excess ^{13}C of soil respiration at six depths and different growth stages of WW. ^{13}C excess was also measured in the DOC, microbial and plant biomass pools. There was a strong yield decline in successive WW rotations accompanied by distinct changes in root growth. Higher ^{13}C excess of soil respiration was measured in W1 compared to W4, especially in the topsoil during later growth stages. Higher ^{13}C excess of the DOC and the C_{mic} was also traced in W1 and W4 compared to W2. Less ^{13}C was taken up by successive WW rotations. This study revealed a mechanism through which the rotational position of WW affects the allocation of freshly assimilated C above- and belowground. WW after oilseed rape sustains belowground allocation of freshly assimilated C for a longer time than successively grown WW and incorporates more of this C to its biomass.

In *Chapter* 5, we aimed to address the yield decline phenomenon by adopting a sustainable farming practice. Using a quadruple isotope labeling study (^{13}C, ^{15}N, ^{2}H and ^{18}O), we investigated the effects of the rotational position and green-waste compost application on productivity of WW, grown either after oilseed rape or in self-succession, during the flowering and grain ripening stage. The initial high soil nutrient content after oilseed rape created a long-lasting soil legacy that gave an advantage to W1 with higher soil NO_3^-, NH_4^+, DOC, and C_{mic} than in W2. Compost significantly compensated for the disadvantage of W2, and by the grain ripening stage, these effects were reflected in enhanced root growth and nutrient uptake in the compost-amended W2. Above- and belowground allocation of freshly assimilated C and ^{15}N from the ^{15}N-labelled fertilizer were also higher in the compost-amended W2 compared to the unamended W2. Compost also increased the contribution of the topsoil and decreased the contribution of the subsoil to total plant water uptake, which resulted in enhanced plant growth and yield gains in the compost-amended W2. Our findings highlight the capacity of compost to buffer negative PSFs in monotonous crop rotations, while simultaneously improving plant growth and yield.

In *Chapter 6*, we assessed the potential of plant growth-promoting *B. pumilus* on the early growth of successively grown WW. We conducted an outdoor experiment using newly designed temperature-regulated rhizotrons. W1 and W2 were either non-inoculated or inoculated with *B. pumilus* at seed germination. The plants were grown until the end of tillering. We measured several plant and soil biochemical parameters and performed zymography to localize the enzymatic hotspots of BGU and LAP in the rhizosphere of the plants. *B. pumilus* significantly compensated for the early growth reduction of W2, and this effect was largely linked to changes in root plasticity with a higher RLD and a smaller SRL in inoculated W2 compared to non-inoculated W2. Inoculated W2 had a higher enzymatic LAP activity than non-inoculated W2, followed by a reduction in soil NO_3^-, most probably due to an enhanced nutrient uptake capacity. This was also reflected in an increased K content of the inoculated W2 compared to its non-inoculated

counterpart. Our study showed that *B. pumilus* can mitigate the negative PSF in successive WW rotations and provides strong evidence for the beneficial effect of PGPR application in promoting WW productivity in such rotations.

7.2 Synthesis

"Soil sickness" has been a well-documented phenomenon since the beginning of agriculture, which has led to the implementation of crop rotation. While this term effectively encompasses the idea of soil health, using the term PSF broadens the scope of soil sickness to include plant health and productivity. To date, there is a plethora of studies researching PSF in a variety of plants and ecosystems with several potential drivers reported, namely maternal effects, plant litter-soil feedback, self-DNA, plant-plant competition, climate, herbivory, greenhouse gases, soil nutrients (De Long et al., 2023). The focus of this thesis falls within the temporal diversity of the rotation and its associated PSF. Plant functional traits, such as root morphology, litter quality and nutrient composition, influence soil properties and microbial communities and drive PSF in WW rotations. Even though the observation of the yield decline in successive WW rotations is common, a strong mechanistic understanding is lacking. By looking at this phenomenon through the PSF perspective, this thesis gained a significant insight into the main drivers of WW productivity in contrasting crop rotations.

I conducted a series of experiments using novel experimental systems to study rhizosphere processes in WW rotations on two contrasting soil types. I used newly designed rhizotrons (Reichel et al., 2022) in *Chapters* 2, 3 and 4 and further optimized them to improve the quality of the experimental conditions and observations as presented in *Chapter* 6. The use of rhizotrons aimed to facilitate easy access to the rhizosphere and the use of the novel enzymatic imaging techniques zymography and GLU imaging as described in *Chapters* 2 and 6. The rhizotrons in *Chapter* 3 were equipped with gas-permeable tubing and connected to a novel manifold system to trace freshly assimilated C from pulse-labelled $^{13}CO_2$. This approach allowed for real-time quantification of freshly assimilated root-derived C along six soil depths and over several WW growth stages. In *Chapter* 5, I developed a new soil mesocosm system that was placed in an outdoor space, subjecting the plants to realistic ambient weather conditions and to realistic soil temperature regimes. The mesocosms allowed for minimally invasive soil sampling at various growth stages, and several rhizosphere processes were observed using a multiple isotopic approach. Strong multidisciplinary collaboration was at the core of this thesis, with significant advances made through the characterization of soil samples for biogeochemical, microbiological and enzymatic properties. The outcome of this collaboration highlighted the strong soil legacy of the preceding crops on WW growth and productivity.

In *Chapter* 2, we found that there is an early microbial immobilization of soil mineral N in successive WW rotations that is quickly locked up by the soil microbes and reflected by the higher C_{mic} values. This is obviously a residual effect of the preceding crop, with oilseed rape supplying higher amounts of mineral N to the following crop after harvest. This means that there is a lot of mineral N available for plant uptake during early growth, which translates into a higher plant

biomass during early growth as shown in *Chapter* 2. However, it is known that WW takes up low amounts of mineral N during the winter period, leaving a considerable pool of available N in the form of NO_3^- that could potentially be leached (Reichel et al., 2018). Indeed, in *Chapter* 3 we recorded a much higher soil NO_3^- content in the subsoil of non-successional WW, which might be leached under conditions of high precipitation and in soils with a high sand content. Therefore, adopting suitable agricultural management practices, such as compost application, is very important to address this environmental issue and be able to improve WW productivity at the same time. In *Chapter* 3, we found that the higher LAP activity in the non-successional WW rotation was associated with an enhanced mineralization of the pre-crop residues, resulting in a more efficient mineral N supply. At the same time, successive WW was faced with higher N losses due to the elevated *nirS* gene abundance that was also evident by the reduced soil NO_3^- content at tillering. We also found that AOB outnumbered AOA as the main ammonia-oxidizers in our soil. AOB abundance is usually greater in fertilized agricultural soils due to their lower enzymatic affinity and copiotrophic lifestyle under these N-rich conditions, while the higher substrate affinity of AOA make them more abundant under conditions of lower N availability (Lehtovirta-Morley, 2018). In the successional WW, the higher initial NH_4^+ was accompanied by an increase in *amoA* from AOB and explained the decreasing and increasing trend for soil NH_4^+ and NO_3^- respectively through the growth season. The increase in *nifH* gene abundance suggests that diazotrophs increase under the soil N limiting conditions of successional WW resulting in distinct N cycling patterns in the contrasting WW rotations. This was further evidenced by the differences in the microbial community composition that we found in *Chapters* 2 and 3, where it is clear that the PSF in WW rotations is highly dependent on the shape of the microbial assemblage.

In *Chapter* 4, we further researched potential mechanism of PSF in WW rotations and found strong evidence of the reduction in belowground C allocation in successive WW rotations compared to WW grown after oilseed rape. The higher translocation of freshly assimilated C belowground was sustained at higher rates in non-successional WW, while the microbial communities of continuous WW showed a slower consumption of rhizodeposited C. We showed that the reduced allocation of belowground C allocation in successive WW rotations may be an adaptive strategy to promote plant defense over growth and to outcompete soil microbes for the lower mineral N sources. Above ground, changes in allocation patterns reflected differences in root growth and soil nutrient content, with increased allocation of freshly assimilated C in the biomass of non-successional WW. Rhizodeposition stimulates microbial activity and mineralization of available organic nutrient sources, a mechanism by which the plants invest C in return for nutrients and water. It has been proposed that under C source limitation in grasslands, plants preferentially allocate C belowground to sustain microbial activity and ensure their survival (Hartmann et al., 2020). We found that this survival mechanism most probably depends on the extent of this source limitation and is an efficient coping strategy until a certain threshold. In *Chapter* 4, we showed that this threshold is largely exceeded and both above- and belowground allocation is severely restricted. Under these substrate-limiting conditions, the reduced rhizodeposition was a resource-saving strategy for the plants and therefore, an unfavorable investment (Noë and Kiers, 2018).

There is a great need to enhance SOC content in order to improve soil health and the resilience of farming systems to climate variability (Amelung et al., 2020), bearing in mind that there is an upper threshold, estimated at 1.4 % of SOC, to achieve high cereal yields. Several global change stressors, including but not limited to extreme weather events, aridity and human influence, have been shown to negatively affect SOC stocks globally (Sáez-Sandino et al., 2024). The adoption of sustainable practices like compost application is therefore among the potential agricultural adaptations which are both feasible to implement and promote SOC supply without compromising yield, as shown in *Chapter* 5. It is important to consider that the aim of boosting positive PSF and/or reducing negative PSF in successive WW rotations must balance the need for sufficient yield and food provision on the one hand, and soil multifunctionality on the other, concepts that do not necessarily converge (Garland et al., 2021). Rather than focusing solely on C sequestration, the adoption of "soil-smart" agricultural practices to sustain crop yields, such as fostering positive PSF in successive WW rotations, might go hand-in-hand with promoting SOC stocks (Moinet et al., 2023). In *Chapter* 5, the compost application successfully compensated for the yield decline in the successive WW rotation. There was a 25 % yield reduction in the successive WW rotation, which was fully mitigated by compost application. Successively grown WW benefited from the increased supply of organic and inorganic N and DOC that were rapidly utilized by the soil microbes and incorporated into microbial biomass. As a result, soil and especially BGU enzymatic activity was increased. This was also associated with the higher shoot and root allocation of freshly assimilated C, ultimately leading to higher yield. Another very important finding was the higher ^{15}N recovery from the ^{15}N-labeled fertilizer taken up by the successively grown WW in the compost-amended soil. This was directly linked with the effect of the compost on enhanced N uptake by WW due to the increase in root growth. Simultaneously, it decreased the contribution of the subsoil to plant water uptake as shown by the increased ^{2}H uptake from the topsoil and the decreased ^{18}O uptake from the subsoil. Compost application created a completely different root ideotype, which was optimized for the increased nutrient mineralization and availability in the topsoil. This was also evident by the higher proportion of thicker roots compared to the non-amended successional WW. The application rate of 40 t compost fresh weight ha^{-1} exceeded the maximum application rates of 20-30 t compost fresh weight ha^{-1} allowed in Germany within 3 years, while research has shown that both lower or higher rates than 40 t compost fresh weight ha^{-1} are beneficial to reduce the risk of take-all disease (Tilston et al., 2005; Demelash et al., 2014). The risk of nutrient leaching due to compost application was outside the scope of this thesis. However, previous research has shown that it is unlikely to be a major concern, while other measures, such as mixing compost with biochar or co-composting biochar, may increase the available surface area for NO_3^- sorption and effectively address this concern (Iqbal et al., 2015; Castro-Herrera et al., 2022). Although there are some emerging issues regarding compost application in agriculture, such as the potential contamination with microplastics (Braun et al., 2021, 2023), the multiple benefits to both plant and soil make a strong case for the widespread adoption of compost as a sustainable tool to increase yields in successive WW rotations and promote key soil functions.

PGPR inoculation also proved to be a very promising approach to mitigate productivity losses in successive WW rotations. The emerging market for biostimulants and the multiple benefits associated with PGPR can be considered a supplementary management option to compost. PGPR mechanisms of growth reduction compensation in successive WW rotations most likely differ from those of compost. Compost provides both a direct and indirect benefit to WW growth by supplying mineral nutrients and stimulating soil enzymatic activity that accelerates the mineralization of organic nutrients. At the same time, it could promote soil physical properties, such as soil porosity and soil aggregation, improving water retention and access for the plants. On the other hand, compost may introduce beneficial microorganisms that effectively control harmful soil pathogens of WW. Based on the findings in *Chapter* 6, *B. pumilus* may have worked in a different way. The application of *B. pumilus* could have stimulated changes in the rhizobiome assemblage, thereby influencing nutrient cycling and especially N cycling as shown by the differences in mineral N and especially soil NO_3^-. These changes in the microbial community composition might have stimulated LAP activity, enabling plants to access organic N. Another possible mechanism of growth promotion by *B. pumilus* could be the hormonal induction of WW (e.g., by auxin and cytokinin), which improved root growth and therefore direct access to soil nutrients. The increase in LAP activity and the release of organic N following the larger root system of WW could have reduced the competition between plants and soil microbes for N. Roots contribute to organic N uptake by direct secretion of proteases and by the indirect contact between proteins and proteases bound to root cell walls, although the contribution of root-derived protease activity is estimated to be about 1/5 of total soil protease activity (Godlewski and Adamczyk, 2007; Greenfield et al., 2020). Therefore, the stimulating effect of *B. pumilus* on the root growth of successively grown WW had a big influence on LAP activity and its associated soil functions. However, we should keep in mind that extracellular proteases have functions in addition to N cycling, such as defense against plant pathogens and root cell expansion (Greenfield et al., 2020), and the higher LAP in the successive WW rotation following *B. pumilus* inoculation may provide additional benefits to enhanced organic N supply. The influence of *B. pumilus* on the transcriptome of WW could have induced the changes in root growth patterns or could have stimulated stress resistance genes in the soil of successive WW rotations, promoting plant growth. In addition, changes in gene expression related to protein synthesis and metabolites (such as flavonoids and other phenolic compounds) can be a major pathway driving the observed response of WW to *B. pumilus* inoculation (Liu et al., 2023; Zhao et al., 2023).

7.3 Conclusions and outlook

This thesis demonstrated that PSF are major drivers of plant productivity and microbial functioning. We now know that yield loss due to repetitive WW cultivation is a multifaceted phenomenon that is associated with intense plant-microbial interactions, C and N transfer in the rhizosphere and within the plant, water uptake and distinct root plastic responses. The results of this thesis were consistent in two different soil types and have important agricultural implications for extrapolating the main findings of the experiments. This knowledge should be taken into

account when designing agricultural systems that aim to achieve simultaneous ecosystem multifunctionality and productivity, and in areas where continuous WW cultivation is a common practice to achieve food security and agricultural profitability. This thesis also showed that the implementation of two sustainable management practices, i.e., application of compost and PGPR, could be an important addition in the toolbox of farmers to sustain WW yield and improve soil fertility by capitalizing on positive PSFs, which stimulate rhizosphere processes and nutrient availability for WW. Given the importance of the yield decline in consecutive WW rotations, it is important to focus future research efforts on:

i. Validating our results in long-term field experiments to strengthen the predictability of the PSF and the proposed mechanisms: The experimental setup of this thesis allowed for both indoor and outdoor experiments where plants were exposed to ambient climatic conditions similar to field experiments. Nevertheless, certain limitations exist in mesocosm and rhizotron studies, and therefore field experiments will strengthen the power of the mechanisms that this thesis researched.
ii. Conducting experiments to evaluate the effects of PGPR over a longer period to fully comprehend their modulating role in plant growth enhancement: PGPR proved to be a suitable method to mitigate biomass losses in continuous WW. However, it remains to be studied whether this effect is sustained over time and is reflected in the final grain yield.
iii. Evaluating the changes in the plant's transcriptome and metabolome following PGPR and compost application to understand their beneficial effects in compensating for yield losses in successive WW rotations. Several genes encoding the biosynthesis of important compounds and secondary metabolites might be differentially expressed following PGPR and compost addition, providing important insights into how they mitigate yield losses in successive WW rotations.

Appendices

Appendix A: Supplementary material for *Chapter 2*

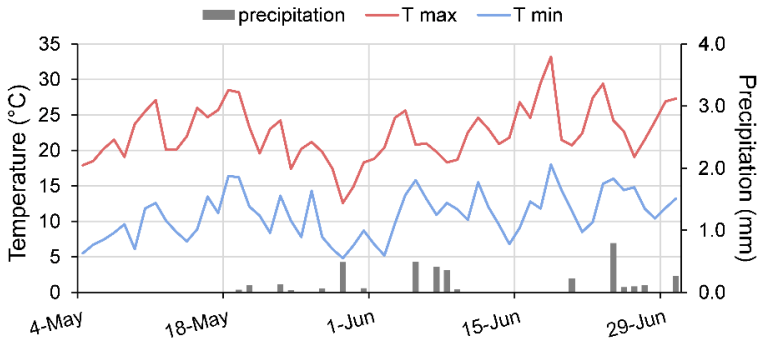

Figure A.1 Minimum and maximum temperature and precipitation throughout the course of the experiment.

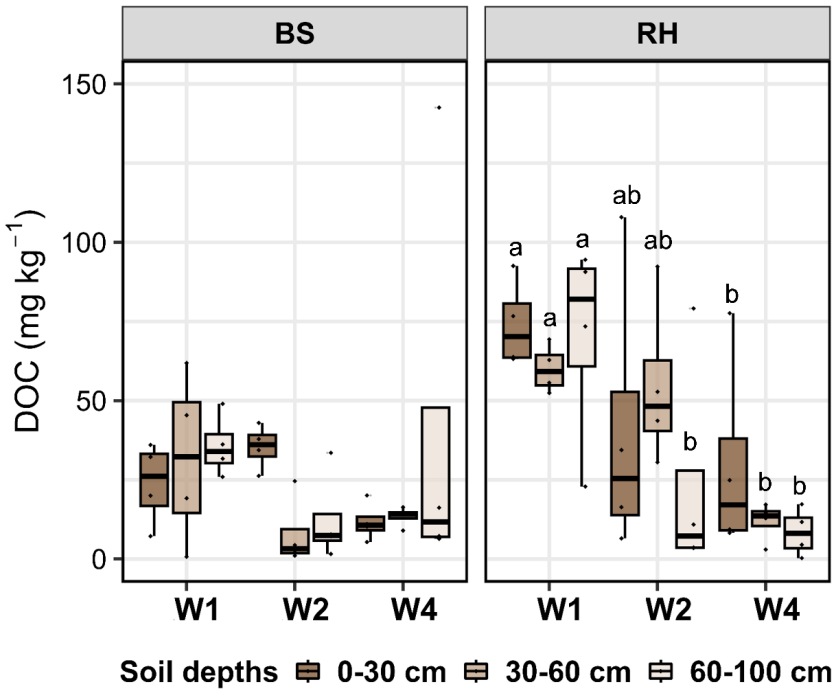

Figure A.2 Effect of the rotational positions on dissolved organic carbon (DOC) of the following winter wheat at the onset of stem elongation (BBCH 30), at soil depths 0-30 cm, 30-60 cm and 60-100 cm and in two soil compartments bulk soil (BS) and rhizosphere soil (RH). W1 = first wheat, W2 = second wheat, and W4 = fourth wheat after oilseed rape in soil from the experimental farm Hohenschulen in Kiel, Germany. Within each soil depth and soil compartment, different lowercase letters denote significant differences between rotational positions at $p \leq 0.05$ according to ANOVA with Bonferroni correction for multiple comparisons. No letters indicate non-significant differences.

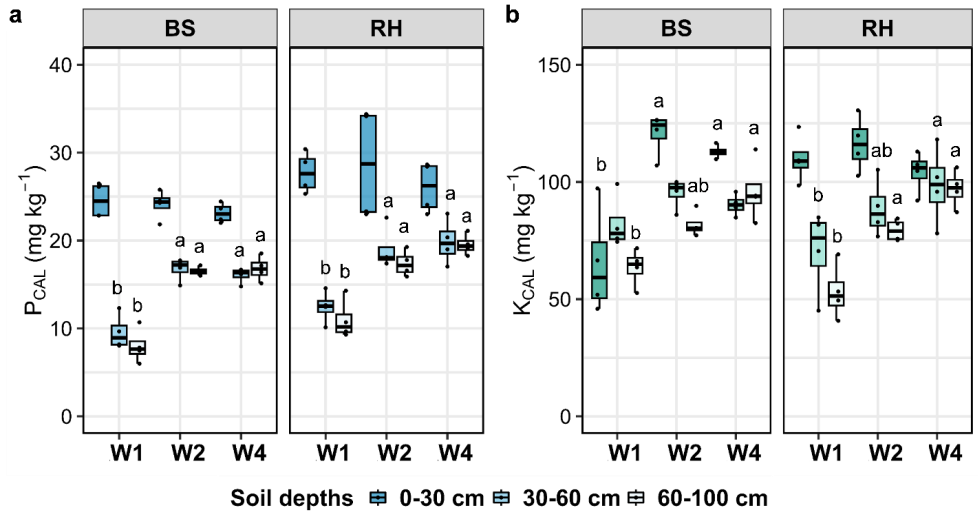

Figure A.3 Effect of the rotational positions on dissolved organic carbon soil P_{CAL} (a) and soil K_{CAL}(b) of the following winter wheat at onset of stem elongation (BBCH 30) at the three soil depths 0-30 cm, 30-60 cm and 60-100 cm and in two soil compartments bulk soil (BS) and rhizosphere soil (RH). W1 = first wheat, W2 = second wheat, and W4 = fourth wheat after oilseed rape in soil from the experimental farm Hohenschulen in Kiel, Germany. Uppercase letters denote significant differences between rotational positions. Within each soil depth and soil compartment, different lowercase letters denote significant differences between rotational positions at $p \leq 0.05$ according to ANOVA with Bonferroni correction for multiple comparisons. No letters indicate non-significant differences.

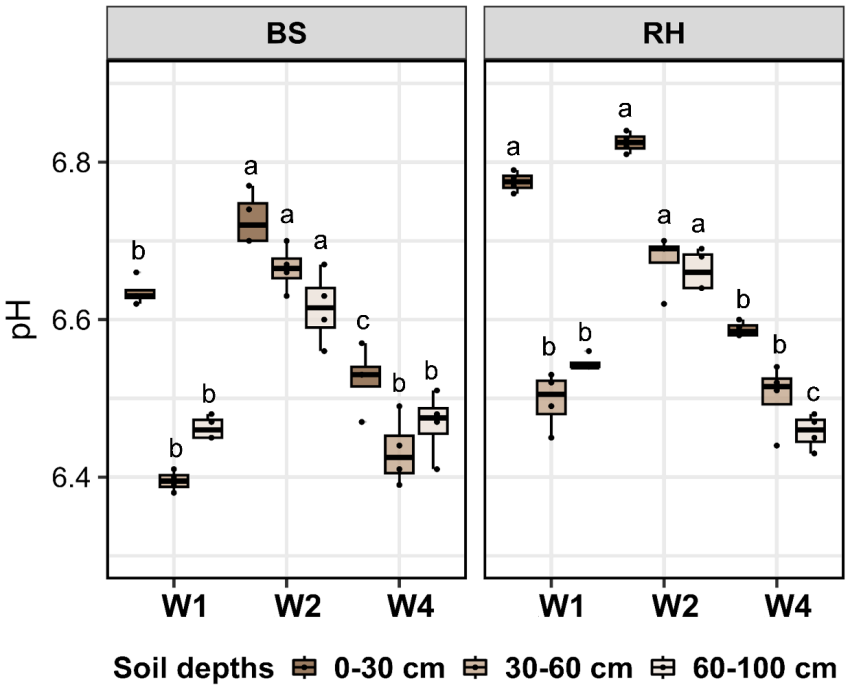

Figure A.4 Effect of the rotational positions on dissolved organic carbon soil pH of the following winter wheat at onset of stem elongation (BBCH 30) at the three soil depths 0-30 cm, 30-60 cm and 60-100 cm and in two soil compartments bulk soil (BS) and rhizosphere soil (RH). W1 = first wheat, W2 = second wheat, and W4 = fourth wheat after oilseed rape in soil from the experimental farm Hohenschulen in Kiel, Germany. Uppercase letters denote significant differences between rotational positions. Within each soil depth and soil compartment, different lowercase letters denote significant differences between rotational positions at $p \leq 0.05$ according to ANOVA with Bonferroni correction for multiple comparisons. No letters indicate non-significant differences.

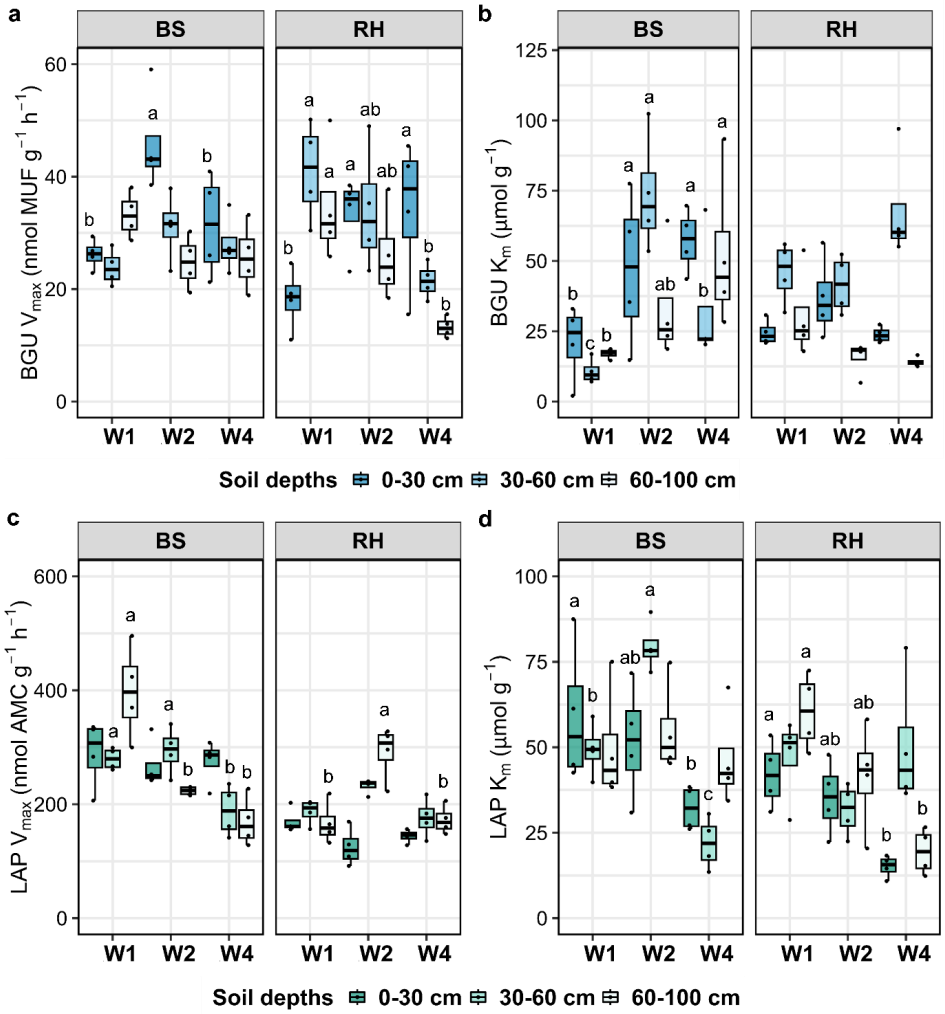

Figure A.5 Effect of the rotational positions on maximum velocity (V_{max}) and enzyme affinity (K_m) of *β*-glucosidase (BGU) (a and b) and leucine aminopeptidase (LAP) (c and d) of the following winter wheat at onset of stem elongation (BBCH 30), at soil depths 0-30 cm, 30-60 cm and 60-100 cm and in two soil compartments bulk soil (BS) and rhizosphere soil (RH). W1 = first wheat, W2 = second wheat, and W4 = fourth wheat after oilseed rape in soil from the experimental farm Hohenschulen in Kiel, Germany. Within each soil depth and soil compartment, different lowercase letters denote significant differences between rotational positions at $p \leq 0.05$ according to ANOVA with Bonferroni correction for multiple comparisons. No letters indicate non-significant differences.

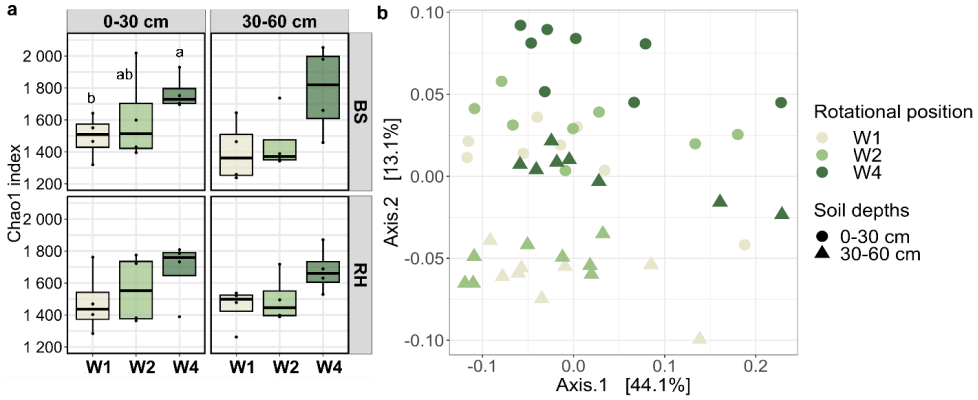

Figure A.6 Effect of the rotational positions on the microbial alpha diversity index Chao1 (a) and PCoA plots of beta diversity (b) of the following winter wheat at onset of stem elongation (BBCH 30), at soil depths 0-30 cm and 30-60 cm, and in two soil compartments bulk soil (BS) and rhizosphere soil (RH). W1 = first wheat, W2 = second wheat, and W4 = fourth wheat after oilseed rape in soil from the experimental farm Hohenschulen in Kiel, Germany. Within each soil depth and soil compartment, different lowercase letters denote significant differences between rotational positions at $p \leq 0.05$ according to the Kruskal Wallis test.

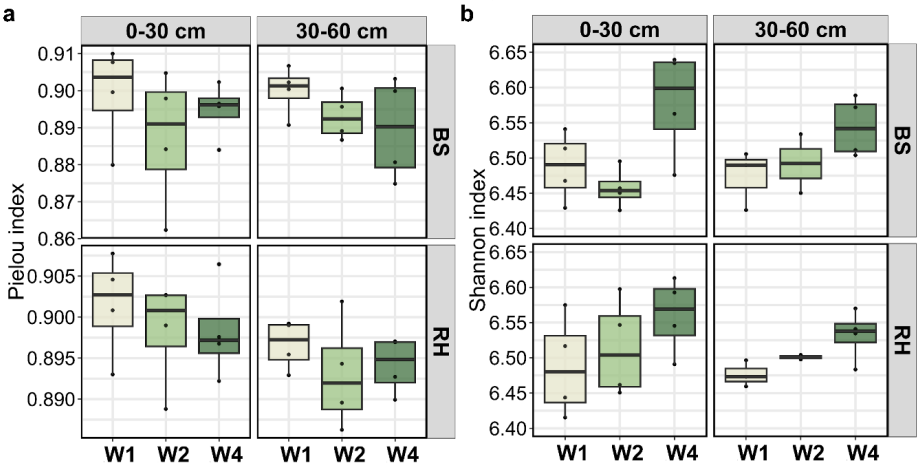

Figure A.7. Effect of the rotational positions on the microbial alpha diversity indices ((a) Pielou and (b) Shannon) of the following winter wheat at onset of stem elongation (BBCH 30), at soil depths 0-30 cm and 30-60 cm, and in two soil compartments bulk soil (BS) and rhizosphere soil (RH). W1 = first wheat, W2 = second wheat, and W4 = fourth wheat after oilseed rape in soil from the experimental farm Hohenschulen in Kiel, Germany. Within each soil depth and soil compartment, different lowercase letters denote significant differences between rotational positions at $p \leq 0.05$ according to Kruskal Wallis test followed by Wilcoxon–Mann–Whitney test. No letters indicate non-significant differences.

Table A.1 Impact of rotational position (Rot_pos), plant part (Plant_part) and their interactions on winter wheat total dry weight (Plant DW) as well as total C:N ratio (Plant C:N). For the individual dry weight and C:N ratio of the plant parts (root, stem and leaf) the main effect of rotational position in mentioned. Log transformation was used for Plant DW. Significant values at $p \leq 0.05$ are indicated in bold.

ANOVA results		Plant DW		Root DW		Stem DW		Leaf DW	
	d.f.	F	*p* value	F	*p* value	F	*p* value	F	*p* value
Rot_pos	2	31.08	< 0.001	20.45	< 0.001	24.83	< 0.001	5.43	0.028
Plant_part	2	53.52	< 0.001						
Rot_pos * Plant_part	4	2.13	0.104						
		Plant C:N		Root C:N		Stem C:N		Leaf C:N	
	d.f.	F	*p* value	F	*p* value	F	*p* value	F	*p* value
Rot_pos	2	34.95	< 0.001	25.83	< 0.001	9.20	0.007	24.80	< 0.001
Plant_part	2	391.90	< 0.001						
Rot_pos * Plant_part	4	6.07	0.001						

Table A.2 Impact of rotational position (Rot_pos), soil depth (Depth) and their interactions on root length density (RLD), root tissue density (RTD), root diameter (R_{dia}), specific root length (SRL), microbial biomass carbon (C_{mic}) and microbial biomass nitrogen (N_{mic}). The Box-Cox transformation was used for Rida. Significant values at $p \leq 0.05$ are indicated in bold.

ANOVA results		RLD		RTD		R_{dia}	
	d.f.	F	*p* value	F	*p* value	F	*p* value
Rot_pos	2	15.16	< 0.001	18.52	< 0.001	35.83	< 0.001
Depth	2	4.77	0.017	8.80	0.001	1.94	0.163
Rot_pos * Depth	4	3.438	0.021	3.07	0.033	0.83	0.516
		SRL		C_{mic}		N_{mic}	
	d.f.	F	*p* value	F	*p* value	F	*p* value
Rot_pos	2	22.71	< 0.001	25.45	< 0.001	17.66	< 0.001
Depth	2	100.71	< 0.001	27.11	< 0.001	28.25	< 0.001
Rot_pos * Depth	4	3.09	0.032	0.57	0.686	2.09	0.109

Table A.3 Impact of rotational position (Rot_pos), soil depth (Depth), soil compartment (Comp) and their interactions on soil $N\text{-}NH_4^+$, $N\text{-}NO_3^-$, dissolved organic carbon (DOC) and total nitrogen (TN). The Yeo-Johnson transformation was used for $N\text{-}NH_4^+$, $N\text{-}NO_3^-$ while the Box-Cox transformation was used for DOC and TN. Significant values at $p \leq 0.05$ are indicated in bold.

ANOVA results		$N\text{-}NH_4^+$		$N\text{-}NO_3^-$		DOC		TN	
	d.f.	F	*p* value	F	*p* value	F	*p* value	F	*p* value
Rot_pos	2	10.50	< 0.001	6.97	0.002	10.53	< 0.001	3.80	0.029
Depth	2	11.32	< 0.001	6.87	0.002	1.21	0.307	0.10	0.908
Comp	1	89.81	< 0.001	0.04	0.847	6.61	0.013	21.63	< 0.001
Rot_pos * Depth	4	0.92	0.459	0.21	0.929	0.98	0.426	2.59	0.047
Rot_pos * Comp	2	0.85	0.434	0.09	0.917	3.73	0.030	0.27	0.761
Depth * Comp	2	0.46	0.637	0.20	0.817	2.34	0.106	1.00	0.376
Rot_pos * Depth * Comp	4	0.61	0.655	0.11	0.977	1.96	0.114	0.31	0.873

Table A.4 Impact of rotational position (Rot_pos), soil depth (Depth), soil compartment (Comp) and their interactions on maximum velocity (V_{max}), enzyme substrate affinity (K_m), catalytic efficiency (K_a) and turnover time (Tt) of *β*-glucosidase (BGU V_{max}, BGU K_m, BGU K_a, BGU Tt) and leucine aminopeptidase (LAP V_{max}, LAP K_m, LAP K_a, LAP Tt). The Yeo-Johnson transformation was used for BGU K_m, BGU K_a, BGU Tt, LAP K_a and LAP Tt. Significant values at $p \leq 0.05$ are indicated in bold.

ANOVA results		BGU V_{max}		BGU K_m		BGU K_a		BGU Tt	
	d.f.	F	*p* value	F	*p* value	F	*p* value	F	*p* value
Rot_pos	2	5.33	0.008	10.14	< 0.001	12.59	< 0.001	7.56	0.001
Depth	2	3.21	0.048	7.71	0.001	3.45	0.039	2.16	0.125
Comp	1	0.77	0.384	0.18	0.674	0.29	0.589	1.38	0.245
Rot_pos * Depth	4	8.44	< 0.001	2.41	0.060	2.33	0.068	9.15	< 0.001
Rot_pos * Comp	2	2.34	0.106	14.87	< 0.001	10.35	< 0.001	1.25	0.295
Depth * Comp	2	3.27	0.046	8.83	< 0.001	3.77	0.029	1.72	0.189
Rot_pos * Depth * Comp	4	3.74	0.009	4.06	0.006	4.96	0.002	5.27	0.001
		LAP V_{max}		LAP K_m		LAP K_a		LAP Tt	
	d.f.	F	*p* value	F	*p* value	F	*p* value	F	*p* value
Rot_pos	2	16.75	< 0.001	18.75	< 0.001	8.27	0.001	6.84	0.002
Depth	2	2.44	0.097	2.40	0.100	0.41	0.665	1.99	0.147
Comp	1	75.14	< 0.001	14.71	< 0.001	0.89	0.350	59.71	< 0.001
Rot_pos * Depth	4	5.58	0.001	1.13	0.353	3.14	0.022	6.28	< 0.001
Rot_pos * Comp	2	13.32	< 0.001	6.08	0.004	10.39	< 0.001	11.98	< 0.001
Depth * Comp	2	7.67	0.001	0.92	0.405	1.85	0.168	10.27	< 0.001
Rot_pos * Depth * Comp	4	10.57	< 0.001	8.55	< 0.001	13.30	< 0.001	11.88	< 0.001

Table A.5 Impact of rotational position (Rot_pos), soil depth (Depth) and their interactions on glucose rhizosphere extent (GLU RH extent), activity (GLU activity), hotspot area (GLU hotspot), *β*-glucosidase rhizosphere extent (BGU RH extent), activity (BGU activity), hotspot area (BGU hotspot), leucine aminopeptidase rhizosphere extent (LAP extent), activity (LAP activity) and hotspot percentage (LAP hotspot). The Yeo-Johnson transformation was used for GLU RH extent. Significant values at $p \leq 0.05$ are indicated in bold.

ANOVA results		GLU RH extent		GLU activity		GLU hotspot	
	d.f.	F	*p* value	F	*p* value	F	*p* value
Rot_pos	2	3.16	0.066	3.26	0.062	7.27	0.005
Depth	2	15.89	< 0.001	0.72	0.502	37.27	< 0.001
Rot_pos * Depth	4	0.56	0.696	0.80	0.543	0.80	0.544
		BGU RH extent		BGU activity		BGU hotspot	
	d.f.	F	*p* value	F	*p* value	F	*p* value
Rot_pos	2	15.11	0.000	2.91	0.081	0.33	0.726
Depth	2	15.82	0.000	3.13	0.068	3.40	0.056
Rot_pos * Depth	4	3.793	0.021	1.11	0.384	1.87	0.159
		LAP RH extent		LAP activity		LAP hotspot	
	d.f.	F	*p* value	F	*p* value	F	*p* value
Rot_pos	2	1.70	0.211	0.93	0.412	1.18	0.329
Depth	2	2.65	0.098	0.68	0.521	3.99	0.037
Rot_pos * Depth	4	2.52	0.077	0.19	0.940	1.29	0.310

Table A.6 Impact of rotational position (Rot_pos), soil depth (Depth), soil compartment (Comp) and their interactions on plant-available P (soil P_{CAL}), K (soil K_{CAL}) and pH. Significant values at $p \leq 0.05$ are indicated in bold.

ANOVA results		soil P_{CAL}		soil K_{CAL}		pH	
	d.f.	F	*p* value	F	*p* value	F	*p* value
Rot_pos	2	36.32	< 0.001	36.16	< 0.001	277.98	< 0.001
Depth	2	148.44	< 0.001	32.94	< 0.001	191.22	< 0.001
Comp	1	28.60	< 0.001	0.15	0.698	88.22	< 0.001
Rot_pos * Depth	4	11.89	< 0.001	3.46	0.014	20.04	< 0.001
Rot_pos * Comp	2	0.45	0.639	1.56	0.219	8.62	0.001
Depth * Comp	2	0.53	0.589	3.06	0.055	6.09	0.004
Rot_pos * Depth * Comp	4	0.51	0.729	6.85	< 0.001	2.13	0.090

Table A.7 Impact of rotational position (Rot_pos), soil depth (Depth) and their interactions on root length proportion for six fine-root diameter classes. Significant values at $p \leq 0.05$ are indicated in bold.

Soil depth cm	Root diameter ≤ 0.05 mm %			Root diameter 0.05 - 0.1 mm %		
	W1	W2	W4	W1	W2	W4
0-30	0.96 ± 0.10	0.87 ± 0.08	0.84 ± 0.04	7.94 ± 1.21 b	11.0 ± 1.04 ab	14.11 ± 1.25 a
30-60	1.05 ± 0.13	0.81 ± 0.12	1.09 ± 0.03	8.90 ± 1.03 b	6.15 ± 1.07 b	12.28 ± 0.27 a
60-100	1.10 ± 0.17	0.91 ± 0.12	0.79 ± 0.05	3.13 ± 0.33	3.20 ± 0.41	5.62 ± 0.82
	Rotational	F = 2.3; P = 0.122		Rotational	F = 19.1; P < 0.001	
ANOVA	Depth	F = 0.56; P = 0.576		Depth	F = 48.6; P < 0.001	
	Two-way	F = 1.2; P = 0.333		Two-way	F = 3.3; P = 0.026	
Soil depth cm	Root diameter 0.1 - 0.5 mm %			Root diameter 0.5 - 1 mm %		
	W1	W2	W4	W1	W2	W4
0-30	85.55 ± 1.31	84.98 ± 1.30	82.01 ± 1.01	4.35 ± 0.31 a	2.64 ± 0.25 b	2.77 ± 0.28 ab
30-60	85.01 ± 1.54 b	89.70 ± 1.23 a	83.59 ± 0.27 b	4.29 ± 0.32	2.99 ± 0.30	2.88 ± 0.42
60-100	87.02 ± 1.17	89.62 ± 0.79	87.04 ± 0.89	7.62 ± 0.82 a	5.73 ± 0.78 b	6.11 ± 0.15 ab
	Rotational	F = 9.2; P = 0.001		Rotational	F = 11.6; P < 0.001	
ANOVA	Depth	F = 8.4; P = 0.001		Depth	F = 47.3; P < 0.001	
	Two-way	F = 1.9; P = 0.145		Two-way	F = 0.1; P = 0.971	
Soil depth cm	Root diameter 1 - 1.5 mm %			Root diameter 1.5 - 2 mm %		
	W1	W2	W4	W1	W2	W4
0-30	0.92 ± 0.10 a	0.43 ± 0.05 ab	0.24 ± 0.07 b	0.22 ± 0.04 a	0.07 ± 0.02 b	0.03 ± 0.01 b
30-60	0.63 ± 0.08 a	0.32 ± 0.04 ab	0.15 ± 0.04 b	0.10 ± 0.02 a	0.02 ± 0.01 ab	0.01 ± 0.00 b
60-100	0.95 ± 0.19 a	0.47 ± 0.11 b	0.39 ± 0.12 b	0.15 ± 0.05 a	0.05 ± 0.02 b	0.04 ± 0.01 b
	Rotational	F = 26.9; P < 0.001		Rotational	F = 25.9; P < 0.001	
ANOVA	Depth	F = 4.6; P = 0.020		Depth	F = 5.1; P = 0.013	
	Two-way	F = 0.4; P = 0.816		Two-way	F = 1.6; P = 0.202	

Table A.8 Impact of rotational position (Rot_pos), soil depth (Depth) and their interactions on root length proportion for the coarse root diameter class. Significant values at $p \leq 0.05$ are indicated in bold.

Soil depth cm	Root diameter ≥ 2 mm %		
	W1	W2	W4
0-30	0.06 ± 0.02 a	0.01 ± 0.00 b	0.00 ± 0.00 c
30-60	0.02 ± 0.01	0.00 ± 0.00	0.00 ± 0.00
60-100	0.04 ± 0.02	0.01 ± 0.00	0.01 ± 0.00
ANOVA	Rotational position	F = 11.5; P < 0.001	
	Depth	F = 2.6; P = 0.094	
	Two-way	F = 1.1; P = 0.364	

Table A.9 Pearson correlation coefficients of the correlations of plant growth, biochemical and microbial response variables of W1 at 0-30 cm and 30-60 cm. Asterisks indicate significant correlation coefficients at: *$p \leq 0.05$; **$p \leq 0.01$; ***$p \leq 0.001$.

0-30 cm / 30-60 cm	DW root	NH_4^+ RH	NH_4^+ BS	NO_3^- RH	NO_3^- BS	DOC RH	DOC BS	pH RH	pH BS	P RH	P BS	K RH	K BS	BGU V_{max} RH	BGU V_{max} BS	LAP V_{max} RH	LAP V_{max} BS	C_{mic}	N_{mic}	RLD	SRL	Rdia	Chloroflexi RH	Chloroflexi BS	Gemmatimonadota RH	Gemmatimonadota BS	Acidobacteriota RH	Acidobacteriota BS	Nitrospirota RH	Nitrospirota BS	BGU extent	BGU hotspot	LAP extent	LAP hotspot	GLU extent	GLU hotspot
DW root		-0.17	-0.44	0.51	.963*	0.93	0.58	0.88	-0.72	0.85	0.61	.950*	-0.22	-0.83	0.72	-0.46	0.40	0.38	0.55	0.91	0.32	0.47	-.967*	-0.77	0.77	0.06	-0.10	-.966*	.988*	0.03	-0.70	0.75	-0.21	-0.10	0.07	-0.19
NH_4^+ RH	-0.75		0.93	0.58	-0.05	0.17	-0.84	0.29	-0.20	0.37	0.67	-0.06	0.91	-0.07	-0.81	-0.27	-0.92	-0.02	-0.06	-0.56	-.959*	0.67	0.05	0.61	-0.21	0.49	.968*	0.38	-0.04	0.32	0.94	-0.20	0.98	0.95	-0.94	-0.81
NH_4^+ BS	-0.21	0.64		0.47	-0.28	-0.09	-.980*	-0.04	0.16	0.07	0.43	-0.39	0.79	0.07	-0.94	0.07	-.995*	0.06	-0.04	-0.74	-0.90	0.36	0.37	0.85	-0.54	0.60	0.94	0.65	-0.34	0.47	0.97	-0.26	0.95	0.91	-0.90	-0.75
NO_3^- RH	0.56	-0.14	0.66		0.70	0.78	-0.38	0.64	-0.27	0.76	0.89	0.40	0.27	-0.84	-0.13	-0.03	-0.53	0.71	0.75	0.24	-0.33	0.52	-0.45	0.15	0.00	0.83	0.73	-0.28	0.55	0.74	0.25	0.69	0.73	0.80	-0.82	-0.94
NO_3^- BS	-0.17	-0.51	-0.55	-0.38		.971*	0.40	0.84	-0.58	0.87	0.70	0.86	-0.22	-0.95	0.60	-0.28	0.22	0.59	0.74	0.85	0.27	0.43	-0.89	-0.59	0.58	0.32	0.07	-0.87	0.95	0.30	-0.52	0.88	0.03	0.13	-0.17	-0.41
DOC RH	0.68	-0.20	-0.16	0.20	-0.68		0.24	0.93	-0.69	.958*	0.84	0.88	0.02	-0.92	0.43	-0.41	0.05	0.50	0.65	0.72	0.03	0.63	-0.90	-0.49	0.60	0.35	0.26	-0.81	.950*	0.28	-0.34	0.78	0.22	0.32	-0.36	-0.58
DOC BS	-0.35	0.40	-0.37	-0.75	-0.31	0.37		0.23	-0.35	0.11	-0.27	0.56	-0.68	-0.16	.959*	-0.25	.980*	-0.10	0.04	0.80	0.81	-0.17	-0.54	-0.94	0.70	-0.61	-0.87	-0.77	0.50	-0.52	-0.98	0.29	-0.92	-0.88	0.86	0.70
pH RH	0.62	-0.87	-0.90	-0.26	0.41	0.39	0.10		-0.89	.986*	0.87	0.94	0.27	-0.72	0.33	-0.71	0.03	0.17	0.34	0.59	-0.17	0.84	-0.94	-0.54	0.76	0.11	0.29	-0.77	0.94	-0.01	-0.29	0.50	0.27	0.36	-0.40	-0.62
pH BS	0.35	-0.86	-0.89	-0.37	0.77	-0.05	-0.08	0.90		-0.81	-0.65	-0.90	-0.38	0.35	-0.32	0.94	-0.19	0.28	0.10	-0.45	0.21	-0.86	0.87	0.64	-0.91	0.32	-0.09	0.70	-0.80	0.44	0.73	-0.12	0.25	0.15	-0.11	0.14
P RH	-0.29	-0.19	0.08	0.08	0.78	-0.90	-0.69	-0.15	0.28		0.93	0.88	0.29	-0.79	0.25	-0.61	-0.10	0.30	0.45	0.55	-0.22	0.82	-0.89	-0.42	0.64	0.27	0.41	-0.71	0.91	0.16	-0.14	0.57	0.42	0.51	-0.54	-0.74
P BS	0.83	-0.33	0.38	0.90	-0.51	0.58	-0.51	0.06	-0.20	-0.27		0.64	0.52	-0.72	-0.11	-0.48	-0.46	0.34	0.44	0.24	-0.50	0.85	-0.67	-0.06	0.36	0.51	0.71	-0.41	0.70	0.36	0.31	0.46	0.78	0.84	-0.86	-0.96
K RH	-0.79	0.28	-0.43	-0.92	0.53	-0.56	0.52	-0.01	0.25	0.26	-.999**		0.00	-0.66	0.63	-0.71	0.38	0.09	0.28	0.79	0.14	0.66	-.998**	-0.80	0.91	-0.14	-0.07	-0.93	.977*	-0.21	-0.75	0.52	-0.28	-0.18	0.15	-0.11
K BS	0.30	-0.28	-0.74	-0.53	-0.15	0.70	0.74	0.70	0.42	-0.73	-0.11	0.15		0.21	-0.75	-0.54	-0.74	-0.42	-0.43	-0.61	-.980*	0.75	0.02	0.44	0.01	0.09	0.78	0.37	-0.08	-0.09	1.000**	-0.50	0.83	0.77	-0.74	-0.55
BGU V_{max} RH	0.25	-0.37	0.36	0.68	0.39	-0.47	-.993**	-0.13	0.10	0.77	0.41	-0.42	-0.78		-0.41	0.03	0.00	-0.80	-0.89	-0.72	-0.19	-0.33	0.71	0.32	-0.30	-0.60	-0.24	0.69	-0.80	-0.58	0.31	-0.95	-0.25	-0.35	0.38	0.61
BGU V_{max} BS	0.82	-0.54	-0.45	0.12	-0.35	0.93	0.25	0.70	0.32	-0.72	0.54	-0.50	0.77	-0.34		-0.13	0.91	0.18	0.32	0.93	0.86	-0.16	-0.63	-0.92	0.65	-0.36	-0.76	-0.86	0.62	-0.27	-0.99	0.55	-0.78	-0.72	0.69	0.48
LAP V_{max} RH	0.51	0.16	0.33	0.46	-0.93	0.88	0.23	-0.08	-0.50	-0.84	0.70	-0.70	0.33	-0.33	0.65		-0.13	0.57	0.42	-0.19	0.36	-0.84	0.67	0.52	-0.84	0.50	-0.09	0.47	-0.56	0.64	0.31	0.22	0.78	0.84	-0.86	-0.96
LAP V_{max} BS	0.44	-0.77	-0.19	0.38	0.68	-0.35	-0.84	0.40	0.61	0.72	0.27	-0.26	-0.38	0.85	-0.05	-0.48		-0.16	-0.06	0.69	0.85	-0.34	-0.36	-0.86	0.57	-0.67	-0.95	-0.62	0.31	-0.56	-0.95	0.17	-0.97	-0.94	0.93	0.80
C_{mic}	0.58	-0.16	0.64	1.000**	-0.37	0.20	-0.75	-0.24	-0.35	0.08	0.91	-0.92	-0.52	0.68	0.14	0.46	0.39		.981*	0.42	0.30	-0.20	-0.16	0.11	-0.30	0.84	0.23	-0.24	0.30	0.90	-0.18	0.89	0.38	0.47	-0.50	-0.71
N_{mic}	0.68	-0.47	0.38	0.93	-0.04	0.09	-0.89	0.03	0.00	0.29	0.84	-0.85	-0.49	0.83	0.17	0.22	0.69	0.93		0.57	0.34	-0.08	-0.35	-0.06	-0.10	0.77	0.18	-0.42	0.48	0.82	-0.28	.958*	0.28	0.37	-0.41	-0.63
RLD	0.95	-0.91	-0.33	0.49	0.15	0.44	-0.50	0.71	0.57	-0.01	0.69	-0.66	0.20	0.43	0.68	0.21	0.69	0.51	0.72		0.69	0.07	-0.81	-0.86	0.67	-0.07	-0.46	-.955*	0.83	-0.01	-0.89	0.78	-0.50	-0.41	0.38	0.13
SRL	0.51	-0.92	-0.52	0.13	0.75	-0.19	-0.60	0.69	0.85	0.55	0.15	-0.12	-0.03	0.60	0.18	-0.48	0.93	0.14	0.49	0.76		-0.65	-0.16	-0.60	0.18	-0.25	-0.86	-0.49	0.18	-0.08	-.999*	0.46	-0.87	-0.81	0.79	0.61
Rdia	-0.19	0.67	.994**	0.64	-0.64	-0.06	-0.29	-0.89	-0.93	-0.03	0.40	-0.45	-0.66	0.27	-0.37	0.42	-0.28	0.63	0.34	-0.34	-0.60		-0.65	-0.17	0.58	0.04	0.58	-0.34	0.60	-0.15	0.67	0.02	0.96	0.99	-0.99	-0.99
Chloroflexi RH	-0.26	0.78	0.46	-0.03	-0.89	0.45	0.62	-0.54	-0.80	-0.74	0.05	-0.08	0.20	-0.65	0.09	0.69	-0.93	-0.04	-0.39	-0.56	-.961*	0.55		0.78	-0.88	0.08	0.04	0.94	-.989*	0.14	0.71	-0.57	0.22	0.12	-0.08	0.18
Chloroflexi BS	-0.23	0.80	0.62	0.15	-0.92	0.40	0.45	-0.64	-0.89	-0.66	0.17	-0.20	0.03	-0.49	0.03	0.72	-0.85	0.14	-0.23	-0.52	-0.95	0.70	.981*		-0.89	0.56	0.65	0.91	-0.73	0.52	1.000**	-0.35	0.85	0.79	-0.76	-0.57
Gemmatimonadota RH	-.952*	0.70	-0.02	-0.76	0.13	-0.49	0.60	-0.42	-0.23	0.08	-0.90	0.89	0.00	-0.51	-0.62	-0.43	-0.58	-0.78	-0.87	-0.93	-0.54	-0.02	0.34	0.24		-0.54	-0.31	-0.84	0.80	-0.60	-.999*	0.17	-0.82	-0.75	0.73	0.53
Gemmatimonadota BS	-0.56	0.16	-0.65	-.999**	0.35	-0.17	0.77	0.25	0.35	-0.11	-0.89	0.91	0.55	-0.70	-0.11	-0.43	-0.41	-.999**	-0.94	-0.50	-0.16	-0.63	0.06	-0.12	0.77		0.69	0.17	0.05	.980*	0.44	0.57	0.86	0.91	-0.92	-0.99
Acidobacteriota RH	-0.59	0.85	0.91	0.30	-0.40	-0.40	-0.14	-.999**	-0.89	0.17	-0.03	-0.02	-0.73	0.18	-0.71	0.07	-0.36	0.28	0.02	-0.68	-0.66	0.90	0.51	0.62	0.38	-0.29		0.35	0.00	0.55	0.85	0.01	1.000*	0.99	-0.99	-0.91
Acidobacteriota BS	-0.25	-0.29	-0.07	-0.01	0.87	-0.87	-0.64	0.00	0.42	.988*	-0.32	0.32	-0.61	0.72	-0.64	-0.89	0.76	-0.01	0.24	0.05	0.64	-0.18	-0.82	-0.76	0.07	-0.02	0.03		-0.94	0.16	0.88	-0.66	0.49	0.39	-0.36	-0.11
Nitrospirota RH	0.87	-0.41	0.29	0.87	-0.46	0.61	-0.49	0.16	-0.12	-0.28	.996**	-.989*	-0.05	0.39	0.60	0.68	0.31	0.87	0.84	0.75	0.22	0.31	0.00	0.11	-0.93	-0.86	-0.13	-0.32		0.00	-0.63	0.68	-0.12	-0.01	-0.02	-0.28
Nitrospirota BS	0.38	-0.25	0.56	0.88	0.06	-0.24	-.966*	-0.24	-0.14	0.53	0.65	-0.67	-0.77	0.94	-0.20	-0.01	0.69	0.88	0.93	0.45	0.40	0.49	-0.40	-0.22	-0.64	-0.90	0.29	0.45	0.62		0.34	0.62	0.80	0.85	-0.87	-0.97
BGU extent	-0.87	0.98	0.47	-0.45	-0.44	-0.28	0.94	-0.87	-0.71	-0.52	-0.53	0.49	-0.20	-0.97	-0.83	0.10	-0.98	-0.47	-0.78	-0.98	-0.92	0.49	0.83	0.75	0.84	0.48	0.85	-0.52	-0.59	-0.74		-0.49	0.84	0.78	-0.76	-0.57
BGU hotspot	0.93	-0.46	0.03	0.64	-0.52	0.84	-0.19	0.38	0.01	-0.54	0.91	-0.89	0.31	0.08	0.84	0.79	0.13	0.65	0.61	0.77	0.17	0.08	0.10	0.15	-0.88	-0.62	-0.36	-0.54	0.93	0.31	-0.61		0.06	0.16	-0.20	-0.44
LAP extent	-0.91	0.95	0.39	-0.53	-0.36	-0.36	0.96	-0.83	-0.65	-0.44	-0.60	0.57	-0.11	-0.99	-0.87	0.01	-0.95	-0.55	-0.83	-0.99	-0.88	0.41	0.77	0.69	0.88	0.56	0.81	-0.45	-0.66	-0.80	1.00	-0.68		0.99	-0.99	-0.92
LAP hotspot	0.84	-0.26	0.56	1.000**	-0.59	0.98	-0.75	-0.02	-0.29	-0.51	.997*	-.999*	-0.77	0.67	0.88	0.83	0.26	1.000**	0.92	0.65	0.09	0.55	0.11	0.24	-0.87	-1.000**	0.06	-0.51	0.99	0.94	-0.47	0.98	-0.54		-.999*	-0.96
GLU extent	-0.76	1.000*	0.64	-0.27	-0.61	-0.08	0.85	-0.95	-0.84	-0.68	-0.35	0.31	-0.39	-0.90	-0.70	0.29	-1.000*	-0.29	-0.64	-0.91	-0.98	0.65	0.92	0.86	0.71	0.30	0.94	-0.68	-0.42	-0.60	0.98	-0.45	0.96	-0.28		0.97
GLU hotspot	0.95	-0.50	0.33	0.96	-0.36	0.89	-0.89	0.24	-0.03	-0.27	0.98	-0.97	-0.58	0.84	0.97	0.66	0.50	0.97	0.99	0.82	0.34	0.31	-0.15	-0.02	-0.97	-0.97	-0.20	-0.27	0.99	1.00	-0.68	1.00	-0.74	0.97	-0.52	

Table A.10 Pearson correlation coefficients of the correlations of plant growth, biochemical and microbial response variables of W2 at 0-30 cm and 30-60 cm. Asterisks indicate significant correlation coefficients at: *$p \leq 0.05$; **$p \leq 0.01$; ***$p \leq 0.001$.

0-30 cm / 30-60 cm	DW root	NH_4^+ RH	NH_4^+ BS	NO_3^- RH	NO_3^- BS	DOC RH	DOC BS	pH RH	pH BS	P RH	P BS	K RH	K BS	BGU V_{max} RH	BGU V_{max} BS	LAP V_{max} RH	LAP V_{max} BS	C_{mic}	N_{mic}	RLD	SRL	Rdia	Chloroflexi RH	Chloroflexi BS	Gemmatimonadota RH	Gemmatimonadota BS	Acidobacteriota RH	Acidobacteriota BS	Nitrospirota RH	Nitrospirota BS	BGU extent	BGU hotspot	LAP extent	LAP hotspot	GLU extent	GLU hotspot
DW root		0.51	0.27	-0.04	0.32	0.02	-0.59	0.03	0.34	-0.61	-0.48	-0.71	-0.24	-0.25	0.02	0.52	0.19	-0.59	0.15	0.87	0.62	-0.68	-0.26	-0.13	-0.81	-0.88	-0.32	-.982*	-0.34	-0.94	-0.34	0.42	0.69	-0.31	-0.47	0.77
NH_4^+ RH	-0.06		0.93	0.32	.958*	0.83	0.21	0.02	0.68	0.36	0.14	0.11	0.50	0.29	-0.66	0.82	-0.39	-0.13	-0.61	0.12	-0.21	0.29	-0.79	-0.43	-0.03	-0.12	0.64	-0.34	0.29	-0.67	-0.95	0.00	0.99	0.58	0.43	0.97
NH_4^+ BS	0.16	0.24		0.11	0.88	.968*	0.24	-0.26	0.83	0.57	0.08	0.20	0.43	0.16	-0.55	0.89	-0.25	-0.19	-0.86	-0.20	-0.53	0.50	-0.62	-0.18	0.09	0.19	0.82	-0.10	0.20	-0.53	-0.96	-0.35	0.99	0.58	0.43	0.97
NO_3^- RH	0.81	0.53	0.20		0.55	0.11	0.76	0.92	-0.45	0.33	0.89	0.65	0.89	.969*	-0.88	-0.28	-.968*	0.82	0.20	0.12	0.20	0.32	-0.83	-.987*	0.56	-0.07	0.27	0.14	0.93	0.20	-0.63	0.69	0.26	0.97	.998*	0.14
NO_3^- BS	-0.55	0.75	-0.33	0.00		0.83	0.47	0.22	0.50	0.53	0.41	0.38	0.73	0.55	-0.85	0.65	-0.63	0.16	-0.57	0.00	-0.26	0.46	-0.91	-0.62	0.23	0.01	0.74	-0.14	0.55	-0.45	-1.000**	0.09	0.92	0.79	0.67	0.87
DOC RH	0.93	0.21	0.44	0.89	-0.43		0.39	-0.29	0.78	0.74	0.19	0.38	0.50	0.21	-0.56	0.79	-0.30	-0.05	-0.94	-0.44	-0.72	0.69	-0.56	-0.14	0.30	0.43	0.93	0.15	0.28	-0.31	-0.99	-0.49	0.95	0.72	0.59	0.91
DOC BS	0.94	-0.18	0.43	0.67	-0.74	0.92		0.54	-0.26	0.82	.963*	.986*	0.93	0.90	-0.82	-0.23	-0.89	0.90	-0.24	-0.55	-0.44	0.83	-0.63	-0.68	.951*	0.59	0.67	0.70	0.95	0.57	-0.50	0.10	0.10	0.92	0.97	-0.02
pH RH	0.20	0.72	0.83	0.54	0.13	0.54	0.31		-0.72	-0.01	0.75	0.43	0.64	0.83	-0.63	-0.54	-0.80	0.77	0.57	0.35	0.52	-0.02	-0.60	-0.90	0.37	-0.30	-0.13	0.01	0.76	0.24	-0.29	0.89	-0.12	0.81	0.90	-0.24
pH BS	0.71	-0.67	0.25	0.19	-.975*	0.57	0.84	-0.12		0.25	-0.46	-0.25	-0.13	-0.41	0.00	.968*	0.33	-0.66	-0.84	-0.16	-0.51	0.20	-0.11	0.37	-0.30	0.12	0.53	-0.25	-0.37	-0.65	-0.62	-0.64	0.89	0.01	-0.16	0.93
P RH	-0.27	-0.83	-0.69	-0.68	-0.26	-0.59	-0.30	-.973*	0.20		0.64	0.87	0.72	0.54	-0.63	0.19	-0.56	0.51	-0.73	-0.83	-0.86	.997**	-0.45	-0.26	0.85	0.84	0.94	0.75	0.64	0.40	-0.72	-0.45	0.37	0.99	.998*	0.26
P BS	-.975*	-0.12	-0.32	-0.89	0.46	-.989*	-0.93	-0.41	-0.62	0.48		0.92	0.93	.970*	-0.83	-0.39	-0.95	.964*	0.01	-0.34	-0.18	0.65	-0.66	-0.81	0.88	0.38	0.47	0.58	.986*	0.56	-0.42	0.35	0.02	0.89	0.95	-0.10
K RH	-0.37	-0.89	-0.42	-0.82	-0.39	-0.62	-0.28	-0.84	0.27	0.94	0.55		0.86	0.82	-0.72	-0.26	-0.80	0.87	-0.30	-0.68	-0.55	0.88	-0.50	-0.54	.988*	0.71	0.69	0.81	0.88	0.66	-0.42	-0.04	0.01	0.88	0.95	-0.10
K BS	-0.94	0.37	-0.20	-0.57	0.80	-0.83	-.963*	-0.04	-0.91	0.05	0.88	0.08		.954*	-.973*	-0.02	-.973*	0.79	-0.25	-0.27	-0.26	0.70	-0.87	-0.86	0.77	0.31	0.68	0.39	.970*	0.24	-0.74	0.29	0.40	1.00	1.00	0.29
BGU V_{max} RH	0.85	-0.56	0.15	0.38	-0.89	0.69	0.90	-0.11	.971*	0.13	-0.75	0.14	-.976*		-0.91	-0.28	-.995**	0.90	0.05	-0.13	-0.03	0.53	-0.80	-0.93	0.74	0.18	0.43	0.37	.992**	0.36	-0.57	0.51	0.19	0.95	0.99	0.07
BGU V_{max} BS	0.87	-0.15	-0.35	0.68	-0.34	0.67	0.67	-0.21	0.53	0.07	-0.77	-0.16	-0.78	0.71		-0.15	0.94	-0.65	0.28	0.11	0.17	-0.59	.962*	0.89	-0.60	-0.14	-0.66	-0.18	-0.91	-0.01	0.86	-0.34	-0.58	-0.99	-0.96	-0.49
LAP V_{max} RH	0.13	0.80	0.77	0.53	0.25	0.47	0.21	.992**	-0.24	-.981*	-0.34	-0.87	0.06	-0.22	-0.25		0.18	-0.62	-0.76	0.03	-0.35	0.13	-0.30	0.16	-0.35	-0.06	0.51	-0.41	-0.26	-0.78	-0.70	-0.43	0.93	0.12	-0.06	0.96
LAP V_{max} BS	-0.94	-0.09	0.11	-0.87	0.28	-0.84	-0.76	-0.10	-0.48	0.24	0.91	0.44	0.80	-0.67	-.950*	-0.06		-0.85	0.02	0.11	0.05	-0.54	0.86	0.94	-0.71	-0.16	-0.49	-0.31	-.987*	-0.27	0.66	-0.49	-0.29	-0.98	-1.000*	-0.18
C_{mic}	-0.90	-0.37	-0.33	-.972*	0.23	-.974*	-0.82	-0.55	-0.40	0.65	.967*	0.74	0.72	-0.56	-0.70	-0.51	0.88		0.20	-0.33	-0.09	0.54	-0.46	-0.72	0.87	0.38	0.27	0.64	0.91	0.72	-0.16	0.40	-0.25	0.73	0.84	-0.36
N_{mic}	-0.54	0.86	0.26	0.04	0.82	-0.24	-0.56	0.60	-0.86	-0.63	0.35	-0.59	0.74	-0.86	-0.62	0.69	0.42	0.11		0.62	0.87	-0.70	0.24	-0.19	-0.26	-0.60	-0.88	-0.28	-0.04	0.19	0.97	0.76	-0.98	-0.62	-0.48	-0.96
RLD	.997**	-0.07	0.22	0.80	-0.59	0.94	.961*	0.23	0.74	-0.29	-.979*	-0.37	-.952*	0.86	0.83	0.16	-0.91	-0.90	-0.54		0.93	-0.87	-0.12	-0.24	-0.74	-.999**	-0.67	-0.91	-0.25	-0.64	0.12	0.74	0.29	-0.70	-0.81	0.40
SRL	-.984*	0.02	0.00	-0.83	0.44	-0.89	-0.86	-0.11	-0.62	0.22	0.94	0.37	0.89	-0.79	-0.94	-0.05	.984*	0.89	0.52	-.968*		-0.86	0.01	-0.27	-0.57	-0.91	-0.83	-0.70	-0.15	-0.31	0.82	0.85	-0.51	-.999*	-0.98	-0.41
Rdia	0.80	-0.50	-0.37	0.41	-0.59	0.53	0.68	-0.43	0.73	0.35	-0.65	0.18	-0.84	0.85	0.93	-0.49	-0.80	-0.49	-0.86	0.77	-0.84		-0.39	-0.23	0.87	0.88	0.91	0.80	0.63	0.47	-0.65	-0.46	0.28	0.98	.999*	0.17
Chloroflexi RH	0.87	0.45	0.26	.992**	-0.12	0.94	0.75	0.54	0.30	-0.66	-0.94	-0.78	-0.66	0.48	0.70	0.51	-0.89	-.993**	-0.05	0.86	-0.87	0.46		0.88	-0.36	0.10	-0.56	0.09	-0.78	0.25	0.96	-0.43	-0.77	-0.93	-0.85	-0.69
Chloroflexi BS	-0.30	0.07	0.88	-0.28	-0.21	-0.03	0.02	0.60	0.04	-0.40	0.16	-0.08	0.17	-0.14	-0.73	0.56	0.57	0.16	0.35	-0.23	0.46	-0.64	-0.23		-0.44	0.20	-0.24	0.01	-0.88	-0.04	0.75	-0.73	-0.42	-.998*	-0.99	-0.31
Gemmatimonadota RH	0.70	-0.76	-0.15	0.16	-0.86	0.44	0.71	-0.44	0.92	0.45	-0.54	0.41	-0.87	0.94	0.71	-0.53	-0.57	-0.31	-.978*	0.70	-0.67	0.91	0.25	-0.33		0.78	0.63	0.89	0.82	0.76	-0.28	-0.11	-0.14	0.81	0.90	-0.25
Gemmatimonadota BS	0.59	-0.38	0.70	0.23	-0.89	0.64	0.83	0.33	0.86	-0.20	-0.60	0.00	-0.76	0.78	0.19	0.21	-0.28	-0.45	-0.50	0.64	-0.44	0.34	0.34	0.50	0.60		0.67	0.93	0.30	0.67	-0.13	-0.70	-0.29	0.70	0.82	-0.39
Acidobacteriota RH	0.91	0.21	0.50	0.88	-0.44	.998**	0.92	0.58	0.57	-0.62	-.978*	-0.63	-0.81	0.68	0.62	0.51	-0.80	-.964*	-0.22	0.93	-0.85	0.49	0.93	0.03	0.42	0.67		0.48	0.52	0.06	-0.95	-0.48	0.73	0.95	0.88	0.65
Acidobacteriota BS	0.85	-0.14	-0.38	0.67	-0.31	0.65	0.65	-0.23	0.51	0.08	-0.75	-0.15	-0.76	0.69	1.000**	-0.26	-0.95	-0.68	-0.61	0.82	-0.93	0.93	0.69	-0.75	0.70	0.16	0.60		0.46	0.89	0.11	-0.43	-0.51	0.52	0.66	-0.60
Nitrospirota RH	0.00	0.46	-0.74	0.32	0.71	-0.10	-0.35	-0.24	-0.56	0.02	0.03	-0.29	0.26	-0.37	0.39	-0.15	-0.34	-0.11	0.25	-0.07	-0.17	0.14	0.22	-0.82	-0.26	-0.81	-0.15	0.41		0.41	-0.56	0.40	0.18	0.95	0.99	0.06
Nitrospirota BS	0.65	0.72	0.32	.965*	0.17	0.81	0.53	0.71	-0.01	-0.84	-0.78	-0.94	-0.38	0.17	0.47	0.71	-0.71	-0.91	0.29	0.64	-0.66	0.16	0.94	-0.12	-0.09	0.14	0.81	0.47	0.32		0.43	-0.10	-0.76	0.20	0.37	-0.83
BGU extent	0.98	-0.06	-0.11	0.89	-0.97	0.84	0.89	0.04	0.99	-0.18	-0.91	-0.44	-0.98	.999*	0.97	-0.02	-.999*	-0.87	-0.77	0.96	-1.00	0.91	0.88	-0.59	0.92	0.55	0.80	0.96	0.46	0.75		-0.15	-0.91	-0.79	-0.68	-0.86
BGU hotspot	-0.79	-0.56	-0.34	-.990*	0.03	-0.92	-0.69	-0.65	-0.20	0.76	0.89	0.86	0.56	-0.37	-0.60	-0.63	0.81	.978*	-0.09	-0.79	0.79	-0.33	-.989*	0.14	-0.11	-0.31	-0.91	-0.59	-0.21	-.977*	-0.81		-0.26	0.72	0.83	-0.37
LAP extent	0.09	-0.97	-0.98	-0.17	-0.05	-0.26	-0.16	-0.94	0.18	0.88	0.12	0.72	-0.13	0.25	0.54	-0.96	-0.27	0.21	-0.84	0.03	-0.22	0.67	-0.18	-0.95	0.66	-0.63	-0.32	0.56	0.99	-0.41	0.30	0.31		0.48	0.32	0.99
LAP hotspot	-0.59	-0.89	-0.87	-0.77	0.62	-0.83	-0.76	-0.93	-0.51	0.98	0.74	.998*	0.55	-0.44	-0.14	-0.91	0.42	0.80	-0.28	-0.63	0.47	0.02	-0.78	-0.51	0.00	-0.98	-0.86	-0.12	0.64	-0.91	-0.39	0.86	0.76		0.99	0.37
GLU extent	0.69	0.83	0.80	0.85	-0.72	0.90	0.84	0.88	0.62	-0.94	-0.82	-.997*	-0.65	0.55	0.27	0.85	-0.54	-0.87	0.15	0.73	-0.59	0.11	0.86	0.39	0.13	.999*	0.92	0.25	-0.53	0.95	0.51	-0.92	-0.66	-0.99		0.21
GLU hotspot	0.90	-0.28	-0.32	0.76	-0.89	0.70	0.77	-0.18	0.94	0.04	-0.80	-0.24	-0.92	0.96	.999*	-0.23	-0.97	-0.74	-0.89	0.88	-0.95	0.98	0.76	-0.75	0.98	0.35	0.65	.998*	0.64	0.58	0.98	-0.66	0.51	-0.18	0.31	

Table A.11 Pearson correlation coefficients of the correlations of plant growth, biochemical and microbial response variables of W4 at 0-30 cm and 30-60 cm. Asterisks indicate significant correlation coefficients at: *$p \leq 0.05$; **$p \leq 0.01$; ***$p \leq 0.001$.

0-30 cm / 30-60 cm	DW root	NH_4^+ RH	NH_4^+ BS	NO_3^- RH	NO_3^- BS	DOC RH	DOC BS	pH RH	pH BS	P RH	P BS	K RH	K BS	BGU V_{max} RH	BGU V_{max} BS	LAP V_{max} RH	LAP V_{max} BS	C_{mic}	N_{mic}	RLD	SRL	Rdia	Chloroflexi RH	Chloroflexi BS	Gemmatimonadota RH	Gemmatimonadota BS	Acidobacteriota RH	Acidobacteriota BS	Nitrospirota RH	Nitrospirota BS	BGU extent	BGU hotspot	LAP extent	LAP hotspot	GLU extent	GLU hotspot
DW root		-0.76	0.50	0.15	0.25	-0.13	0.11	0.46	-0.05	0.33	-0.46	0.72	0.47	0.25	-0.63	-0.59	-0.53	0.29	0.56	0.79	-0.78	0.70	-.969*	-0.74	-0.05	-0.44	0.57	-0.59	0.43	-.979*	0.59	0.33	-0.84	-0.78	-0.54	-0.64
NH_4^+ RH	-0.49		0.15	0.52	0.44	0.74	-0.62	0.22	0.59	-0.02	0.21	-0.52	-0.82	0.16	0.18	0.88	0.73	0.38	0.06	-0.26	.960*	-0.84	0.88	0.64	0.42	0.88	-0.07	0.62	0.06	0.65	-0.99	-0.63	0.98	0.99	0.98	-0.10
NH_4^+ BS	0.15	0.66		0.81	0.87	0.70	-0.78	.986*	0.83	0.19	-0.16	0.18	-0.19	0.80	-0.87	0.12	-0.07	0.83	0.79	0.72	-0.01	0.11	-0.27	-0.46	0.20	0.39	0.92	-0.30	0.49	-0.65	-0.72	-0.54	0.42	0.51	0.76	-0.85
NO_3^- RH	-0.19	-0.51	-.972*		.993**	.957*	-0.67	0.89	0.72	0.56	-0.45	0.28	-0.72	0.39	-0.42	0.65	0.53	.988*	0.88	0.69	0.48	-0.46	0.04	0.14	0.71	0.82	0.51	0.32	0.77	-0.26	-.997*	-0.38	0.90	0.94	1.000*	-0.32
NO_3^- BS	0.25	-0.53	-0.79	0.86		0.93	-0.70	0.94	0.74	0.53	-0.43	0.30	-0.63	0.47	-0.52	0.55	0.43	.992**	0.91	0.74	0.38	-0.36	-0.04	0.02	0.64	0.75	0.61	0.21	0.76	-0.36	-0.98	-0.39	0.85	0.90	0.99	-0.42
DOC RH	0.16	-0.92	-0.68	0.50	0.31		-0.76	0.78	0.78	0.41	-0.26	0.03	-0.83	0.39	-0.29	0.79	0.64	0.90	0.71	0.45	0.69	-0.63	0.33	0.30	0.68	0.93	0.40	0.44	0.61	0.01	-.999*	-0.53	0.92	0.95	1.000**	-0.29
DOC BS	0.55	-.979*	-0.70	0.59	0.68	0.83		-0.75	-.997**	0.23	-0.34	0.43	0.35	-0.86	0.66	-0.36	-0.08	-0.60	-0.37	-0.16	-0.40	0.18	-0.35	0.18	-0.03	-0.58	-0.73	0.14	-0.06	0.09	0.76	0.93	-0.47	-0.56	-0.80	0.82
pH RH	-0.38	0.24	0.47	-0.61	-0.91	0.07	-0.43		0.80	0.33	-0.28	0.26	-0.33	0.70	-0.78	0.25	0.09	0.91	0.87	0.77	0.10	-0.02	-0.24	-0.33	0.36	0.50	0.84	-0.14	0.62	-0.59	-0.84	-0.47	0.58	0.66	0.87	-0.74
pH BS	0.11	-0.24	0.34	-0.55	-0.70	0.43	0.06	0.84		-0.17	0.28	-0.36	-0.35	0.86	-0.69	0.35	0.09	0.65	0.44	0.24	0.38	-0.16	0.29	-0.20	0.07	0.59	0.76	-0.14	0.13	-0.15	-0.77	-0.90	0.48	0.57	0.80	-0.81
P RH	0.79	-0.82	-0.48	0.44	0.74	0.53	0.91	-0.66	-0.15		-.983*	0.86	-0.56	-0.44	0.18	0.45	0.60	0.63	0.75	0.73	0.18	-0.41	-0.34	0.38	0.90	0.42	-0.13	0.57	0.95	-0.25	-0.51	0.55	0.79	0.72	0.46	0.71
P BS	0.85	0.03	0.59	-0.55	-0.06	-0.35	0.05	-0.25	0.02	0.40		-0.93	0.39	0.46	-0.15	-0.27	-0.46	-0.55	-0.72	-0.76	0.00	0.24	0.50	-0.25	-0.80	-0.24	0.12	-0.44	-0.92	0.37	0.33	-0.66	-0.65	-0.57	-0.28	-0.83
K RH	0.50	-0.88	-0.78	0.73	0.86	0.69	.958*	-0.66	-0.23	0.92	0.03		-0.05	-0.36	-0.04	-0.08	0.11	0.41	0.67	0.82	-0.36	0.12	-0.77	-0.08	0.55	-0.08	0.02	0.12	0.80	-0.62	0.14	0.73	0.23	0.12	-0.20	0.99
K BS	0.01	0.24	0.73	-0.86	-0.94	-0.07	-0.40	0.90	0.87	-0.47	0.20	-0.64		0.16	-0.30	-.990**	-.961*	-0.64	-0.45	-0.18	-0.91	0.95	-0.55	-0.78	-0.86	-.964*	0.18	-0.87	-0.58	-0.43	0.87	0.18	-0.99	-0.97	-0.84	-0.27
BGU V_{max} RH	-0.55	-0.26	-0.89	0.93	0.62	0.39	0.30	-0.35	-0.48	0.07	-0.81	0.44	-0.72		-0.91	-0.17	-0.43	0.37	0.27	0.20	-0.11	0.35	-0.03	-0.65	-0.37	0.10	0.92	-0.62	-0.13	-0.43	-0.35	-0.83	-0.01	0.09	0.40	-0.99
BGU V_{max} BS	0.18	-0.10	0.53	-0.71	-0.79	0.24	-0.08	0.84	.976*	-0.21	0.19	-0.36	0.94	-0.65		0.35	0.54	-0.46	-0.49	-0.53	0.40	-0.55	0.43	0.82	0.28	0.07	-.993**	0.73	-0.11	0.77	0.23	0.53	0.14	0.03	-0.29	1.000*
LAP V_{max} RH	-0.19	-0.72	-0.67	0.49	0.14	0.93	0.60	0.28	0.46	0.21	-0.64	0.46	0.01	0.52	0.25		.958*	0.55	0.33	0.04	.957*	-.974*	0.66	0.82	0.79	.958*	-0.24	0.87	0.46	0.54	-0.87	-0.24	0.99	0.97	0.84	0.27
LAP V_{max} BS	-0.16	0.76	0.94	-0.93	-0.91	-0.66	-0.84	0.66	0.39	-0.73	0.29	-0.93	0.79	-0.73	0.55	-0.53		0.46	0.31	0.07	0.88	-.974*	0.54	0.91	0.87	0.86	-0.44	.970*	0.54	0.54	-0.70	0.05	0.91	0.86	0.66	0.52
C_{mic}	0.05	0.83	0.92	-0.81	-0.59	-0.91	-0.81	0.20	-0.04	-0.51	0.55	-0.78	0.44	-0.73	0.17	-0.88	0.87		0.94	0.79	0.36	-0.36	-0.11	0.05	0.71	0.73	0.55	0.26	0.84	-0.39	-1.00	-0.27	0.90	0.94	1.000*	-0.33
N_{mic}	0.91	-0.49	0.31	-0.42	-0.09	0.27	0.47	0.03	0.50	0.60	0.77	0.30	0.39	-0.70	0.56	-0.02	0.06	0.06		0.95	0.08	-0.15	-0.42	-0.10	0.68	0.50	0.54	0.13	0.92	-0.61	-.999*	-0.01	0.91	0.95	1.000**	-0.30
RLD	0.81	-0.11	0.15	-0.05	0.46	-0.29	0.27	-0.73	-0.45	0.65	0.84	0.38	-0.36	-0.37	-0.33	-0.61	-0.16	0.28	0.53		-0.23	0.12	-0.69	-0.30	0.53	0.20	0.55	-0.07	0.87	-0.80	-0.98	0.20	0.84	0.90	0.99	-0.43
SRL	-0.27	0.68	0.12	0.12	0.26	-0.80	-0.52	-0.54	-0.87	-0.26	0.07	-0.26	-0.52	0.17	-0.77	-0.75	0.10	0.49	-0.57	0.35		-.958*	0.85	0.83	0.59	0.90	-0.29	0.81	0.19	0.72	-0.89	-0.39	0.99	0.98	0.86	0.22
Rdia	0.23	-0.43	0.19	-0.42	-0.54	0.58	0.25	0.73	.980**	0.04	0.04	-0.03	0.77	-0.41	0.93	0.56	0.22	-0.20	0.59	-0.38	-0.95		-0.72	-0.93	-0.75	-0.87	0.45	-0.95	-0.35	-0.69	0.74	0.11	-0.94	-0.89	-0.70	-0.46
Chloroflexi RH	0.76	-0.38	0.45	-0.60	-0.36	0.26	0.30	0.31	0.71	0.37	0.68	0.08	0.63	-0.79	0.78	0.04	0.26	0.14	.958*	0.30	-0.67	0.76		0.67	0.08	0.57	-0.36	0.54	-0.36	0.90	-0.93	-0.53	1.000**	0.99	0.90	0.14
Chloroflexi BS	-0.03	-0.35	0.11	-0.33	-0.59	0.59	0.15	0.83	.967*	-0.15	-0.21	-0.13	0.75	-0.24	0.89	0.66	0.22	-0.26	0.35	-0.61	-0.92	.964*	0.56		0.65	0.62	-0.75	.972*	0.21	0.80	-0.42	0.17	0.72	0.64	0.37	0.78
Gemmatimonadota RH	-0.09	-0.06	-0.63	0.79	0.87	-0.10	0.24	-0.89	-0.94	0.34	-0.18	0.50	-.984*	0.69	-.987*	-0.15	-0.68	-0.30	-0.48	0.36	0.66	-0.87	-0.71	-0.84		0.76	-0.19	0.81	0.88	0.08	-0.72	0.25	0.92	0.88	0.68	0.50
Gemmatimonadota BS	-0.37	0.39	0.61	-0.72	-.967*	-0.10	-0.57	.984*	0.78	-0.73	-0.16	-0.77	0.92	-0.45	0.81	0.11	0.78	0.37	0.01	-0.66	-0.40	0.64	0.30	0.73	-0.88		0.05	0.71	0.52	0.35	-0.97	-0.42	0.99	1.000**	0.95	0.00
Acidobacteriota RH	-0.86	0.15	-0.19	0.11	-0.41	0.25	-0.30	0.67	0.36	-0.67	-0.88	-0.38	0.28	0.44	0.24	0.58	0.13	-0.28	-0.61	-.994**	-0.26	0.28	-0.40	0.52	-0.27	0.60		-0.64	0.17	-0.73	-0.36	-0.58	-0.01	0.10	0.41	-0.99
Acidobacteriota BS	-0.06	-0.44	-0.02	-0.20	-0.49	0.68	0.24	0.77	0.93	-0.09	-0.29	-0.03	0.66	-0.12	0.82	0.75	0.10	-0.38	0.31	-0.64	-0.94	0.94	0.50	.991**	-0.76	0.65	0.55		0.43	0.64	-0.50	0.22	0.78	0.72	0.46	0.71
Nitrospirota RH	0.93	-0.36	0.06	-0.02	0.48	-0.04	0.48	-0.66	-0.26	0.80	0.84	0.53	-0.29	-0.39	-0.17	-0.39	-0.27	0.10	0.71	.960*	0.08	-0.14	0.48	-0.40	0.24	-0.63	-.977*	-0.41		-0.41	-0.83	0.30	0.98	0.95	0.80	0.33
Nitrospirota BS	-0.34	-0.65	-0.82	0.68	0.31	0.86	0.57	0.12	0.21	0.18	-0.77	0.50	-0.22	0.73	-0.01	.962*	-0.65	-0.93	-0.24	-0.61	-0.54	0.31	-0.22	0.45	0.10	-0.05	0.61	0.56	-0.44		-0.23	-0.13	0.57	0.48	0.18	0.88
BGU extent	0.94	-0.86	0.29	-0.15	0.43	-.999*	0.78	-0.67	-0.39	0.95	0.90	0.61	-0.27	-0.47	-0.24	-.997*	-0.14	0.60	0.68	1.00	0.44	-0.34	0.42	-0.60	0.27	-0.61	-1.000**	-0.68	1.000**	-0.90		0.63	-0.93	-0.96	-.999*	0.25
BGU hotspot	0.58	-0.83	-0.16	-0.05	-0.01	0.80	0.73	0.23	0.71	0.58	0.20	0.50	0.34	-0.24	0.63	0.62	-0.27	-0.50	0.77	0.00	-0.93	0.83	0.78	0.72	-0.50	0.11	-0.09	0.74	0.28	0.42	0.12		-0.30	-0.40	-0.67	0.91
LAP extent	0.43	-0.98	-0.45	0.57	0.93	-0.70	1.00	-.997*	-0.92	0.90	0.34	0.99	-0.86	0.26	-0.84	-0.67	-0.79	-0.12	-0.02	0.79	0.94	-0.90	-0.32	-0.99	0.86	-0.99	-0.73	-.998*	0.71	-0.35	0.72	-0.60		0.99	0.91	0.12
LAP hotspot	0.11	0.72	0.85	-0.92	-0.98	0.22	-0.80	0.89	0.99	-0.54	0.20	-0.92	1.000*	-0.73	1.000**	0.18	0.99	0.62	0.54	-0.35	-0.98	1.00	0.77	0.92	-1.000*	0.92	0.26	0.88	-0.24	-0.19	-0.25	0.93	-0.85		0.95	0.02
GLU extent	0.64	0.21	.999**	-0.98	-0.72	-0.36	-0.34	0.49	0.75	0.02	0.71	-0.56	0.82	-0.99	0.84	-0.39	0.89	0.95	0.91	0.23	-0.71	0.78	0.99	0.56	-0.83	0.55	-0.32	0.47	0.33	-0.70	0.32	0.98	-0.42	0.83		-0.30
GLU hotspot	-0.99	0.51	-0.71	0.60	0.04	0.90	-0.40	0.24	-0.09	-0.70	-1.000*	-0.16	-0.21	0.83	-0.24	0.91	-0.34	-0.91	-0.94	-0.83	0.03	-0.14	-0.80	0.16	0.22	0.17	0.88	0.26	-0.89	.999*	-0.88	-0.57	-0.31	-0.23	-0.73	

Appendix B: Supplementary material for *Chapter 3*

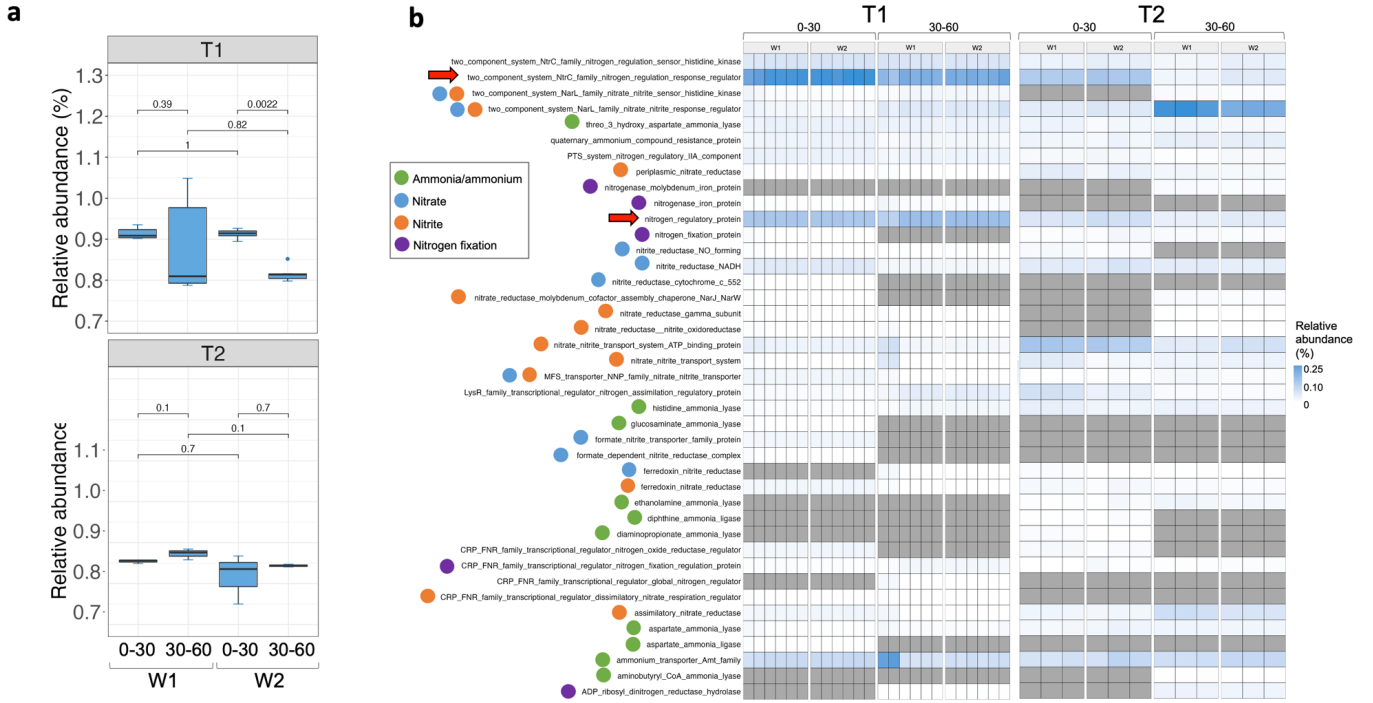

Figure B.1 Functional features related to nitrogen metabolism predicted by Tax4Fun2. (a) Relative abundance of the total nitrogen-related genes; (b) Description of the genes related to the nitrogen cycle in samples. The arrows correspond to regulator genes, and round shapes represent the different groups of nitrogen-related genes, green = ammonia/ammonium; blue = nitrate; orange = nitrite; purple = nitrogen fixation genes. W1 = first wheat after oilseed rape as a pre-crop; W2 = second wheat after oilseed rape at two plant developmental stages: T1 (BBCH 29, 28 DAS, tillering) and T2 (BBCH 90, 180 DAS, grain ripening), separated by soil depth (0-30 cm; 30-60 cm). Three plant replicates were analyzed for the response variables (n = 24 for T1 and n = 12 for T2).

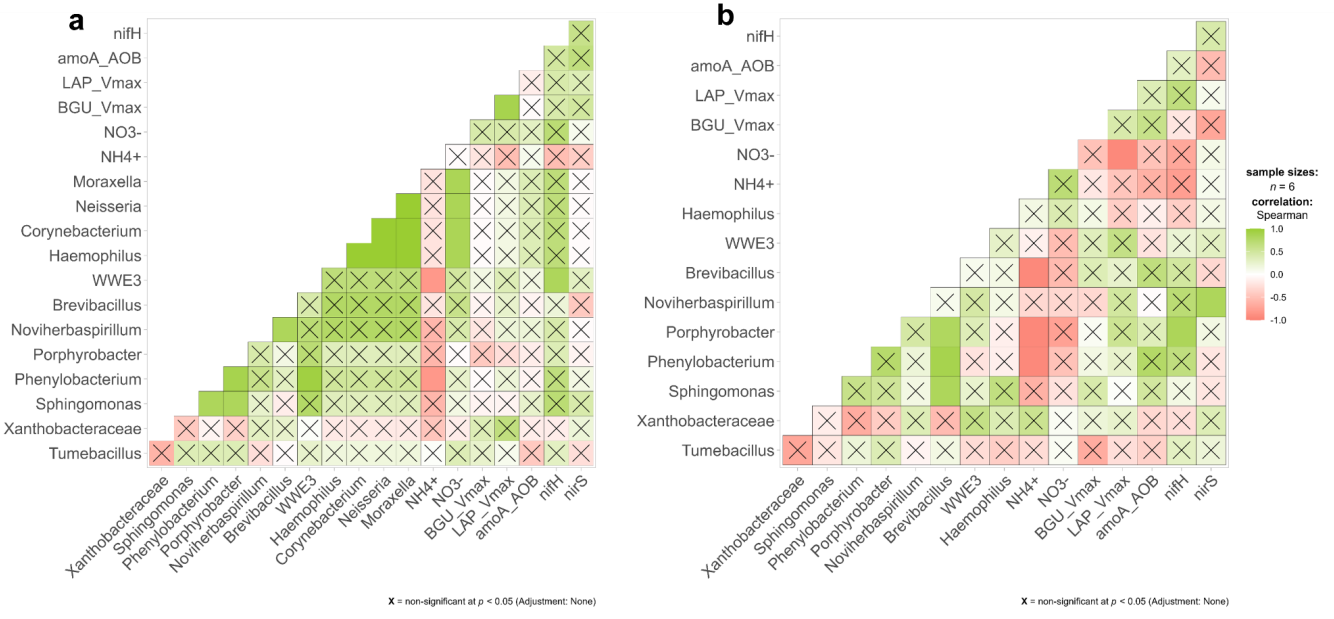

Figure B.2 Spearman rank correlation matrices visualizations for the biochemical variables at tillering (BBCH 29, 28DAS, T1) between (a) 1st winter wheat after oilseed rape (W1) and (b) 2nd winter wheat after oilseed rape (W2) and at 0-30 cm soil depth.

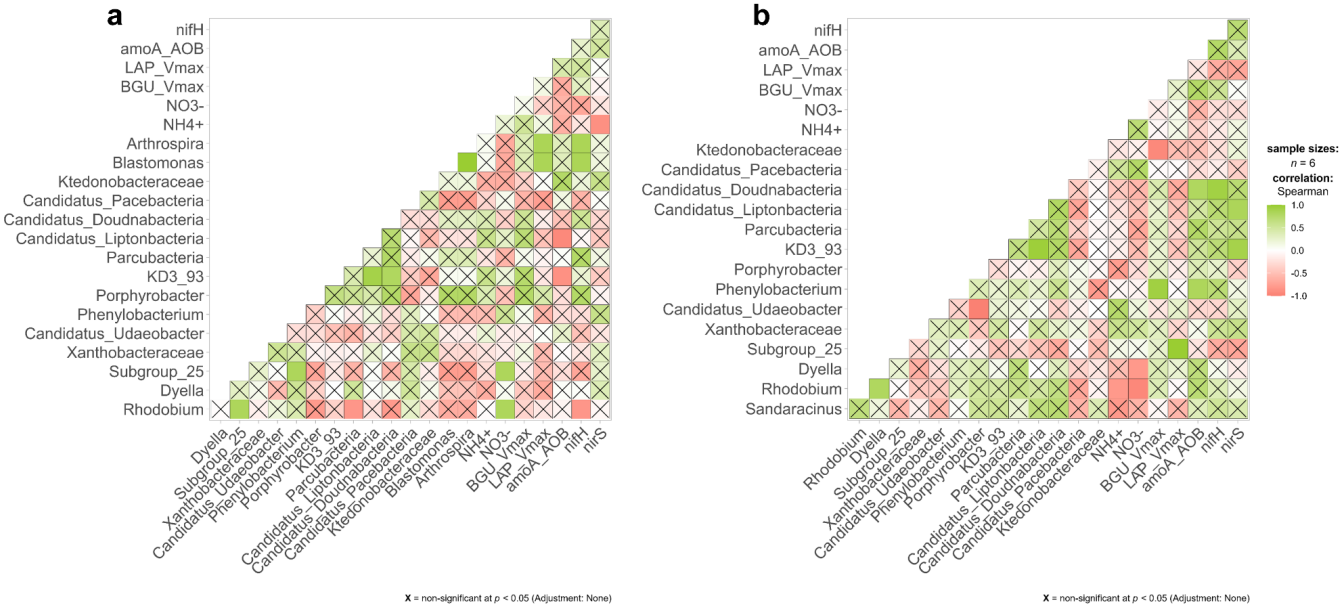

Figure B.3 Spearman rank correlation matrices visualizations for the biochemical variables at tillering (BBCH 29, 28 DAS, T1) between (a) 1st winter wheat after oilseed rape (W1) and (b) 2nd winter wheat after oilseed rape (W2) and at 30-60 cm soil depth.

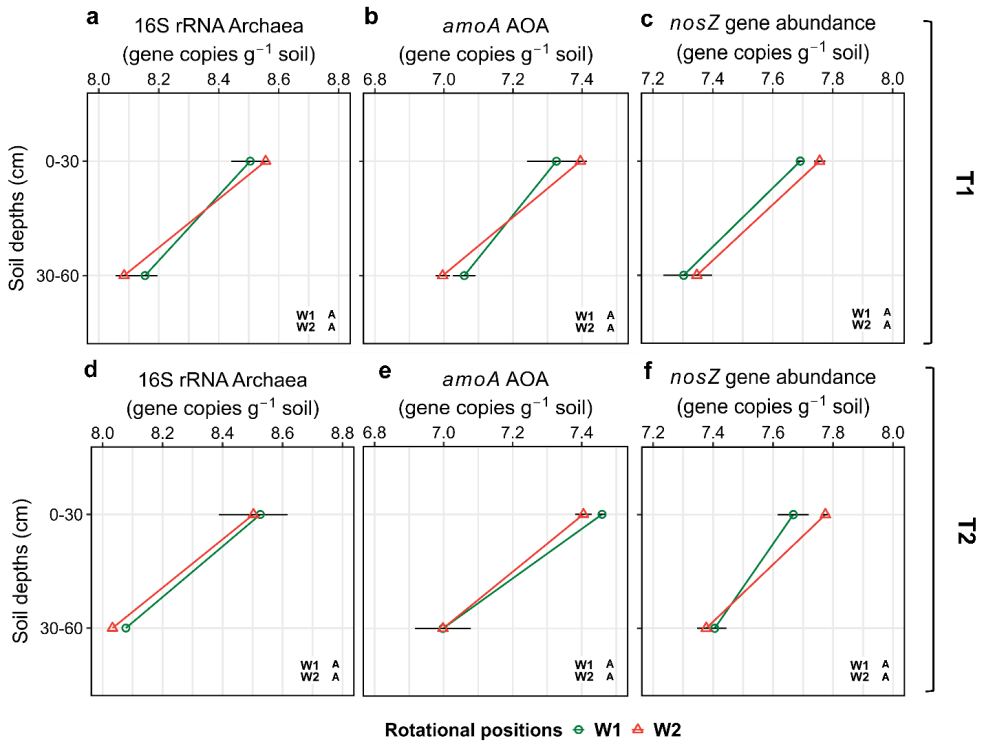

Figure B.4 Effect of the rotational positions on the 16S rRNA of Archaea (a, d), ammonia-oxidizing archaea *amoA* gene abundance (b, e) and bacterial *nosZ* gene abundance (c, f) of the following winter wheat at tillering (BBCH 29, 28 DAS) and grain ripening (BBCH 90, 180 DAS). W1 = first wheat and W2 = second wheat after oilseed rape. Different uppercase letters in each subplot indicate significant differences between the rotational positions. Within each soil depth, different lowercase letters denote significant differences between rotational positions at $p \leq 0.05$ level according to ANOVA with Bonferroni correction for multiple comparisons. No letters indicate non-significant differences. Three plant replicates were analyzed for the response variables (n = 24 for T1 and n = 12 for T2).

Table B.1 Effect of rotational position (Rot_pos), soil depth (Depth) and their interactions on ammonium ($N\text{-}NH_4^+$), nitrate ($N\text{-}NO_3^-$), *β*-glucosidase maximum velocity (BGU V_{max}) and leucine aminopeptidase maximum velocity (LAP V_{max}) at tillering (28 DAS, T1) and grain ripening (180 DAS, T2). Significant values at $p \leq 0.05$ level are indicated in bold. Data on $N\text{-}NH_4^+$, nitrate $N\text{-}NO_3^-$ were transformed, using the Yeo-Johnson transformation, prior to the analysis.

	ANOVA results	$N\text{-}NH_4^+$			$N\text{-}NO_3^-$			BGU V_{max}		LAP V_{max}	
		d.f.	F	*p* value	F	*p* value	d.f.	F	*p* value	F	*p* value
T1	Rot_pos	1	15.10	**0.001**	12.85	**0.002**	1	64.55	**0.000**	13.00	**0.007**
	Depth	2	3.37	0.057	21.92	**0.000**	1	1.38	0.275	0.14	0.723
	Rot_pos × Depth	2	0.07	0.932	1.61	0.228	1	1.81	0.216	3.25	0.109
T2	Rot_pos	1	15.33	**0.001**	29.80	**0.000**	1	0.02	0.899	0.37	0.551
	Depth	4	13.52	**0.000**	3.98	**0.015**	1	3.93	0.061	0.86	0.365
	Rot_pos × Depth	4	0.77	0.557	0.65	0.636	1	0.25	0.621	0.00	0.984

Table B.2 Effect of rotational position (Rot_pos), soil depth (Depth) and their interactions on 16S rRNA genes from bacteria, AMOgenes from ammonia-oxidizing bacteria (*amoA* AOB), bacterial NO_2^- reductase genes (*nirS*) and bacterial N_2-fixing nitrogenase genes (*nifH*) at tillering (28 DAS, T1) and grain ripening (180 DAS, T2). Significant values at $p \leq 0.05$ level are indicated in bold.

	ANOVA results	16S rRNA Bacteria		*amoA* AOB		*nirS*		*nifH*	
		d.f.	F	*p* value	F	*p* value	F	*p* value	F	*p* value
T1	Rot_pos	1	0.03	0.864	6.77	**0.017**	18.28	**0.000**	3.68	0.069
	Depth	1	232.90	**0.000**	22.66	**0.000**	28.85	**0.000**	6.90	**0.016**
	Rot_pos × Depth	1	0.80	0.382	11.82	**0.003**	0.01	0.909	0.91	0.353
T2	Rot_pos	1	0.32	0.589	3.74	0.089	4.40	0.069	4.90	0.058
	Depth	1	99.41	**0.000**	42.91	**0.000**	8.20	**0.021**	24.92	**0.001**
	Rot_pos × Depth	1	0.04	0.856	4.28	0.072	0.28	0.614	0.05	0.833

Table B.3 Effect of rotational position (Rot_pos), soil depth (Depth) and their interactions on 16S rRNA genes from archaea, ammonia monooxygenase genes from ammonia-oxidizing archaea and N_2O reductase genes from bacteria (*nosZ*) at tillering (28 DAS, T1) and grain ripening (180 DAS, T2). Significant values at $p \leq 0.05$ level are indicated in bold. Data on *amoA* AOA were transformed using the Yeo-Johnson transformation prior to the analyses.

	ANOVA results		16S rRNA archaea		*amoA* AOA		*nosZ*	
		d.f.	F	*p* value	F	*p* value	F	*p* value
T1	Rot_pos	1	0.05	0.824	0.09	0.773	1.15	0.297
	Depth	1	101.31	**0.000**	10.24	**0.004**	80.62	**0.000**
	Rot_pos × Depth	1	2.20	0.153	0.60	0.449	3.38	0.081
T2	Rot_pos	1	0.20	0.667	0.30	0.597	1.50	0.255
	Depth	1	36.49	**0.000**	78.31	**0.000**	81.47	**0.000**
	Rot_pos × Depth	1	0.02	0.890	0.31	0.596	0.05	0.821

Table B.4 Effect of rotational position (Rot_pos), soil depth (Depth) and their interactions on plant biomass and plant C:N. Significant values at $p \leq 0.05$ level are indicated in bold. Data were transformed, using the Yeo-Johnson transformation, prior to the analysis.

ANOVA results		Plant Biomass		C:N ratio	
	d.f.	F	*p* value	F	*p* value
Rot_pos	2	32.27	**0.000**	2.52	0.123
Plant_part	4	85.91	**0.000**	19.78	**0.000**
Rot_pos × Plant_part	8	1.55	0.212	1.09	0.381

Table B.5. Effect of rotational position (Rot_pos), soil depth (Depth) and their interactions on root dry weight (RDW) and root mass density (RMD). Significant values at $p \leq 0.05$ level are indicated in bold. Data on RMD were transformed, using the Yeo-Johnson transformation, prior to the analysis. Data have been adapted from Kaloterakis et al. (2024b).

ANOVA results		RDW		RMD	
	d.f.	F	*p* value	F	*p* value
Rot_pos	2	11.82	**0.000**	8.53	**0.001**
Depth	4	5.55	**0.001**	27.77	**0.000**
Rot_pos × Depth	12	1.26	0.290	0.69	0.696

Table B.6 Effect of rotational position (Rot_pos), soil depth (Depth) and their interactions on root *β*-glucosidase (BGU) and leucine aminopeptidase (LAP) substrate affinity (K_m) at tillering (28 DAS, T1) and grain ripening (180 DAS, T2). Significant values at $p \leq 0.05$ level are indicated in bold. Data on BGU at both T1 and T2 were transformed, using the Yeo-Johnson transformation, prior to the analysis.

	ANOVA results		BGU K_m		LAP K_m	
		d.f.	F	*p* value	F	*p* value
T1	Rot_pos	1	20.31	**0.000**	2.51	0.129
	Depth	1	0.52	0.479	0.81	0.378
	Rot_pos × Depth	2	0.06	0.804	0.26	0.615
T2	Rot_pos	1	5.65	**0.045**	36.34	**0.000**
	Depth	1	6.03	**0.040**	0.06	0.806
	Rot_pos × Depth	1	0.17	0.695	0.00	0.984

Appendix C: Supplementary material for *Chapter 4*

Figure C.1 Left: Visual illustration of the plant-labeling chamber used for the $^{13}CO_2$ pulse labeling. Right: The chamber fitted onto the rhizotron.

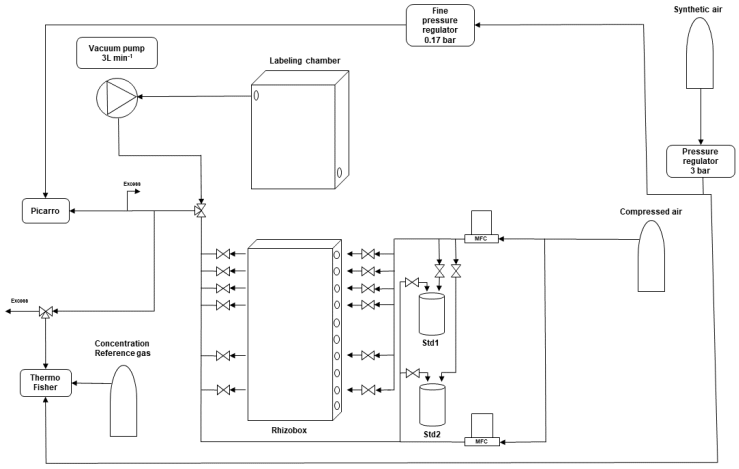

Figure C.2 Schematic representation of the experimental setup for sampling CO_2 and water vapor at different soil depths of the rhizotron, the plant-labeling chamber and from the two standards (500 ‰ $H_2{}^{18}O$ and D_2O enriched standard (Std1) and depleted Std2). Adjusted from Rothfuss et al. (2015). The setup consisted of two valve stands each supporting six 3/2-way valves (Bürkert GmbH and Co. KG, Ingelfingen, Germany) with brass and stainless steel connections (Swagelok, Düsseldorf, Germany) suitable for creating airtight conditions when connected to the gas permeable tubing. Dry synthetic air (20.5% O_2, 79.5% N_2; Air Liquide, Düsseldorf, Germany) was directed to the isotope-specific analyzers. A vacuum pump with a needle valve was connected to the outlet of the plant chamber fitted onto the rhizotron and pumped air from the chamber interior to the isotope-specific analyzers at a rate of 3 L min^{-1}. Synthetic air could be directed either to the valves connected to the side ports of the rhizotron, to the isotope standard vessels prepared as per Rothfuss et al. (2013) or to isotope-specific analyzers. Two pressure regulators were used to control pressure (1 bar, 5 ml min^{-1}, Distrelec Deutschland GmbH, Bremen, Germany) and mass flow controllers (MFC) (Bronkhorst Deutschland Nord GmbH, Kamen, Germany) were used to control airflow.

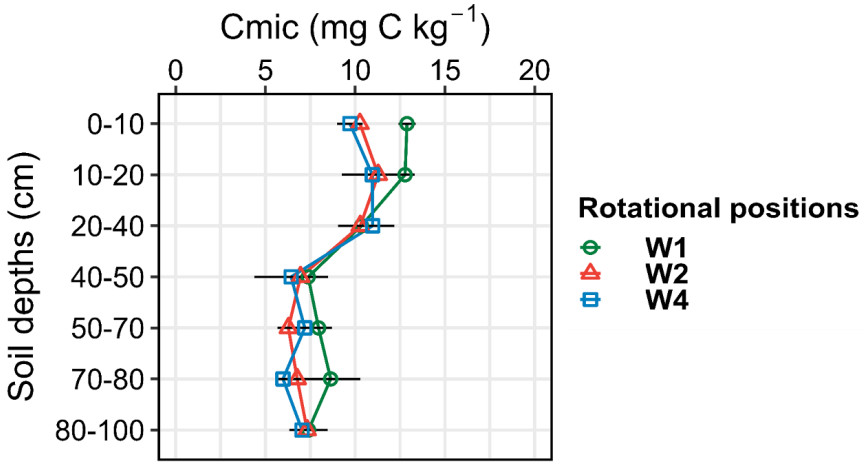

Figure C.3 Microbial biomass C (C_{mic}) of in three rotational position of winter wheat at grain ripening stage (BBCH 92). W1 = first wheat, W2 = second wheat, and W4 = fourth wheat after oilseed rape.

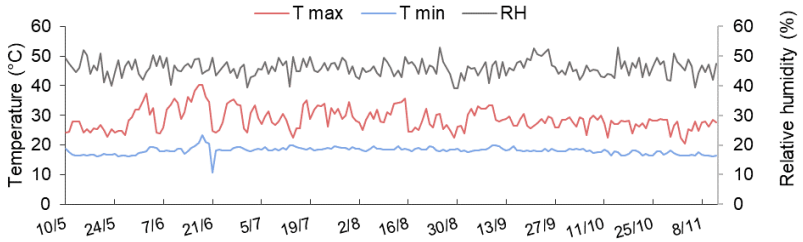

Figure C.4 Time courses of maximum (T max) and minimum (T min) temperature and relative humidity fluctuation in the greenhouse throughout the growing season of the plants.

Table C.1 Effect of days after labeling (DAL), rotational position (Rot_pos) and soil depth (Depth) and their interactions on excess ^{13}C of soil respiration fluxes tested with repeated measured ANOVA. Significant values at $p \leq 0.05$ level are indicated in bold. Data were log transformed prior to the analysis.

ANOVA results	Excess ^{13}C of soil respiration		
	d.f.	F	*p* value
DAL	2.973	231.4	**< 0.001**
DAL × Rot_pos	2.973	20.0	**< 0.001**
DAL × Depth	8.918	22.1	**< 0.001**
DAL × Rot_pos × Depth	8.918	1.5	0.178

Table C.2 Effect of rotational position (Rot_pos), plant part (Plant_part) and their interactions on absolute and relative excess ^{13}C of different plant parts as well as on total plant biomass. Significant values at $p \leq 0.05$ level are indicated in bold. Data were transformed, using the Yeo-Johnson transformation, prior to the analysis.

ANOVA results		Absolute excess		Relative excess		Total plant biomass	
	d.f.	F	*p* value	F	*p* value	F	*p* value
Rot_pos	2	29.42	**0.000**	0.61	0.549	30.60	**0.000**
Plant_part	4	21.80	**0.000**	34.92	**0.000**	307.54	**0.000**
Rot_pos × Plant_part	8	2.77	**0.020**	6.01	**0.000**	7.26	**0.000**

Table C.3 Effect of rotational position (Rot_pos), soil depth (Depth) and their interaction on absolute excess ^{13}C of microbial biomass C (C_{mic}), dissolved organic carbon (DOC) and root biomass. Significant values at $p \leq 0.05$ level are indicated in bold. Data were transformed, using the Yeo-Johnson transformation, prior to the analysis.

ANOVA results		Excess ^{13}C C_{mic}		Excess ^{13}C DOC		Excess ^{13}C root	
	d.f.	F	*p* value	F	*p* value	F	*p* value
Rot_pos	2	7.64	**0.001**	8.98	**0.001**	9.81	**0.000**
Depth	6	6.10	**0.000**	5.61	**0.000**	7.36	**0.000**
Rot_pos × Depth	12	0.83	0.619	0.88	0.569	0.73	0.718

Table C.4 Effect of rotational position (Rot_pos), soil depth (Depth) and their interaction on root dry weight (RDW), root mass density (RMD) and root length density (RLD). Significant values at $p \leq 0.05$ level are indicated in bold. Data on RMD were transformed, using the Yeo-Johnson transformation, prior to the analysis.

ANOVA results		RDW		RMD		RLD	
	d.f.	F	*p* value	F	*p* value	F	*p* value
Rot_pos	2	11.82	**0.000**	8.53	**0.001**	7.44	**0.002**
Depth	4	5.55	**0.001**	27.77	**0.000**	2.16	0.089
Rot_pos × Depth	12	1.26	0.290	0.69	0.696	2.94	**0.010**

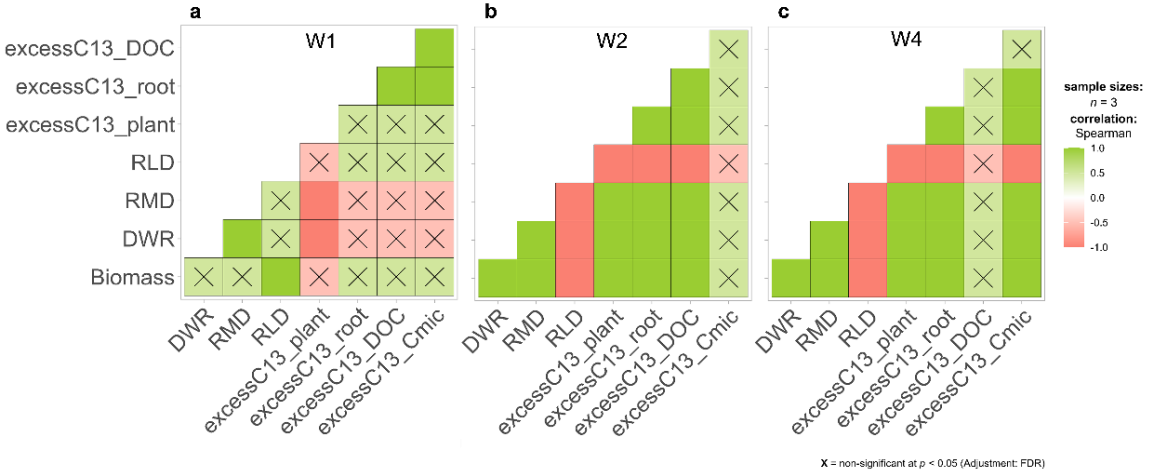

Figure C.5 Spearman rank correlation matrices visualizations with false discovery rate (FDR) adjustment between excess ^{13}C of plant material, root, dissolved organic carbon (DOC), microbial biomass carbon (C_{mic}), root dry weight (DWR), root mass density (RMD) and root length density (RLD) for (a) 1st winter wheat after oilseed rape (W1), (b) 2nd winter wheat after oilseed rape (W2) and (c) 4th winter wheat after oilseed rape (W4).

Appendix D: Supplementary material for *Chapter 5*

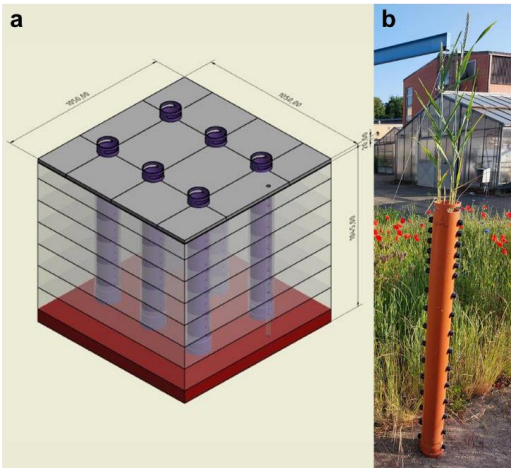

Figure D.1 (a) Diagram of the stacked styrofoam plates with the PVC pipes/mesocosms, (b) PVC mesocosm with the sampling ports at different depths used in the experiment.

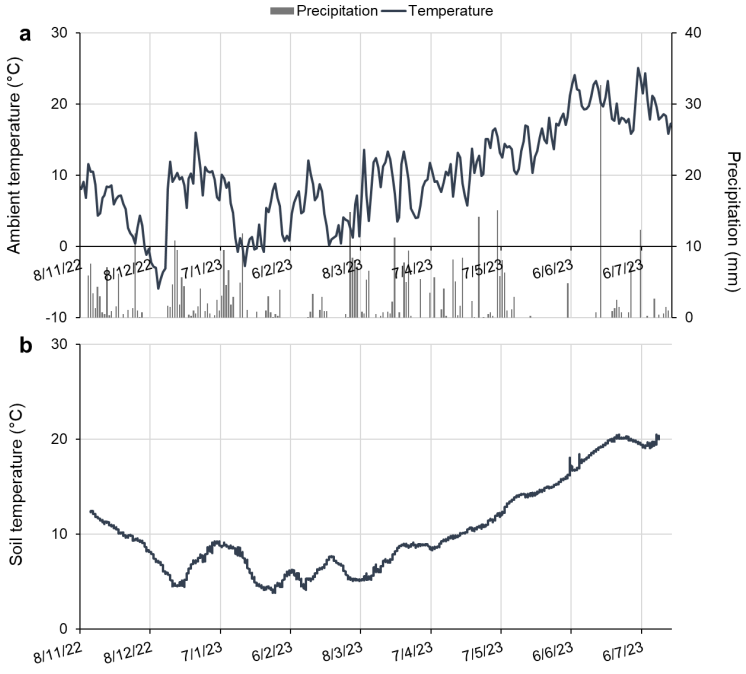

Figure D.2 (a) Time courses of temperature and precipitation, and (b) soil temperature throughout the growing season.

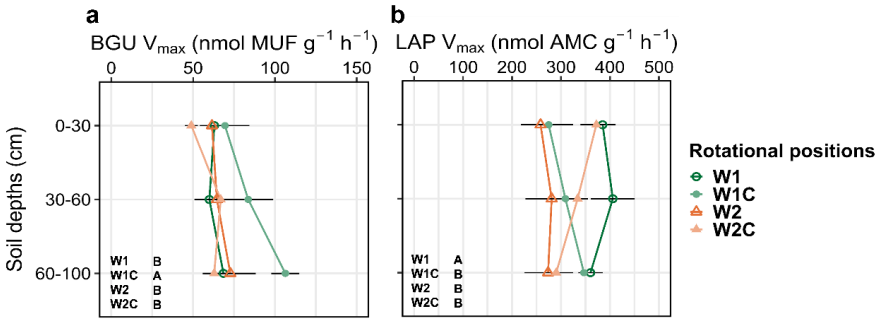

Figure D.3 Effect of the rotational positions on (a) the V_{max} of *β*-glucosidase (BGU) and (b) leucine-aminopeptidase (LAP) of the following winter wheat at flowering (BBCH 61, T1). First wheat after oilseed rape without (W1) and with (W1C) compost addition, and second wheat after oilseed rape without (W2) and with (W2C) compost addition. Different uppercase letters in each subplot indicate significant differences between the rotational positions. Within each soil depth, different lowercase letters denote significant differences between rotational positions at $p \leq 0.05$ level according to PERMANOVA with Benjamini-Hochberg p adjustment. Absence of letters indicates non-significant differences.

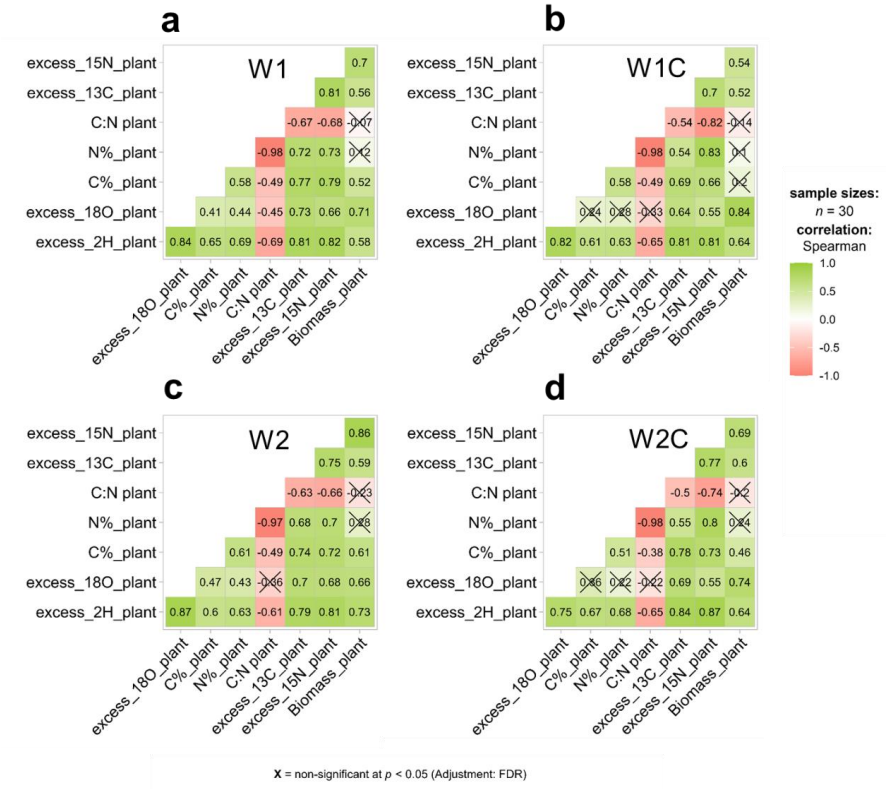

Figure D.4 Spearman rank correlation matrices visualizations with false discovery rate (FDR) adjustment between the absolute ^{13}C excess of plant material for (a) 1st winter wheat after oilseed rape without (W1) and (b) with (W1C) compost addition; (c) 2nd winter wheat after oilseed rape without (W2) and (d) with (W2C) compost addition.

Table D.1 Effect of rotational position (Rot_pos), organic amendment (OA), soil depth (Depth) and their interactions on ammonium ($N\text{-}NH_4^+$), nitrate ($N\text{-}NO_3^-$), dissolved organic C (DOC), total extractable N (TN), β-glucosidase reaction rate (BGU V_{max}), leucine aminopeptidase reaction rate (LAP V_{max}), absolute ^{13}C excess of the soil, DOC, C_{mic} and absolute ^{15}N excess of the soil at flowering (BBCH 61, T1). Significant values at $p \leq 0.05$ level are indicated in bold. Pseudo F is the modeled analogous to the F statistic in ANOVA.

ANOVA results		$N\text{-}NH_4^+$		$N\text{-}NO_3^-$		DOC		C_{mic}		BGU V_{max}	
	df	Pseudo F	*p* value	Pseudo F	*p* value	Pseudo F	*p* value	Pseudo F	*p* value	Pseudo F	*p* value
Rot_pos	1	6.32	**0.007**	13.04	**0.000**	4.37	**0.040**	5.93	**0.017**	3.97	**0.048**
OA	1	30.32	**0.000**	4.35	**0.039**	3.24	0.080	5.29	**0.024**	1.68	0.199
Depth	2	5.00	**0.005**	7.95	**0.000**	10.51	**0.002**	14.15	**0.000**	5.17	**0.028**
Rot_pos × OA	1	4.05	**0.039**	7.46	**0.007**	0.90	0.352	4.17	**0.047**	6.79	**0.011**
Rot_pos × Depth	2	1.28	0.297	2.03	0.141	0.21	0.660	0.88	0.425	1.69	0.198
OA × Depth	2	1.60	0.214	0.47	0.639	0.15	0.696	0.23	0.800	0.04	0.851
Rot_pos × OA × Depth	2	0.78	0.486	0.35	0.720	0.00	0.964	1.74	0.181	0.55	0.455
		LAP V_{max}		$^{13}C_{soil}$ excess		$^{13}C_{DOC}$ excess		$^{13}C_{mic}$ excess		$^{15}N_{soil}$ excess	
		Pseudo F	*p* value	Pseudo F	*p* value	Pseudo F	*p* value	Pseudo F	*p* value	Pseudo F	*p* value
Rot_pos	1	6.95	**0.009**	2.66	0.113	6.19	**0.012**	0.00	0.999	0.52	0.475
OA	1	0.03	0.873	12.41	**0.001**	0.02	0.900	0.45	0.519	0.38	0.537
Depth	2	11.42	**0.002**	2.09	0.134	7.05	**0.001**	5.31	**0.005**	3.70	**0.030**
Rot_pos × OA	1	13.20	**0.001**	0.70	0.416	5.69	**0.017**	2.30	0.144	0.15	0.700
Rot_pos × Depth	2	6.97	**0.010**	0.24	0.782	0.29	0.770	1.99	0.150	0.14	0.870
OA × Depth	2	0.20	0.656	1.60	0.209	0.71	0.513	2.53	0.087	0.07	0.930
Rot_pos × OA × Depth	2	2.68	0.110	0.14	0.870	3.41	**0.034**	3.44	**0.036**	0.47	0.638

Table D.2 Effect of rotational position (Rot_pos), organic amendment (OA), soil depth (Depth) and their interactions on ammonium ($N\text{-}NH_4^+$), nitrate ($N\text{-}NO_3^-$), dissolved organic C (DOC), total extractable N (TN), absolute ^{13}C excess of the soil, DOC, C_{mic} and absolute ^{15}N excess of the soil at grain ripening (BBCH 90, T2). Significant values at $p \leq 0.05$ level are indicated in bold. Pseudo F is the modeled analogous to the F statistic in ANOVA.

ANOVA results		$N\text{-}NH_4^+$		$N\text{-}NO_3^-$		DOC		C_{mic}	
	df	Pseudo F	*p* value	Pseudo F	*p* value	Pseudo F	*p* value	Pseudo F	*p* value
Rot_pos	1	0.50	0.483	1.42	0.241	3.49	0.054	0.12	0.736
OA	1	0.00	0.990	0.48	0.487	0.65	0.464	14.32	**0.000**
Depth	2	1.53	0.229	0.12	0.737	1.70	0.212	67.41	**0.000**
Rot_pos × OA	1	0.22	0.648	0.10	0.764	1.16	0.318	0.22	0.640
Rot_pos × Depth	2	0.74	0.390	1.20	0.282	0.52	0.506	6.15	**0.004**
OA × Depth	2	0.05	0.808	0.01	0.921	0.62	0.467	5.29	**0.009**
Rot_pos × OA × Depth	2	2.24	0.135	0.77	0.383	0.07	0.818	0.56	0.576
		$^{13}C_{soil}$ excess		$^{13}C_{DOC}$ excess		$^{13}C_{mic}$ excess		$^{15}N_{soil}$ excess	
		Pseudo F	*p* value	Pseudo F	*p* value	Pseudo F	*p* value	Pseudo F	*p* value
Rot_pos	1	0.24	0.628	0.11	0.769	0.09	0.773	5.44	**0.022**
OA	1	0.00	0.987	0.80	0.403	1.47	0.226	3.32	0.071
Depth	2	8.37	**0.001**	2.91	**0.045**	21.31	**0.000**	0.03	0.967
Rot_pos × OA	1	0.88	0.363	0.02	0.896	0.00	0.975	0.82	0.373
Rot_pos × Depth	2	0.04	0.958	0.12	0.909	1.55	0.219	0.53	0.600
OA × Depth	2	0.04	0.963	2.94	**0.044**	3.13	0.051	0.36	0.705
Rot_pos × OA × Depth	2	0.06	0.947	0.14	0.898	0.50	0.612	0.30	0.735

Table D.3 Effect of rotational position (Rot_pos), organic amendment (OA), plant part (Plant_part) and their interaction on plant dry weight (Plant DW) and plant C:N ratio. Significant values at $p \leq 0.05$ level are indicated in bold. Pseudo F is the modeled analogous to the F statistic in ANOVA.

ANOVA results		Plant DW		Plant C:N	
	df	Pseudo F	*p* value	Pseudo F	*p* value
Rot_pos	1	22.57	**0.000**	6.01	**0.017**
OA	1	26.97	**0.000**	13.45	**0.000**
Plant_part	4	425.06	**0.000**	120.70	**0.000**
Rot_pos × OA	1	35.89	**0.000**	17.05	**0.000**
Rot_pos × Plant_part	4	2.45	**0.048**	0.81	0.532
OA × Plant_part	4	9.43	**0.000**	9.15	**0.000**
Rot_pos × OA × Plant_part	4	2.28	0.070	0.87	0.485

Table D.4 Effect of rotational position (Rot_pos), organic amendment (OA), plant part (Plant_part) and their interaction on absolute ^{13}C excess, ^{15}N, ^{2}H and ^{18}O and relative ^{13}C excess of plant material. Significant values at $p \leq 0.05$ level are indicated in bold. Pseudo F is the modeled analogous to the F statistic in ANOVA.

ANOVA results		$^{13}C_{plant}$ excess		fraction $^{13}C_{plant}$		$^{15}N_{plant}$ excess		$^{2}H_{plant}$ excess		$^{18}O_{plant}$ excess	
	df	Pseudo F	*p* value	Pseudo F	*p* value	Pseudo F	*p* value	Pseudo F	*p* value	Pseudo F	*p* value
Rot_pos	1	19.70	**0.000**	0.00	1.000	5.30	**0.022**	0.15	0.697	4.96	**0.026**
OA	1	2.07	0.157	0.00	1.000	8.84	**0.005**	28.27	**0.000**	19.88	**0.000**
Plant_part	4	167.38	**0.000**	425.28	**0.000**	140.77	**0.000**	327.18	**0.000**	65.26	**0.000**
Rot_pos × OA	1	25.72	**0.000**	0.00	1.000	12.13	**0.001**	5.12	**0.028**	0.09	0.772
Rot_pos × Plant_part	4	6.65	**0.000**	3.40	**0.012**	1.26	0.292	1.01	0.406	3.03	**0.018**
OA × Plant_part	4	0.81	0.529	2.98	**0.024**	11.02	**0.000**	6.78	**0.000**	6.39	**0.000**
Rot_pos × OA × Plant_part	4	4.83	**0.001**	1.40	0.241	2.54	**0.047**	1.01	0.406	0.08	0.987

Table D.5 Effect of rotational position (Rot_pos), organic amendment (OA), soil depth (Depth) and their interaction on root dry weight (RDW), root length density (RLD), absolute ^{13}C and ^{15}N excess of roots. Significant values at $p \leq 0.05$ level are indicated in bold. Pseudo F is the modeled analogous to the F statistic in ANOVA.

ANOVA results		RDW		RLD		$^{13}C_{root}$ excess		$^{15}N_{root}$ excess	
	df	Pseudo F	*p* value	Pseudo F	*p* value	Pseudo F	*p* value	Pseudo F	*p* value
Rot_pos	1	14.12	**0.001**	1.76	0.190	15.91	0.000	1.61	0.203
OA	1	39.20	**0.000**	0.01	0.914	4.35	**0.043**	15.77	**0.000**
Depth	2	192.72	**0.000**	1.11	0.339	21.18	**0.000**	166.51	**0.000**
Rot_pos × OA	1	5.02	**0.030**	0.35	0.539	0.02	0.885	9.53	**0.003**
Rot_pos × Depth	2	11.13	**0.000**	0.37	0.691	7.32	**0.001**	4.99	**0.031**
OA × Depth	2	12.17	**0.000**	0.00	1.000	1.22	0.300	4.95	**0.032**
Rot_pos × OA × Depth	2	2.06	0.137	0.49	0.614	1.47	**0.240**	7.52	**0.008**

Appendix E: Supplementary material for *Chapter 6*

Figure E.1 Custom-made rhizotrons with passive and active temperature regulation.

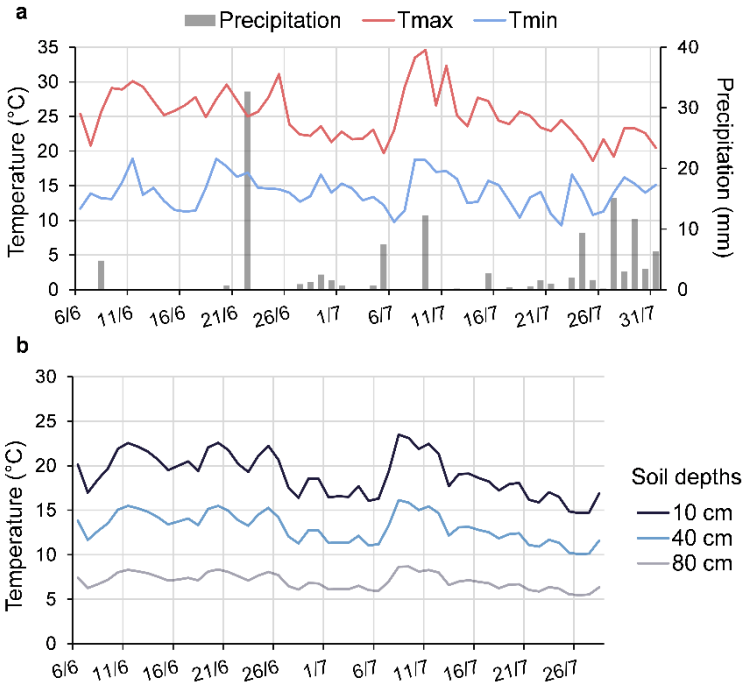

Figure E.2 Ambient minimum and maximum temperature and precipitation (a), and soil temperature of the rhizotron at 10 cm, 40 cm and 80 cm (b) during the course of the experiment.

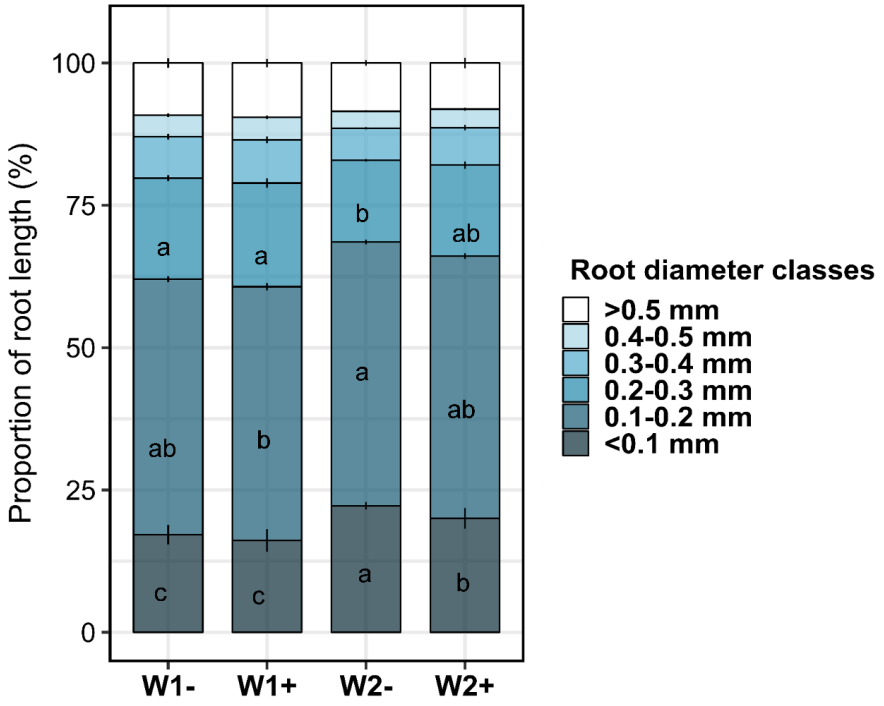

Figure E.3 Proportion of root length for six root diameter classes of two rotational positions of winter wheat at end of tillering (BBCH 29). First wheat after oilseed rape without (W1-) and with (W1+) *Bacillus pumilus* and second wheat after oilseed rape without (W2-) and with (W2+) *Bacillus pumilus*. Within each root diameter class, different lowercase letters indicate significant differences between the rotational positions at $p \leq 0.05$ level according to PERMANOVA. Absence of letters indicate non-significant differences.

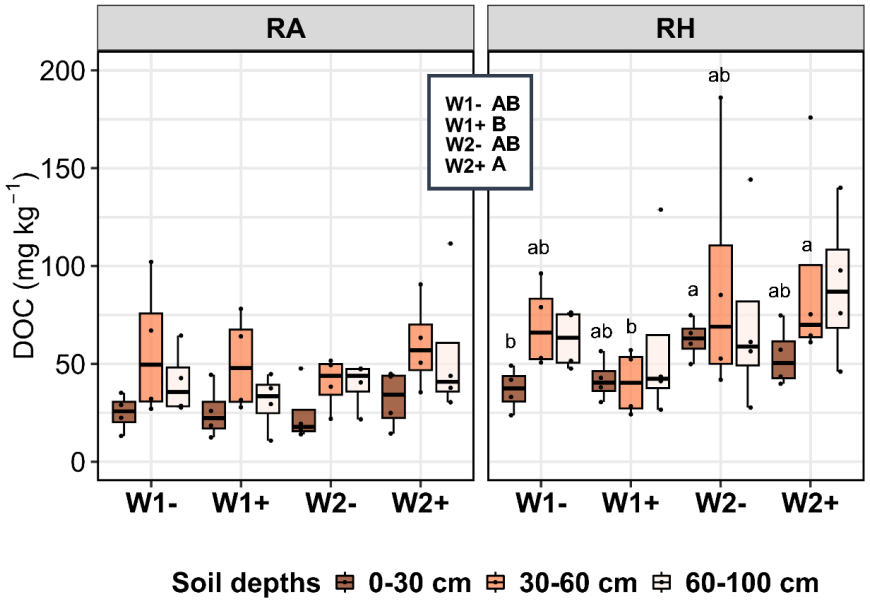

Figure E.4 Effect of the rotational positions on dissolved organic C (DOC of the following winter wheat at end of tillering (BBCH 29) at soil depth 0-30 cm, 30-60 cm and 60-100 cm and two soil compartments: root-affected soil (RA) and rhizosphere soil (RH). First wheat after oilseed rape without (W1-) and with (W1+) *Bacillus pumilus* and second wheat after oilseed rape without (W2-) and with (W2+) *Bacillus pumilus*. Different uppercase letters indicate significant differences between the rotational positions. Within each soil depth, different lowercase letters indicate significant differences between the rotational positions at $p \leq 0.05$ level according to PERMANOVA. Absence of letters indicate non-significant differences.

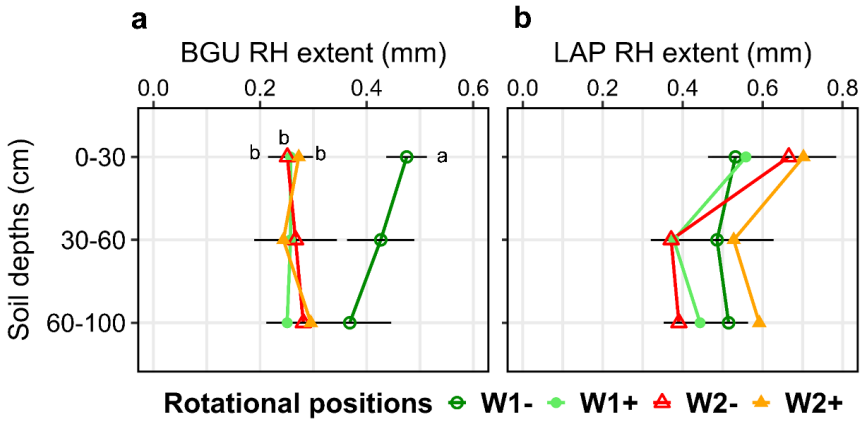

Figure E.5 Rhizosphere extent of *β*-glucosidase (BGU; a) and leucine aminopeptidase (LAP; b) of two rotational positions of winter wheat at end of tillering (BBCH 29) at soil depths 0-30 cm, 30-60 cm and 60-100 cm. First wheat after oilseed rape without (W1-) and with (W1+) *Bacillus pumilus* and second wheat after oilseed rape without (W2-) and with (W2+) *Bacillus pumilus*. Within each soil depth, different lowercase letters indicate significant differences between the rotational positions at $p \leq 0.05$ level according to PERMANOVA. Absence of letters indicate non-significant differences.

Table E.1 Effect of rotational position (Rot_pos), plant growth-promoting rhizobacterium (PGPR), plant part (Plant_part) and their interaction on plant dry weight (Plant DW), plant phosphorus concentration (P%), plant potassium concentration (K%) and plant iron concentration (Fe%). Significant values at $p \leq 0.05$ level are indicated in bold. Pseudo F is the modeled analogous to the F statistic in ANOVA.

ANOVA results		Plant DW		Plant P%		Plant K%		Plant Fe%	
	df	Pseudo F	*p* value	Pseudo F	*p* value	Pseudo F	*p* value	Pseudo F	*p* value
Rot_pos	1	21.02	**0.000**	0.09	0.771	1.18	0.293	0.05	0.823
PGPR	1	10.64	**0.003**	2.81	0.106	0.03	0.851	3.46	0.067
Plant_part	2	22.08	**0.000**	14.01	**0.001**	154.02	**0.000**	36.41	**0.000**
Rot_pos × PGPR	1	12.84	**0.001**	0.71	0.414	34.06	**0.000**	0.56	0.463
Rot_pos × Plant_part	2	1.12	0.344	3.16	0.086	3.32	0.088	1.85	0.173
PGPR × Plant_part	2	4.07	**0.027**	2.04	0.164	0.24	0.630	0.91	0.408
Rot_pos × PGPR × Plant_part	2	3.53	**0.041**	1.48	0.242	13.45	**0.002**	0.27	0.762

Table E.2 Effect of rotational position (Rot_pos), plant growth-promoting rhizobacterium (PGPR), soil depth (Depth) and their interaction on root dry weight (RDW), root length density (RLD), average root diameter (R_{dia}), specific root length (SRL). Significant values at $p \leq 0.05$ level are indicated in bold. Pseudo F is the modeled analogue to the F statistic in ANOVA.

ANOVA results		RDW		RLD		R_{dia}		SRL
		Pseudo F	*p* value	Pseudo F	*p* value	Pseudo F	*p* value	Pseudo F
Rot_pos	1	41.44	**0.000**	22.50	**0.000**	13.22	**0.001**	3.39
PGPR	1	105.59	**0.000**	23.09	**0.000**	8.68	**0.007**	16.86
Depth	2	40.77	**0.000**	40.05	**0.000**	12.53	**0.000**	28.67
Rot_pos × PGPR	1	170.55	**0.000**	12.31	**0.002**	3.81	0.058	41.02
Rot_pos × Depth	2	4.33	**0.020**	4.54	**0.020**	2.18	0.127	6.44
PGPR × Depth	2	2.40	0.105	0.84	0.443	11.21	**0.001**	6.37
Rot_pos × PGPR × Depth	2	1.06	0.362	2.09	0.134	9.86	**0.001**	2.96

Table E.3 Effect of rotational position (Rot_pos), plant growth-promoting rhizobacterium (PGPR), soil depth (Depth) and their interaction on the proportion of total root length in the < 0.1 mm diameter class (P1), in the 0.1 - 0.2 mm diameter class (P2), in the 0.2 - 0.3 mm diameter class (P3), in the 0.3 - 0.4 mm diameter class (P4), in the 0.4 - 0.5 mm diameter class (P5), in the > 0.5 mm diameter class (P6). Significant values at p ≤ 0.05 level are indicated in bold. Pseudo F is the modeled analogue to the F statistic in ANOVA.

ANOVA results		P1		P2		P3	
	df	Pseudo F	*p* value	Pseudo F	*p* value	Pseudo F	*p* value
Rot_pos	1	13.19	**0.001**	30.27	**0.000**	31.36	**0.000**
PGPR	1	7.89	**0.008**	12.83	**0.001**	14.66	**0.001**
Depth	2	11.77	**0.000**	14.60	**0.000**	22.20	**0.000**
Rot_pos × PGPR	1	2.55	0.113	1.44	0.239	6.42	**0.016**
Rot_pos × Depth	2	2.07	0.137	12.72	**0.000**	1.95	0.153
PGPR × Depth	2	4.87	**0.012**	6.19	**0.003**	1.25	0.289
Rot_pos × PGPR × Depth	2	4.09	**0.025**	5.53	**0.005**	0.86	0.424
		P4		P5		P6	
		Pseudo F	*p* value	Pseudo F	*p* value	Pseudo F	*p* value
Rot_pos	1	18.27	**0.000**	27.02	**0.000**	8.82	**0.007**
PGPR	1	11.72	**0.003**	13.86	**0.001**	5.38	0.026
Depth	2	17.28	**0.000**	19.49	**0.000**	7.15	**0.003**
Rot_pos × PGPR	1	3.81	0.059	1.20	0.284	0.43	0.515
Rot_pos × Depth	2	2.77	0.076	2.57	0.089	6.66	**0.004**
PGPR × Depth	2	2.58	0.087	6.03	**0.007**	20.41	**0.000**
Rot_pos × PGPR × Depth	2	1.26	0.301	1.36	0.269	15.23	**0.000**

Table E.4 Effect of rotational position (Rot_pos), plant growth-promoting rhizobacterium (PGPR), soil compartment (Comp), soil depth (Depth) and their interaction on ammonium ($N\text{-}NH_4^+$), nitrate ($N\text{-}NO_3^-$) and dissolved organic C (DOC). Significant values at $p \leq 0.05$ level are indicated in bold. Pseudo F is the modeled analogue to the F statistic in ANOVA.

ANOVA results		$N\text{-}NH_4^+$		$N\text{-}NO_3^-$		DOC	
	df	Pseudo F	*p* value	Pseudo F	*p* value	Pseudo F	*p* value
Rot_pos	1	7.83	**0.003**	3.63	0.059	5.99	**0.015**
PGPR	1	0.82	0.386	33.97	**0.000**	0.03	0.867
Comp	1	15.90	**0.000**	60.85	**0.000**	17.03	**0.000**
Depth	2	3.61	**0.023**	15.57	**0.000**	6.42	**0.003**
Rot_pos × PGPR	1	0.02	0.894	0.27	0.606	1.90	0.175
Rot_pos × Comp	1	4.41	**0.032**	6.55	**0.011**	3.32	0.074
PGPR × Comp	1	3.08	0.079	9.69	**0.003**	0.36	0.563
Rot_pos × Depth	2	2.61	0.072	0.85	0.433	0.10	0.901
PGPR × Depth	2	0.48	0.657	21.09	**0.000**	0.18	0.845
Comp × Depth	2	3.31	**0.032**	4.46	**0.014**	0.17	0.850
Rot_pos × PGPR × Comp	1	0.00	0.977	3.77	0.055	0.10	0.757
Rot_pos × PGPR × Depth	2	0.82	0.470	0.71	0.496	0.70	0.508
Rot_pos × Comp × Depth	2	2.09	0.124	4.18	**0.017**	0.71	0.508
PGPR × Comp × Depth	2	0.92	0.423	6.40	**0.002**	0.34	0.725
Rot_pos × PGPR × Comp × Depth	2	1.42	0.252	0.30	0.746	0.10	0.904

Table E.5 Effect of rotational position (Rot_pos), plant growth-promoting rhizobacterium (PGPR), soil compartment (Comp), soil depth (Depth) and their interaction on β-glucosidase maximum reaction rate (BGU V_{max}), BGU substrate affinity (BGU K_m), leucine aminopeptidase maximum reaction rate (LAP V_{max}) and LAP substrate affinity (LAP K_m). Significant values at $p \leq 0.05$ level are indicated in bold. Pseudo F is the modeled analogue to the F statistic in ANOVA.

ANOVA results		BGU V_{max}		BGU K_m		LAP Vmax		LAP Km	
	df	Pseudo F	*p* value	Pseudo F	*p* value	Pseudo F	*p* value	Pseudo F	*p* value
Rot_pos	1	0.02	0.885	6.41	**0.015**	7.85	**0.007**	1.26	0.266
PGPR	1	2.14	0.148	2.99	0.092	28.60	0.000	2.46	0.123
Comp	1	111.01	**0.000**	0.06	0.821	7.33	**0.009**	13.32	**0.000**
Depth	2	11.86	**0.000**	15.69	**0.000**	1.60	0.214	1.25	0.288
Rot_pos × PGPR	1	2.52	0.117	0.21	0.649	14.41	**0.001**	1.79	0.184
Rot_pos × Comp	1	9.29	**0.003**	1.92	0.163	0.85	0.356	0.07	0.793
PGPR × Comp	1	1.24	0.270	4.81	**0.032**	0.46	0.499	0.02	0.883
Rot_pos × Depth	2	4.57	**0.011**	1.20	0.310	0.18	0.833	1.81	0.166
PGPR × Depth	2	4.17	**0.017**	1.03	0.364	1.30	0.282	0.93	0.410
Comp × Depth	2	2.03	0.135	2.48	0.090	0.35	0.711	0.78	0.470
Rot_pos × PGPR × Comp	1	0.79	0.376	3.21	0.076	3.71	0.059	0.46	0.495
Rot_pos × PGPR × Depth	2	7.81	**0.001**	4.38	**0.015**	1.48	0.238	1.50	0.223
Rot_pos × Comp × Depth	2	0.93	0.403	0.54	0.593	1.04	0.365	0.39	0.684
PGPR × Comp × Depth	2	3.48	**0.034**	4.08	**0.021**	0.27	0.762	0.34	0.716
Rot_pos × PGPR × Comp × Depth	2	3.47	**0.035**	8.61	**0.001**	1.15	0.323	1.32	0.269

Table E.6 Effect of rotational position (Rot_pos), plant growth-promoting rhizobacterium (PGPR), soil depth (Depth) and their interaction on β-glucosidase (BGU) and leucine aminopeptidase (LAP) hotspot area percentage, rhizosphere (RH) extent and activity. Significant values at $p \leq 0.05$ level are indicated in bold. Pseudo F is the modeled analogue to the F statistic in ANOVA.

ANOVA results		BGU hotspot		BGU RH extent		BGU activity	
	df	Pseudo F	*p* value	Pseudo F	*p* value	Pseudo F	*p* value
Rot_pos	1	0.06	0.811	5.97	**0.020**	3.54	0.071
PGPR	1	0.01	0.906	8.04	**0.006**	2.41	0.125
Depth	2	3.73	0.062	0.18	0.675	0.65	0.428
Rot_pos × PGPR	1	0.00	0.970	8.89	**0.005**	0.09	0.776
Rot_pos × Depth	2	0.46	0.499	1.37	0.244	0.01	0.942
PGPR × Depth	2	0.29	0.596	0.43	0.506	0.18	0.684
Rot_pos × PGPR × Depth	2	0.12	0.734	0.58	0.458	0.15	0.697
		LAP hotspot		LAP RH extent		LAP activity	
		Pseudo F	*p* value	Pseudo F	*p* value	Pseudo F	*p* value
Rot_pos	1	0.02	0.902	5.97	**0.020**	1.94	0.176
PGPR	1	0.07	0.798	8.04	**0.008**	0.15	0.700
Depth	2	6.20	**0.017**	0.18	0.671	12.08	**0.002**
Rot_pos × PGPR	1	0.11	0.729	8.89	**0.005**	0.73	0.400
Rot_pos × Depth	2	1.36	0.245	1.37	0.247	0.24	0.628
PGPR × Depth	2	1.05	0.322	0.43	0.515	0.78	0.376
Rot_pos × PGPR × Depth	2	0.01	0.925	0.58	0.451	0.23	0.632

References

Adesina, M.F., Lembke, A., Costa, R., Speksnijder, A., Smalla, K., 2007. Screening of bacterial isolates from various European soils for in vitro antagonistic activity towards *Rhizoctonia solani* and *Fusarium oxysporum*: Site-dependent composition and diversity revealed. Soil Biology and Biochemistry 39, 2818–2828. doi:10.1016/j.soilbio.2007.06.004

Agegnehu, G., Srivastava, A.K., Bird, M.I., 2017. The role of biochar and biochar-compost in improving soil quality and crop performance: A review. Applied Soil Ecology 119, 156–170. doi:10.1016/j.apsoil.2017.06.008

Al-Bataina, B.B., Young, T.M., Ranieri, E., 2016. Effects of compost age on the release of nutrients. International Soil and Water Conservation Research 4, 230–236. doi: 10.1016/j.iswcr.2016.07.003

Alegria Terrazas, R., Robertson-Albertyn, S., Corral, A.M., Escudero-Martinez, C., Kapadia, R., Balbirnie-Cumming, K., Morris, J., Hedley, P.E., Barret, M., Torres-Cortes, G., Paterson, E., Baggs, E.M., Abbott, J., Bulgarelli, D., 2022. Defining Composition and Function of the Rhizosphere Microbiota of Barley Genotypes Exposed to Growth-Limiting Nitrogen Supplies. MSystems 7, e00934-22. doi:10.1128/msystems.00934-22

Alves, R.J.E., Minh, B.Q., Urich, T., von Haeseler, A., Schleper, C., 2018. Unifying the global phylogeny and environmental distribution of ammonia-oxidising archaea based on *amoA* genes. Nature Communications 9, 1517. doi:10.1038/s41467-018-03861-1

Amelung, W., Bossio, D., de Vries, W., Kögel-Knabner, I., Lehmann, J., Amundson, R., Bol, R., Collins, C., Lal, R., Leifeld, J., Minasny, B., Pan, G., Paustian, K., Rumpel, C., Sanderman, J., van Groenigen, J.W., Mooney, S., van Wesemael, B., Wander, M., Chabbi, A., 2020. Towards a global-scale soil climate mitigation strategy. Nature Communications 11, 1–10. doi:10.1038/s41467-020-18887-7

Amlinger, F., Götz, B., Dreher, P., Geszti, J., Weissteiner, C., 2003. Nitrogen in biowaste and yard waste compost: dynamics of mobilisation and availability—a review. European Journal of Soil Biology 39, 107–116. doi:10.1016/S1164-5563(03)00026-8

Angus, J.F., Kirkegaard, J.A., Hunt, J.R., Ryan, M.H., Ohlander, L., Peoples, M.B., 2015. Break crops and rotations for wheat. Crop and Pasture Science 66, 523–552. doi:10.1071/CP14252

Arnhold, J., Grunwald, D., Braun-Kiewnick, A., Koch, H.-J., 2023a. Effect of crop rotational position and nitrogen supply on root development and yield formation of winter wheat. Frontiers in Plant Science 14. doi:10.3389/fpls.2023.1265994

Arnhold, J., Grunwald, D., Kage, H., Koch, H.-J., 2023b. No differences in soil structure under winter wheat grown in different crop rotational positions. Canadian Journal of Soil Science 103, 643–649. doi:10.1139/cjss-2023-0030

Awad, Y.M., Blagodatskaya, E., Ok, Y.S., Kuzyakov, Y., 2012. Effects of polyacrylamide, biopolymer, and biochar on decomposition of soil organic matter and plant residues as determined by ^{14}C and enzyme activities. European Journal of Soil Biology 48, 1–10. doi:10.1016/j.ejsobi.2011.09.005

Babin, D., Deubel, A., Jacquiod, S., Sørensen, S.J., Geistlinger, J., Grosch, R., Smalla, K., 2019. Impact of long-term agricultural management practices on soil prokaryotic communities. Soil Biology and Biochemistry 129, 17–28. doi:10.1016/j.soilbio.2018.11.002

Bacilio-Jiménez, M., Aguilar-Flores, S., del Valle, M.., Pérez, A., Zepeda, A., Zenteno, E., 2001. Endophytic bacteria in rice seeds inhibit early colonization of roots by *Azospirillum*

brasilense. Soil Biology and Biochemistry 33, 167–172. doi:10.1016/S0038-0717(00)00126-7

Backer, R., Rokem, J.S., Ilangumaran, G., Lamont, J., Praslickova, D., Ricci, E., Subramanian, S., Smith, D.L., 2018. Plant Growth-Promoting Rhizobacteria: Context, Mechanisms of Action, and Roadmap to Commercialization of Biostimulants for Sustainable Agriculture. Frontiers in Plant Science 9. doi:10.3389/fpls.2018.01473

Bahn, M., Lattanzi, F.A., Hasibeder, R., Wild, B., Koranda, M., Danese, V., Brüggemann, N., Schmitt, M., Siegwolf, R., Richter, A., 2013. Responses of belowground carbon allocation dynamics to extended shading in mountain grassland. New Phytologist 198, 116–126. doi:10.1111/nph.12138

Bahn, M., Schmitt, M., Siegwolf, R., Richter, A., Brüggemann, N., 2009. Does photosynthesis affect grassland soil-respired CO_2 and its carbon isotope composition on a diurnal timescale? New Phytologist 182, 451–460. doi:10.1111/j.1469-8137.2008.02755.x

Banerjee, S., Kirkby, C.A., Schmutter, D., Bissett, A., Kirkegaard, J.A., Richardson, A.E., 2016. Network analysis reveals functional redundancy and keystone taxa amongst bacterial and fungal communities during organic matter decomposition in an arable soil. Soil Biology and Biochemistry 97, 188–198. doi:10.1016/j.soilbio.2016.03.017

Bass, E., 2024. Getting to the root of divergent outcomes in the modulation of plant–soil feedbacks by benzoxazinoids. New Phytologist 241, 2316–2319. doi:10.1111/nph.19545

Beneduzi, A., Ambrosini, A., Passaglia, L.M.P., 2012. Plant growth-promoting rhizobacteria (PGPR): Their potential as antagonists and biocontrol agents. Genetics and Molecular Biology 35, 1044–1051. doi:10.1590/S1415-47572012000600020

Benizri, E., Nguyen, C., Piutti, S., Slezack-Deschaumes, S., Philippot, L., 2007. Additions of maize root mucilage to soil changed the structure of the bacterial community. Soil Biology and Biochemistry 39, 1230–1233. doi:10.1016/j.soilbio.2006.12.026

Bennett, J.A., Klironomos, J., 2019. Mechanisms of plant–soil feedback: interactions among biotic and abiotic drivers. New Phytologist 222, 91–96. doi:10.1111/nph.15603

Bilyera, N., Zhang, X., Duddek, P., Fan, L., Banfield, C.C., Schlüter, S., Carminati, A., Kaestner, A., Ahmed, M.A., Kuzyakov, Y., Dippold, M.A., Spielvogel, S., Razavi, B.S., 2021. Maize genotype-specific exudation strategies: An adaptive mechanism to increase microbial activity in the rhizosphere. Soil Biology and Biochemistry 162, 108426. doi:10.1016/J.SOILBIO.2021.108426

Blagodatskaya, E. V, Blagodatsky, S.A., Anderson, T.-H., Kuzyakov, Y., 2009. Contrasting effects of glucose, living roots and maize straw on microbial growth kinetics and substrate availability in soil. European Journal of Soil Science 60, 186–197. doi:10.1111/j.1365-2389.2008.01103.x

Bommarco, R., Kleijn, D., Potts, S.G., 2013. Ecological intensification: Harnessing ecosystem services for food security. Trends in Ecology and Evolution 28, 230–238. doi:10.1016/j.tree.2012.10.012

Bongiorno, G., Postma, J., Bünemann, E.K., Brussaard, L., de Goede, R.G.M., Mäder, P., Tamm, L., Thuerig, B., 2019. Soil suppressiveness to *Pythium ultimum* in ten European long-term field experiments and its relation with soil parameters. Soil Biology and Biochemistry 133, 174–187. doi:10.1016/j.soilbio.2019.03.012

Borrelli, P., Robinson, D.A., Fleischer, L.R., Lugato, E., Ballabio, C., Alewell, C., Meusburger, K., Modugno, S., Schütt, B., Ferro, V., Bagarello, V., Oost, K. Van, Montanarella, L., Panagos, P., 2017. An assessment of the global impact of 21st century land use change on soil erosion. Nature Communications 8, 2013. doi:10.1038/s41467-017-02142-7

Bowles, T.M., Jilling, A., Morán-Rivera, K., Schnecker, J., Grandy, A.S., 2022. Crop rotational complexity affects plant-soil nitrogen cycling during water deficit. Soil Biology and Biochemistry 166, 108552. doi:10.1016/j.soilbio.2022.108552

Box, G.E.P., Cox, D.R., 1964. An Analysis of Transformations. Journal of the Royal Statistical Society. Series B (Methodological) 26, 211–252. doi:10.1111/J.2517-6161.1964.TB00553.X

Bozal-Leorri, A., Subbarao, G. V, Kishii, M., Urmeneta, L., Kommerell, V., Karwat, H., Braun, H.-J., Aparicio-Tejo, P.M., Ortiz-Monasterio, I., González-Murua, C., González-Moro, M.B., 2022. Biological nitrification inhibitor-trait enhances nitrogen uptake by suppressing nitrifier activity and improves ammonium assimilation in two elite wheat varieties. Frontiers in Plant Science 13. doi:10.3389/fpls.2022.1034219

Braun-Kiewnick, A., Giongo, A., Zamberlan, P.M., Pluta, P., Koch, H.-J., Kage, H., Smalla, K., Babin, D., 2024. The microbiome of continuous wheat rotations: minor shifts in bacterial and archaeal communities but a source for functionally active plant-beneficial bacteria. Phytobiomes Journal. doi:10.1094/PBIOMES-05-24-0054-R

Braun, M., Mail, M., Heyse, R., Amelung, W., 2021. Plastic in compost: Prevalence and potential input into agricultural and horticultural soils. Science of The Total Environment 760, 143335. doi:10.1016/j.scitotenv.2020.143335

Braun, M., Mail, M., Krupp, A.E., Amelung, W., 2023. Microplastic contamination of soil: Are input pathways by compost overridden by littering? Science of The Total Environment 855, 158889. doi:10.1016/j.scitotenv.2022.158889

Brazelton, J.N., Pfeufer, E.E., Sweat, T.A., Gardener, B.B.M., Coenen, C., 2008. 2,4-Diacetylphloroglucinol Alters Plant Root Development. Molecular Plant-Microbe Interactions 21, 1349–1358. doi:10.1094/MPMI-21-10-1349

Brisson, N., Gate, P., Gouache, D., Charmet, G., Oury, F.X., Huard, F., 2010. Why are wheat yields stagnating in Europe? A comprehensive data analysis for France. Field Crops Research 119, 201–212. doi:10.1016/j.fcr.2010.07.012

Brüggemann, N., Gessler, A., Kayler, Z., Keel, S.G., Badeck, F., Barthel, M., Boeckx, P., Buchmann, N., Brugnoli, E., Esperschütz, J., Gavrichkova, O., Ghashghaie, J., Gomez-Casanovas, N., Keitel, C., Knohl, A., Kuptz, D., Palacio, S., Salmon, Y., Uchida, Y., Bahn, M., 2011. Carbon allocation and carbon isotope fluxes in the plant-soil-atmosphere continuum: A review. Biogeosciences 8, 3457–3489. doi:10.5194/bg-8-3457-2011

Bziuk, N., Maccario, L., Douchkov, D., Lueck, S., Babin, D., Sørensen, S.J., Schikora, A., Smalla, K., 2021. Tillage shapes the soil and rhizosphere microbiome of barley—but not its susceptibility towards *Blumeria graminis* f.sp. *hordei*. FEMS Microbiology Ecology 97, fiab018. doi:10.1093/femsec/fiab018

Calderini, D.F., Slafer, G.A., 1998. Changes in yield and yield stability in wheat during the 20th century. Field Crops Research 57, 335–347. doi:10.1016/S0378-4290(98)00080-X

Callahan, B.J., McMurdie, P.J., Rosen, M.J., Han, A.W., Johnson, A.J.A., Holmes, S.P., 2016. DADA2: High-resolution sample inference from Illumina amplicon data. Nature Methods 13, 581–583. doi:10.1038/nmeth.3869

Camenzind, T., Mason-Jones, K., Mansour, I., Rillig, M.C., Lehmann, J., 2023. Formation of necromass-derived soil organic carbon determined by microbial death pathways. Nature Geoscience 16, 115–122. doi:10.1038/s41561-022-01100-3

Canarini, A., Kaiser, C., Merchant, A., Richter, A., Wanek, W., 2019. Root exudation of primary metabolites: Mechanisms and their roles in plant responses to environmental stimuli. Frontiers in Plant Science 10. doi:10.3389/fpls.2019.00157

Caporaso, J.G., Lauber, C.L., Walters, W.A., Berg-Lyons, D., Lozupone, C.A., Turnbaugh, P.J.,

Fierer, N., Knight, R., 2011. Global patterns of 16S rRNA diversity at a depth of millions of sequences per sample. Proceedings of the National Academy of Sciences of the United States of America 108, 4516–4522. doi:10.1073/pnas.1000080107
Castro-Herrera, D., Prost, K., Schäfer, Y., Kim, D.-G., Yimer, F., Tadesse, M., Gebrehiwot, M., Brüggemann, N., 2022. Nutrient dynamics during composting of human excreta, cattle manure, and organic waste affected by biochar. Journal of Environmental Quality 51, 19–32. doi:10.1002/jeq2.20312
Cenini, V.L., Fornara, D.A., McMullan, G., Ternan, N., Carolan, R., Crawley, M.J., Clément, J.C., Lavorel, S., 2016. Linkages between extracellular enzyme activities and the carbon and nitrogen content of grassland soils. Soil Biology and Biochemistry 96, 198–206. doi:10.1016/j.soilbio.2016.02.015
Cerecetto, V., Leoni, C., Jurburg, S.D., Kampouris, I.D., Smalla, K., Babin, D., 2024. Pasture-crop rotations modulate the soil and rhizosphere microbiota and preserve soil structure supporting oat cultivation in the Pampa biome. Soil Biology and Biochemistry 195, 109451. doi:10.1016/j.soilbio.2024.109451
Chai, Y.N., Schachtman, D.P., 2022. Root exudates impact plant performance under abiotic stress. Trends in Plant Science 27, 80–91. doi:10.1016/j.tplants.2021.08.003
Chandregowda, M.H., Tjoelker, M.G., Pendall, E., Zhang, H., Churchill, A.C., Power, S.A., 2023. Belowground carbon allocation, root trait plasticity, and productivity during drought and warming in a pasture grass. Journal of Experimental Botany 74, 2127–2145. doi:10.1093/jxb/erad021
Chen, D., Wang, X., Carrión, V.J., Yin, S., Yue, Z., Liao, Y., Dong, Y., Li, X., 2022. Acidic amelioration of soil amendments improves soil health by impacting rhizosphere microbial assemblies. Soil Biology and Biochemistry 167, 108599. doi:10.1016/j.soilbio.2022.108599
Chen, G., Dresbøll, D.B., Thorup-Kristensen, K., 2021. Dual labelling by ^{2}H and ^{15}N revealed differences in uptake potential by deep roots of chicory. Rhizosphere 19, 100368. doi:10.1016/j.rhisph.2021.100368
Chen, Q., Long, C., Bao, Y., Men, X., Zhang, Y., Cheng, X., 2024. The dominant genera of nitrogenase (*nifH*) affects soil biological nitrogen fixation along an elevational gradient in the Hengduan mountains. Chemosphere 347, 140722. doi:10.1016/j.chemosphere.2023.140722
Chen, Y., Li, Y., Qiu, T., He, H., Liu, J., Duan, C., Cui, Y., Huang, M., Wu, C., Fang, L., 2023. High nitrogen fertilizer input enhanced the microbial network complexity in the paddy soil. Soil Ecology Letters 6, 230205. doi:10.1007/s42832-023-0205-3
Cheng, W., Kuzyakov, Y., 2015. Root Effects on Soil Organic Matter Decomposition, in: Roots and Soil Management: Interactions between Roots and the Soil, Agronomy Monographs. pp. 119–143. doi:10.2134/agronmonogr48.c7
Chieb, M., Gachomo, E.W., 2023. The role of plant growth promoting rhizobacteria in plant drought stress responses. BMC Plant Biology 23, 407. doi:10.1186/s12870-023-04403-8
Contosta, A.R., Frey, S.D., Cooper, A.B., 2011. Seasonal dynamics of soil respiration and N mineralization in chronically warmed and fertilized soils. Ecosphere 2, art36. doi:10.1890/ES10-00133.1
Cook, R.J., 2003. Take-all of wheat. Physiological and Molecular Plant Pathology 62, 73–86. doi:10.1016/S0885-5765(03)00042-0
Cope, J.E., Berckx, F., Galinski, A., Lentz, J., Nagel, K.A., Fiorani, F., Weih, M., 2024. Precrop-treated soil influences wheat (*Triticum aestivum* L.) root system architecture and its response to drought. Frontiers in Plant Science 15. doi:10.3389/fpls.2024.1389593
Cortois, R., Schröder-Georgi, T., Weigelt, A., van der Putten, W.H., De Deyn, G.B., 2016. Plant–

soil feedbacks: role of plant functional group and plant traits. Journal of Ecology 104, 1608–1617. doi:10.1111/1365-2745.12643

Costa, O.Y.A., Raaijmakers, J.M., Kuramae, E.E., 2018. Microbial extracellular polymeric substances: Ecological function and impact on soil aggregation. Frontiers in Microbiology 9, 1–14. doi:10.3389/fmicb.2018.01636

Crespo-Herrera, L.A., Crossa, J., Huerta-Espino, J., Vargas, M., Mondal, S., Velu, G., Payne, T.S., Braun, H., Singh, R.P., 2018. Genetic gains for grain yield in cimmyt's semi-arid wheat yield trials grown in suboptimal environments. Crop Science 58, 1890–1898. doi:10.2135/cropsci2018.01.0017

Crowther, T.W., Todd-Brown, K.E.O., Rowe, C.W., Wieder, W.R., Carey, J.C., Machmuller, M.B., Snoek, B.L., Fang, S., Zhou, G., Allison, S.D., Blair, J.M., Bridgham, S.D., Burton, A.J., Carrillo, Y., Reich, P.B., Clark, J.S., Classen, A.T., Dijkstra, F.A., Elberling, B., Emmett, B.A., Estiarte, M., Frey, S.D., Guo, J., Harte, J., Jiang, L., Johnson, B.R., Kröel-Dulay, G., Larsen, K.S., Laudon, H., Lavallee, J.M., Luo, Y., Lupascu, M., Ma, L.N., Marhan, S., Michelsen, A., Mohan, J., Niu, S., Pendall, E., Peñuelas, J., Pfeifer-Meister, L., Poll, C., Reinsch, S., Reynolds, L.L., Schmidt, I.K., Sistla, S., Sokol, N.W., Templer, P.H., Treseder, K.K., Welker, J.M., Bradford, M.A., 2016. Quantifying global soil carbon losses in response to warming. Nature 540, 104–108. doi:10.1038/nature20150

D'Acunto, L., Andrade, J.F., Poggio, S.L., Semmartin, M., 2018. Diversifying crop rotation increased metabolic soil diversity and activity of the microbial community. Agriculture, Ecosystems & Environment 257, 159–164. doi:10.1016/j.agee.2018.02.011

Daims, H., Lebedeva, E. V, Pjevac, P., Han, P., Herbold, C., Albertsen, M., Jehmlich, N., Palatinszky, M., Vierheilig, J., Bulaev, A., Kirkegaard, R.H., von Bergen, M., Rattei, T., Bendinger, B., Nielsen, P.H., Wagner, M., 2015. Complete nitrification by *Nitrospira* bacteria. Nature 528, 504–509. doi:10.1038/nature16461

Danhorn, T., Fuqua, C., 2007. Biofilm Formation by Plant-Associated Bacteria. Annual Review of Microbiology 61, 401–422. doi:10.1146/annurev.micro.61.080706.093316

De Long, J.R., Heinen, R., Heinze, J., Morriën, E., Png, G.K., Sapsford, S.J., Teste, F.P., Fry, E.L., 2023. Plant-soil feedback: incorporating untested influential drivers and reconciling terminology. Plant and Soil 485, 7–43. doi:10.1007/s11104-023-05908-9

de Vries, F., Lau, J., Hawkes, C., Semchenko, M., 2023. Plant&Soil feedback under drought: does history shape the future? Trends in Ecology & Evolution 38, 708–718. doi:10.1016/j.tree.2023.03.001

De Zutter, N., Ameye, M., Bekaert, B., Verwaeren, J., De Gelder, L., Audenaert, K., 2022. Uncovering New Insights and Misconceptions on the Effectiveness of Phosphate Solubilizing Rhizobacteria in Plants: A Meta-Analysis. Frontiers in Plant Science 13. doi:10.3389/fpls.2022.858804

Demelash, N., Bayu, W., Tesfaye, S., Ziadat, F., Sommer, R., 2014. Current and residual effects of compost and inorganic fertilizer on wheat and soil chemical properties. Nutrient Cycling in Agroecosystems 100, 357–367. doi:10.1007/s10705-014-9654-5

Dijkstra, F.A., Carrillo, Y., Pendall, E., Morgan, J.A., 2013. Rhizosphere priming: a nutrient perspective. Frontiers in Microbiology 4. doi:10.3389/fmicb.2013.00216

Dobrzyński, J., Jakubowska, Z., Dybek, B., 2022. Potential of *Bacillus pumilus* to directly promote plant growth. Frontiers in Microbiology 13. doi:10.3389/fmicb.2022.1069053

Donn, S., Kirkegaard, J.A., Perera, G., Richardson, A.E., Watt, M., 2015. Evolution of bacterial communities in the wheat crop rhizosphere. Environmental Microbiology 17, 610–621. doi:10.1111/1462-2920.12452

Dorodnikov, M., Blagodatskaya, E., Blagodatsky, S., Marhan, S., Fangmeier, A., Kuzyakov, Y., 2009. Stimulation of microbial extracellular enzyme activities by elevated CO_2 depends on soil aggregate size. Global Change Biology 15, 1603–1614. doi:10.1111/J.1365-2486.2009.01844.X

Duan, C., Li, J., Zhang, B., Wu, S., Fan, J., Feng, H., He, J., Siddique, K.H.M., 2023. Effect of bio-organic fertilizer derived from agricultural waste resources on soil properties and winter wheat (*Triticum aestivum* L.) yield in semi-humid drought-prone regions. Agricultural Water Management 289, 108539. doi:10.1016/j.agwat.2023.108539

Elias, D.M.O., Rowe, R.L., Pereira, M.G., Stott, A.W., Barnes, C.J., Bending, G.D., McNamara, N.P., 2017. Functional differences in the microbial processing of recent assimilates under two contrasting perennial bioenergy plantations. Soil Biology and Biochemistry 114, 248–262. doi:10.1016/j.soilbio.2017.07.026

Emmett, B.D., Buckley, D.H., Drinkwater, L.E., 2020. Plant growth rate and nitrogen uptake shape rhizosphere bacterial community composition and activity in an agricultural field. New Phytologist 225, 960–973. doi:10.1111/nph.16171

Enghiad, A., Ufer, D., Countryman, A.M., Thilmany, D.D., 2017. An Overview of Global Wheat Market Fundamentals in an Era of Climate Concerns. International Journal of Agronomy 2017, 3931897. doi:10.1155/2017/3931897

Erenstein, O., Jaleta, M., Mottaleb, K.A., Sonder, K., Donovan, J., Braun, H.-J., 2022. Global Trends in Wheat Production, Consumption and Trade BT - Wheat Improvement: Food Security in a Changing Climate, in: Reynolds, M.P., Braun, H.-J. (Eds.). Springer International Publishing, Cham, pp. 47–66. doi:10.1007/978-3-030-90673-3_4

Feifel, M., Durner, W., Hohenbrink, T.L., Peters, A., 2024. Effects of improved water retention by increased soil organic matter on the water balance of arable soils: A numerical analysis. Vadose Zone Journal 23, 1–13. doi:10.1002/vzj2.20302

Flores-Félix, J.D., Silva, L.R., Rivera, L.P., Marcos-García, M., García-Fraile, P., Martínez-Molina, E., Mateos, P.F., Velázquez, E., Andrade, P., Rivas, R., 2015. Plants probiotics as a tool to produce highly functional fruits: The case of *Phyllobacterium* and vitamin C in strawberries. PLoS ONE 10, 1–10. doi:10.1371/journal.pone.0122281

Freschet, G.T., Pagès, L., Iversen, C.M., Comas, L.H., Rewald, B., Roumet, C., Klimešová, J., Zadworny, M., Poorter, H., Postma, J.A., Adams, T.S., Bagniewska-Zadworna, A., Bengough, A.G., Blancaflor, E.B., Brunner, I., Cornelissen, J.H.C., Garnier, E., Gessler, A., Hobbie, S.E., Meier, I.C., Mommer, L., Picon-Cochard, C., Rose, L., Ryser, P., Scherer-Lorenzen, M., Soudzilovskaia, N.A., Stokes, A., Sun, T., Valverde-Barrantes, O.J., Weemstra, M., Weigelt, A., Wurzburger, N., York, L.M., Batterman, S.A., Gomes de Moraes, M., Janeček, Š., Lambers, H., Salmon, V., Tharayil, N., McCormack, M.L., 2021. A starting guide to root ecology: strengthening ecological concepts and standardising root classification, sampling, processing and trait measurements. New Phytologist 232, 973–1122. doi:10.1111/nph.17572

Frey, S.D., 2019. Mycorrhizal Fungi as Mediators of Soil Organic Matter Dynamics. Annual Review of Ecology, Evolution, and Systematics 50, 237–259. doi:10.1146/annurev-ecolsys-110617-062331

Galloway, A.F., Knox, P., Krause, K., 2020. Sticky mucilages and exudates of plants: putative microenvironmental design elements with biotechnological value. New Phytologist 225, 1461–1469. doi:10.1111/nph.16144

Gao, Z., Han, M., Hu, Y., Li, Z., Liu, C., Wang, X., Tian, Q., Jiao, W., Hu, J., Liu, L., Guan, Z., Ma, Z., 2019. Effects of Continuous Cropping of Sweet Potato on the Fungal Community

Structure in Rhizospheric Soil. Frontiers in Microbiology 10, 2269. doi:10.3389/fmicb.2019.02269
Garland, G., Edlinger, A., Banerjee, S., Degrune, F., García-Palacios, P., Pescador, D.S., Herzog, C., Romdhane, S., Saghai, A., Spor, A., Wagg, C., Hallin, S., Maestre, F.T., Philippot, L., Rillig, M.C., van der Heijden, M.G.A., 2021. Crop cover is more important than rotational diversity for soil multifunctionality and cereal yields in European cropping systems. Nature Food 2, 28–37. doi:10.1038/s43016-020-00210-8
George, T.S., Bulgarelli, D., Carminati, A., Chen, Y., Jones, D., Kuzyakov, Y., Schnepf, A., Wissuwa, M., Roose, T., 2024. Bottom-up perspective – The role of roots and rhizosphere in climate change adaptation and mitigation in agroecosystems. Plant and Soil 500, 297–323. doi:10.1007/s11104-024-06626-6
German, D.P., Chacon, S.S., Allison, S.D., 2011. Substrate concentration and enzyme allocation can affect rates of microbial decomposition. Ecology 92, 1471–1480. doi:10.1890/10-2028.1
Gfeller, V., Thoenen, L., Erb, M., 2024. Root-exuded benzoxazinoids can alleviate negative plant–soil feedbacks. New Phytologist 241, 2575–2588. doi:10.1111/nph.19401
Giongo, A., Arnhold, J., Grunwald, D., Smalla, K., Braun-Kiewnick, A., 2024. Soil depths and microhabitats shape soil and root-associated bacterial and archaeal communities more than crop rotation in wheat. Frontiers in Microbiomes 3, 1–14. doi:10.3389/frmbi.2024.1335791
Godlewski, M., Adamczyk, B., 2007. The ability of plants to secrete proteases by roots. Plant Physiology and Biochemistry 45, 657–664. doi:10.1016/j.plaphy.2007.06.001
Goswami, D., Thakker, J.N., Dhandhukia, P.C., 2016. Portraying mechanics of plant growth promoting rhizobacteria (PGPR): A review. Cogent Food & Agriculture 2, 1127500. doi:10.1080/23311932.2015.1127500
Grassini, P., Eskridge, K.M., Cassman, K.G., 2013. Distinguishing between yield advances and yield plateaus in historical crop production trends. Nature Communications 4, 2918. doi:10.1038/ncomms3918
Greenfield, L.M., Hill, P.W., Paterson, E., Baggs, E.M., Jones, D.L., 2020. Do plants use root-derived proteases to promote the uptake of soil organic nitrogen? Plant and Soil 456, 355–367. doi:10.1007/s11104-020-04719-6
Groeneveld, M., Grunwald, D., Piepho, H.P., Koch, H.J., 2024. Crop rotation and sowing date effects on yield of winter wheat. Journal of Agricultural Science 162, 139–149. doi:10.1017/S0021859624000261
Groppa, M.D., Benavides, M.P., Zawoznik, M.S., 2012. Root hydraulic conductance, aquaporins and plant growth promoting microorganisms: A revision. Applied Soil Ecology 61, 247–254. doi:10.1016/j.apsoil.2011.11.013
Guber, A., Blagodatskaya, E., Juyal, A., Razavi, B.S., Kuzyakov, Y., Kravchenko, A., 2021. Time-lapse approach to correct deficiencies of 2D soil zymography. Soil Biology and Biochemistry 157, 108225. doi:10.1016/j.soilbio.2021.108225
Gutiérrez-Mañero, F.J., Ramos-Solano, B., Probanza, A., Mehouachi, J., R. Tadeo, F., Talon, M., 2001. The plant-growth-promoting rhizobacteria *Bacillus pumilus* and *Bacillus licheniformis* produce high amounts of physiologically active gibberellins. Physiologia Plantarum 111, 206–211. doi:10.1034/j.1399-3054.2001.1110211.x
Hansen, J.C., Schillinger, W.F., Sullivan, T.S., Paulitz, T.C., 2019. Soil microbial biomass and fungi reduced with canola introduced into long-term monoculture wheat rotations. Frontiers in Microbiology 10, 1488. doi:10.3389/fmicb.2019.01488
Hao, J., Feng, Y., Wang, Xing, Yu, Q., Zhang, F., Yang, G., Ren, G., Han, X., Wang, Xiaojiao, Ren, C., 2022. Soil microbial nitrogen-cycling gene abundances in response to crop

diversification: A meta-analysis. Science of The Total Environment 838, 156621. doi:10.1016/j.scitotenv.2022.156621
Hartmann, H., Bahn, M., Carbone, M., Richardson, A.D., 2020. Plant carbon allocation in a changing world – challenges and progress: introduction to a Virtual Issue on carbon allocation. New Phytologist 227, 981–988. doi:10.1111/nph.16757
He, X., Xu, M., Qiu, G.Y., Zhou, J., 2009. Use of 15N stable isotope to quantify nitrogen transfer between mycorrhizal plants. Journal of Plant Ecology 2, 107–118. doi:10.1093/jpe/rtp015
Hegewald, H., Wensch-Dorendorf, M., Sieling, K., Christen, O., 2018. Impacts of break crops and crop rotations on oilseed rape productivity: A review. European Journal of Agronomy 101, 63–77. doi:10.1016/j.eja.2018.08.003
Heil, M., 2002. Fitness costs of induced resistance: emerging experimental support for a slippery concept. Trends in Plant Science 7, 61–67. doi:10.1016/S1360-1385(01)02186-0
Heinemann, H., Hirte, J., Seidel, F., Don, A., 2023. Increasing root biomass derived carbon input to agricultural soils by genotype selection – a review. Plant and Soil. doi:10.1007/s11104-023-06068-6
Heisey, S., Ryals, R., Maaz, T.M.C., Nguyen, N.H., 2022. A Single Application of Compost Can Leave Lasting Impacts on Soil Microbial Community Structure and Alter Cross-Domain Interaction Networks. Frontiers in Soil Science 2, 1–16. doi:10.3389/fsoil.2022.749212
Henneron, L., Balesdent, J., Alvarez, G., Barré, P., Baudin, F., Basile-Doelsch, I., Cécillon, L., Fernandez-Martinez, A., Hatté, C., Fontaine, S., 2022. Bioenergetic control of soil carbon dynamics across depth. Nature Communications 13, 7676. doi:10.1038/s41467-022-34951-w
Henry, S., Bru, D., Stres, B., Hallet, S., Philippot, L., 2006. Quantitative detection of the *nosZ* gene, encoding nitrous oxide reductase, and comparison of the abundances of 16S rRNA, *narG*, *nirK*, and *nosZ* genes in soils. Applied and Environmental Microbiology 72, 5181–5189. doi:10.1128/AEM.00231-06
Hernández-Calderón, E., Aviles-Garcia, M.E., Castulo-Rubio, D.Y., Macías-Rodríguez, L., Ramírez, V.M., Santoyo, G., López-Bucio, J., Valencia-Cantero, E., 2018. Volatile compounds from beneficial or pathogenic bacteria differentially regulate root exudation, transcription of iron transporters, and defense signaling pathways in Sorghum bicolor. Plant Molecular Biology 96, 291–304. doi:10.1007/s11103-017-0694-5
Hervé, M., 2023. RVAideMemoire: Testing and Plotting Procedures for Biostatistics Available.
Hettiarachchi, H., Bouma, J., Caucci, S., Zhang, L., 2020. Organic Waste Composting Through Nexus Thinking: Linking Soil and Waste as a Substantial Contribution to Sustainable Development BT - Organic Waste Composting through Nexus Thinking: Practices, Policies, and Trends, in: Hettiarachchi, H., Caucci, S., Schwärzel, K. (Eds.). Springer International Publishing, Cham, pp. 1–15. doi:10.1007/978-3-030-36283-6_1
Hilton, S., Bennett, A.J., Chandler, D., Mills, P., Bending, G.D., 2018. Preceding crop and seasonal effects influence fungal, bacterial and nematode diversity in wheat and oilseed rape rhizosphere and soil. Applied Soil Ecology 126, 34–46. doi:10.1016/j.apsoil.2018.02.007
Hoang, D.T.T., Rashtbari, M., Anh, L.T., Wang, S., Tu, D.T., Hiep, N.V., Razavi, B.S., 2022. Mutualistic interaction between arbuscular mycorrhiza fungi and soybean roots enhances drought resistant through regulating glucose exudation and rhizosphere expansion. Soil Biology and Biochemistry 171, 108728. doi:10.1016/J.SOILBIO.2022.108728
Hou, J., McCormack, M.L., Reich, P.B., Sun, T., Phillips, R.P., Lambers, H., Chen, H.Y.H., Ding, Y., Comas, L.H., Valverde-Barrantes, O.J., Solly, E.F., Freschet, G.T., 2024. Linking fine root lifespan to root chemical and morphological traits—A global analysis. Proceedings of

the National Academy of Sciences 121, e2320623121. doi:10.1073/pnas.2320623121
Hu, L., Robert, C.A.M.M., Cadot, S., Zhang, X., Ye, M., Li, B., Manzo, D., Chervet, N., Steinger, T., van der Heijden, M.G.A.A., Schlaeppi, K., Erb, M., 2018. Root exudate metabolites drive plant-soil feedbacks on growth and defense by shaping the rhizosphere microbiota. Nature Communications 9, 2738. doi:10.1038/s41467-018-05122-7
Idbella, M., Bonanomi, G., De Filippis, F., Foscari, A., Zotti, M., Abd-ElGawad, A.M., Fechtali, T., Incerti, G., Mazzoleni, S., 2024. Negative plant-soil feedback in Arabidopsis thaliana: Disentangling the effects of soil chemistry, microbiome, and extracellular self-DNA. Microbiological Research 281, 127634. doi:10.1016/j.micres.2024.127634
Imparato, V., Hansen, V., Santos, S.S., Nielsen, T.K., Giagnoni, L., Hauggaard-Nielsen, H., Johansen, A., Renella, G., Winding, A., 2016. Gasification biochar has limited effects on functional and structural diversity of soil microbial communities in a temperate agroecosystem. Soil Biology and Biochemistry 99, 128–136. doi:10.1016/j.soilbio.2016.05.004
Iqbal, H., Garcia-Perez, M., Flury, M., 2015. Effect of biochar on leaching of organic carbon, nitrogen, and phosphorus from compost in bioretention systems. Science of The Total Environment 521–522, 37–45. doi:10.1016/j.scitotenv.2015.03.060
Jeewani, P.H., Luo, Y., Yu, G., Fu, Y., He, X., Van Zwieten, L., Liang, C., Kumar, A., He, Y., Kuzyakov, Y., Qin, H., Guggenberger, G., Xu, J., 2021. Arbuscular mycorrhizal fungi and goethite promote carbon sequestration via hyphal-aggregate mineral interactions. Soil Biology and Biochemistry 162, 108417. doi:10.1016/j.soilbio.2021.108417
Joergensen, R.G., 1996. The fumigation-extraction method to estimate soil microbial biomass: Calibration of the kEC value. Soil Biology and Biochemistry 28, 25–31. doi:10.1016/0038-0717(95)00102-6
Jones, D.L., Nguyen, C., Finlay, R.D., 2009. Carbon flow in the rhizosphere: Carbon trading at the soil-root interface. Plant and Soil 321, 5–33. doi:10.1007/s11104-009-9925-0
Jones, P., Garcia, B.J., Furches, A., Tuskan, G.A., Jacobson, D., 2019. Plant host-associated mechanisms for microbial selection. Frontiers in Plant Science 10, 1–14. doi:10.3389/fpls.2019.00862
Kaloterakis, N., Kummer, S., Le Gall, S., Rothfuss, Y., Reichel, R., Brüggemann, N., 2024a. Reduced belowground allocation of freshly assimilated C contributes to negative plant-soil feedback in successive winter wheat rotations. Plant and Soil 505, 687–701. doi:10.1007/s11104-024-06696-6
Kaloterakis, N., Rashtbari, M., Razavi, B.S., Braun-Kiewnick, A., Giongo, A., Smalla, K., Kummer, C., Kummer, S., Reichel, R., Brüggemann, N., 2024b. Preceding crop legacy modulates the early growth of winter wheat by influencing root growth dynamics, rhizosphere processes, and microbial interactions. Soil Biology and Biochemistry 191, 109343. doi:10.1016/j.soilbio.2024.109343
Kaloterakis, N., van Delden, S.H., Hartley, S., De Deyn, G.B., 2021. Silicon application and plant growth promoting rhizobacteria consisting of six pure Bacillus species alleviate salinity stress in cucumber (*Cucumis sativus* L). Scientia Horticulturae 288, 110383. doi:10.1016/j.scienta.2021.110383
Kavamura, V.N., Robinson, R.J., Hughes, D., Clark, I., Rossmann, M., Melo, I.S. de, Hirsch, P.R., Mendes, R., Mauchline, T.H., 2020. Wheat dwarfing influences selection of the rhizosphere microbiome. Scientific Reports 10, 1–11. doi:10.1038/s41598-020-58402-y
Keeling, A.A., McCallum, K.R., Beckwith, C.P., 2003. Mature green waste compost enhances growth and nitrogen uptake in wheat (*Triticum aestivum* L.) and oilseed rape (*Brassica napus*

L.) through the action of water-extractable factors. Bioresource Technology 90, 127–132. doi:10.1016/S0960-8524(03)00125-1

Kelly, C., Haddix, M.L., Byrne, P.F., Cotrufo, M.F., Schipanski, M., Kallenbach, C.M., Wallenstein, M.D., Fonte, S.J., 2022. Divergent belowground carbon allocation patterns of winter wheat shape rhizosphere microbial communities and nitrogen cycling activities. Soil Biology and Biochemistry 165, 108518. doi:10.1016/j.soilbio.2021.108518

Kerdraon, L., Balesdent, M.-H., Barret, M., Laval, V., Suffert, F., 2019. Crop Residues in Wheat-Oilseed Rape Rotation System: a Pivotal, Shifting Platform for Microbial Meetings. Microbial Ecology 77, 931–945. doi:10.1007/s00248-019-01340-8

Khoso, M.A., Wagan, S., Alam, I., Hussain, A., Ali, Q., Saha, S., Poudel, T.R., Manghwar, H., Liu, F., 2024. Impact of plant growth-promoting rhizobacteria (PGPR) on plant nutrition and root characteristics: Current perspective. Plant Stress 11, 100341. doi:10.1016/j.stress.2023.100341

Kielak, A.M., Barreto, C.C., Kowalchuk, G.A., van Veen, J.A., Kuramae, E.E., 2016. The ecology of Acidobacteria: Moving beyond genes and genomes. Frontiers in Microbiology 7. doi:10.3389/fmicb.2016.00744

Kindler, R., Siemens, J., Kaiser, K., Walmsley, D.C., Bernhofer, C., Buchmann, N., Cellier, P., Eugster, W., Gleixner, G., Grunwald, T., Heim, A., Ibrom, A., Jones, S.K., Jones, M., Klumpp, K., Kutsch, W., Larsen, K.S., Lehuger, S., Loubet, B., Mckenzie, R., Moors, E., Osborne, B., Pilegaard, K., Rebmann, C., Saunders, M., Schmidt, M.W.I., Schrumpf, M., Seyfferth, J., Skiba, U., Soussana, J.F., Sutton, M.A., Tefs, C., Vowinckel, B., Zeeman, M.J., Kaupenjohann, M., 2011. Dissolved carbon leaching from soil is a crucial component of the net ecosystem carbon balance. Global Change Biology 17, 1167–1185. doi:10.1111/j.1365-2486.2010.02282.x

Kirkegaard, J., Christen, O., Krupinsky, J., Layzell, D., 2008. Break crop benefits in temperate wheat production. Field Crops Research 107, 185–195. doi:10.1016/j.fcr.2008.02.010

Köberl, M., Ramadan, E.M., Adam, M., Cardinale, M., Hallmann, J., Heuer, H., Smalla, K., Berg, G., 2013. *Bacillus* and *Streptomyces* were selected as broad-spectrum antagonists against soilborne pathogens from arid areas in Egypt. FEMS Microbiology Letters 342, 168–178. doi:10.1111/1574-6968.12089

Koprivova, A., Kopriva, S., 2022. Plant secondary metabolites altering root microbiome composition and function. Current Opinion in Plant Biology 67, 102227. doi:10.1016/j.pbi.2022.102227

Korenblum, E., Dong, Y., Szymanski, J., Panda, S., Jozwiak, A., Massalha, H., Meir, S., Rogachev, I., Aharoni, A., 2020. Rhizosphere microbiome mediates systemic root metabolite exudation by root-to-root signaling. Proceedings of the National Academy of Sciences of the United States of America 117, 3874–3883. doi:10.1073/pnas.1912130117

Kowaljow, E., Gonzalez-Polo, M., Mazzarino, M.J., 2017. Understanding compost effects on water availability in a degraded sandy soil of Patagonia. Environmental Earth Sciences 76, 255. doi:10.1007/s12665-017-6573-1

Kramer-Walter, K.R., Bellingham, P.J., Millar, T.R., Smissen, R.D., Richardson, S.J., Laughlin, D.C., 2016. Root traits are multidimensional: specific root length is independent from root tissue density and the plant economic spectrum. Journal of Ecology 104, 1299–1310. doi:10.1111/1365-2745.12562

Kumar, A., Singh, S., Mukherjee, A., Rastogi, R.P., Verma, J.P., 2021. Salt-tolerant plant growth-promoting *Bacillus pumilus* strain JPVS11 to enhance plant growth attributes of rice and improve soil health under salinity stress. Microbiological Research 242, 126616.

doi:10.1016/j.micres.2020.126616
Kumar, V., Pathania, N., Sharma, S., Sharma, R., 2024. Dynamics of plant nutrient signaling through compost. The Microbe 2, 100047. doi:10.1016/j.microb.2024.100047
Kuppe, C.W., Postma, J.A., 2024. Benefits and limits of biological nitrification inhibitors for plant nitrogen uptake and the environment. Scientific Reports 14, 15027. doi:10.1038/s41598-024-65247-2
Kuzyakov, Y., Domanski, G., 2000. Carbon input by plants into the soil. Review. Journal of Plant Nutrition and Soil Science 163, 421–431. doi:10.1002/1522-2624(200008)163:4<421::AID-JPLN421>3.0.CO;2-R
Kuzyakov, Y., Jones, D.L., 2006. Glucose uptake by maize roots and its transformation in the rhizosphere. Soil Biology and Biochemistry 38, 851–860. doi:10.1016/j.soilbio.2005.07.012
Kuzyakov, Y., Larionova, A.A., 2005. Root and rhizomicrobial respiration: A review of approaches to estimate respiration by autotrophic and heterotrophic organisms in soil. Journal of Plant Nutrition and Soil Science 168, 503–520. doi:10.1002/jpln.200421703
Kuzyakov, Y., Razavi, B.S., 2019. Rhizosphere size and shape: Temporal dynamics and spatial stationarity. Soil Biology and Biochemistry 135, 343–360. doi:10.1016/j.soilbio.2019.05.011
Kuzyakov, Y., Xu, X., 2013. Competition between roots and microorganisms for nitrogen: Mechanisms and ecological relevance. New Phytologist 198, 656–669. doi:10.1111/nph.12235
Kwak, Y.S., Weller, D.M., 2013. Take-all of wheat and natural disease suppression: A review. Plant Pathology Journal 29, 125–135. doi:10.5423/PPJ.SI.07.2012.0112
Lahti, L., Shetty, S., 2017. microbiome: Tools for microbiome analysis in R. Available at: https://github.com/microbiome/microbiome/.
Landeta, C., Marchant, F., 2022. Biostimulants: Emerging Trend and Opportunities BT - Biostimulants: Exploring Sources and Applications, in: Ramawat, N., Bhardwaj, V. (Eds.), . Springer Nature Singapore, Singapore, pp. 263–290. doi:10.1007/978-981-16-7080-0_11
Lange, M., Eisenhauer, N., Sierra, C.A., Bessler, H., Engels, C., Griffiths, R.I., Mellado-Vázquez, P.G., Malik, A.A., Roy, J., Scheu, S., Steinbeiss, S., Thomson, B.C., Trumbore, S.E., Gleixner, G., 2015. Plant diversity increases soil microbial activity and soil carbon storage. Nature Communications 6. doi:10.1038/ncomms7707
Lee, H.H., Kim, S.U., Han, H.R., Hur, D.Y., Owens, V.N., Kumar, S., Hong, C.O., 2021. Mitigation of global warming potential and greenhouse gas intensity in arable soil with green manure as source of nitrogen. Environmental Pollution 288, 117724. doi:10.1016/j.envpol.2021.117724
Lehtovirta-Morley, L.E., 2018. Ammonia oxidation: Ecology, physiology, biochemistry and why they must all come together. FEMS Microbiology Letters 365, fny058. doi:10.1093/femsle/fny058
Leininger, S., Urich, T., Schloter, M., Schwark, L., Qi, J., Nicol, G.W., Prosser, J.I., Schuster, S.C., Schleper, C., 2006. Archaea predominate among ammonia-oxidizing prokaryotes in soils. Nature 442, 806–809. doi:10.1038/nature04983
Levičnik-Höfferle, Š., Nicol, G.W., Ausec, L., Mandić-Mulec, I., Prosser, J.I., 2012. Stimulation of thaumarchaeal ammonia oxidation by ammonia derived from organic nitrogen but not added inorganic nitrogen. FEMS Microbiology Ecology 80, 114–123. doi:10.1111/j.1574-6941.2011.01275.x
Li, J., Pei, J., Dijkstra, F.A., Nie, M., Pendall, E., 2021. Microbial carbon use efficiency, biomass residence time and temperature sensitivity across ecosystems and soil depths. Soil Biology and Biochemistry 154, 108117. doi:10.1016/j.soilbio.2020.108117

Liao, L., Wang, J., Dijkstra, F.A., Lei, S., Zhang, L., Wang, X., Liu, G., Zhang, C., 2024. Nitrogen enrichment stimulates rhizosphere multi-element cycling genes via mediating plant biomass and root exudates. Soil Biology and Biochemistry 190, 109306. doi:10.1016/j.soilbio.2023.109306

Ling, N., Wang, T., Kuzyakov, Y., 2022. Rhizosphere bacteriome structure and functions. Nature Communications 13, 836. doi:10.1038/s41467-022-28448-9

Liu, H., Colombi, T., Jäck, O., Westerbergh, A., Weih, M., 2022. Linking wheat nitrogen use to root traits: Shallow and thin embryonic roots enhance uptake but reduce conversion efficiency of nitrogen. Field Crops Research 285, 108603. doi:10.1016/j.fcr.2022.108603

Liu, H., Wang, Z., Xu, W., Zeng, J., Li, L., Li, S., Gao, Z., 2020. *Bacillus pumilus* LZP02 Promotes Rice Root Growth by Improving Carbohydrate Metabolism and Phenylpropanoid Biosynthesis. Molecular Plant-Microbe Interactions 33, 1222–1231. doi:10.1094/MPMI-04-20-0106-R

Liu, R., Liu, Y., Gao, Y., Zhao, F., Wang, J., 2023. The Nitrogen Cycling Key Functional Genes and Related Microbial Bacterial Community α−Diversity Is Determined by Crop Rotation Plans in the Loess Plateau. Agronomy. doi:10.3390/agronomy13071769

Liu, S., He, F., Kuzyakov, Y., Xiao, H., Hoang, D.T.T., Pu, S., Razavi, B.S., 2022. Nutrients in the rhizosphere: A meta-analysis of content, availability, and influencing factors. Science of The Total Environment 826, 153908. doi:10.1016/j.scitotenv.2022.153908

Liu, X., Du, Y., Na, X., Wang, M., Qu, Y., Ge, L., Wang, Y., Gao, L., Bai, W., Bi, Y., Zhou, L., 2023. Integrative transcriptome and metabolome revealed the molecular mechanism of *Bacillus megaterium* BT22-mediated growth promotion in *Arabidopsis thaliana*. Journal of Plant Physiology 285, 153995. doi:10.1016/j.jplph.2023.153995

Loeppmann, S., Forbush, K., Cheng, W., Pausch, J., 2019. Subsoil biogeochemical properties induce shifts in carbon allocation pattern and soil C dynamics in wheat. Plant and Soil 442, 369–383. doi:10.1007/s11104-019-04204-9

Lopez, G., Ahmadi, S.H., Amelung, W., Athmann, M., Ewert, F., Gaiser, T., Gocke, M.I., Kautz, T., Postma, J., Rachmilevitch, S., Schaaf, G., Schnepf, A., Stoschus, A., Watt, M., Yu, P., Seidel, S.J., 2023. Nutrient deficiency effects on root architecture and root-to-shoot ratio in arable crops. Frontiers in Plant Science 13, 1–18. doi:10.3389/fpls.2022.1067498

Love, M.I., Huber, W., Anders, S., 2014. Moderated estimation of fold change and dispersion for RNA-seq data with DESeq2. Genome Biology 15, 550. doi:10.1186/s13059-014-0550-8

Luan, H., Liu, Y., Huang, S., Qiao, W., Chen, J., Guo, T., Zhang, Xiaojia, Guo, S., Zhang, Xuemei, Qi, G., 2022. Successive walnut plantations alter soil carbon quantity and quality by modifying microbial communities and enzyme activities. Frontiers in Microbiology 13, 1–14. doi:10.3389/fmicb.2022.953552

Lugtenberg, B., Kamilova, F., 2009. Plant-growth-promoting rhizobacteria. Annual Review of Microbiology 63, 541–556. doi:10.1146/annurev.micro.62.081307.162918

Lynch, J.P., 2013. Steep, cheap and deep: an ideotype to optimize water and N acquisition by maize root systems. Annals of Botany 112, 347–357. doi:10.1093/aob/mcs293

Ma, X., Zarebanadkouki, M., Kuzyakov, Y., Blagodatskaya, E., Pausch, J., Razavi, B.S., 2018. Spatial patterns of enzyme activities in the rhizosphere: Effects of root hairs and root radius. Soil Biology and Biochemistry 118, 69–78. doi:10.1016/j.soilbio.2017.12.009

Ma, Y., Rajkumar, M., Freitas, H., 2009. Improvement of plant growth and nickel uptake by nickel resistant-plant-growth promoting bacteria. Journal of Hazardous Materials 166, 1154–1161. doi:10.1016/j.jhazmat.2008.12.018

Macias-Benitez, S., Garcia-Martinez, A.M., Caballero Jimenez, P., Gonzalez, J.M., Tejada Moral,

M., Parrado Rubio, J., 2020. Rhizospheric Organic Acids as Biostimulants: Monitoring Feedbacks on Soil Microorganisms and Biochemical Properties. Frontiers in Plant Science 11. doi:10.3389/fpls.2020.00633

Mäder, P., Kaiser, F., Adholeya, A., Singh, R., Uppal, H.S., Sharma, A.K., Srivastava, R., Sahai, V., Aragno, M., Wiemken, A., Johri, B.N., Fried, P.M., 2011. Inoculation of root microorganisms for sustainable wheat–rice and wheat–black gram rotations in India. Soil Biology and Biochemistry 43, 609–619. doi:10.1016/j.soilbio.2010.11.031

Maheshwari, A., Jones, C.M., Tiemann, M., Hallin, S., 2023. Carbon substrate selects for different lineages of N_2O reducing communities in soils under anoxic conditions. Soil Biology and Biochemistry 177, 108909. doi:10.1016/j.soilbio.2022.108909

Mariutto, M., Ongena, M., 2015. Molecular Patterns of Rhizobacteria Involved in Plant Immunity Elicitation, Advances in Botanical Research. Elsevier Ltd. doi:10.1016/bs.abr.2015.07.002

Mayer, Z., Sasvári, Z., Szentpéteri, V., Rétháti, B.P., Vajna, B., Posta, K., 2019. Effect of long-term cropping systems on the diversity of the soil bacterial communities. Agronomy 9, 1–10. doi:10.3390/agronomy9120878

Mazzoleni, S., Bonanomi, G., Incerti, G., Chiusano, M.L., Termolino, P., Mingo, A., Senatore, M., Giannino, F., Cartenì, F., Rietkerk, M., Lanzotti, V., 2015. Inhibitory and toxic effects of extracellular self-DNA in litter: a mechanism for negative plant–soil feedbacks? New Phytologist 205, 1195–1210. doi:10.1111/nph.13121

McMurdie, P.J., Holmes, S., 2013. Phyloseq: An R Package for Reproducible Interactive Analysis and Graphics of Microbiome Census Data. PLoS ONE 8, e61217. doi:10.1371/journal.pone.0061217

Meier, I.C., Finzi, A.C., Phillips, R.P., 2017. Root exudates increase N availability by stimulating microbial turnover of fast-cycling N pools. Soil Biology and Biochemistry 106, 119–128. doi:10.1016/j.soilbio.2016.12.004

Meng, F., Dungait, J.A.J.J., Zhang, X., He, M., Guo, Y., Wu, W., 2013. Investigation of photosynthate-C allocation 27 days after ^{13}C-pulse labeling of *Zea mays* L. at different growth stages. Plant and Soil 373, 755–764. doi:10.1007/s11104-013-1841-7

Meyer, A., Focks, A., Radl, V., Keil, D., Welzl, G., Schöning, I., Boch, S., Marhan, S., Kandeler, E., Schloter, M., 2013. Different land use intensities in grassland ecosystems drive ecology of microbial communities involved in nitrogen turnover in soil. PloS One 8, e73536. doi:10.1371/journal.pone.0073536

Mohan, S., Kiran Kumar, K., Sutar, V., Saha, S., Rowe, J., Davies, K.G., 2020. Plant Root-Exudates Recruit Hyperparasitic Bacteria of Phytonematodes by Altered Cuticle Aging: Implications for Biological Control Strategies. Frontiers in Plant Science 11. doi:10.3389/fpls.2020.00763

Moinet, G.Y.K., Hijbeek, R., van Vuuren, D.P., Giller, K.E., 2023. Carbon for soils, not soils for carbon. Global Change Biology 29, 2384–2398. doi:10.1111/gcb.16570

Moore, F.C., Lobell, D.B., 2015. The fingerprint of climate trends on european crop yields. Proceedings of the National Academy of Sciences of the United States of America 112, 2970–2975. doi:10.1073/pnas.1409606112

Moran, J., McGrath, C., 2021. Comparison of Methods for Mapping Rhizosphere Processes in the Context of Their Surrounding Root and Soil Environments. BioTechniques 71, 604–614. doi:10.2144/btn-2021-0021

Mwendwa, J.M., Weston, P.A., Weidenhamer, J.D., Fomsgaard, I.S., Wu, H., Gurusinghe, S., Weston, L.A., 2021. Metabolic profiling of benzoxazinoids in the roots and rhizosphere of commercial winter wheat genotypes. Plant and Soil 466, 467–489. doi:10.1007/s11104-021-

04996-9
Nacry, P., Canivenc, G., Muller, B., Azmi, A., Van Onckelen, H., Rossignol, M., Doumas, P., 2005. A Role for Auxin Redistribution in the Responses of the Root System Architecture to Phosphate Starvation in Arabidopsis. Plant Physiology 138, 2061–2074. doi:10.1104/pp.105.060061
Nannipieri, P., Hannula, S.E., Pietramellara, G., Schloter, M., Sizmur, T., Pathan, S.I., 2023. Legacy effects of rhizodeposits on soil microbiomes: A perspective. Soil Biology and Biochemistry 184, 109107. doi:10.1016/j.soilbio.2023.109107
Näsholm, T., Kielland, K., Ganeteg, U., 2009. Uptake of organic nitrogen by plants. New Phytologist 182, 31–48. doi:10.1111/j.1469-8137.2008.02751.x
Navarro-Noya, Y.E., Gómez-Acata, S., Montoya-Ciriaco, N., Rojas-Valdez, A., Suárez-Arriaga, M.C., Valenzuela-Encinas, C., Jiménez-Bueno, N., Verhulst, N., Govaerts, B., Dendooven, L., 2013. Relative impacts of tillage, residue management and crop-rotation on soil bacterial communities in a semi-arid agroecosystem. Soil Biology and Biochemistry 65, 86–95. doi:10.1016/j.soilbio.2013.05.009
Ngo, N.P., Yamada, T., Higuma, S., Ueno, N., Saito, K., Kojima, K., Maeda, M., Yamaya-Ito, H., Ohkama-Ohtsu, N., Kanekatsu, M., Yokoyama, T., 2019. Spore inoculation of *Bacillus pumilus* TUAT1 strain, a biofertilizer microorganism, enhances seedling growth by promoting root system development in rice. Soil Science and Plant Nutrition 65, 598–604. doi:10.1080/00380768.2019.1689795
Nguyen, T.-T., Fuentes, S., Marschner, P., 2012. Effects of compost on water availability and gas exchange in tomato during drought and recovery. Plant, Soil and Environment 58, 495–502. doi:10.17221/403/2012-PSE
Ni, X., Liao, S., Tan, S., Peng, Y., Wang, D., Yue, K., Wu, F., Yang, Y., 2020. The vertical distribution and control of microbial necromass carbon in forest soils. Global Ecology and Biogeography 29, 1829–1839. doi:10.1111/geb.13159
Nkebiwe, P.M., Stevens Lekfeldt, J.D., Symanczik, S., Thonar, C., Mäder, P., Bar-Tal, A., Halpern, M., Biró, B., Bradáčová, K., Caniullan, P.C., Choudhary, K.K., Cozzolino, V., Di Stasio, E., Dobczinski, S., Geistlinger, J., Lüthi, A., Gómez-Muñoz, B., Kandeler, E., Kolberg, F., Kotroczó, Z., Kulhanek, M., Mercl, F., Tamir, G., Moradtalab, N., Piccolo, A., Maggio, A., Nassal, D., Szalai, M.Z., Juhos, K., Fora, C.G., Florea, A., Poşta, G., Lauer, K.F., Toth, B., Tlustoš, P., Mpanga, I.K., Weber, N., Weinmann, M., Yermiyahu, U., Magid, J., Müller, T., Neumann, G., Ludewig, U., de Neergaard, A., 2024. Effectiveness of bio-effectors on maize, wheat and tomato performance and phosphorus acquisition from greenhouse to field scales in Europe and Israel: a meta-analysis. Frontiers in Plant Science 15. doi:10.3389/fpls.2024.1333249
Nobile, C., Lebrun, M., Védère, C., Honvault, N., Aubertin, M.-L., Faucon, M.-P., Girardin, C., Houot, S., Kervroëdan, L., Dulaurent, A.-M., Rumpel, C., Houben, D., 2022. Biochar and compost addition increases soil organic carbon content and substitutes P and K fertilizer in three French cropping systems. Agronomy for Sustainable Development 42, 119. doi:10.1007/s13593-022-00848-7
Noë, R., Kiers, E.T., 2018. Mycorrhizal Markets, Firms, and Co-ops. Trends in Ecology & Evolution 33, 777–789. doi:10.1016/j.tree.2018.07.007
Oksanen, J., Simpson, G.L., Blanchet, F.G., Kindt, R., Legendre, P., Minchin, P.R., O'Hara, R.B., Solymos, P., Stevens, M.H.H., Szoecs, E., Wagner, H., Barbour, M., Bedward, M., Bolker, B., Borcard, D., Carvalho, G., Chirico, M., De Caceres, M., Durand, S., Evangelista, H.B.A., FitzJohn, R., Friendly, M., Furneaux, B., Hannigan, G., Hill, M.O., Lahti, L., McGlinn, D.,

Ouellette, M.-H., Ribeiro Cunha, E., Smith, T., Stier, A., Ter Braak, C.J.F., Weedon, J., 2022. vegan: Community Ecology Package. R Package Version 2.6-8. doi:10.32614/CRAN.package.vegan

Oldfield, E.E., Bradford, M.A., Wood, S.A., 2019. Global meta-analysis of the relationship between soil organic matter and crop yields. SOIL 5, 15–32. doi:10.5194/soil-5-15-2019

Osborne, S.-J., McMillan, V.E., White, R., Hammond-Kosack, K.E., 2018. Elite UK winter wheat cultivars differ in their ability to support the colonization of beneficial root-infecting fungi. Journal of Experimental Botany 69, 3103–3115. doi:10.1093/jxb/ery136

Palma-Guerrero, J., Chancellor, T., Spong, J., Canning, G., Hammond, J., McMillan, V.E., Hammond-Kosack, K.E., 2021. Take-All Disease: New Insights into an Important Wheat Root Pathogen. Trends in Plant Science 26, 836–848. doi:10.1016/j.tplants.2021.02.009

Panagos, P., Borrelli, P., 2017. Soil erosion in Europe: Current status, challenges and future developments, In: All That Soil Erosion: the Global Task to Conserve Our Soil Resources, 03-07 December 2017, Marriott Hotel, Seoul, Korea, Asia-EC JRC Joint Conference 2017 "All That Soil Erosion: the Global Task to Conserve Our Soil Resources." Soil Environment Center of the Korea, Seoul (South Korea).

Panchal, P., Preece, C., Peñuelas, J., Giri, J., 2022. Soil carbon sequestration by root exudates. Trends in Plant Science 27, 749–757. doi:10.1016/j.tplants.2022.04.009

Pang, Z., Chen, J., Wang, T., Gao, C., Li, Z., Guo, L., Xu, J., Cheng, Y., 2021. Linking Plant Secondary Metabolites and Plant Microbiomes: A Review. Frontiers in Plant Science 12. doi:10.3389/fpls.2021.621276

Panikov, N.S., Blagodatsky, S.A., Blagodatskaya, J. V., Glagolev, M. V., 1992. Determination of microbial mineralization activity in soil by modified Wright and Hobbie method. Biology and Fertility of Soils 14, 280–287. doi:10.1007/BF00395464

Pascault, N., Cécillon, L., Mathieu, O., Hénault, C., Sarr, A., Lévêque, J., Farcy, P., Ranjard, L., Maron, P.-A., 2010. In Situ Dynamics of Microbial Communities during Decomposition of Wheat, Rape, and Alfalfa Residues. Microbial Ecology 60, 816–828. doi:10.1007/s00248-010-9705-7

Paterson, E., Gebbing, T., Abel, C., Sim, A., Telfer, G., 2007. Rhizodeposition shapes rhizosphere microbial community structure in organic soil. New Phytologist 173, 600–610. doi:10.1111/j.1469-8137.2006.01931.x

Patil, I., 2021. Visualizations with statistical details : the 'ggstatsplot' approach. Journal of Open Source Software 6, 1–5. doi:10.21105/joss.03167

Paungfoo-Lonhienne, C., Lonhienne, T.G.A., Rentsch, D., Robinson, N., Christie, M., Webb, R.I., Gamage, H.K., Carroll, B.J., Schenk, P.M., Schmidt, S., 2008. Plants can use protein as a nitrogen source without assistance from other organisms. Proceedings of the National Academy of Sciences of the United States of America 105, 4524–4529. doi:10.1073/pnas.0712078105

Pausch, J., Kuzyakov, Y., 2018. Carbon input by roots into the soil: Quantification of rhizodeposition from root to ecosystem scale. Global Change Biology 24, 1–12. doi:10.1111/gcb.13850

Pausch, J., Tian, J., Riederer, M., Kuzyakov, Y., 2013. Estimation of rhizodeposition at field scale: upscaling of a 14C labeling study. Plant and Soil 364, 273–285. doi:10.1007/s11104-012-1363-8

Penna, D., Geris, J., Hopp, L., Scandellari, F., 2020. Water sources for root water uptake: Using stable isotopes of hydrogen and oxygen as a research tool in agricultural and agroforestry systems. Agriculture, Ecosystems & Environment 291, 106790.

doi:10.1016/j.agee.2019.106790
Peralta, A.L., Sun, Y., McDaniel, M.D., Lennon, J.T., 2018. Crop rotational diversity increases disease suppressive capacity of soil microbiomes. Ecosphere 9, e02235. doi:10.1002/ecs2.2235
Philippot, L., Raaijmakers, J.M., Lemanceau, P., Van Der Putten, W.H., 2013. Going back to the roots: The microbial ecology of the rhizosphere. Nature Reviews Microbiology 11, 789–799. doi:10.1038/nrmicro3109
Pieterse, C.M.J., Pelt, J. a V. a N., Verhagen, B. a S.W.M., 2003. Induced Systemic Resistance by Plant Growth- Promoting Rhizobacteria. Symbiosis 35, 39–54.
Pineda, A., Kaplan, I., Hannula, S.E., Ghanem, W., Bezemer, T.M., 2020. Conditioning the soil microbiome through plant–soil feedbacks suppresses an aboveground insect pest. New Phytologist 226, 595–608. doi:10.1111/nph.16385
Pivato, B., Semblat, A., Guégan, T., Jacquiod, S., Martin, J., Deau, F., Moutier, N., Lecomte, C., Burstin, J., Lemanceau, P., 2021. Rhizosphere Bacterial Networks, but Not Diversity, Are Impacted by Pea-Wheat Intercropping. Frontiers in Microbiology 12, 1–13. doi:10.3389/fmicb.2021.674556
Poly, F., Ranjard, L., Nazaret, S., Gourbière, F., Monrozier, L.J., 2001. Comparison of *nifH* gene pools in soils and soil microenvironments with contrasting properties. Applied and Environmental Microbiology 67, 2255–2262. doi:10.1128/AEM.67.5.2255-2262.2001
Qi, B., Zhang, K., Qin, S., Lyu, D., He, J., 2022. Glucose addition promotes C fixation and bacteria diversity in C-poor soils, improves root morphology, and enhances key N metabolism in apple roots. PLOS ONE 17, e0262691. doi:10.1371/journal.pone.0262691
Quast, C., Pruesse, E., Yilmaz, P., Gerken, J., Schweer, T., Yarza, P., Peplies, J., Glöckner, F.O., 2013. The SILVA ribosomal RNA gene database project: Improved data processing and web-based tools. Nucleic Acids Research 41, 590–596. doi:10.1093/nar/gks1219
R Core Team, 2022. R: a language and environment for statistical computing, R Foundation for Statistical Computing, Vienna, Austria. <http://www.r-project.org>.
Ramanauskienė, J., Semaškienė, R., Jonavičienė, A., Ronis, A., 2018. The effect of crop rotation and fungicide seed treatment on take-all in winter cereals in Lithuania. Crop Protection 110, 14–20. doi:10.1016/j.cropro.2018.03.011
Ray, D.K., Mueller, N.D., West, P.C., Foley, J.A., 2013. Yield Trends Are Insufficient to Double Global Crop Production by 2050. PLoS ONE 8. doi:10.1371/journal.pone.0066428
Raymond, N.S., Gómez-Muñoz, B., van der Bom, F.J.T., Nybroe, O., Jensen, L.S., Müller-Stöver, D.S., Oberson, A., Richardson, A.E., 2021. Phosphate-solubilising microorganisms for improved crop productivity: a critical assessment. New Phytologist 229, 1268–1277. doi:10.1111/nph.16924
Razavi, B.S., Liu, S., Kuzyakov, Y., 2017. Hot experience for cold-adapted microorganisms: Temperature sensitivity of soil enzymes. Soil Biology and Biochemistry 105, 236–243. doi:10.1016/j.soilbio.2016.11.026
Razavi, B.S., Zarebanadkouki, M., Blagodatskaya, E., Kuzyakov, Y., 2016. Rhizosphere shape of lentil and maize: Spatial distribution of enzyme activities. Soil Biology and Biochemistry 96, 229–237. doi:10.1016/j.soilbio.2016.02.020
Razavi, B.S., Zhang, X., Bilyera, N., Guber, A., Zarebanadkouki, M., 2019. Soil zymography: Simple and reliable? Review of current knowledge and optimization of the method. Rhizosphere 11, 100161. doi:10.1016/j.rhisph.2019.100161
Reichel, R., Kamau, C.W., Kumar, A., Li, Z., Radl, V., Temperton, V.M., Schloter, M., Brüggemann, N., 2022. Spring barley performance benefits from simultaneous shallow straw

incorporation and top dressing as revealed by rhizotrons with resealable sampling ports. Biology and Fertility of Soils 58, 375–388. doi:10.1007/s00374-022-01624-1
Reichel, R., Wei, J., Islam, M.S., Schmid, C., Wissel, H., Schröder, P., Schloter, M., Brüggemann, N., 2018. Potential of wheat straw, spruce sawdust, and lignin as high organic carbon soil amendments to improve agricultural nitrogen retention capacity: An incubation study. Frontiers in Plant Science 9, 1–13. doi:10.3389/fpls.2018.00900
Reichstein, M., Bahn, M., Ciais, P., Frank, D., Mahecha, M.D., Seneviratne, S.I., Zscheischler, J., Beer, C., Buchmann, N., Frank, D.C., Papale, D., Rammig, A., Smith, P., Thonicke, K., van der Velde, M., Vicca, S., Walz, A., Wattenbach, M., 2013. Climate extremes and the carbon cycle. Nature 500, 287–295. doi:10.1038/nature12350
Remus, R., Pandey, D., Lüttschwager, D., 2022. What regulates the rhizodeposition of winter oilseed rape during growth? Plant and Soil 478, 283–310. doi:10.1007/s11104-022-05441-1
Ren, C., Chen, J., Deng, J., Zhao, F., Han, X., Yang, G., Tong, X., Feng, Y., Shelton, S., Ren, G., 2017. Response of microbial diversity to C:N:P stoichiometry in fine root and microbial biomass following afforestation. Biology and Fertility of Soils 53, 457–468. doi:10.1007/s00374-017-1197-x
Reyes-Torres, M., Oviedo-Ocaña, E.R., Dominguez, I., Komilis, D., Sánchez, A., 2018. A systematic review on the composting of green waste: Feedstock quality and optimization strategies. Waste Management 77, 486–499. doi:10.1016/j.wasman.2018.04.037
Rillig, M.C., Caldwell, B.A., Wösten, H.A.B., Sollins, P., 2007. Role of proteins in soil carbon and nitrogen storage: Controls on persistence. Biogeochemistry 85, 25–44. doi:10.1007/s10533-007-9102-6
Rolfe, S.A., Griffiths, J., Ton, J., 2019. Crying out for help with root exudates: adaptive mechanisms by which stressed plants assemble health-promoting soil microbiomes. Current Opinion in Microbiology 49, 73–82. doi:10.1016/j.mib.2019.10.003
Rosa, S.D., Silva, C.A., Carletti, P., Sawaya, A.C.H.F., 2021. Maize Growth and Root Organic Acid Exudation in Response to Water Extract of Compost Application. Journal of Soil Science and Plant Nutrition 21, 2770–2780. doi:10.1007/s42729-021-00564-3
Rose, L., 2017. Pitfalls in root trait calculations: How ignoring diameter heterogeneity can lead to overestimation of functional traits. Frontiers in Plant Science 8, 1–5. doi:10.3389/fpls.2017.00898
Rosier, A., Medeiros, F.H.V., Bais, H.P., 2018. Defining plant growth promoting rhizobacteria molecular and biochemical networks in beneficial plant-microbe interactions. Plant and Soil. doi:10.1007/s11104-018-3679-5
Rothfuss, Y., Merz, S., Vanderborght, J., Hermes, N., Weuthen, A., Pohlmeier, A., Vereecken, H., Brüggemann, N., 2015. Long-term and high-frequency non-destructive monitoring of water stable isotope profiles in an evaporating soil column. Hydrology and Earth System Sciences 19, 4067–4080. doi:10.5194/hess-19-4067-2015
Rotthauwe, J.H., Witzel, K.P., Liesack, W., 1997. The ammonia monooxygenase structural gene amoA as a functional marker: molecular fine-scale analysis of natural ammonia-oxidizing populations. Applied and Environmental Microbiology 63, 4704–4712. doi:10.1128/aem.63.12.4704-4712.1997
Sæbø, A., Ferrini, F., 2006. The use of compost in urban green areas – A review for practical application. Urban Forestry & Urban Greening 4, 159–169. doi:10.1016/j.ufug.2006.01.003
Sáez-Sandino, T., Maestre, F.T., Berdugo, M., Gallardo, A., Plaza, C., García-Palacios, P., Guirado, E., Zhou, G., Mueller, C.W., Tedersoo, L., Crowther, T.W., Delgado-Baquerizo, M., 2024. Increasing numbers of global change stressors reduce soil carbon worldwide.

Nature Climate Change 14, 740–745. doi:10.1038/s41558-024-02019-w
Sakai, K., Yamauchi, N., Tatsuo, F., Ohe, T., 1996. Biodegradation of Cellulose Acetate by Neisseria sicca. Bioscience, Biotechnology, and Biochemistry 60, 1617–1622. doi:10.1271/bbb.60.1617
Sanders, G.J., Arndt, S.K., 2012. Osmotic Adjustment Under Drought Conditions BT - Plant Responses to Drought Stress: From Morphological to Molecular Features, in: Aroca, R. (Ed.). Springer Berlin Heidelberg, Berlin, Heidelberg, pp. 199–229. doi:10.1007/978-3-642-32653-0_8
Santana, M.M., Dias, T., Gonzalez, J.M., Cruz, C., 2021. Transformation of organic and inorganic sulfur– adding perspectives to new players in soil and rhizosphere. Soil Biology and Biochemistry 160, 108306. doi:10.1016/j.soilbio.2021.108306
Santana, M.M., Portillo, M.C., Gonzalez, J.M., Clara, M.I.E., 2013. Characterization of new soil thermophilic bacteria potentially involved in soil fertilization. Journal of Plant Nutrition and Soil Science 176, 47–56. doi:10.1002/jpln.201100382
Sasse, J., Martinoia, E., Northen, T., 2018. Feed Your Friends: Do Plant Exudates Shape the Root Microbiome? Trends in Plant Science 23, 25–41. doi:10.1016/j.tplants.2017.09.003
Scavino, A.F., Pedraza, R.O., 2013. The Role of Siderophores in Plant Growth-Promoting Bacteria, in: Maheshwari, D.K., Saraf, M., Aeron, A. (Eds.), Bacteria in Agrobiology: Crop Productivity. Springer Berlin Heidelberg, Berlin, Heidelberg, pp. 265–285. doi:10.1007/978-3-642-37241-4_11
Schauberger, B., Ben-Ari, T., Makowski, D., Kato, T., Kato, H., Ciais, P., 2018. Yield trends, variability and stagnation analysis of major crops in France over more than a century. Scientific Reports 8, 16865. doi:10.1038/s41598-018-35351-1
Schauss, K., Focks, A., Leininger, S., Kotzerke, A., Heuer, H., Thiele-Bruhn, S., Sharma, S., Wilke, B.-M., Matthies, M., Smalla, K., Munch, J.C., Amelung, W., Kaupenjohann, M., Schloter, M., Schleper, C., 2009. Dynamics and functional relevance of ammonia-oxidizing archaea in two agricultural soils. Environmental Microbiology 11, 446–456. doi:10.1111/j.1462-2920.2008.01783.x
Scheifes, D.J.P., te Beest, M., Olde Venterink, H., Jansen, A., Kinsbergen, D.T.P., Wassen, M.J., 2024. The plant root economics space in relation to nutrient limitation in Eurasian herbaceous plant communities. Ecology Letters 27, e14402. doi:10.1111/ele.14402
Schloss, P.D., 2024. Rarefaction is currently the best approach to control for uneven sequencing effort in amplicon sequence analyses. MSphere 9, e00354-23. doi:10.1128/msphere.00354-23
Schneider, H.M., Lynch, J.P., 2020. Should Root Plasticity Be a Crop Breeding Target? Frontiers in Plant Science 11, 1–16. doi:10.3389/fpls.2020.00546
Schreiter, S., Ding, G.-C., Heuer, H., Neumann, G., Sandmann, M., Grosch, R., Kropf, S., Smalla, K., 2014. Effect of the soil type on the microbiome in the rhizosphere of field-grown lettuce. Frontiers in Microbiology 5. doi:10.3389/fmicb.2014.00144
Semenov, M.A., Shewry, P.R., 2011. Modelling predicts that heat stress, not drought, will increase vulnerability of wheat in Europe. Scientific Reports 1, 66. doi:10.1038/srep00066
Senapati, N., Halford, N.G., Semenov, M.A., 2021. Vulnerability of European wheat to extreme heat and drought around flowering under future climate. Environmental Research Letters 16, 24052. doi:10.1088/1748-9326/abdcf3
Sharma, N., Sharma, G., Kour, S., Chadha, B.S., Ohri, P., 2024. Unravelling the role of plant growth promoting rhizobacteria in boosting plant growth and phytoremediation of heavy metals. Applied Soil Ecology 199, 105416. doi:10.1016/j.apsoil.2024.105416

Shewry, P.R., Hey, S.J., 2015. The contribution of wheat to human diet and health. Food and Energy Security 4, 178–202. doi:10.1002/FES3.64
Shi, Y., Sheng, L., Wang, Z., Zhang, X., He, N., Yu, Q., 2016. Responses of soil enzyme activity and microbial community compositions to nitrogen addition in bulk and microaggregate soil in the temperate steppe of Inner Mongolia. Eurasian Soil Science 49, 1149–1160. doi:10.1134/S1064229316100124
Siedt, M., Schäffer, A., Smith, K.E.C., Nabel, M., Roß-Nickoll, M., van Dongen, J.T., 2021. Comparing straw, compost, and biochar regarding their suitability as agricultural soil amendments to affect soil structure, nutrient leaching, microbial communities, and the fate of pesticides. Science of The Total Environment 751, 141607. doi:10.1016/j.scitotenv.2020.141607
Sieling, K., 2005. Growth stage-specific application of slurry and mineral N to oilseed rape, wheat and barley. Journal of Agricultural Science 142, 495–502. doi:10.1017/S0021859604004757
Sieling, K., Christen, O., 2015. Crop rotation effects on yield of oilseed rape, wheat and barley and residual effects on the subsequent wheat. Archives of Agronomy and Soil Science 61, 1531–1549. doi:10.1080/03650340.2015.1017569
Sieling, K., Günther-Borstel, O., Teebken, T., Hanus, H., 1999. Soil mineral N and N net mineralization during autumn and winter under an oilseed rape – winter wheat – winter barley rotation in different crop management systems. The Journal of Agricultural Science 132, 127–137. doi:10.1017/S0021859698006273
Sieling, K., Kage, H., 2006. N balance as an indicator of N leaching in an oilseed rape – winter wheat – winter barley rotation. Agriculture, Ecosystems & Environment 115, 261–269. doi:10.1016/j.agee.2006.01.011
Sieling, K., Stahl, C., Winkelmann, C., Christen, O., 2005. Growth and yield of winter wheat in the first 3 years of a monoculture under varying N fertilization in NW Germany. European Journal of Agronomy 22, 71–84. doi:10.1016/j.eja.2003.12.004
Simonet, P., Grosjean, M.C., Misra, A.K., Nazaret, S., Cournoyer, B., Normand, P., 1991. Frankia genus-specific characterization by polymerase chain reaction. Applied and Environmental Microbiology 57, 3278–3286. doi:10.1128/aem.57.11.3278-3286.1991
Singh, G., Verma, A.K., Kumar, V., 2016. Catalytic properties, functional attributes and industrial applications of β-glucosidases. 3 Biotech 6, 1–14. doi:10.1007/s13205-015-0328-z
Smagacz, J., Kozieł, M., Martyniuk, S., 2016. Soil properties and yields of winter wheat after long-term growing of this crop in two contrasting rotations. Plant, Soil and Environment 62, 566–570. doi:10.17221/582/2016-PSE
Sokolova, M.G., Akimova, G.P., Vaishlya, O.B., 2011. Effect of phytohormones synthesized by rhizosphere bacteria on plants. Applied Biochemistry and Microbiology 47, 274–278. doi:10.1134/S0003683811030148
Sommer, J., Dippold, M.A., Flessa, H., Kuzyakov, Y., 2016. Allocation and dynamics of C and N within plant–soil system of ash and beech. Journal of Plant Nutrition and Soil Science 179, 376–387. doi:10.1002/jpln.201500384
Song, X., Razavi, B.S., Ludwig, B., Zamanian, K., Zang, H., Kuzyakov, Y., Dippold, M.A., Gunina, A., 2020. Combined biochar and nitrogen application stimulates enzyme activity and root plasticity. Science of the Total Environment 735, 139393. doi:10.1016/j.scitotenv.2020.139393
Soudek, P., Langhansová, L., Dvořáková, M., Revutska, A., Petrová, Š., Hirnerová, A., Bouček, J., Trakal, L., Hošek, P., Soukupová, M., 2024. The impact of the application of compochar on soil moisture, stress, yield and nutritional properties of legumes under drought stress.

Science of The Total Environment 914, 169914. doi:10.1016/j.scitotenv.2024.169914
Sterngren, A.E., Hallin, S., Bengtson, P., 2015. Archaeal Ammonia Oxidizers Dominate in Numbers, but Bacteria Drive Gross Nitrification in N-amended Grassland Soil. Frontiers in Microbiology 6, 1350. doi:10.3389/fmicb.2015.01350
Stumpp, C., Brüggemann, N., Wingate, L., 2018. Stable Isotope Approaches in Vadose Zone Research. Vadose Zone Journal 17, 180096. doi:10.2136/vzj2018.05.0096
Subbarao, G. V, Kishii, M., Bozal-Leorri, A., Ortiz-Monasterio, I., Gao, X., Ibba, M.I., Karwat, H., Gonzalez-Moro, M.B., Gonzalez-Murua, C., Yoshihashi, T., Tobita, S., Kommerell, V., Braun, H.-J., Iwanaga, M., 2021. Enlisting wild grass genes to combat nitrification in wheat farming: A nature-based solution. Proceedings of the National Academy of Sciences 118, e2106595118. doi:10.1073/pnas.2106595118
Sun, L., Wang, S., Narsing Rao, M.P., Shi, Y., Lian, Z.-H., Jin, P.-J., Wang, W., Li, Y.-M., Wang, K.-K., Banerjee, A., Cui, X.-Y., Wei, D., 2023. The shift of soil microbial community induced by cropping sequence affect soil properties and crop yield. Frontiers in Microbiology 14. doi:10.3389/fmicb.2023.1095688
Sun, Y., Yang, X., Elsgaard, L., Du, T., Siddique, K.H.M., Kang, S., Butterbach-Bahl, K., 2024. Diversified crop rotations improve soil microbial communities and functions in a six-year field experiment. Journal of Environmental Management 370, 122604. doi:10.1016/j.jenvman.2024.122604
Sun, Z., Chen, Q., Han, X., Bol, R., Qu, B., Meng, F., 2018. Allocation of photosynthesized carbon in an intensively farmed winter wheat-soil system as revealed by $^{14}CO_2$ pulse labelling. Scientific Reports 8, 6–15. doi:10.1038/s41598-018-21547-y
Sun, Z., Wu, S., Zhu, B., Zhang, Y., Bol, R., Chen, Q., Meng, F., 2019. Variation of ^{13}C and ^{15}N enrichments in different plant components of labeled winter wheat (Triticum aestivum L.). PeerJ 7, e7738. doi:10.7717/peerj.7738
Sundberg, C., Al-Soud, W.A., Larsson, M., Alm, E., Yekta, S.S., Svensson, B.H., Sørensen, S.J., Karlsson, A., 2013. 454 Pyrosequencing Analyses of Bacterial and Archaeal Richness in 21 Full-Scale Biogas Digesters. FEMS Microbiology Ecology 85, 612–626. doi:10.1111/1574-6941.12148
Suzuki, M.T., Taylor, L.T., DeLong, E.F., 2000. Quantitative analysis of small-subunit rRNA genes in mixed microbial populations via 5'-nuclease assays. Applied and Environmental Microbiology 66, 4605–4614. doi:10.1128/AEM.66.11.4605-4614.2000
Tavi, N.M., Martikainen, P.J., Lokko, K., Kontro, M., Wild, B., Richter, A., Biasi, C., 2013. Linking microbial community structure and allocation of plant-derived carbon in an organic agricultural soil using $^{13}CO_2$ pulse-chase labelling combined with ^{13}C-PLFA profiling. Soil Biology and Biochemistry 58, 207–215. doi:10.1016/j.soilbio.2012.11.013
Thakur, M.P., van der Putten, W.H., Wilschut, R.A., Veen, G.F. (Ciska), Kardol, P., van Ruijven, J., Allan, E., Roscher, C., van Kleunen, M., Bezemer, T.M., 2021. Plant–Soil Feedbacks and Temporal Dynamics of Plant Diversity–Productivity Relationships. Trends in Ecology & Evolution 36, 651–661. doi:10.1016/j.tree.2021.03.011
Thion, C.E., Poirel, J.D., Cornulier, T., De Vries, F.T., Bardgett, R.D., Prosser, J.I., 2016. Plant nitrogen-use strategy as a driver of rhizosphere archaeal and bacterial ammonia oxidiser abundance. FEMS Microbiology Ecology 92, fiw091. doi:10.1093/femsec/fiw091
Thorup-Kristensen, K., 2001. Are differences in root growth of nitrogen catch crops important for their ability to reduce soil nitrate-N content, and how can this be measured? Plant and Soil 230, 185–195. doi:10.1023/A:1010306425468
Throbäck, I.N., Enwall, K., Jarvis, A., Hallin, S., 2004. Reassessing PCR primers targeting *nirS*,

nirK and *nosZ* genes for community surveys of denitrifying bacteria with DGGE. FEMS Microbiology Ecology 49, 401–417. doi:10.1016/j.femsec.2004.04.011

Tian, J., Dippold, M., Pausch, J., Blagodatskaya, E., Fan, M., Li, X., Kuzyakov, Y., 2013. Microbial response to rhizodeposition depending on water regimes in paddy soils. Soil Biology and Biochemistry 65, 195–203. doi:10.1016/j.soilbio.2013.05.021

Tian, P., Razavi, B.S., Zhang, X., Wang, Q., Blagodatskaya, E., 2020. Microbial growth and enzyme kinetics in rhizosphere hotspots are modulated by soil organics and nutrient availability. Soil Biology and Biochemistry 141, 107662. doi:10.1016/j.soilbio.2019.107662

Tilman, D., Balzer, C., Hill, J., Befort, B.L., 2011. Global food demand and the sustainable intensification of agriculture. Proceedings of the National Academy of Sciences of the United States of America 108, 20260–20264. doi:10.1073/pnas.1116437108

Tilston, E.L., Pitt, D., Fuller, M.P., Groenhof, A.C., 2005. Compost increases yield and decreases take-all severity in winter wheat. Field Crops Research 94, 176–188. doi:10.1016/j.fcr.2005.01.003

Tittonell, P., 2014. Ecological intensification of agriculture-sustainable by nature. Current Opinion in Environmental Sustainability 8, 53–61. doi:10.1016/j.cosust.2014.08.006

Town, J.R., Dumonceaux, T., Tidemann, B., Helgason, B.L., 2023. Crop rotation significantly influences the composition of soil, rhizosphere, and root microbiota in canola (*Brassica napus* L.). Environmental Microbiome 18, 1–14. doi:10.1186/s40793-023-00495-9

Trinsoutrot, I., Recous, S., Bentz, B., Linères, M., Chèneby, D., Nicolardot, B., 2000. Biochemical Quality of Crop Residues and Carbon and Nitrogen Mineralization Kinetics under Nonlimiting Nitrogen Conditions. Soil Science Society of America Journal 64, 918–926. doi:10.2136/sssaj2000.643918x

Turner, B.L., Hopkins, D.W., Haygarth, P.M., Ostle, N., 2002. β-Glucosidase activity in pasture soils. Applied Soil Ecology 20, 157–162. doi:10.1016/S0929-1393(02)00020-3

Uhlig, D., Berns, A.E., Wu, B., Amelung, W., 2023. Mean nutrient uptake depths of cereal crops change with compost incorporation into subsoil – evidence from 87Sr/86Sr ratios. Plant and Soil 489, 613–628. doi:10.1007/s11104-023-06047-x

Vacheron, J., Desbrosses, G., Bouffaud, M.-L., Touraine, B., Moënne-Loccoz, Y., Muller, D., Legendre, L., Wisniewski-Dyé, F., Prigent-Combaret, C., 2013. Plant growth-promoting rhizobacteria and root system functioning. Frontiers in Plant Science 4, 1–19. doi:10.3389/fpls.2013.00356

Van de Broek, M., Ghiasi, S., Decock, C., Hund, A., Abiven, S., Friedli, C., Werner, R.A., Six, J., 2020. The soil organic carbon stabilization potential of old and new wheat cultivars: A 13CO2-labeling study. Biogeosciences 17, 2971–2986. doi:10.5194/bg-17-2971-2020

van der Putten, W.H., Bardgett, R.D., Bever, J.D., Bezemer, T.M., Casper, B.B., Fukami, T., Kardol, P., Klironomos, J.N., Kulmatiski, A., Schweitzer, J.A., Suding, K.N., Van de Voorde, T.F.J., Wardle, D.A., 2013. Plant–soil feedbacks: the past, the present and future challenges. Journal of Ecology 101, 265–276. doi:10.1111/1365-2745.12054

Vandooren, J., Geurts, N., Martens, E., Van den Steen, P.E., Opdenakker, G., 2013. Zymography methods for visualizing hydrolytic enzymes. Nature Methods 10, 211–220. doi:10.1038/nmeth.2371

Veres, Z., Kotroczó, Z., Fekete, I., Tóth, J.A., Lajtha, K., Townsend, K., Tóthmérész, B., 2015. Soil extracellular enzyme activities are sensitive indicators of detrital inputs and carbon availability. Applied Soil Ecology 92, 18–23. doi:10.1016/j.apsoil.2015.03.006

Verma, V.C., Singh, S.K., Prakash, S., 2011. Bio-control and plant growth promotion potential of siderophore producing endophytic Streptomyces from *Azadirachta indica* A. Juss. Journal of

Basic Microbiology 51, 550–556. doi:10.1002/jobm.201000155
Vetterlein, D., Carminati, A., Kögel-Knabner, I., Bienert, G.P., Smalla, K., Oburger, E., Schnepf, A., Banitz, T., Tarkka, M.T., Schlüter, S., 2020. Rhizosphere Spatiotemporal Organization–A Key to Rhizosphere Functions. Frontiers in Agronomy 2. doi:10.3389/fagro.2020.00008
Viretto, A., Gontard, N., Angellier-Coussy, H., 2021. Urban parks and gardens green waste: A valuable resource for the production of fillers for biocomposites applications. Waste Management 120, 538–548. doi:10.1016/j.wasman.2020.10.018
Vlot, A.C., Sales, J.H., Lenk, M., Bauer, K., Brambilla, A., Sommer, A., Chen, Y., Wenig, M., Nayem, S., 2020. Systemic propagation of immunity in plants. New Phytologist 229, 1234–1250. doi:10.1111/nph.16953
Vujanovic, V., Mavragani, D., Hamel, C., 2012. Fungal communities associated with durum wheat production system: A characterization by growth stage, plant organ and preceding crop. Crop Protection 37, 26–34. doi:10.1016/j.cropro.2012.02.006
Wang, B., Li, L., Feng, P., Chen, C., Luo, J.-J., Taschetto, A.S., Harrison, M.T., Liu, K., Liu, D.L., Yu, Q., Guo, X., 2024. Probabilistic analysis of drought impact on wheat yield and climate change implications. Weather and Climate Extremes 45, 100708. doi:10.1016/j.wace.2024.100708
Wang, D., Lin, J.Y., Sayre, J.M., Schmidt, R., Fonte, S.J., Rodrigues, J.L.M., Scow, K.M., 2022. Compost amendment maintains soil structure and carbon storage by increasing available carbon and microbial biomass in agricultural soil – A six-year field study. Geoderma 427, 116117. doi:10.1016/j.geoderma.2022.116117
Wang, Q., Ding, J., Zhang, Z., Liang, C., Lambers, H., Zhu, B., Wang, D., Wang, J., Zhang, P., Li, N., Yin, H., 2025. Rhizosphere as a hotspot for microbial necromass deposition into the soil carbon pool. Journal of Ecology 113, 168–179. doi:10.1111/1365-2745.14448
Wang, R., Bicharanloo, B., Shirvan, M.B., Cavagnaro, T.R., Jiang, Y., Keitel, C., Dijkstra, F.A., 2021. A novel ^{13}C pulse-labelling method to quantify the contribution of rhizodeposits to soil respiration in a grassland exposed to drought and nitrogen addition. New Phytologist 230, 857–866. doi:10.1111/nph.17118
Wang, X., Chen, R., Jing, Z., Yao, T., Feng, Y., Lin, X., 2018. Root derived carbon transport extends the rhizosphere of rice compared to wheat. Soil Biology and Biochemistry 122, 211–219. doi:10.1016/j.soilbio.2018.03.024
Wang, Y., Zhang, H., Zhang, Y., Fei, J., Xiangmin, R., Peng, J., Luo, G., 2023. Crop rotation-driven changes in rhizosphere metabolite profiles regulate soil microbial diversity and functional capacity. Agriculture, Ecosystems & Environment 358, 108716. doi:10.1016/j.agee.2023.108716
Wang, Y., Zhang, Y., Li, Z.-Z., Zhao, Q., Huang, X.-Y., Huang, K.-F., 2019. Effect of continuous cropping on the rhizosphere soil and growth of common buckwheat. Plant Production Science 23, 81–90. doi:10.1080/1343943X.2019.1685895
Wassermann, B., Cernava, T., Goertz, S., Zur, J., Rietz, S., Kögl, I., Abbadi, A., Berg, G., 2023. Low nitrogen fertilization enriches nitrogen-fixing bacteria in the Brassica seed microbiome of subsequent generations. Journal of Sustainable Agriculture and Environment 2, 87–98. doi:10.1002/sae2.12046
Watt, M., Kirkegaard, J.A., Rebetzke, G.J., 2005. A wheat genotype developed for rapid leaf growth copes well with the physical and biological constraints of unploughed soil. Functional Plant Biology 32, 695–706. doi:10.1071/FP05026
Wei, W., Isobe, K., Nishizawa, T., Zhu, L., Shiratori, Y., Ohte, N., Koba, K., Otsuka, S., Senoo, K., 2015. Higher diversity and abundance of denitrifying microorganisms in environments

than considered previously. The ISME Journal 9, 1954–1965. doi:10.1038/ismej.2015.9
Weiser, C., Fuß, R., Kage, H., Flessa, H., 2017. Do farmers in Germany exploit the potential yield and nitrogen benefits from preceding oilseed rape in winter wheat cultivation? Archives of Agronomy and Soil Science 64, 25–37. doi:10.1080/03650340.2017.1326031
Wemheuer, F., Taylor, J.A., Daniel, R., Johnston, E., Meinicke, P., Thomas, T., Wemheuer, B., 2020. Tax4Fun2: prediction of habitat-specific functional profiles and functional redundancy based on 16S rRNA gene sequences. Environmental Microbiome 15, 11. doi:10.1186/s40793-020-00358-7
Wen, T., Yu, G.H., Hong, W.D., Yuan, J., Niu, G.Q., Xie, P.H., Sun, F.S., Guo, L.D., Kuzyakov, Y., Shen, Q.R., 2022. Root exudate chemistry affects soil carbon mobilization via microbial community reassembly. Fundamental Research 2, 697–707. doi:10.1016/j.fmre.2021.12.016
Weng, Z.H., Van Zwieten, L., Singh, B.P., Tavakkoli, E., Joseph, S., Macdonald, L.M., Rose, T.J., Rose, M.T., Kimber, S.W.L., Morris, S., Cozzolino, D., Araujo, J.R., Archanjo, B.S., Cowie, A., 2017. Biochar built soil carbon over a decade by stabilizing rhizodeposits. Nature Climate Change 7, 371–376. doi:10.1038/nclimate3276
Werner, R.A., Brand, W.A., 2001. Referencing strategies and techniques in stable isotope ratio analysis. Rapid Communications in Mass Spectrometry 15, 501–519. doi:10.1002/rcm.258
Werth, M., Kuzyakov, Y., 2008. Root-derived carbon in soil respiration and microbial biomass determined by ^{14}C and ^{13}C. Soil Biology and Biochemistry 40, 625–637. doi:10.1016/j.soilbio.2007.09.022
Wickham, H., 2016. ggplot2: Elegant Graphics for Data Analysis. Springer-Verlag New York.
Williams, A., de Vries, F.T., 2020. Plant root exudation under drought: implications for ecosystem functioning. New Phytologist 225, 1899–1905. doi:10.1111/nph.16223
Win, K.T., Oo, A.Z., Ohkama-Ohtsu, N., Yokoyama, T., 2018. *Bacillus pumilus* Strain TUAT-1 and Nitrogen Application in Nursery Phase Promote Growth of Rice Plants under Field Conditions. Agronomy. doi:10.3390/agronomy8100216
Wolińska, A., Kuźniar, A., Zielenkiewicz, U., Banach, A., Izak, D., Stępniewska, Z., Błaszczyk, M., 2017. Metagenomic Analysis of Some Potential Nitrogen-Fixing Bacteria in Arable Soils at Different Formation Processes. Microbial Ecology 73, 162–176. doi:10.1007/s00248-016-0837-2
Woo, S.L., De Filippis, F., Zotti, M., Vandenberg, A., Hucl, P., Bonanomi, G., 2022. Pea-Wheat Rotation Affects Soil Microbiota Diversity, Community Structure, and Soilborne Pathogens. Microorganisms. doi:10.3390/microorganisms10020370
Wu, J., Joergensen, R.G., Pommerening, B., Chaussod, R., Brookes, P.C., 1990. Measurement of soil microbial biomass C by fumigation-extraction—an automated procedure. Soil Biology and Biochemistry 22, 1167–1169. doi:10.1016/0038-0717(90)90046-3
Wu, L., Chen, J., Xiao, Z., Zhu, X., Wang, J., Wu, H., Wu, Y., Zhang, Z., Lin, W., 2018. Barcoded Pyrosequencing Reveals a Shift in the Bacterial Community in the Rhizosphere and Rhizoplane of *Rehmannia glutinosa* under Consecutive Monoculture. International Journal of Molecular Sciences. doi:10.3390/ijms19030850
Xiong, W., Guo, S., Jousset, A., Zhao, Q., Wu, H., Li, R., Kowalchuk, G.A., Shen, Q., 2017. Bio-fertilizer application induces soil suppressiveness against *Fusarium* wilt disease by reshaping the soil microbiome. Soil Biology and Biochemistry 114, 238–247. doi:10.1016/j.soilbio.2017.07.016
Yahya, M., Islam, E. ul, Rasul, M., Farooq, I., Mahreen, N., Tawab, A., Irfan, M., Rajput, L., Amin, I., Yasmin, S., 2021. Differential Root Exudation and Architecture for Improved Growth of Wheat Mediated by Phosphate Solubilizing Bacteria. Frontiers in Microbiology

12, 1–23. doi:10.3389/fmicb.2021.744094
Yang, X., Wang, B., Fakher, A., An, S., Kuzyakov, Y., 2023. Contribution of roots to soil organic carbon: From growth to decomposition experiment. CATENA 231, 107317. doi:10.1016/j.catena.2023.107317
Yang, Yonghui, Li, M., Wu, J., Pan, X., Gao, C., Tang, D.W.S., 2022. Impact of Combining Long-Term Subsoiling and Organic Fertilizer on Soil Microbial Biomass Carbon and Nitrogen, Soil Enzyme Activity, and Water Use of Winter Wheat. Frontiers in Plant Science 12, 1–13. doi:10.3389/fpls.2021.788651
Yang, Yajun, Liu, H., Lv, J., 2022. Response of N_2O emission and denitrification genes to different inorganic and organic amendments. Scientific Reports 12, 3940. doi:10.1038/s41598-022-07753-9
Yeo, I.N.K., Johnson, R.A., 2000. A new family of power transformations to improve normality or symmetry. Biometrika 87, 954–959. doi:10.1093/biomet/87.4.954
Yin, C., Schlatter, D.C., Hagerty, C.H., Hulbert, S.H., Paulitz, T.C., 2022. Disease-induced assemblage of the rhizosphere fungal community in successive plantings of wheat. Phytobiomes Journal 7, 100–112. doi:10.1094/pbiomes-12-22-0101-r
Yu, P., He, X., Baer, M., Beirinckx, S., Tian, T., Moya, Y.A.T., Zhang, X., Deichmann, M., Frey, F.P., Bresgen, V., Li, C., Razavi, B.S., Schaaf, G., von Wirén, N., Su, Z., Bucher, M., Tsuda, K., Goormachtig, S., Chen, X., Hochholdinger, F., 2021. Plant flavones enrich rhizosphere Oxalobacteraceae to improve maize performance under nitrogen deprivation. Nature Plants 7, 481–499. doi:10.1038/s41477-021-00897-y
Yu, T., Hou, X., Fang, X., Razavi, B., Zang, H., Zeng, Z., Yang, Y., 2024. Short-term continuous monocropping reduces peanut yield mainly via altering soil enzyme activity and fungal community. Environmental Research 245, 117977. doi:10.1016/j.envres.2023.117977
Yu, Y., Lee, C., Kim, J., Hwang, S., 2005. Group-specific primer and probe sets to detect methanogenic communities using quantitative real-time polymerase chain reaction. Biotechnology and Bioengineering 89, 670–679. doi:10.1002/bit.20347
Yuan, J., Zhao, J., Wen, T., Zhao, M., Li, R., Goossens, P., Huang, Q., Bai, Y., Vivanco, J.M., Kowalchuk, G.A., Berendsen, R.L., Shen, Q., 2018. Root exudates drive the soil-borne legacy of aboveground pathogen infection. Microbiome 6, 156. doi:10.1186/s40168-018-0537-x
Yuan, L., Gao, Y., Mei, Y., Liu, J., Kalkhajeh, Y.K., Hu, H., Huang, J., 2023. Effects of continuous straw returning on bacterial community structure and enzyme activities in rape-rice soil aggregates. Scientific Reports 13, 2357. doi:10.1038/s41598-023-28747-1
Zadoks, J.C., Chang, T.T., Konzak, C.F., 1974. A decimal code for the growth stages of cereals. Weed Research 14, 415–421. doi:10.1111/j.1365-3180.1974.tb01084.x
Zhang, T., van der Wiel, K., Wei, T., Screen, J., Yue, X., Zheng, B., Selten, F., Bintanja, R., Anderson, W., Blackport, R., Glomsrød, S., Liu, Y., Cui, X., Yang, X., 2022. Increased wheat price spikes and larger economic inequality with 2°C global warming. One Earth 5, 907–916. doi:10.1016/j.oneear.2022.07.004
Zhang, X., Kuzyakov, Y., Zang, H., Dippold, M.A., Shi, L., Spielvogel, S., Razavi, B.S., 2020. Rhizosphere hotspots: Root hairs and warming control microbial efficiency, carbon utilization and energy production. Soil Biology and Biochemistry 148, 107872. doi:10.1016/j.soilbio.2020.107872
Zhao, G., Sun, T., Zhang, Z., Zhang, J., Bian, Y., Hou, C., Zhang, D., Han, S., Wang, D., 2023. Management of take-all disease caused by *Gaeumannomyces graminis* var. *tritici* in wheat through Bacillus subtilis strains. Frontiers in Microbiology 14. doi:10.3389/fmicb.2023.1118176

Zhao, H., Zhang, L., Kirkham, M.B., Welch, S.M., Nielsen-Gammon, J.W., Bai, G., Luo, J., Andresen, D.A., Rice, C.W., Wan, N., Lollato, R.P., Zheng, D., Gowda, P.H., Lin, X., 2022. U.S. winter wheat yield loss attributed to compound hot-dry-windy events. Nature Communications 13, 7233. doi:10.1038/s41467-022-34947-6

Zhao, S., Zhang, S., 2018. Linkages between straw decomposition rate and the change in microbial fractions and extracellular enzyme activities in soils under different long-term fertilization treatments. PLoS ONE 13, e0202660. doi:10.1371/journal.pone.0202660

Zhao, Y., Zhang, F., Mickan, B., Wang, D., 2023. Inoculation of wheat with *Bacillus* sp. *wp-6* altered amino acid and flavonoid metabolism and promoted plant growth. Plant Cell Reports 42, 165–179. doi:10.1007/s00299-022-02947-x

Zheng, J., Fujii, K., Koba, K., Wanek, W., Müller, C., Jansen-Willems, A.B., Nakajima, Y., Wagai, R., Canarini, A., 2023. Revisiting process-based simulations of soil nitrite dynamics: Tighter cycling between nitrite and nitrate than considered previously. Soil Biology and Biochemistry 178, 108958. doi:10.1016/j.soilbio.2023.108958

Zhou, M., Diwu, Z., Panchuk-Voloshina, N., Haugland, R.P., 1997. A Stable Nonfluorescent Derivative of Resorufin for the Fluorometric Determination of Trace Hydrogen Peroxide: Applications in Detecting the Activity of Phagocyte NADPH Oxidase and Other Oxidases. Analytical Biochemistry 253, 162–168. doi:10.1006/ABIO.1997.2391

Zhou, Y., Yang, Z., Liu, J., Li, Xudong, Wang, X., Dai, C., Zhang, T., Carrión, V.J., Wei, Z., Cao, F., Delgado-Baquerizo, M., Li, Xiaogang, 2023. Crop rotation and native microbiome inoculation restore soil capacity to suppress a root disease. Nature Communications 14, 8126. doi:10.1038/s41467-023-43926-4

Zhu, P., Burney, J., Chang, J., Jin, Z., Mueller, N.D., Xin, Q., Xu, J., Yu, L., Makowski, D., Ciais, P., 2022. Warming reduces global agricultural production by decreasing cropping frequency and yields. Nature Climate Change 12, 1016–1023. doi:10.1038/s41558-022-01492-5

Zumft, W.G., 1997. Cell biology and molecular basis of denitrification. Microbiology and Molecular Biology Reviews 61, 533–616. doi:10.1128/mmbr.61.4.533-616.1997

Band / Volume 672
Exploring Plant Responses to Changing Environments: Integrating Phenotyping and Modeling Across Scales
F. M. Bauer (2025), xxix, 188 pp
ISBN: 978-3-95806-845-2

Band / Volume 673
A constitutive theory to represent non-idealities in contacting of SOC interconnect contacts
R. M. Pinto (2025), xii, 139 pp
ISBN: 978-3-95806-846-9

Band / Volume 674
Strontium titanate based materials for use as oxygen transport membranes in membrane reactors
Y. Tang (2025), XIV, 132 pp
ISBN: 978-3-95806-849-0

Band / Volume 675
Scaling Methods for the Production of Tungsten Fiber-Reinforced Composites via Chemical Vapor Deposition
A. Lau (2025), untersch. Pag.
ISBN: 978-3-95806-851-3

Band / Volume 676
Nanoscale analysis of high-temperature oxidation mechanisms of Cr_2AlC MAX phase and W-Cr-Y self-passivating tungsten alloy
A.J. S. Reuban (2025), ix, 142 pp
ISBN: 978-3-95806-855-1

Band / Volume 677
First principles simulations of high-entropy materials for energy storage
Y. Ting (2025), xviii, 169 pp
ISBN: 978-3-95806-858-2

Band / Volume 678
Deployment of Fuel Cell Vehicles in Road Transport and the Expansion of the Hydrogen Refueling Station Network
T. Grube, M. Sander (2025), iv, 61 pp
ISBN: 978-3-95806-859-9

Band / Volume 679
Entwicklung von nickelbasierten katalysatorbeschichteten Diaphragmen für die alkalische Wasserelektrolyse
C. B. Karacan (2025), 146 pp
ISBN: 978-3-95806-860-5

Band / Volume 680
Bewertung lokaler Eigenspannungsverteilungen bei der lokalen Bauteilreparatur durch Kaltgasspritzen
J.-C. Schmitt (2025), 154, xxvii pp
ISBN: 978-3-95806-861-2

Band / Volume 681
First principles study of the effect of substitution\doping on the performance of layered oxide cathode materials for secondary batteries
N. Yacoob (2025), iii, 126 pp
ISBN: 978-3-95806-864-3

Band / Volume 682
Field assisted sintering technology/spark plasma sintering in the direct recycling of hot-deformed Nd-Fe-B scrap and PM T15 steel swarf
M. T. M. Keszler (2025), viii, 173 pp
ISBN: 978-3-95806-866-7

Band / Volume 683
Assessment of erosion in recessed areas of fusion devices using multi-scale computer simulations
S. Rode (2025), viii, 196 pp
ISBN: 978-3-95806-867-4

Band / Volume 684
Europäische Energiewende – Deutschland im Herzen Europas
T. Klütz, P. Dunkel, T. Busch, J. Linssen, D. Stolten (2025), IV, 56 pp
ISBN: 978-3-95806-870-4

Band / Volume 685
Performance and stability of solar cells and modules: From laboratory characterization to field data analysis
T. S. Vaas (2025), xvii, 146 pp
ISBN: 978-3-95806-871-1

Band / Volume 686
From Soil Legacy to Wheat Yield Decline: Studying the Plant-Soil Feedback Mechanisms in Wheat Rotations
N. Kaloterakis (2025), XXIX, 188 pp
ISBN: 978-3-95806-874-2

Energie & Umwelt / Energy & Environment
Band / Volume 686
ISBN 978-3-95806-874-2

Mitglied der Helmholtz-Gemeinschaft

JÜLICH
Forschungszentrum